Universität Bielefeld – Fakultät für Physik
Theorie der kondensierten Materie

Numerical Renormalization Group Calculations of the Magnetization of Kondo Impurities

Dissertation
zur Erlangung des Doktorgrades
an der Fakultät für Physik
der Universität Bielefeld

vorgelegt von

Martin Höck

im

Juni 2013

betreut durch

Prof. Dr. Jürgen Schnack

"If you can't do something smart, do something right."
Joss Whedon (from the motion picture *Serenity*)

Contents

Acknowledgments

I would like to express my gratitude to the following people:

Jürgen Schnack

As my adviser, he has been extremely dedicated, taking a lot of time to discuss my research with me. In particular, I would like to thank him for giving me the chance to see Japan. Above all things, I have always admired his passion for teaching and I will certainly remember him as one of the greatest guys that I have met in my life.

Theo Costi

I feel very fortunate that I could consult Mr. Costi, one of the leading experts on NRG. In particular, I would like to thank him for carefully reading and critically commenting on the (very long) manuscript included in chapter 8. His suggestions have definitely helped to improve the quality of the paper.

Henning-Timm Langwald

He wrote his own NRG code from scratch based on chapter 4 and, in the process, tested and verified this part. Furthermore, he carefully read the complete draft of this thesis and made a lot of helpful suggestions for improvement. While not being quite as critical as I am, he came rather close ;).

Hanne Litschewsky

She has done a lot of things, far exceeding her job description as a secretary, for all of us on the floor E5. In my opinion, her dedication should not be taken for granted.

Jörg Ummethum

He was a helpful colleague at all times and I have enjoyed working with him very much.

Nedko Ivanov

He always explained things to me thoroughly whenever I asked him a question.

Roman Schnalle

During his time in Bielefeld, he regularly took the time to listen to my ideas, which must have been quite crude at this early stage.

My parents

They have always had a lot of patience with me, in particular during the roller coaster ride the result of which you are (actually or figuratively) holding in your hands. For all the things they have done for me, I am forever thankful.

Part I.

Introduction

1. Introduction, motivation, and outline

This thesis presents Numerical Renormalization Group (NRG) calculations of thermodynamic (static) observables for isotropic and anisotropic single-channel single-impurity Kondo models with impurity spin $S \geq 1/2$ in zero and non-zero magnetic field. It pursues the following goals:

1. To give a comprehensive and easily understandable introduction to basic quantum impurity physics, using the Kondo model and some of its generalizations as an example.

2. To provide a pedagogic description of the NRG method as employed for the investigation of the thermodynamics of the single-channel Kondo model with arbitrary ratio g_e/g_S of electron and impurity g-factors. This explanation is intended to be so detailed that it can be directly used for the development of a NRG code from scratch.

3. To clarify, for the Kondo model, the difference between defining the magnetization as an impurity contribution or as a local observable, and to study the effect of a non-zero electron g-factor on the properties of the model.

4. To investigate the magnetic properties of the Kondo model with additional uniaxial anisotropy of the impurity spin $S \geq 1$ by calculating magnetization curves.

The Kondo model with additional uniaxial anisotropy is relevant to the description of magnetic atoms and molecules that are deposited on a non-magnetic metallic substrate. Bistable magnetic molecules such as single molecule magnets (SMMs) have special properties which, in principle, make it possible to encode and store information in their magnetic state. This has given rise to the idea that at some point in the future a single magnetic molecule could be used to represent one bit of information. Should this become possible on a technologically relevant scale, it could significantly push the limits of attainable storage densities. However, in order to employ a single molecule for information storage purposes, one needs to be able to address individual molecules in the first place. A controlled deposition on a suitable substrate already allows to probe single atoms and molecules by means of scanning tunneling microscopy (STM) and spectroscopy (STS) techniques. "Anchoring" molecules to a surface should, however, be expected to modify their properties because of the interaction with the constituents

of the substrate (e.g., the conduction electrons of a metallic surface). As a first step, it therefore seems worthwhile to theoretically study the magnetic features of minimal models for the description of the so-called surface Kondo effect, which deposited magnetic atoms and molecules can display. We have decided to focus on the calculation and interpretation of magnetization curves. The field-dependent magnetic moment of deposited atoms and molecules can be measured using, e.g., X-ray magnetic circular dichroism (XMCD) and spin-polarized scanning tunneling spectroscopy (SP-STS). For a more detailed motivation that also provides suitable references, please refer to the introduction of the manuscript included in chapter 8.

The remainder of this thesis is organized as follows. Chapter 2 begins with an overview of the history of the Kondo effect, as it occurs in dilute magnetic alloys. The chapter continues with a discussion of the single-channel single-impurity Kondo Hamiltonian, its symmetry properties, and its relation to the single-impurity Anderson model. Furthermore, minimal models are introduced in order to describe isolated magnetic molecules (in particular, SMMs) and deposited magnetic atoms and molecules showing the surface Kondo effect, respectively. After a brief overview of the different steps that a NRG calculation is comprised of in chapter 3, the Numerical Renormalization Group method for the investigation of the thermodynamics of the single-channel Kondo model is explained *in detail* in chapter 4. Note that this chapter is very long and quite technical. In chapters 5 and 6, NRG calculations of the thermodynamic properties of the single-channel Kondo model with impurity spin $S \geq 1/2$ in zero and non-zero magnetic field, respectively, are presented and used to illustrate basic concepts of quantum impurity physics. Chapter 7 is concerned with a discussion of the Bethe ansatz solution for the zero-temperature impurity contribution to the magnetization of the isotropic Kondo model with arbitrary impurity spin. As the main result of this thesis, chapter 8 contains a NRG investigation of the single-channel single-impurity Kondo model with and without uniaxial anisotropy in non-zero magnetic field. This part focusses on the calculation and interpretation of magnetization curves. In particular, the different definitions of the magnetization are compared and the effect of the g-factor ratio of electrons and impurity on the magnetic properties of the model is illustrated. After summarizing the contents and results of this thesis, the initialization of the iterative diagonalization of the so-called Wilson chain, which has to be carried out as part of a NRG calculation, is considered in the appendix.

2. The single-channel single-impurity Kondo model

In order to provide some historical background on the concept of a so-called "quantum impurity model", we begin this chapter in Sec. 2.1 with a brief discussion of the physical phenomenon that has become known as "the Kondo effect". Starting from a real-space representation, the Hamiltonian of the *single-channel single-impurity Kondo model* is then introduced in Sec. 2.2. In particular, we address the relation between the Kondo model and the more fundamental single-impurity Anderson model. In a certain parameter regime, the Anderson model approximately maps to a spin-1/2 Kondo model. This mapping constitutes one possible "derivation" of the Kondo Hamiltonian. The particular form of the Kondo model that we intend to use for the description of deposited magnetic molecules is the topic of Sec. 2.3. Symmetry properties of a model are immensely helpful when trying to calculate its properties. They can already be discussed on the level of the Hamiltonian, and we do so for the Kondo model in Sec. 2.4.

2.1. The Kondo effect

For the moment, let us consider a non-magnetic metal with a low concentration of other atoms carrying a magnetic moment due to a spin degree of freedom (we consider the case of magnetic atoms or molecules deposited on a non-magnetic metallic substrate in Sec. 2.3). The presence of local magnetic moments can modify the physical properties of the host metal at low temperatures. Historically, effects due to dissolved magnetic atoms were first observed in samples that had previously been thought to be "pure". For this reason, the local moments are referred to as *impurities* from now on. If the concentration of impurity atoms is sufficiently low, it might be possible to neglect impurity-impurity interactions. As an approximation, the observed phenomena can then be considered as the result of additive contributions from the individual magnetic atoms (i.e., they can be effectively described using a single-impurity picture). On the other hand, the interaction with the conduction electrons of the metal is also expected to affect the physical properties of the localized moments.

The low-temperature behavior of the electrical resistivity of certain metals containing dilute amounts of magnetic atoms constitutes one of the most famous examples of an impurity-related effect. As first observed for a gold sample by de Haas, de Boer, and van den Berg in 1934 (cf. p. xvi of the book [Hew93]), the resistivity of a metal can display a minimum as a function of the temperature.

This was a surprising and at that time completely obscure result ([Hew93], p. xvi). Typically, at finite temperature, the resistivity of a metal is mainly determined by the presence of phonons. Since the scattering of electrons with phonons decreases upon reducing the temperature, the resistivity is usually expected to decline monotonically until, at very low temperature, (non-magnetic) impurities and defects become dominant and lead to a non-zero limiting value as $T \to 0$ (cf. p. 29 of Ref. [Hew93]). The minimum was later suspected to be an effect related to magnetic impurities, after linking resistivity and magnetic susceptibility measurements (see the introduction of Ref. [Kon64]). Furthermore, the position of the minimum was found to depend on the concentration of impurities ([Hew93], p. 39 f.).

It turned out that the resistance minimum can be explained in the framework of the *s-d exchange model*, which had originally been proposed by Zener to describe the interaction between conduction electrons and electrons from d-shells [Zen51]. This model comprises a localized spin S that couples to non-interacting delocalized electrons via an exchange interaction J (cf. p. 16 of Ref. [Hew93]). In 1964 Kondo studied the resistance minimum using a multi-impurity extension of the *s-d* exchange model [Kon64]. He argued, however, that due to the low concentrations in the actual samples the impurities can be treated as uncorrelated (making the minimum essentially a single-impurity effect). With this assumption, Kondo calculated the resistivity in third-order perturbation theory and found that a temperature-dependent correction appears in third order in J, which for antiferromagnetic coupling increases as $|\ln(k_B T/W)|$ (where W is the bandwidth of the conduction electrons) upon lowering the temperature (cf. p. 44 of Ref. [Hew93]). Combined with the phonon contribution, this result is sufficient to explain the occurrence of a resistance minimum [Kon64]. Kondo demonstrated that experimental resistivity curves can be well described using the logarithmic correction and, by treating J as a fit parameter, obtained antiferromagnetic couplings of the order of 0.2 eV. Because of Kondo's convincing explanation, the resistance minimum and, more generally, the physics behind it have become known as the *Kondo effect*. Nowadays, the *s-d* exchange model is usually referred to as the *Kondo model*, too.

Although very successful, Kondo's perturbational result breaks down at low temperature. In particular, it predicts a divergence of the resistivity for $T \to 0$ in case of antiferromagnetic exchange coupling because of the logarithmic temperature dependence. Moreover, perturbation theory in J for the antiferromagnetic Kondo model with a summation of the logarithmically divergent terms in leading order produces singularities in various observables at some finite temperature (see p. xvii and p. 49 of Ref. [Hew93]). This breakdown of the perturbative expansions can be used to qualitatively define a characteristic temperature scale T_K which is called the *Kondo temperature* ([Hew93], p. 49). With $\rho(\varepsilon_F)$ as the density of states of the conduction electrons at the Fermi energy, a functional dependence of the form $k_B T_K/W \approx \exp(-1/\rho(\varepsilon_F)J)$ is found. For temperatures smaller than T_K, the system is said to be in the *strong coupling regime* in which it is no longer possible to treat the exchange coupling J as a small perturbation. This conclusion follows, e.g., from the *scaling picture* for the Kondo model which originated from

Renormalization Group ideas and culminated in Anderson's "poor man's scaling" [And70]. In this scaling approach, the Kondo model is approximately mapped to the same model with a renormalized ("running") exchange coupling valid on a reduced energy scale by perturbatively eliminating electron states near the upper and lower band edge (cf. p. 58 ff. of Ref. [Hew93]). In case of an antiferromagnetic interaction, the effective coupling parameter grows when reducing the energy scale and eventually cannot be considered as small anymore. The scaling picture furthermore shows that $k_B T_K$ is the only energy scale that characterizes the low-temperature (strong-coupling) physics of the Kondo model ([Hew93], p. 61 f.). For magnetic impurities in non-magnetic metals, the experimentally determined Kondo temperatures span several orders of magnitude and can reach from the sub-Kelvin regime to (and beyond) room temperature (see p. 1564 of Ref. [GZ74], p. 982 of Ref. [Grü74], and p. 457 f. of Ref. [TW83]).

The investigation of the Kondo model for temperatures $T < T_K$ posed a great theoretical challenge and became known as the "Kondo problem" ([Hew93], p. xvii). In order to study the strong-coupling regime, a non-perturbative treatment of the exchange interaction between impurity spin and conduction electrons is necessary. Making use of Renormalization Group ideas, Wilson managed to devise an approximate numerical method called the *Numerical Renormalization Group*, which was presented in 1975 [Wil75] and allowed for the first time to calculate observables of the spin-1/2 Kondo model (such as the magnetic susceptibility, cf. p. 836 of Ref. [Wil75], Ref. [KmWW75], and p. 1025 of Ref. [KmWW80a]) over the whole temperature range. In particular, the method gives access to the low-temperature regime $T \ll T_K$ in which the Kondo model approaches a stable strong-coupling fixed point [Wil75]. By connecting to Wilson's numerical results, Nozières found a quasiparticle description of the spin-1/2 Kondo model in the vicinity of the low-temperature fixed point based on Landau's Fermi liquid theory [Noz74]. At the beginning of the 1980s, it even became possible to exactly diagonalize the Kondo model with arbitrary impurity spin by applying the *Bethe ansatz* and to derive numerically solvable equations that describe the thermodynamics at non-zero temperature [TW83, AFL83].

All these results confirmed the following physical picture of the Kondo effect, that had in part already been developed earlier. An antiferromagnetic exchange coupling between the conduction electrons and an impurity with $S = 1/2$ leads to *Kondo screening* of the impurity spin at zero temperature and zero magnetic field. A singlet groundstate is then formed [Yos66, Mat67] in which the magnetic moment of the impurity is quenched so that the impurity becomes non-magnetic. In particular, the screening effect causes the impurity magnetic susceptibility at zero field to approach a finite non-zero value for $T \ll T_K$ [Wil75]. This behavior of the susceptibility is different from, e.g., that described by a Curie law for a free spin. Note that, depending on the impurity spin S and the properties of the conduction electrons, the impurity might only be partially screened so that a magnetic moment remains at zero temperature [Mat67, CL79a]. Remarkably, it took about 40 years to confirm the theoretical prediction of this so-called *underscreened Kondo effect* experimentally (however, the effect was not observed for a dilute alloy, but for a

"molecular quantum dot" [RFC+09] and a single magnetic molecule in a break junction [PCC+10]).

As part of the screening effect, conduction electrons develop spin-spin correlations with the impurity, which oscillate and decline in magnitude with increasing distance to the impurity spin [Bor07, BGK09]. These correlations can be used to define a "Kondo screening cloud" which is thought to form in the metal around the impurity spin [Bor07]. Note, however, that the Kondo effect is a quantum mechanical *many-particle correlation phenomenon* and that, e.g., the net magnetization of the conduction electrons in a non-zero magnetic field is not necessarily significantly affected by the screening of the impurity spin [BHS70, Low84]. Theoretical estimates assuming typical parameters (e.g., $T_K \sim 1$ K) indicate that at low temperature the spatial extent of the Kondo cloud could reach an order of magnitude of about 1 μm [Bor07]. A comparison of this estimate with typical lattice constants of the order of several angstroms suggests that any theoretical method that is supposed to accurately capture Kondo physics needs to be able to effectively describe a very large (by today's standards) system. In particular, this rules out simple approaches such as a direct numerical diagonalization of the Kondo model for some finite lattice size. This challenge can also be expressed in a slightly different way: The relevant low-temperature scale T_K of the Kondo effect might be orders of magnitude smaller than, say, the bandwidth of the conduction electrons (which can, e.g., be of the order of several eV). For this reason, any theoretical method that is supposed to accurately describe the Kondo effect at low temperature has to (effectively) treat a large system size in order to resolve the relevant small energy differences (cf. p. 399 of Ref. [BCP08]).

Kondo screening leads to characteristic features in thermodynamic and dynamic quantities (we study thermodynamic observables of the Kondo model in chapters 5 and 6). As regards the latter, the appearance of a narrow many-particle resonance in the one-electron density of states at the Fermi level at low temperature $T < T_K$ is another important manifestation of the Kondo effect besides the resistivity minimum. This peak is known as the *Kondo resonance* or the *Abrikosov-Suhl resonance* ([Hew93], p. 107). For example, it can be observed in the impurity spectral density[1] of the Anderson model (see p. 127 ff. of Ref. [Hew93]), of which the Kondo model is a certain limiting case as discussed in Sec. 2.2.1, or, in the form of an antiresonance, in the spectral density at the zeroth site of the Wilson chain[2] (see p. 89 for the Kondo model and p. 215 for the Anderson model, respectively, of Ref. [Žit07]). The width of the Kondo peak at zero temperature is proportional to T_K (see, e.g., Ref. [CO03] and references therein). Non-zero temperature broadens the resonance and eventually suppresses it for $T \gg T_K$ ([Hew93], p. 128 f.). Since spectral densities are related to thermodynamic expectation values (compare, e.g.,

[1] The impurity spectral density is the quantity $\mathcal{S}_{d_\mu d_\mu^\dagger}(E)$ according to the definition (4.83) with the impurity state $\underset{\sim}{d}_\mu$ from Hamiltonian (2.19).

[2] This is the quantity $\mathcal{S}_{f_{0\mu} f_{0\mu}^\dagger}(E)$ with the state $\underset{\sim}{f}_{0\mu}$ for the Kondo model defined in Eq. (4.20). The operator $\underset{\sim}{f}_{0\mu}$ for the Anderson model is obtained by suitably adapting the definition (4.20) to the energy representation (2.21) of the Anderson Hamiltonian.

the spectral theorem (4.90)), the Kondo resonance can also be seen as the "origin" of the characteristic features observed in thermodynamic observables (cf. p. xx and 109 of Ref. [Hew93]).

2.2. The Hamiltonian of the single-channel single-impurity Kondo model

The Kondo model is one of the canonical examples of a so-called *quantum impurity model*. Generally speaking, a quantum impurity model comprises two (usually strongly) interacting subsystems. On the one hand, there is an extended fermionic (or bosonic) system with a continuous or quasi-continuous energy spectrum, which is also called "the bath". On the other hand, we have a localized system with few energy levels that, for historical reasons (cf. Sec. 2.1), is referred to as "the impurity". A typical question for such a model is how the physical properties of either subsystem are influenced by the interaction with the other subsystem.

As a quantum mechanical model, the Kondo model is defined by specifying a Hamilton operator and the corresponding Hilbert space. According to the time-independent Schrödinger equation, a "solution" of the model then amounts to solving the eigenvalue problem of the Hamilton operator. The Kondo model is typically expressed using the formalism of second quantization, i.e., its Hamiltonian is written as a Fock space operator by introducing creation and destruction operators. The fermionic Fock space is the direct sum of all antisymmetrized product Hilbert spaces with a particle number allowed by the Pauli principle.

For didactic reasons, we first show a real-space representation of the Kondo Hamiltonian which is then mapped to the reciprocal space by using a Fourier transformation. Let us consider a *tight-binding model* (see, e.g., Ref. [EFG$^+$05]) describing non-interacting electrons on a d-dimensional hypercubic lattice with L sites *per dimension* (normally, we are interested in the case of an arbitrarily large lattice with $L \gg 1$) and periodic boundary conditions in each dimension:

$$\underset{\sim}{H}_{\text{electrons}} \equiv \sum_{\substack{i \neq j \\ \sigma}} t_{ij} \underset{\sim}{d}^{\dagger}_{i\sigma} \underset{\sim}{d}_{j\sigma} + g_e \mu_B B \underset{\sim}{s}^{z}_{\text{total}} \,. \tag{2.1}$$

Whereas $\underset{\sim}{d}^{\dagger}_{i\sigma}$ creates an electron with magnetic quantum number $\sigma = \pm 1/2$ of the z-component of the electron spin at lattice site i, $\underset{\sim}{d}_{j\sigma}$ destroys an equivalent electron at site j. t_{ij} is thus a "hopping parameter" that describes the transition of an electron from site j to i. For the Hamiltonian to be Hermitian, we have to require that $t_{ij} = t^{*}_{ji}$. In order to obtain properly normalized and antisymmetrized states, the creation and destruction operators must fulfill standard fermionic anticommutation relations. Introducing the anticommutator $\{\underset{\sim}{A}, \underset{\sim}{B}\} \equiv \underset{\sim}{A}\underset{\sim}{B} + \underset{\sim}{B}\underset{\sim}{A}$, we thus have

$$\left\{ \underset{\sim}{d}_{i\mu}, \underset{\sim}{d}^{\dagger}_{j\nu} \right\} = \delta_{ij} \delta_{\mu\nu} \,, \tag{2.2}$$

with all remaining anticommutators being zero. By using Hamiltonian (2.1) it is assumed that an external magnetic field B only couples to the spin moment of the electrons, i.e., all effects related to orbital magnetism are neglected. The interaction with the spin moment is modeled by a standard Zeeman term with electron g-factor g_e, Bohr magneton μ_B, and the z-component of the *total* electron spin $\underset{\sim}{s}^z_{\text{total}}$ which, according to the rules of second quantization, can be written as:

$$\underset{\sim}{s}^z_{\text{total}} = \sum_i \underset{\sim}{s}^z_i = \frac{1}{2} \sum_i \left(\underset{\sim}{n}_{i\uparrow} - \underset{\sim}{n}_{i\downarrow} \right) . \tag{2.3}$$

Here, $\underset{\sim}{n}_{i\sigma} \equiv \underset{\sim}{d}^\dagger_{i\sigma} \underset{\sim}{d}_{i\sigma}$ is the particle-number operator for lattice site i and spin projection σ.

The localized subsystem (the impurity) is taken as a single spin $\underset{\sim}{\boldsymbol{S}}$ with quantum number S, and we assume that it exclusively interacts with the electronic spin at one site of the lattice. Since we consider all sites to be equivalent due to translational invariance, the choice of the lattice site to which the impurity spin couples is arbitrary. Let us henceforth label it with the index "0". Introducing the vector of Pauli matrices $\boldsymbol{\sigma} \equiv (\sigma^x, \sigma^y, \sigma^z)$, the electronic spin at lattice site 0 is written in second quantization as:

$$\boxed{\underset{\sim}{\boldsymbol{s}}_0 = \sum_{\mu,\nu} \underset{\sim}{d}^\dagger_{0\mu} \frac{\boldsymbol{\sigma}_{\mu\nu}}{2} \underset{\sim}{d}_{0\nu} .} \tag{2.4}$$

In the simplest case, the coupling between impurity and electrons is described by a *local* exchange interaction which takes the general anisotropic form:

$$\underset{\sim}{H}_{\text{interaction}} \equiv \sum_\alpha J^\alpha \underset{\sim}{S}^\alpha \underset{\sim}{s}^\alpha_0 = J^x \underset{\sim}{S}^x \underset{\sim}{s}^x_0 + J^y \underset{\sim}{S}^y \underset{\sim}{s}^y_0 + J^z \underset{\sim}{S}^z \underset{\sim}{s}^z_0 . \tag{2.5}$$

Normally, the isotropic ($J \equiv J^x \equiv J^y \equiv J^z$) or the XXZ-anisotropic case ($J_\perp \equiv J^x \equiv J^y$, $J_\parallel \equiv J^z$) with an antiferromagnetic exchange interaction (i.e., $J > 0$ or $J_\perp, J_\parallel > 0$) are considered.

By combining Hamiltonians (2.1) and (2.5) and adding a further field-dependent impurity Hamiltonian $\underset{\sim}{H}_{\text{imp}}(B)$, we obtain the real-space representation of a single-impurity (and single-channel, see below) Kondo model in non-zero magnetic field:

$$\boxed{\underset{\sim}{H}_{\text{Kondo}} \equiv \sum_{\substack{i \neq j \\ \sigma}} t_{ij} \underset{\sim}{d}^\dagger_{i\sigma} \underset{\sim}{d}_{j\sigma} + g_e \mu_B B \underset{\sim}{s}^z_{\text{total}} + \sum_\alpha J^\alpha \underset{\sim}{S}^\alpha \underset{\sim}{s}^\alpha_0 + \underset{\sim}{H}_{\text{imp}}(B) .} \tag{2.6}$$

The usual form of the Kondo Hamiltonian is obtained by performing a discrete Fourier transformation to the reciprocal space with the (vectorial) shift quantum number (or momentum) $\boldsymbol{k}$ (cf. Ref. [EFG+05]):

$$\underset{\sim}{c}^\dagger_{\boldsymbol{k}\sigma} \equiv \frac{1}{\sqrt{L^d}} \sum_j \mathrm{e}^{2\pi \mathrm{i}\, \boldsymbol{k} \cdot \boldsymbol{R}_j / L} \underset{\sim}{d}^\dagger_{j\sigma} , \tag{2.7}$$

with the inverse transformation

$$\underset{\sim}{d}^{\dagger}_{j\sigma} = \frac{1}{\sqrt{L^d}} \sum_{\boldsymbol{k}} \mathrm{e}^{-2\pi \mathrm{i}\, \boldsymbol{R}_j \cdot \boldsymbol{k}/L} \underset{\sim}{c}^{\dagger}_{\boldsymbol{k}\sigma} \; . \tag{2.8}$$

Here, $\boldsymbol{R}_j$ is the vector with the coordinates of lattice site j. Transformation (2.7) preserves the normalization and symmetry properties of the states, i.e.,

$$\left\{ \underset{\sim}{c}_{\boldsymbol{k}\mu}, \underset{\sim}{c}^{\dagger}_{\boldsymbol{q}\nu} \right\} = \delta_{\boldsymbol{k}\boldsymbol{q}} \delta_{\mu\nu} \; , \tag{2.9}$$

and makes the electronic Hamiltonian (2.1) diagonal:

$$\underset{\sim}{H}_{\text{electrons}} = \sum_{\boldsymbol{k},\sigma} \varepsilon_{\boldsymbol{k}} \underset{\sim}{c}^{\dagger}_{\boldsymbol{k}\sigma} \underset{\sim}{c}_{\boldsymbol{k}\sigma} + g_e \mu_B B \underset{\sim}{s}^{z}_{\text{total}} \; . \tag{2.10}$$

The dispersion relation $\varepsilon_{\boldsymbol{k}}$ assigns an energy ε to a momentum $\boldsymbol{k}$ (as an example, the dispersion relation for a one-dimensional lattice with nearest-neighbor hopping is derived in Sec. 4.3). Introducing $\underset{\sim}{n}_{\boldsymbol{k}\sigma} \equiv \underset{\sim}{c}^{\dagger}_{\boldsymbol{k}\sigma} \underset{\sim}{c}_{\boldsymbol{k}\sigma}$ and replacing the sum over the lattice sites i with a sum over the modes $\boldsymbol{k}$, the expression for the z-component of the total electron spin is analogous to Eq. (2.3),

$$\underset{\sim}{s}^{z}_{\text{total}} = \sum_{\boldsymbol{k}} \underset{\sim}{s}^{z}_{\boldsymbol{k}} = \frac{1}{2} \sum_{\boldsymbol{k}} \left(\underset{\sim}{n}_{\boldsymbol{k}\uparrow} - \underset{\sim}{n}_{\boldsymbol{k}\downarrow} \right) \; , \tag{2.11}$$

so that by defining

$$\boxed{\begin{aligned} h &\equiv g_e \mu_B B \; , && (2.12) \\ \varepsilon_{\boldsymbol{k}\sigma} &\equiv \varepsilon_{\boldsymbol{k}} + \sigma h \; , && (2.13) \end{aligned}}$$

the Zeeman term can be formally absorbed into a spin-dependent dispersion relation. Without loss of generality, we can assume that $\boldsymbol{R}_0$ is the null vector so that $\underset{\sim}{\boldsymbol{s}}_0$ from Eq. (2.4) transforms to:

$$\boxed{\underset{\sim}{\boldsymbol{s}}_0 = \frac{1}{L^d} \sum_{\substack{\boldsymbol{k},\boldsymbol{q} \\ \mu,\nu}} \underset{\sim}{c}^{\dagger}_{\boldsymbol{k}\mu} \frac{\boldsymbol{\sigma}_{\mu\nu}}{2} \underset{\sim}{c}_{\boldsymbol{q}\nu} \; .} \tag{2.14}$$

In summary, the Fourier transformation (2.7) leads to the following $\boldsymbol{k}$-space representation of the Kondo Hamiltonian (2.6):

$$\boxed{\underset{\sim}{H}_{\text{Kondo}} = \sum_{\boldsymbol{k},\sigma} \varepsilon_{\boldsymbol{k}\sigma} \underset{\sim}{c}^{\dagger}_{\boldsymbol{k}\sigma} \underset{\sim}{c}_{\boldsymbol{k}\sigma} + \sum_{\alpha} J^{\alpha} \underset{\sim}{S}^{\alpha} \underset{\sim}{s}^{\alpha}_{0} + \underset{\sim}{H}_{\text{imp}}(B) \; .} \tag{2.15}$$

Since the (single) impurity spin couples only to one "flavor" of electrons via the spin $\underset{\sim}{\boldsymbol{s}}_0$, i.e., to one *electron channel*, Hamiltonian (2.15) is classified as a *single-channel single-impurity Kondo model*. In his explanation of the resistance minimum [Kon64], Kondo considered the case of zero magnetic field and studied a

multi-impurity generalization of the model (2.15) with uniform isotropic exchange interactions J between impurity spins and conduction electrons. Assuming a sufficiently low concentration of impurity atoms, correlation effects between the localized spins were neglected and, in particular, $\underset{\sim}{H}_{\mathrm{imp}} = 0$ was used.

For practical reasons, it might be necessary to study the thermodynamics of the Kondo model using the grand-canonical ensemble. This applies, in particular, to a Numerical Renormalization Group calculation in which the "effective system size" changes so that a constant filling of the electron band requires a variable particle number. In the grand-canonical density operator, Hamiltonian (2.15) is complemented by the term $-\mu_{\mathrm{chem}}\underset{\sim}{N}$, where μ_{chem} is the chemical potential and $\underset{\sim}{N} = \sum_{i,\sigma} \underset{\sim}{n}_{i\sigma} = \sum_{\boldsymbol{k},\sigma} \underset{\sim}{n}_{\boldsymbol{k}\sigma}$ is the total electron number operator. In an actual calculation, it is convenient to absorb the term $-\mu_{\mathrm{chem}}\underset{\sim}{N}$ into the Hamiltonian and define

$$\underset{\sim}{H}_{\mathrm{GC}} \equiv \underset{\sim}{H} - \mu_{\mathrm{chem}}\underset{\sim}{N} \;, \tag{2.16}$$

so that

$$\boxed{\underset{\sim}{H}^{\mathrm{Kondo}}_{\mathrm{GC}} = \sum_{\boldsymbol{k},\sigma} (\varepsilon_{\boldsymbol{k}\sigma} - \mu_{\mathrm{chem}}) \underset{\sim}{c}^{\dagger}_{\boldsymbol{k}\sigma} \underset{\sim}{c}_{\boldsymbol{k}\sigma} + \sum_{\alpha} J^{\alpha} \underset{\sim}{S}^{\alpha} \underset{\sim}{s}^{\alpha}_{0} + \underset{\sim}{H}_{\mathrm{imp}}(B) \;.} \tag{2.17}$$

The chemical potential is typically used to determine the filling of the *non-interacting* electron band at zero temperature and zero magnetic field. To this end, for a system with a (quasi-)continuous energy spectrum, μ_{chem} is set equal to the Fermi energy ε_F according to Fermi-Dirac statistics for the ideal Fermi gas:

$$\boxed{\mu_{\mathrm{chem}} \equiv \varepsilon_F \;.} \tag{2.18}$$

There are no quantum fluctuations of $\underset{\sim}{N}$ at zero temperature (since $\underset{\sim}{N}$ is a conserved quantity of the model, see Sec. 2.4.1), but there are of course thermal fluctuations for non-zero temperature. These can, e.g., be quantified by considering the mean square deviation $\left\langle \left(\underset{\sim}{N} - \langle \underset{\sim}{N} \rangle\right)^2 \right\rangle = \langle \underset{\sim}{N}^2 \rangle - \langle \underset{\sim}{N} \rangle^2$ of the total electron number which, however, depends on the details of the electronic system. In case of particle-hole symmetry (i.e., energies occur only in symmetric pairs relative to μ_{chem}), the non-interacting electron band is on average half-filled for all temperatures and magnetic fields.

A solution of the "Kondo problem" (i.e., a study of the properties of the Kondo model for all temperatures) requires a non-perturbative treatment of the exchange interaction in Hamiltonian (2.17) (cf. Sec. 2.1). This makes analytical approaches to the Kondo problem difficult. Nevertheless, certain variants of the Kondo model can be exactly diagonalized based on an idea known as "the Bethe ansatz" [TW83, AFL83]. Furthermore, in the framework of these exact solutions numerically solvable equations describing the thermodynamics at non-zero temperature can be derived (we consider results obtained using the Bethe ansatz in chapters 5, 7,

and 8). Among the numerical methods that can be applied to the Kondo model are the *Numerical Renormalization Group* [Wil75, KmWW80a, Cos99, BCP08] (which is used in this thesis and described at length in chapter 4) and Quantum Monte Carlo [HF86, FH89, Fye94, GWPT08, GML+11].

2.2.1. Relation between the Kondo model and the Anderson model

The Kondo model with $S = 1/2$ is related to a more fundamental quantum impurity model that has been introduced by Anderson for the description of local magnetic moments in metals [And61] and is known as the *single-impurity Anderson model (SIAM)* [BCP08]. In zero magnetic field, its Hamiltonian can be written as [Hew93, Cos99, BCP08]:

$$\underset{\sim}{H}_{\mathrm{SIAM}} \equiv \sum_{\boldsymbol{k},\mu} \varepsilon_{\boldsymbol{k}}\, \underset{\sim}{c}^{\dagger}_{\boldsymbol{k}\mu} \underset{\sim}{c}_{\boldsymbol{k}\mu} + \frac{1}{\sqrt{L^d}} \sum_{\boldsymbol{k},\mu} \Big(V_{\boldsymbol{k}}\, \underset{\sim}{d}^{\dagger}_{\mu} \underset{\sim}{c}_{\boldsymbol{k}\mu} + V^{*}_{\boldsymbol{k}}\, \underset{\sim}{c}^{\dagger}_{\boldsymbol{k}\mu} \underset{\sim}{d}_{\mu} \Big) + \underbrace{\sum_{\mu} \epsilon_d\, \underset{\sim}{n}_{d,\mu} + U \underset{\sim}{n}_{d,\uparrow} \underset{\sim}{n}_{d,\downarrow}}_{= \underset{\sim}{H}_{\mathrm{imp}}} \; . \tag{2.19}$$

This model describes a single impurity orbital $\underset{\sim}{d}_{\mu}$ with on-site energy ϵ_d and on-site Coulomb repulsion $U > 0$ that "hybridizes" with the conduction electrons via a "hopping term" with parameters $V_{\boldsymbol{k}}$. In contrast to the Kondo model, the SIAM thus also takes charge fluctuations between impurity and conduction band into account. The occupation-number operators for the impurity orbital are $\underset{\sim}{n}_{d,\mu} \equiv \underset{\sim}{d}^{\dagger}_{\mu} \underset{\sim}{d}_{\mu}$, with the total electron-number operator given by $\underset{\sim}{N} = \sum_{\boldsymbol{k},\mu} \underset{\sim}{n}_{\boldsymbol{k}\mu} + \underset{\sim}{n}_{d,\uparrow} + \underset{\sim}{n}_{d,\downarrow}$. Let us assume in the following that $\varepsilon_F = 0$. It turns out that all the information about the properties of the conduction electrons can be embedded in a quantity called *hybridization function*,[3] which we define as (note that a factor π

[3] By introducing states of distinct energy $\bar{\underset{\sim}{a}}_{\mu}(\varepsilon)$, similar to Eq. (4.9), for $\varepsilon_F = 0$ and $B = 0$,

$$\bar{\underset{\sim}{a}}_{\mu}(\varepsilon) \equiv \frac{1}{\sqrt{(2\pi)^d \Delta(\varepsilon)}} \int \mathrm{d}\boldsymbol{k}\, V(\boldsymbol{k})\, \delta\big(\varepsilon - \varepsilon(\boldsymbol{k})\big)\, \underset{\sim}{a}_{\mu}(\boldsymbol{k}) \; , \tag{2.20}$$

which involve the hybridization function $\Delta(\varepsilon)$ from Eq. (2.22) instead of the density of states $\rho(\varepsilon)$ defined in Eq. (4.6), a continuous energy representation analogous to the one for the Kondo model given by Eq. (4.12) can be obtained for the SIAM Hamiltonian:

$$\underset{\sim}{H}_{\mathrm{SIAM}} \to \sum_{\mu} \int_{-W}^{W} \mathrm{d}\varepsilon\, \varepsilon\, \bar{\underset{\sim}{a}}^{\dagger}_{\mu}(\varepsilon) \bar{\underset{\sim}{a}}_{\mu}(\varepsilon) + \sum_{\mu} \int_{-W}^{W} \mathrm{d}\varepsilon\, \sqrt{\Delta(\varepsilon)} \Big(\underset{\sim}{d}^{\dagger}_{\mu} \bar{\underset{\sim}{a}}_{\mu}(\varepsilon) + \bar{\underset{\sim}{a}}^{\dagger}_{\mu}(\varepsilon) \underset{\sim}{d}_{\mu} \Big) + \underset{\sim}{H}_{\mathrm{imp}} \; . \tag{2.21}$$

The hybridization function thus encodes the information about the conduction electrons in much the same way as the density of states does in case of the Kondo model.

is missing compared to the conventional definition [Cos99, BCP08]):

$$\Delta(\varepsilon) \equiv \frac{1}{L^d} \sum_{\boldsymbol{k}} |V_{\boldsymbol{k}}|^2 \, \delta(\varepsilon - \varepsilon_{\boldsymbol{k}}) \; . \tag{2.22}$$

If we add the irrelevant constant $-\epsilon_d$ to Hamiltonian (2.19), introduce $\underset{\sim}{n}_d \equiv \underset{\sim}{n}_{d,\uparrow} + \underset{\sim}{n}_{d,\downarrow}$, and define $\delta \equiv \epsilon_d + U/2$, the impurity part can be alternatively expressed as (see p. 93 of Ref. [Žit07] and Ref. [KmWW80a], and note that $\big(\underset{\sim}{n}_{d,\mu}\big)^2 = \underset{\sim}{n}_{d,\mu}$):

$$\underset{\sim}{H}'_{\text{imp}} \equiv \underset{\sim}{H}_{\text{imp}} - \epsilon_d = \delta\big(\underset{\sim}{n}_d - 1\big) + \frac{U}{2}\big(\underset{\sim}{n}_d - 1\big)^2 \; . \tag{2.23}$$

This form makes certain symmetry properties of the model more transparent. In particular, $\delta = 0$ corresponds to the particle-hole symmetric point at which the Hamiltonian is invariant under the particle-hole transformation $\underset{\sim}{\bar{a}}_\mu(\varepsilon) \to \underset{\sim}{\bar{a}}^\dagger_\mu(-\varepsilon)$ and $\underset{\sim}{d}_\mu \to -\underset{\sim}{d}^\dagger_\mu$ (the states $\underset{\sim}{\bar{a}}_\mu(\varepsilon)$ are defined in Eq. (2.20)), provided that $\Delta(\varepsilon) = \Delta(-\varepsilon)$ (cf. Ref. [KmWW80a] and note that $(\underset{\sim}{n}_d - 1) \to -(\underset{\sim}{n}_d - 1)$). We discuss particle-hole symmetry for the Kondo model in Sec. 2.4.4.

If it is possible to add one electron to the impurity orbital because of $\epsilon_d < \varepsilon_F$, but energetically unfavorable to add another due to the Coulomb repulsion and $\epsilon_d + U > \varepsilon_F$, then the impurity site is preferably singly occupied at low energy ([Hew93], p. 19). In this case, the impurity carries a magnetic moment and its two configurations (corresponding to a spin-down or a spin-up electron) can be identified with the states of a spin-1/2 (on the other hand, the empty and doubly occupied orbital can be shown to have $S = 0$). Provided that the hybridization parameters $|V_{\boldsymbol{k}}|$ are sufficiently small, it is then possible, at low energies, to approximately map the single-impurity Anderson model to an effective Hamiltonian which takes the form of an antiferromagnetic Kondo model with $S = 1/2$ ([Hew93], p. 19).

The relation between the spin-1/2 Kondo model and the SIAM is similar to the relation between the half-filled Hubbard model and the antiferromagnetic spin-1/2 Heisenberg model. If the Coulomb interaction U is large compared to the absolute value of the hopping parameters t_{ij}, the Hubbard model (proposed by Hubbard [Hub63] and Gutzwiller [Gut63], cf. the book [EFG$^+$05]),

$$\underset{\sim}{H}_{\text{Hubbard}} \equiv \sum_{\substack{i,j \\ \mu}} t_{ij} \, \underset{\sim}{c}^\dagger_{i\mu} \underset{\sim}{c}_{j\mu} + U \sum_i \underset{\sim}{n}_{i\uparrow} \underset{\sim}{n}_{i\downarrow} \; , \tag{2.24}$$

at half-filling (i.e., the number of electrons is equal to the number of lattice sites) and low energies approximately maps to a spin-1/2 Heisenberg model. In lowest-order perturbation theory, one obtains the following low-energy effective Hamiltonian (see p. 42 of Ref. [EFG$^+$05]):

$$\underset{\sim}{H}^{\text{eff}}_{\text{Hubbard}} = \sum_{i<j} \frac{4|t_{ij}|^2}{U} \left(\underset{\sim}{\boldsymbol{S}}_i \cdot \underset{\sim}{\boldsymbol{S}}_j - \frac{1}{4} \right) , \tag{2.25}$$

with isotropic antiferromagnetic exchange interactions $J_{ij} \equiv 4|t_{ij}|^2/U > 0$ and $S_i = 1/2$ for all i. This result had already been obtained by Anderson in the context of the "superexchange interaction" [And59], prior to the introduction of the Hubbard model. One possibility for carrying out the perturbative expansion (in principle, to arbitrary order in $1/U$) is to employ a unitary, so-called canonical, transformation with a suitable generator $\underset{\sim}{G}$ so that $\underset{\sim}{H}_{\mathrm{eff}} = \exp\bigl(\mathrm{i}\underset{\sim}{G}\bigr)\underset{\sim}{H}\exp\bigl(-\mathrm{i}\underset{\sim}{G}\bigr)$ [MGY88, MGY90, MGY91, CGP$^+$04, KJ04]. The effect of the canonical transformation is to eliminate terms from the Hamiltonian that couple states with a different number of doubly occupied lattice sites [MGY88].

As a simplification, let us now consider the case $V_{\boldsymbol{k}} \equiv V$ for all $\boldsymbol{k}$ and $\rho(\varepsilon) \equiv \rho \equiv$ const. (the density of states $\rho(\varepsilon)$ is defined in Eq. (4.6)). According to the definition (2.22), we then have $\Delta(\varepsilon) = \rho V^2 \equiv \Gamma > 0$. Note that the *hybridization strength* Γ is again defined without an additional factor π (see, e.g., Ref. [KmWW80a] for the usual definition). For $\Gamma \ll U$ and $|\delta| \ll U$, one can now derive the following effective low-energy Hamiltonian for the SIAM, which is valid to second order in the hybridization V (see p. 95 ff. of Ref. [Žit07]):

$$\underset{\sim}{H}^{\mathrm{eff}}_{\mathrm{SIAM}} = \sum_{\boldsymbol{k},\mu} \varepsilon_{\boldsymbol{k}}\, \underset{\sim}{c}^{\dagger}_{\boldsymbol{k}\mu}\underset{\sim}{c}_{\boldsymbol{k}\mu} + \frac{J}{L^d}\,\underset{\sim}{\boldsymbol{S}}\cdot\sum_{\substack{\boldsymbol{k},\boldsymbol{q}\\ \mu,\nu}} \underset{\sim}{c}^{\dagger}_{\boldsymbol{k}\mu}\frac{\boldsymbol{\sigma}_{\mu\nu}}{2}\underset{\sim}{c}_{\boldsymbol{q}\nu} + \frac{K}{L^d}\sum_{\substack{\boldsymbol{k},\boldsymbol{q}\\ \mu}} \underset{\sim}{c}^{\dagger}_{\boldsymbol{k}\mu}\underset{\sim}{c}_{\boldsymbol{q}\mu}\ , \tag{2.26}$$

with impurity spin $S = 1/2$ and (see p. 97 of Ref. [Žit07] and compare the result for $\delta = 0$ from Ref. [KmWW75]):

$$\rho J = \frac{8\Gamma}{U}\,\frac{1}{1-4(\delta/U)^2}\ , \tag{2.27}$$

$$\rho K = \frac{\delta}{2U}\,\rho J \qquad . \tag{2.28}$$

In the parameter regime $\Gamma \ll U$ and $|\delta| \ll U$, the single-impurity Anderson model is thus approximated at low energy by a spin-1/2 Kondo model with isotropic antiferromagnetic exchange interaction $J > 0$, which features additional *potential scattering* K if the SIAM is *not* particle-hole symmetric (the Kondo model with $S = 1/2$ and potential scattering is studied in Sec. 5.1.3). The relation between the Kondo and Anderson Hamiltonians was first demonstrated in Ref. [SW66] by means of a canonical transformation that is known as the *Schrieffer-Wolff transformation*.

2.3. A minimal model for deposited magnetic atoms and molecules

2.3.1. The bilinear spin Hamiltonian for the description of an isolated magnetic molecule

To begin with, let us consider an *isolated* molecule in zero magnetic field. We assume that the molecule is magnetic due to one or more contained metal ions with unpaired electrons that result in a non-zero magnetic moment at the respective "magnetic center". In the following, the interaction between two such centers is discussed. To this end, we furthermore presume that the groundstate multiplets of both ions are orbitally non-degenerate (typically, this means that the orbital angular momentum is essentially quenched) and that they are well separated in energy from the higher-lying levels. Under these conditions, it might be reasonable to describe the magnetic properties of the molecule at low energy (relative to the groundstate gaps of the ions) by an *effective spin Hamiltonian*, which contains only spin degrees of freedom (cf. p. 20 f. of Ref. [BG90], p. 14 f. of Ref. [GSV06], and p. 369 of Ref. [FW13]). A justification of such an approach based on a more fundamental (microscopic) theory is usually difficult ([BG90], p. 20).

Let $\underset{\sim}{\boldsymbol{S}}_A$ and $\underset{\sim}{\boldsymbol{S}}_B$ be the (effective) spin operators assigned to the two magnetic centers. If we only consider bilinear terms, the Hamiltonian describing the spin-spin interaction takes the following general form ([BG90], p. 21):

$$\underset{\sim}{H}_{AB} \equiv \underset{\sim}{\boldsymbol{S}}_A^T \mathcal{J}_{AB} \underset{\sim}{\boldsymbol{S}}_B \, . \tag{2.29}$$

Here, $\mathcal{J}_{AB}$ is a general real tensor with nine independent entries. In principle, also higher-order terms with an even number of spin operators (e.g., biquadratic terms) have to be added to the Hamiltonian in order to accurately describe the interaction between the magnetic centers. However, it is found that in case of magnetic molecules such terms are usually less important compared to the dominant bilinear terms (cf. p. 34 of Ref. [BG90], as well as p. 16 and 19 of Ref. [GSV06]).

The tensor $\mathcal{J}_{AB}$ can be split up into a symmetric part $\mathcal{S}_{AB}$ and an antisymmetric part $\mathcal{A}_{AB}$ ([BG90], p. 21):

$$\mathcal{S}_{AB} \equiv \frac{1}{2}\left(\mathcal{J}_{AB} + \mathcal{J}_{AB}^T\right) , \tag{2.30}$$

$$\mathcal{A}_{AB} \equiv \frac{1}{2}\left(\mathcal{J}_{AB} - \mathcal{J}_{AB}^T\right) . \tag{2.31}$$

The antisymmetric component is traceless by definition and the symmetric part can be made traceless by subtracting a suitable diagonal matrix ([BG90], p. 21):

$$\mathcal{S}'_{AB} \equiv \mathcal{S}_{AB} - \frac{1}{3}\mathrm{tr}(\mathcal{S}_{AB})\,\mathbb{1} = \mathcal{S}_{AB} - \underbrace{\frac{1}{3}\mathrm{tr}(\mathcal{J}_{AB})}_{\equiv J_{AB}}\mathbb{1} \, . \tag{2.32}$$

The resulting decomposition of the tensor $\mathcal{J}_{AB}$,

$$\mathcal{J}_{AB} = J_{AB}\mathbb{1} + \mathcal{S}'_{AB} + \mathcal{A}_{AB} \ , \tag{2.33}$$

leads to the following equivalent expression for Hamiltonian (2.29):

$$\underset{\sim}{H}_{AB} = J_{AB}\underset{\sim}{\boldsymbol{S}}_A \cdot \underset{\sim}{\boldsymbol{S}}_B + \underset{\sim}{\boldsymbol{S}}_A^T \mathcal{S}'_{AB} \underset{\sim}{\boldsymbol{S}}_B + \underset{\sim}{\boldsymbol{S}}_A^T \mathcal{A}_{AB} \underset{\sim}{\boldsymbol{S}}_B \ . \tag{2.34}$$

As an antisymmetric tensor, $\mathcal{A}_{AB}$ has three independent components (e.g., $\mathcal{A}_{AB}^{xy}$, $\mathcal{A}_{AB}^{xz}$, and $\mathcal{A}_{AB}^{yz}$). We now introduce the vector $\mathbf{d}_{AB} \equiv \left(d_{AB}^x, d_{AB}^y, d_{AB}^z\right)$ and demand:

$$\mathbf{d}_{AB} \cdot \left(\underset{\sim}{\boldsymbol{S}}_A \times \underset{\sim}{\boldsymbol{S}}_B\right) \overset{!}{=} \underset{\sim}{\boldsymbol{S}}_A^T \mathcal{A}_{AB} \underset{\sim}{\boldsymbol{S}}_B \ . \tag{2.35}$$

Equating coefficients leads to nine equations which, using the Levi-Civita symbol ε^{ijk}, can be expressed as:

$$\mathcal{A}_{AB}^{ij} = \sum_k \varepsilon^{ijk} d_{AB}^k \quad \text{for} \quad i,j = x,y,z \ . \tag{2.36}$$

Since $\mathcal{A}_{AB}$ is an antisymmetric tensor, this system of equations is solvable and yields the unique solution ([BG90], p. 22):

$$d_{AB}^x = \ \ \mathcal{A}_{AB}^{yz} \ , \tag{2.37}$$
$$d_{AB}^y = -\mathcal{A}_{AB}^{xz} \ , \tag{2.38}$$
$$d_{AB}^z = \ \ \mathcal{A}_{AB}^{xy} \ . \tag{2.39}$$

We thus have the following equivalent representation of Hamiltonian (2.29) ([BG90], p. 21):

$$\boxed{\underset{\sim}{H}_{AB} = \underbrace{J_{AB}\underset{\sim}{\boldsymbol{S}}_A \cdot \underset{\sim}{\boldsymbol{S}}_B}_{\substack{\text{isotropic} \\ \text{(Heisenberg)}}} + \underbrace{\mathbf{d}_{AB} \cdot \left(\underset{\sim}{\boldsymbol{S}}_A \times \underset{\sim}{\boldsymbol{S}}_B\right)}_{\substack{\text{antisymmetric} \\ \text{(Dzyaloshinski-Moriya)}}} + \underbrace{\underset{\sim}{\boldsymbol{S}}_A^T \mathcal{S}'_{AB} \underset{\sim}{\boldsymbol{S}}_B}_{\substack{\text{anisotropic,} \\ \text{with a symmetric} \\ \text{and traceless tensor}}}} \ . \tag{2.40}$$

Next, we consider the bilinear spin Hamiltonian describing the magnetic properties of a *single* spin by setting $\underset{\sim}{\boldsymbol{S}}_A \equiv \underset{\sim}{\boldsymbol{S}}_B \equiv \underset{\sim}{\boldsymbol{S}}$ in Eq. (2.29). Note that the resulting Hamiltonian can serve as a model for the *whole* molecule if the molecule either contains only one magnetic center or if its groundstate multiplet with good spin quantum number S is energetically well separated from the rest of the spectrum. In the latter case, essential magnetic features of the molecule might be describable using a "giant-spin" approximation which only takes into account the groundstate multiplet and thus reduces all the spin degrees of freedom of the molecule to a single (usually large) spin S (cf. p. 284 of Ref. [Blu07] and p. 404 of Ref. [FW13]).

For $\underset{\sim}{\boldsymbol{S}}_A = \underset{\sim}{\boldsymbol{S}}_B = \underset{\sim}{\boldsymbol{S}}$, the isotropic term in Eq. (2.40) reduces to a constant ($J_{AA}\underset{\sim}{\boldsymbol{S}}^2 = J_{AA}S(S+1)\mathbb{1}$) that can be dropped and the antisymmetric term vanishes so that only the anisotropic part remains. Setting $\mathcal{C} \equiv \mathcal{S}'_{AA}$, we obtain the so-called *crystal-field Hamiltonian*, which describes the effect of the surrounding atoms (the "crystal field") on the spin $\underset{\sim}{\boldsymbol{S}}$ (see p. 15 of Ref. [GSV06]):

$$\boxed{\underset{\sim}{H}_S \equiv \underset{\sim}{\boldsymbol{S}}^T \mathcal{C}\, \underset{\sim}{\boldsymbol{S}}\,.} \tag{2.41}$$

The tensor $\mathcal{C}$ is referred to as the *crystal-field tensor* ([Blu07], p. 284) or the *zero-field-splitting tensor* (because the resulting anisotropy splits up spin multiplets even in zero magnetic field, cf. p. 17 of Ref. [GSV06]). Since $\mathcal{C}$ is symmetric, we may transform to a coordinate system in which the tensor assumes a diagonal form $\mathcal{D}$ ([GSV06], p. 16):

$$\mathcal{D} = \begin{pmatrix} \mathcal{D}^{xx} & 0 & 0 \\ 0 & \mathcal{D}^{yy} & 0 \\ 0 & 0 & \mathcal{D}^{zz} \end{pmatrix}. \tag{2.42}$$

By convention, the z-axis is chosen so that $|\mathcal{D}^{zz}|$ is maximized. Denoting the transformed spin operators by $\underset{\sim}{\boldsymbol{S}}$ as before, Hamiltonian (2.41) then simplifies to:

$$\underset{\sim}{H}_S = \mathcal{D}^{xx}\big(\underset{\sim}{S}^x\big)^2 + \mathcal{D}^{yy}\big(\underset{\sim}{S}^y\big)^2 + \mathcal{D}^{zz}\big(\underset{\sim}{S}^z\big)^2\,. \tag{2.43}$$

Since $\mathcal{C}$, and thus also $\mathcal{D}$, is traceless, only two free parameters remain (e.g., $\mathcal{D}^{xx}$ and $\mathcal{D}^{yy}$). By defining (see p. 16 of Ref. [GSV06])

$$\begin{aligned} D &\equiv \mathcal{D}^{zz} - \frac{1}{2}(\mathcal{D}^{xx} + \mathcal{D}^{yy}) \\ &= -\frac{3}{2}(\mathcal{D}^{xx} + \mathcal{D}^{yy})\,, && (2.44) \\ E &\equiv \frac{1}{2}(\mathcal{D}^{xx} - \mathcal{D}^{yy})\,, && (2.45) \end{aligned}$$

and subtracting a suitable constant, we obtain:

$$\underset{\sim}{H}'_S \equiv \underset{\sim}{H}_S - \frac{1}{2}(\mathcal{D}^{xx} + \mathcal{D}^{yy}) \underbrace{\Big[\big(\underset{\sim}{S}^x\big)^2 + \big(\underset{\sim}{S}^y\big)^2 + \big(\underset{\sim}{S}^z\big)^2\Big]}_{=\,\underset{\sim}{\boldsymbol{S}}^2 = S(S+1)\mathbb{1}} \tag{2.46}$$

$$= D\big(\underset{\sim}{S}^z\big)^2 + E\Big[\big(\underset{\sim}{S}^x\big)^2 - \big(\underset{\sim}{S}^y\big)^2\Big] \tag{2.47}$$

$$= D\big(\underset{\sim}{S}^z\big)^2 + \frac{E}{2}\Big[\big(\underset{\sim}{S}^+\big)^2 + \big(\underset{\sim}{S}^-\big)^2\Big]\,. \tag{2.48}$$

In the last equation, we have introduced the spin raising and lowering operators via $\underset{\sim}{S}^x = \big(\underset{\sim}{S}^+ + \underset{\sim}{S}^-\big)/2$ and $\underset{\sim}{S}^y = \big(\underset{\sim}{S}^+ - \underset{\sim}{S}^-\big)/2\mathrm{i}$. The D-term is called *axial*

anisotropy and the E-term *planar* or *transverse anisotropy* [Blu07, FW13]. For many magnetic molecules it is reasonable to assume that $|E| \ll |D|$ (see Ref. [Blu07] and p. 404 of Ref. [FW13]). In particular, E is zero and the anisotropy thus *uniaxial* if $\mathcal{D}^{xx} = \mathcal{D}^{yy}$. A uniaxial anisotropy with $D < 0$ is said to be of *easy axis* type (since it is energetically favorable for the spin to align parallel to the axis defined by the anisotropy), whereas $D > 0$ (by the same logic) corresponds to *hard axis* or *easy plane* anisotropy ([GSV06], p. 17).

In non-zero magnetic field $\mathbf{B}$, a Zeeman term with a g-tensor $\mathcal{G}$,

$$\boxed{\underset{\sim}{H}_Z(\mathbf{B}) \equiv \mu_B \underset{\sim}{\boldsymbol{S}}^T \mathcal{G}\, \mathbf{B}\ ,} \tag{2.49}$$

has to be added to the spin Hamiltonian in order to describe the interaction between the external field and the magnetic moment $-\mu_B \mathcal{G}^T \underset{\sim}{\boldsymbol{S}}$ of the spin ([GSV06], p. 15 f.). In the simplest case, the field is aligned in such a way that

$$\mathcal{G}\,\mathbf{B} = B\,\mathcal{G}\,\mathbf{e}_B = B \underbrace{\|\mathcal{G}\,\mathbf{e}_B\|}_{\equiv g_S} \mathbf{e}_z\ . \tag{2.50}$$

With this assumption, the total Hamiltonian for a single spin in an applied magnetic field becomes:

$$\boxed{\underset{\sim}{H}'_S(B) \equiv D\big(\underset{\sim}{S}^z\big)^2 + E\Big[\big(\underset{\sim}{S}^x\big)^2 - \big(\underset{\sim}{S}^y\big)^2\Big] + g_S \mu_B B \underset{\sim}{S}^z\ .} \tag{2.51}$$

In particular, as a giant-spin approximation and with $D < 0$, this Hamiltonian corresponds to a minimal model for a so-called *single molecule magnet* (SMM, see Refs. [GSV06, Blu07, FW13]). SMMs constitute a special subclass of magnetic molecules characterized by a large groundstate spin and an easy axis anisotropy, leading to magnetic bistability at low temperature because of an energy barrier that inhibits a reversal of the spin along the anisotropy direction. In experiments on SMMs, this energy barrier gives rise to slow relaxation of the magnetization and magnetic hysteresis at low temperature. Note that the transverse anisotropy E mixes eigenstates of the z-component of the total spin and thus allows transitions through the barrier. This property is related to "quantum tunneling of the magnetization", which is experimentally observed in the magnetic hysteresis curves in the form of characteristic steps. Due to their extraordinary magnetic properties, it is conceivable that at some point in the future SMMs could be used as classical or quantum bits for information storage and processing purposes (see, e.g., Ref. [BW08]).

The first reported SMM was a Mn_{12}-acetate cluster (abbreviated as Mn_{12}ac) with a groundstate spin of $S = 10$ and an easy axis anisotropy parameter inferred from experimental data of $D \approx -0.66$ K ≈ -0.057 meV (see p. 135 ff. of Ref. [GSV06]). Theoretically calculated transverse anisotropy parameters E of the different isomers of Mn_{12}ac (if non-zero at all due to reduced symmetry) do not exceed a few mK ([GSV06], p. 142). It is also possible to compute the values of the anisotropy parameters for individual manganese ions in Mn_{12}ac. Such calculations

give $D \approx -5$ K and $|E/D| < 0.1$ ([GSV06], p. 141). Another well studied SMM, commonly indicated as Fe_8, contains eight iron ions. It has a groundstate with $S = 10$ like Mn_{12}ac and fits to experimental data result in $D \approx -0.3$ K and a rather large ratio $0.15 \leq |E/D| \leq 0.19$ ([GSV06], p. 151 ff.).

2.3.2. A Kondo model for deposited magnetic atoms and molecules

As discussed in Sec. 2.1, quantum impurity models (QIMs) were originally used to describe the anomalous effects that small concentrations of magnetic atoms can cause in non-magnetic metals. Over the last two decades, however, the focus of quantum impurity physics has shifted to other problems and systems, creating a renewed interest in QIMs [BCP08]. From a theoretical point of view, the concept of a quantum impurity gained additional importance since QIMs appear as part of a *dynamical mean-field theory (DMFT)* calculation [MV89, GKKR96]: It turns out that lattice models of correlated electrons such as the Hubbard model, which has been defined in Eq. (2.24), can be exactly mapped onto effective quantum impurity problems in the limit of infinite spatial dimensionality. This way, an approximation for the physically relevant case of, e.g., three dimensions can be obtained.

Regarding further experimental realizations of QIMs, quantum dot devices were theoretically predicted to display signatures of the Kondo effect in their transport properties at low temperature [GR88, NL88, HDW91, MWL93, WM94]. Schematically, a quantum dot is formed by a confined region (e.g., defined in a semiconductor heterostructure) that traps a certain number of electrons and is coupled to leads via tunnel barriers ([BCP08], p. 422). Because of its quantized energy levels, it may be viewed as a kind of artificial atom. At the end of the 1990s, the predicted Kondo effect was indeed experimentally observed in quantum dots [COK98, GGSM$^+$98, GGGK$^+$98, vdWDFF$^+$00]. Quantum dots, which are usually described by an Anderson-type Hamiltonian, are particularly interesting realizations of QIMs since the parameters of the devices can be tuned via the applied gate voltages so that different physical regimes of the models can be studied ([BCP08], p. 422 f.). A few years later, it became possible to build nanometer-scale transistors incorporating single magnetic molecules and to investigate the occurring Kondo effect [LSB$^+$02, PPG$^+$02]. Similar devices have also been fabricated using single molecule magnets, allowing for a study of the transport properties of individual SMMs [JGB$^+$06, HdGF$^+$06].

Around the same time the Kondo effect was experimentally observed in quantum dot systems, it was discovered that magnetic impurities deposited on the surface of a non-magnetic metal can also be Kondo screened. This phenomenon is referred to as the *surface Kondo effect* (see chapter 10 of Ref. [Žit07]). The appearance of a Kondo resonance for magnetic atoms deposited on a metallic substrate was demonstrated by performing scanning tunneling spectroscopy (STS) experiments [LSBD98, MCJ$^+$98, MCJ$^+$01]. Subsequently, similar experimental studies were conducted for "artificial" molecules [MJN$^+$02], magnetic molecules

[WDW+05, IDH06, GJH+07], and finally SMMs [KIL+11] on suitable surfaces. From a technological point of view, attempts at organizing magnetic molecules on substrates and investigations of their properties in contact with the surface seem worthwhile because a controlled deposition could solve the problem of addressability (see Refs. [GCMS09, RDT+09, CMSS11, DBRM12]): In order to use single magnetic molecules as classical or quantum bits, one has to be able to individually address and manipulate them in the first place.

A list of experimentally determined Kondo temperatures for the surface Kondo effect can be found on p. 202 of Ref. [Žit07]. Because of the strong dependence on the microscopic parameters, which has already been observed for bulk systems (cf. Sec. 2.1), the estimated T_K-values extend from above room temperature to below the lowest temperature achievable in the STS experiments of around 5 K. It has been argued that, due to the reduced coordination at a surface, deposited magnetic impurities have significantly smaller Kondo temperatures compared to impurities in the bulk of the metal [KSD+02, QWW+04].

As a model for a single magnetic molecule on the surface of a non-magnetic normal metal, we use Hamiltonian (2.51) with $E \equiv 0$ (i.e., *without* transverse anisotropy) as the impurity part of the Kondo Hamiltonian (2.15):

$$\boxed{\underset{\sim}{H}_{\mathrm{imp}}(B) \equiv D\big(\underset{\sim}{S}^z\big)^2 + g_S \mu_B B \underset{\sim}{S}^z \,.} \tag{2.52}$$

Since the z-component of the total spin (with the corresponding magnetic quantum number M) commutes with the axial, but not with the transverse anisotropy term, setting $E \equiv 0$ makes M a "good" quantum number and thus simplifies calculations (see Sec. 2.4.2). Note that for several reasons besides neglecting the transverse anisotropy the combination of Eqs. (2.15) and (2.52) leads to a very simplified (at best, *minimal*) model of a deposited magnetic molecule. For example:

1. Since we consider a Kondo model, the impurity spin is fixed and no charge transfer between molecule and surface is possible. In the simplest case, charge fluctuations can be described using the single-impurity Anderson model (2.19) which, however, maps to an *isotropic spin-1/2* Kondo model as discussed in Sec. 2.2.1.

2. Orbital contributions to the magnetism are not explicitly taken into account. Note, however, that the anisotropy terms in the spin Hamiltonian (2.51) are at least partly ascribed to effects which are related to the orbital angular momentum (cf. p. 27 ff. of Ref. [BG90] and p. 28 f. of Ref. [GSV06]).

3. The interaction term (2.5) in the Kondo Hamiltonian has a very simple structure considering that a surface necessarily breaks symmetries of the bulk metal. In an Anderson-type model for a deposited magnetic impurity, the hybridization parameters $V_{\boldsymbol{k}}$ are expected to be strongly anisotropic in $\boldsymbol{k}$-space [LCNJ05] (also compare p. 212 of Ref. [Žit07]). Likewise, $\boldsymbol{k}$-dependent exchange parameters $J_{\boldsymbol{kq}}$ in a more realistic interaction term of a Kondo model should be anisotropic in the reciprocal space [ŽPP08].

4. We consider a Kondo model with a single electron band. In general, a deposited molecule is expected to couple to different types of electronic states (e.g., both bulk and surface states can be relevant as pointed out on p. 211 of Ref. [Žit07]). Nevertheless, a single-channel model might still be a reasonable starting point for an effective description. For example, it is possible that the impurity only interacts with a certain symmetrized combination of the different kinds of electron states, leading to a single effective conduction channel ([Žit07], p. 211 f.).

5. The surface can mediate a (possibly long-ranged) indirect interaction of RKKY-type [RK54, Kas56, Yos57, RZK66, ZWL$^+$10] between different deposited impurities. Depending on the properties of the substrate and the spatial separation of different molecules on the surface, it may therefore be insufficient to consider a single-impurity problem as described by Hamiltonian (2.15).

The Kondo Hamiltonian (2.15) with isotropic exchange interaction and the impurity part (2.52) (*including* additional transverse anisotropy E) has already been used to describe SMMs in contact with metallic electrodes [RWHS06b, RWHS06a, RWHS11, RWH08, RWH10]. Furthermore, it has been demonstrated that the spin Hamiltonian (2.51) *alone* is able to describe the surface-induced anisotropy of a single magnetic atom separated from the underlying metallic substrate by an additional decoupling layer [HLO$^+$07, OTvB$^+$08, BG09]. The D-values obtained by fitting the experimental data with such a spin model can be as large as a few meV (with the transverse anisotropy E, if taken into account, being smaller in magnitude by a factor of about 5) [HLO$^+$07, OTvB$^+$08, BG09]. The occurrence of spin-orbit-induced anisotropy for magnetic impurities that are embedded in a metal near a surface was theoretically predicted in Refs. [ÚZG96, ÚZ98].

Note that the single-channel single-impurity Kondo model with axial and transverse anisotropy *in zero magnetic field* has been studied in detail in Ref. [ŽPP08]. There, it is conjectured that the appropriate effective model for the description of the surface Kondo effect could be some anisotropic Kondo model instead of the typically used Anderson model. The authors of Ref. [ŽPP08] subsequently investigated anisotropic Kondo models for deposited magnetic impurities also in non-zero magnetic field, focussing on spectral functions [ŽPP09, ŽP10] and magnetization curves [Žit11a].

2.4. Symmetry properties of the Hamiltonian

The symmetry properties of the Hamiltonian are an important aspect since, e.g., the use of symmetries can simplify and speed up calculations. Moreover, certain calculations may only be possible if enough symmetries are exploited. It is convenient to discuss the symmetry properties of the Kondo model on the basis of the real-space representation (2.6) and the definition (2.16) of $\underset{\sim}{H}_{\mathrm{GC}}$.

2.4.1. SU(2) isospin symmetry

Under certain conditions, the Kondo Hamiltonian possesses a SU(2) symmetry that is referred to as *axial charge* [JVW88], *pseudospin* or *isospin* [TSU97], or η-*pairing symmetry* [EFG$^+$05]. This symmetry only involves the electronic degrees of freedom. The components of the total isospin operator $\underset{\sim}{\boldsymbol{\eta}}_{\text{total}}$ are defined in the following way (see Ref. [TSU97] and p. 34 of Ref. [EFG$^+$05]):

$$\begin{aligned}
\underset{\sim}{\eta}^{z}_{\text{total}} &\equiv \frac{1}{2}\sum_i \left(\underset{\sim}{d}^{\dagger}_{i\uparrow}\underset{\sim}{d}_{i\uparrow} + \underset{\sim}{d}^{\dagger}_{i\downarrow}\underset{\sim}{d}_{i\downarrow} - 1\right) && (2.53)\\
&= \frac{1}{2}\left(\underset{\sim}{N} - L^d\right) , && (2.54)\\
\underset{\sim}{\eta}^{+}_{\text{total}} &\equiv \sum_i \mathcal{S}_i\, \underset{\sim}{d}^{\dagger}_{i\uparrow}\underset{\sim}{d}^{\dagger}_{i\downarrow} , && (2.55)\\
\underset{\sim}{\eta}^{-}_{\text{total}} &\equiv \left(\underset{\sim}{\eta}^{+}_{\text{total}}\right)^{\dagger} = \sum_i \mathcal{S}_i\, \underset{\sim}{d}_{i\downarrow}\underset{\sim}{d}_{i\uparrow} , && (2.56)\\
\underset{\sim}{\eta}^{x}_{\text{total}} &\equiv \frac{1}{2}\left(\underset{\sim}{\eta}^{+}_{\text{total}} + \underset{\sim}{\eta}^{-}_{\text{total}}\right) , && (2.57)\\
\underset{\sim}{\eta}^{y}_{\text{total}} &\equiv \frac{1}{2\mathrm{i}}\left(\underset{\sim}{\eta}^{+}_{\text{total}} - \underset{\sim}{\eta}^{-}_{\text{total}}\right) . && (2.58)
\end{aligned}$$

Here, $\mathcal{S}_i = \pm 1$ is an additional factor that is assigned to lattice site i. Let us now assume that the lattice is *bipartite*, meaning that it can be divided into two sublattices A and B in such a way that there is an interaction only between sites belonging to *different* sublattices. We then define:

$$\mathcal{S}_i \equiv \begin{cases} -1 & , \quad \text{if site } i \text{ belongs to sublattice A} \\ 1 & , \quad \text{if site } i \text{ belongs to sublattice B} \end{cases} . \tag{2.59}$$

According to the above representations of the components of the isospin, the total isospin of the electrons is given by a sum over contributions from the individual lattice sites:

$$\underset{\sim}{\boldsymbol{\eta}}_{\text{total}} = \sum_i \underset{\sim}{\boldsymbol{\eta}}_i . \tag{2.60}$$

The isospin operators are related to the spin operators of the conduction electrons via a particle-hole-type transformation that is called "Shiba transformation" ([EFG$^+$05], p. 34), and they also satisfy SU(2) commutation relations. With the Levi-Civita symbol $\varepsilon^{\alpha\beta\gamma}$ and $\left[\underset{\sim}{A}, \underset{\sim}{B}\right] \equiv \underset{\sim}{A}\underset{\sim}{B} - \underset{\sim}{B}\underset{\sim}{A}$, we thus have ([EFG$^+$05], p. 34):

$$\left[\underset{\sim}{\eta}^{\alpha}_j, \underset{\sim}{\eta}^{\beta}_j\right] = \mathrm{i}\sum_{\gamma\in\{x,y,z\}} \varepsilon^{\alpha\beta\gamma}\underset{\sim}{\eta}^{\gamma}_j \quad \text{for} \quad \alpha,\beta = x,y,z . \tag{2.61}$$

Provided that the lattice is bipartite, the hopping parameters are real and spin-independent, and the chemical potential is zero, the Kondo Hamiltonian displays a SU(2) isospin symmetry for arbitrary magnetic fields:

$$\boxed{\left[\underset{\sim}{H}^{\mathrm{Kondo}}_{\mathrm{GC}}, \underset{\sim}{\eta}^{\alpha}_{\mathrm{total}}\right] = \left[\underset{\sim}{H}_{\mathrm{Kondo}}, \underset{\sim}{\eta}^{\alpha}_{\mathrm{total}}\right] = 0 \quad \text{for} \quad \alpha = x, y, z \; .} \tag{2.62}$$

A non-zero chemical potential breaks the full isospin symmetry because μ_{chem} couples to the total particle-number operator $\underset{\sim}{N} = 2\underset{\sim}{\eta}^{z}_{\mathrm{total}} + L^d$. However, even if the aforementioned conditions are not met, the number of electrons is still conserved so that there is always a U(1) symmetry:

$$\boxed{\left[\underset{\sim}{H}^{\mathrm{Kondo}}_{\mathrm{GC}}, \underset{\sim}{\eta}^{z}_{\mathrm{total}}\right] = 0 \; .} \tag{2.63}$$

2.4.2. SU(2) spin symmetry

Combining the total electron spin $\underset{\sim}{\boldsymbol{s}}_{\mathrm{total}}$, which is a sum over contributions from the individual lattice sites, with the impurity spin $\underset{\sim}{\boldsymbol{S}}$, the total spin operator for the Kondo model is obtained:

$$\boxed{\underset{\sim}{\boldsymbol{S}}_{\mathrm{total}} \equiv \underset{\sim}{\boldsymbol{s}}_{\mathrm{total}} + \underset{\sim}{\boldsymbol{S}} = \sum_i \underset{\sim}{\boldsymbol{s}}_i + \underset{\sim}{\boldsymbol{S}} \; .} \tag{2.64}$$

The components of the total spin are expressed via the creation and destruction operators in the following way (compare the real-space representation of $\underset{\sim}{\boldsymbol{s}}_0$ from Eq. (2.4) and see Refs. [TSU97, EFG+05]):

$$\boxed{\begin{aligned}
\underset{\sim}{S}^{z}_{\mathrm{total}} &= \frac{1}{2}\sum_i \left(\underset{\sim}{d}^{\dagger}_{i\uparrow}\underset{\sim}{d}_{i\uparrow} - \underset{\sim}{d}^{\dagger}_{i\downarrow}\underset{\sim}{d}_{i\downarrow}\right) + \underset{\sim}{S}^{z} \; , && (2.65)\\
\underset{\sim}{S}^{+}_{\mathrm{total}} &= \sum_i \underset{\sim}{d}^{\dagger}_{i\uparrow}\underset{\sim}{d}_{i\downarrow} + \underset{\sim}{S}^{+} \; , && (2.66)\\
\underset{\sim}{S}^{-}_{\mathrm{total}} &= \left(\underset{\sim}{S}^{+}_{\mathrm{total}}\right)^{\dagger} = \sum_i \underset{\sim}{d}^{\dagger}_{i\downarrow}\underset{\sim}{d}_{i\uparrow} + \underset{\sim}{S}^{-} \; , && (2.67)\\
\underset{\sim}{S}^{x}_{\mathrm{total}} &= \frac{1}{2}\left(\underset{\sim}{S}^{+}_{\mathrm{total}} + \underset{\sim}{S}^{-}_{\mathrm{total}}\right) , && (2.68)\\
\underset{\sim}{S}^{y}_{\mathrm{total}} &= \frac{1}{2\mathrm{i}}\left(\underset{\sim}{S}^{+}_{\mathrm{total}} - \underset{\sim}{S}^{-}_{\mathrm{total}}\right) . && (2.69)
\end{aligned}}$$

If the exchange interaction is isotropic (i.e., $J^x = J^y = J^z$) and the magnetic field zero, and if there is no impurity Hamiltonian $\underset{\sim}{H}_{\mathrm{imp}}$, the Kondo model has the full SU(2) spin symmetry for arbitrary values of the chemical potential (the

invariance of the tight-binding term in Eq. (2.6) is shown, e.g., on p. 33 of Ref. [EFG+05]):

$$\left[\underset{\sim}{H}_{\mathrm{GC}}^{\mathrm{Kondo}}, \underset{\sim}{S}_{\mathrm{total}}^{\alpha}\right] = 0 \quad \text{for} \quad \alpha = x, y, z \; . \tag{2.70}$$

In non-zero magnetic field, the full spin symmetry is reduced to a U(1) symmetry,

$$\boxed{\left[\underset{\sim}{H}_{\mathrm{GC}}^{\mathrm{Kondo}}, \underset{\sim}{S}_{\mathrm{total}}^{z}\right] = 0 \; ,} \tag{2.71}$$

since the Zeeman terms for conduction electrons and impurity involve the z-component of the respective spin. Furthermore, an additional uniaxial anisotropy of the impurity spin as in Eq. (2.52) or an exchange anisotropy of XXZ-type break the full invariance under rotations in spin space, but preserve the U(1) symmetry (2.71).

Since the total isospin and the total spin commute (see p. 34 of Ref. [EFG+05]),

$$\left[\underset{\sim}{\eta}_{\mathrm{total}}^{\alpha}, \underset{\sim}{S}_{\mathrm{total}}^{\beta}\right] = 0 \quad \text{for} \quad \alpha, \beta = x, y, z \; , \tag{2.72}$$

the Kondo model may exhibit two separate SU(2) symmetries that can be simultaneously exploited. In all cases that are considered in this thesis, $\underset{\sim}{H}_{\mathrm{GC}}^{\mathrm{Kondo}}$ satisfies Eqs. (2.63) and (2.71), i.e., displays two U(1) symmetries.

2.4.3. Spinflip symmetry

A so-called *spinflip* for the Kondo model corresponds to a unitary transformation $\underset{\sim}{\mathcal{U}}_{\mathrm{sf}}$ with the following effects on the electronic and impurity degrees of freedom:

$$\boxed{\begin{aligned}
\underset{\sim}{\mathcal{U}}_{\mathrm{sf}}\, \underset{\sim}{d}_{i\sigma}\, \underset{\sim}{\mathcal{U}}_{\mathrm{sf}}^{\dagger} &\equiv \underset{\sim}{d}_{i,-\sigma} \; , && (2.73)\\
\underset{\sim}{\mathcal{U}}_{\mathrm{sf}}\, \underset{\sim}{\boldsymbol{\eta}}_{i}\, \underset{\sim}{\mathcal{U}}_{\mathrm{sf}}^{\dagger} &= \left(-\underset{\sim}{\eta}_{i}^{x}, -\underset{\sim}{\eta}_{i}^{y}, +\underset{\sim}{\eta}_{i}^{z}\right) , && (2.74)\\
\underset{\sim}{\mathcal{U}}_{\mathrm{sf}}\, \underset{\sim}{\boldsymbol{s}}_{i}\, \underset{\sim}{\mathcal{U}}_{\mathrm{sf}}^{\dagger} &= \left(+\underset{\sim}{s}_{i}^{x}, -\underset{\sim}{s}_{i}^{y}, -\underset{\sim}{s}_{i}^{z}\right) , && (2.75)\\
\underset{\sim}{\mathcal{U}}_{\mathrm{sf}}\, \underset{\sim}{\boldsymbol{S}}\, \underset{\sim}{\mathcal{U}}_{\mathrm{sf}}^{\dagger} &\equiv \left(+\underset{\sim}{S}^{x}, -\underset{\sim}{S}^{y}, -\underset{\sim}{S}^{z}\right) . && (2.76)
\end{aligned}}$$

Transformation (2.73) maps a spin-down particle to a spin-up particle (and vice versa) and thus "flips its spin". Eqs. (2.74) and (2.75) are obtained by applying the spinflip transformation to the representations of the isospin and electron spin from Secs. 2.4.1 and 2.4.2, respectively. In contrast, the transformation property (2.76) of the impurity spin is *chosen* so as to match that of the electron spin.

Applying the spinflip transformation to the real-space representation (2.6) of the Kondo Hamiltonian, with the impurity part from Eq. (2.52) and additional chemical potential term, we find:

$$\boxed{\underset{\sim}{\mathcal{U}}_{\mathrm{sf}}\, \underset{\sim}{H}_{\mathrm{GC}}^{\mathrm{Kondo}}(B)\, \underset{\sim}{\mathcal{U}}_{\mathrm{sf}}^{\dagger} = \underset{\sim}{H}_{\mathrm{GC}}^{\mathrm{Kondo}}(-B) \; .} \tag{2.77}$$

In particular, $\underset{\sim}{H}_{\mathrm{GC}}^{\mathrm{Kondo}}$ is thus invariant under a spinflip for vanishing magnetic field.

The transformation property (2.77) implies that magnetizations of the Kondo model vanish for $B = 0$ and that magnetization curves exhibit point symmetry with respect to $B = 0$. Schematically, consider a thermodynamic expectation value of the z-component of the impurity spin that is calculated using the density operator $\underset{\sim}{\rho}(B)$:

$$\langle \underset{\sim}{S}^z \rangle(B) \equiv \mathrm{tr}\Big(\underset{\sim}{S}^z \underset{\sim}{\rho}(B) \Big) \; . \tag{2.78}$$

Using Eqs. (2.76) and (2.77) in combination with the cyclic property of the trace, we indeed obtain:

$$\langle \underset{\sim}{S}^z \rangle(B) = \mathrm{tr}\Big(\underset{\sim}{\mathcal{U}}_{\mathrm{sf}} \underset{\sim}{S}^z \underset{\sim}{\mathcal{U}}_{\mathrm{sf}}^\dagger \underset{\sim}{\mathcal{U}}_{\mathrm{sf}} \underset{\sim}{\rho}(B) \underset{\sim}{\mathcal{U}}_{\mathrm{sf}}^\dagger \Big) = -\langle \underset{\sim}{S}^z \rangle(-B) \; . \tag{2.79}$$

2.4.4. Particle-hole symmetry

A particle-hole transformation for the Kondo model (in *arbitrary* magnetic field) again corresponds to a unitary operator $\underset{\sim}{\mathcal{U}}_{\mathrm{ph}}$. It affects the electronic and impurity degrees of freedom in the following way:

$$\begin{aligned}
\underset{\sim}{\mathcal{U}}_{\mathrm{ph}} \underset{\sim}{d}_{i\sigma} \underset{\sim}{\mathcal{U}}_{\mathrm{ph}}^\dagger &\equiv \mathcal{S}_i \, \underset{\sim}{d}_{i,-\sigma}^\dagger \; , && (2.80)\\
\underset{\sim}{\mathcal{U}}_{\mathrm{ph}} \underset{\sim}{\boldsymbol{\eta}}_i \underset{\sim}{\mathcal{U}}_{\mathrm{ph}}^\dagger &= \Big(+ \underset{\sim}{\eta}_i^x, - \underset{\sim}{\eta}_i^y, - \underset{\sim}{\eta}_i^z \Big) \; , && (2.81)\\
\underset{\sim}{\mathcal{U}}_{\mathrm{ph}} \underset{\sim}{\boldsymbol{s}}_i \underset{\sim}{\mathcal{U}}_{\mathrm{ph}}^\dagger &= \big(- \underset{\sim}{s}_i^x, - \underset{\sim}{s}_i^y, + \underset{\sim}{s}_i^z \big) \; , && (2.82)\\
\underset{\sim}{\mathcal{U}}_{\mathrm{ph}} \underset{\sim}{\boldsymbol{S}} \underset{\sim}{\mathcal{U}}_{\mathrm{ph}}^\dagger &\equiv \big(- \underset{\sim}{S}^x, - \underset{\sim}{S}^y, + \underset{\sim}{S}^z \big) \; . && (2.83)
\end{aligned}$$

Transformation (2.80) maps a hole to an electron with opposite spin projection (and vice versa) and, furthermore, adds a sign $\mathcal{S}_i$ according to the definition (2.59). Eq. (2.83) is again chosen so as to match Eq. (2.82). Note that an isospin changes under a particle-hole transformation in the same way as a spin does under a spinflip transformation and vice versa.

For a bipartite lattice with real and spin-independent hopping parameters, a particle-hole transformation turns the Kondo Hamiltonian into (cf. Eq. (2.54)):

$$\boxed{\underset{\sim}{\mathcal{U}}_{\mathrm{ph}} \underset{\sim}{H}_{\mathrm{GC}}^{\mathrm{Kondo}}(\mu_{\mathrm{chem}}) \underset{\sim}{\mathcal{U}}_{\mathrm{ph}}^\dagger = \underset{\sim}{H}_{\mathrm{GC}}^{\mathrm{Kondo}}(-\mu_{\mathrm{chem}}) - 2L^d \mu_{\mathrm{chem}} \; .} \tag{2.84}$$

If the chemical potential is zero, $\underset{\sim}{H}_{\mathrm{GC}}^{\mathrm{Kondo}}$ is equal to $\underset{\sim}{H}_{\mathrm{Kondo}}$ and invariant under the transformation. With an argument analogous to the one leading to Eq. (2.79), we then find:

$$\Big\langle \underset{\sim}{\eta}_{\mathrm{total}}^z \Big\rangle = -\Big\langle \underset{\sim}{\eta}_{\mathrm{total}}^z \Big\rangle \quad \Leftrightarrow \quad \Big\langle \underset{\sim}{\eta}_{\mathrm{total}}^z \Big\rangle = 0 \quad \Leftrightarrow \quad \langle \underset{\sim}{N} \rangle = L^d \; . \tag{2.85}$$

In case of particle-hole symmetry, the conduction band is hence on average half-filled. If the chemical potential coupled to the z-component of the isospin, a particle-hole transformation would simply map μ_{chem} to $-\mu_{\text{chem}}$ according to Eq. (2.81), just in the same way as a spinflip transformation turns the value of the magnetic field into its negative (cf. Eq. (2.77)).

Part II.

The Numerical Renormalization Group for the thermodynamics of the single-channel Kondo model

3. Overview of a Numerical Renormalization Group calculation

Because chapter 4, which describes the Numerical Renormalization Group (NRG) in detail, is rather long and technical, we would like to give a brief introduction to NRG, with a compact overview of the different steps in an actual calculation, before continuing.

NRG is a numerical method originally introduced by Kenneth G. Wilson in 1975 [Wil75] which is intended to *approximately* solve the eigenvalue problem of a quantum impurity model (such as the Kondo model) in the continuum limit. It gives a number of eigenvalues and eigenvectors that can be used to approximate the full energy spectrum of the model in a certain way. This allows, e.g., to calculate thermodynamic expectation values. Although NRG is optimized to produce reliable low-temperature results, it can also be used to study the effect of finite temperature. As a limitation of the method, the bath degrees of freedom (as opposed to the impurity degrees of freedom) are required to be non-interacting so that certain analytical transformations are possible. Furthermore, with growing complexity of the quantum impurity models (i.e., with increasing number of impurities and bath channels), NRG calculations quickly become prohibitively expensive. In practice, the application of NRG is therefore restricted to systems with only a few impurities and channels. On the other hand, if a model can be treated using NRG, there are no principle limitations regarding the parameter space that can be studied since NRG is non-perturbative with respect to all physical parameters [BCP08].

The various approximations that are made in a NRG calculation might seem severe at first sight. However, comparisons with (quasi-)exact results that are available for certain impurity models (e.g., with Bethe ansatz results for the Kondo model [AFL83, TW83]) reveal that NRG can be surprisingly accurate. Nevertheless, the approximations that are made are, strictly speaking, uncontrolled. For example, there is no quantity like the "discarded weight", which can be used to assess the accuracy of the results in Density Matrix Renormalization Group (DMRG) calculations (see, e.g., Ref. [Sch05]). In principle, one has to check for each system that NRG is really applicable. In practice, however, this can only be done by varying the numerical parameters and verifying that this does not appreciably change the obtained results. There are recent attempts to quantify the accuracy of NRG calculations (see, e.g., Ref. [Wei11]).

NRG was originally applied to the Kondo model [Wil75] and the single-impurity Anderson model [KmWW75, KmWW80a, KmWW80b]. Since then, NRG has been used to study the properties of a large number of quantum impurity models (see Ref. [BCP08] for a recent review of available results). While, at first, NRG

was only employed to calculate thermodynamic expectation values, the method was subsequently extended to also allow for the calculation of dynamic quantities (such as the single-particle Green's function and its spectral density). With the temperature-dependent spectral density it is possible to, e.g., determine transport-related properties such as the resistivity and conductance [BCP08]. Among further generalizations of NRG are the treatment of a bosonic bath (bosonic NRG; see, e.g., Ref. [BLTV05]) and the investigation of non-equilibrium transient dynamics (TD-NRG; see Refs. [AS05, AS06]).

Technical aspects of a NRG calculation for the single-impurity Anderson model are described in Refs. [KmWW80a, BCP08], whereas a chapter of Hewson's book [Hew93] and Costi's review [Cos99] concentrate on the application to the Kondo model. A comprehensive overview of the NRG method is also provided by the PhD thesis of Žitko [Žit07].

Let us now turn to a *summary of the Numerical Renormalization Group*. A NRG calculation comprises the following steps:

1. *Transformation to a continuous energy representation (exact, see Sec. 4.1):*
   In the limit of an arbitrarily large electronic lattice (i.e., in the thermodynamic limit), the Hamiltonian is first transformed to a continuous energy representation. The properties of the impurity can then be *exactly* described by keeping only those electronic states to which it *directly* couples. After the transformation, the details of the bath (including its dimensionality and lattice structure) are completely "encoded" in the density of states (DOS) of the electrons.

2. *Logarithmic discretization of the electron band (key approximation of NRG, see Secs. 4.4, 4.5, and 4.7):*
   In order to treat the obtained Hamiltonian numerically, the continuum of electronic states has to be discretized. NRG aims at providing high energy resolution close to the Fermi energy ε_F, i.e., at low temperature. To this end, the electron band is logarithmically discretized around ε_F by defining certain energy intervals and keeping *only one* suitable state per interval. The discretization is called logarithmic since the interval width decreases exponentially upon approaching the Fermi energy so that the electron band is equipartitioned on a logarithmic scale. The electronic state that is chosen in each interval is the *only state* falling into the respective energy window that directly couples to the impurity. For this reason, the interaction term in the Hamiltonian can be exactly expressed via the selected states.

3. *Tridiagonalization (exact, see Sec. 4.9):*
   The resulting discretized Hamiltonian is tridiagonalized, i.e., it is *exactly* mapped onto a semi-infinite so-called *Wilson chain* with the impurity at the closed end. The first (zeroth) state of the Wilson chain, which corresponds to the starting point of the tridiagonalization, is chosen as that electronic state to which the impurity directly couples (this, again, allows for an exact representation of the interaction term). The Hamiltonian of the Wilson chain

has the special and important property that its parameters (i.e., hopping parameters and possibly on-site energies) decrease exponentially along the chain towards the open end. This is a direct consequence of the logarithmic discretization of the electron band.

4. *Iterative diagonalization of the Wilson chain and basis truncation (approximation, see Secs. 4.10 and 4.11):*
   The Hamiltonian of the Wilson chain is iteratively diagonalized. Starting from the closed end with the impurity, the chain is constructed by adding one lattice site at a time, followed by a numerical diagonalization of the enlarged chain fragment in each step. With respect to the considered states, this diagonalization is complete and exact. Since the size of the Hilbert space grows exponentially with the number of included sites, states have to be discarded after a few steps, i.e., the basis has to be truncated. The states to keep are chosen based on their energy: After each step involving a truncation of the basis, only a certain number of the energetically lowest-lying states is retained. This truncation scheme is notably simpler than the one used in a DMRG calculation. However, it only leads to results that are representative of the properties of the full Hamiltonian because of the special structure of the Wilson chain.

5. *Calculation of thermodynamic expectation values for certain temperatures (see Secs. 4.12 and 4.13):*
   The energy spectrum obtained in a certain step of the iterative diagonalization is inaccurate at low energies since the contribution of the remaining part of the semi-infinite Wilson chain is missing. Furthermore, states exceeding a certain energy are not available once the basis has to be truncated. For this reason, the *approximate* eigenstates determined in the current step can only be used to calculate thermodynamic quantities for thermal energies that are large compared to the groundstate gap (so that improperly reproduced fine details in the low-energy spectrum are thermally washed out), but small compared to the energy cutoff (so that the contribution of the missing part of the spectrum can be neglected). This requires some compromise when *assigning one or several temperatures to a chain fragment of a certain length.* In any case, since the groundstate gaps are related to the exponentially decreasing hopping parameters of the Wilson chain, the temperature (or energy scale) declines exponentially along the chain towards the open end. Considering a *longer chain fragment* therefore corresponds to studying the model on a *lower temperature or energy scale.* For the temperatures that are chosen in a certain step, the eigenvalues, eigenstates, and matrix elements that are available in this step can be used to calculate thermodynamic expectation values with respect to the grand-canonical ensemble in a standard way.

4. The Numerical Renormalization Group (NRG)

In this chapter, we are going to describe in considerable detail how to carry out a *Numerical Renormalization Group* calculation for a single-channel Kondo model in order to obtain thermodynamic (static) expectation values with respect to the grand-canonical ensemble.

The starting point for our considerations is Hamiltonian (2.17). In order to keep the notation simple, we assume in this chapter that the exchange interaction is isotropic (i.e., $J^x \equiv J^y \equiv J^z \equiv J$). Note that this restriction is not necessary for the subsequent discussions as long as the total Hamiltonian has the symmetry properties that are exploited in Sec. 4.11. There, the charge Q and the magnetic quantum number M belonging to the z-component of the total spin are assumed to be good quantum numbers. In fact, Hamiltonian (2.17) could, in principle, be generalized to include an arbitrary number of impurity degrees of freedom that either do not interact with the electrons at all or only couple to the states $\underset{\sim}{f}_{0\mu}$ defined in Eq. (4.20), without requiring any fundamental changes of the presented NRG procedure. For example, there could be N_S impurity spins, with the interaction term (2.5) replaced by:

$$\underset{\sim}{H}^{N_S}_{\text{interaction}} \equiv \underset{\sim}{\boldsymbol{s}}_0 \cdot \sum_{i=1}^{N_S} J_i \underset{\sim}{\boldsymbol{S}}_i \; . \tag{4.1}$$

Furthermore, apart from its symmetry properties, the exact form of the impurity part $\underset{\sim}{H}_{\text{imp}}$ of Hamiltonian (2.17) is also irrelevant. The considerations in this chapter therefore apply to a *multi-impurity* single-channel Kondo model.

4.1. Transformation to a continuous energy representation

For an arbitrarily large electronic lattice with $L \gg 1$, the momenta $\boldsymbol{k}$ become (quasi-)continuous so that we can perform a standard continuum limit in $\boldsymbol{k}$-space. To this end, we introduce new operators (cf. App. A of Ref. [KmWW80a]),

$$\sqrt{\frac{L}{2\pi}}^{d} \underset{\sim}{c}_{\boldsymbol{k}\sigma} \longrightarrow \underset{\sim}{a}_{\sigma}(\boldsymbol{k}) \; , \tag{4.2}$$

which still fulfill standard anticommutation relations,

$$\left\{\underset{\sim}{a}_\mu(\boldsymbol{k}), \underset{\sim}{a}^\dagger_\nu(\boldsymbol{q})\right\} = \delta(\boldsymbol{k}-\boldsymbol{q})\delta_{\mu\nu} \;, \tag{4.3}$$

since $(L/2\pi)^d \delta_{\boldsymbol{kq}} \to \delta(\boldsymbol{k}-\boldsymbol{q})$. Replacing sums with integrals,

$$\sum_{\boldsymbol{k}} \cdot = \left(\frac{L}{2\pi}\right)^d \sum_{\boldsymbol{k}} \underbrace{\left(\frac{2\pi}{L}\right)^d}_{=(\Delta k)^d} \cdot \longrightarrow \left(\frac{L}{2\pi}\right)^d \int \mathrm{d}\boldsymbol{k} \cdot \,, \tag{4.4}$$

and using the operators $\underset{\sim}{a}_\sigma(\boldsymbol{k})$, Hamiltonian (2.17) with $\mu_{\mathrm{chem}} \equiv \varepsilon_F$ is transformed to:

$$\begin{aligned} \underset{\sim}{H}{}^{\mathrm{Kondo}}_{\mathrm{GC}} \to \underset{\sim}{H}_{\mathrm{d}\boldsymbol{k}} \;\equiv\; & \sum_\mu \int \mathrm{d}\boldsymbol{k}\, \big(\varepsilon_\mu(\boldsymbol{k}) - \varepsilon_F\big)\, \underset{\sim}{a}^\dagger_\mu(\boldsymbol{k}) \underset{\sim}{a}_\mu(\boldsymbol{k}) \\ & + \frac{J}{L^d}\, \underset{\sim}{\boldsymbol{S}} \cdot \left(\frac{L}{2\pi}\right)^d \sum_{\mu,\nu} \left(\int \mathrm{d}\boldsymbol{k}\, \underset{\sim}{a}^\dagger_\mu(\boldsymbol{k})\right) \frac{\boldsymbol{\sigma}_{\mu\nu}}{2} \left(\int \mathrm{d}\boldsymbol{q}\, \underset{\sim}{a}_\nu(\boldsymbol{q})\right) \\ & + \underset{\sim}{H}_{\mathrm{imp}}(B) \;. \end{aligned} \tag{4.5}$$

We now introduce the density of states (DOS) per lattice site (or mode) and "per spin projection":

$$\boxed{\rho(\varepsilon) \equiv \frac{1}{L^d} \sum_{\boldsymbol{k}} \delta(\varepsilon - \varepsilon_{\boldsymbol{k}}) \;.} \tag{4.6}$$

The DOS is normalized by definition:

$$\int \mathrm{d}\varepsilon\, \rho(\varepsilon) = \frac{1}{L^d} \sum_{\boldsymbol{k}} 1 = 1 \;. \tag{4.7}$$

Measuring energies relative to the Fermi level, i.e.,

$$\tilde{\varepsilon} \equiv \varepsilon - \varepsilon_F \;, \tag{4.8}$$

let us define the following states of distinct energy $\tilde{\varepsilon}$ (cf. Ref. [SDL08], and also observe the corresponding expressions for the two-impurity Kondo model from Refs. [Fye94, ALJ95, CO04]):

$$\boxed{\underset{\sim}{a}_\mu(\tilde{\varepsilon}) \equiv \frac{1}{\sqrt{(2\pi)^d \rho(\tilde{\varepsilon} + \varepsilon_F - \mu h)}} \int \mathrm{d}\boldsymbol{k}\, \delta\big(\tilde{\varepsilon} + \varepsilon_F - \varepsilon_\mu(\boldsymbol{k})\big)\, \underset{\sim}{a}_\mu(\boldsymbol{k}) \;.} \tag{4.9}$$

h and $\varepsilon_{\boldsymbol{k}\mu}$ have been introduced in Eqs. (2.12) and (2.13), respectively. The states $\underset{\sim}{a}_\mu(\tilde{\varepsilon})$ are correctly normalized:

$$\left\{\underset{\sim}{a}_\mu(\tilde{\varepsilon}), \underset{\sim}{a}^\dagger_\nu(\tilde{\omega})\right\} = \delta(\tilde{\varepsilon} - \tilde{\omega})\, \delta_{\mu\nu} \;. \tag{4.10}$$

Let us now assume that $\varepsilon_{\boldsymbol{k}} \in [-W, W]$ for all $\boldsymbol{k}$. W thus denotes the half-bandwidth of the electrons. Comparing the identity

$$\sqrt{2\pi}^{d} \int_{-W^{-}+\mu h}^{W^{+}+\mu h} \mathrm{d}\tilde{\varepsilon}\, \sqrt{\rho(\tilde{\varepsilon}+\varepsilon_F-\mu h)}\, \underset{\sim}{a}_{\mu}(\tilde{\varepsilon}) = \int \mathrm{d}\boldsymbol{k}\, \underset{\sim}{a}_{\mu}(\boldsymbol{k})\;, \tag{4.11}$$

where we have introduced $W^{\pm} \equiv W \mp \varepsilon_F$, with the interaction term in Hamiltonian (4.5) reveals that the states $\underset{\sim}{a}_{\mu}(\tilde{\varepsilon})$ are in fact *the only electronic states which directly couple to the impurity spin*. If we are only interested in impurity properties, we can thus, *without any approximation*, discard all the other states with energy $\tilde{\varepsilon}$ that are different from those defined in Eq. (4.9) (note that, in general, there are infinitely many such states). In this way, we obtain the desired continuous energy representation of the Hamiltonian:

$$\begin{aligned}
\underset{\sim}{H}_{\mathrm{d}\boldsymbol{k}} \to \underset{\sim}{H}_{\mathrm{d}\tilde{\varepsilon}} \equiv & \sum_{\mu} \int_{-W^{-}+\mu h}^{W^{+}+\mu h} \mathrm{d}\tilde{\varepsilon}\, \tilde{\varepsilon}\, \underset{\sim}{a}^{\dagger}_{\mu}(\tilde{\varepsilon}) \underset{\sim}{a}_{\mu}(\tilde{\varepsilon}) \\
& + J \underset{\sim}{\boldsymbol{S}} \cdot \sum_{\mu,\nu} \left(\int_{-W^{-}+\mu h}^{W^{+}+\mu h} \mathrm{d}\tilde{\varepsilon}\, \sqrt{\rho(\tilde{\varepsilon}+\varepsilon_F-\mu h)}\, \underset{\sim}{a}^{\dagger}_{\mu}(\tilde{\varepsilon}) \right) \frac{\boldsymbol{\sigma}_{\mu\nu}}{2} \times \\
& \qquad \left(\int_{-W^{-}+\nu h}^{W^{+}+\nu h} \mathrm{d}\tilde{\omega}\, \sqrt{\rho(\tilde{\omega}+\varepsilon_F-\nu h)}\, \underset{\sim}{a}_{\nu}(\tilde{\omega}) \right) \\
& + \underset{\sim}{H}_{\mathrm{imp}}(B)\;.
\end{aligned} \tag{4.12}$$

In general, the purely electronic terms in Hamiltonians (4.5) and (4.12) are *not* equivalent since electron states are discarded in the transformation $\underset{\sim}{H}_{\mathrm{d}\boldsymbol{k}} \to \underset{\sim}{H}_{\mathrm{d}\tilde{\varepsilon}}$. However, in the special case that the dispersion relation $\varepsilon(\boldsymbol{k})$ is a bijective map between energy ε and shift quantum number $\boldsymbol{k}$ (i.e., all states are retained), we indeed have

$$\sum_{\mu} \int_{-W^{-}+\mu h}^{W^{+}+\mu h} \mathrm{d}\tilde{\varepsilon}\, \tilde{\varepsilon}\, \underset{\sim}{a}^{\dagger}_{\mu}(\tilde{\varepsilon}) \underset{\sim}{a}_{\mu}(\tilde{\varepsilon}) \;\overset{\varepsilon \leftrightarrow \boldsymbol{k}}{=}\; \sum_{\mu} \int \mathrm{d}\boldsymbol{k}\, \big(\varepsilon_{\mu}(\boldsymbol{k}) - \varepsilon_F\big)\, \underset{\sim}{a}^{\dagger}_{\mu}(\boldsymbol{k}) \underset{\sim}{a}_{\mu}(\boldsymbol{k})\;. \tag{4.13}$$

Finally, note that $\tilde{\varepsilon} = 0$ corresponds to $\varepsilon = \varepsilon_F$ and that Hamiltonian (4.12) does not explicitly depend on the number of lattice sites L or the dimension d anymore.

4.2. Transformation to a dimensionless representation

For the physically reasonable case $h < W^{\pm}$, we now introduce abbreviations for the integration boundaries in Eq. (4.12),

$$\mathcal{B}_{\mu}^{\pm} \equiv |\pm W^{\pm} + \mu h| \,, \tag{4.14}$$

and use them to define rescaled integration variables and electron operators (cf. Ref. [KmWW80a]):

$$\xi_{\mu}^{+} \equiv \frac{\tilde{\varepsilon}}{\mathcal{B}_{\mu}^{+}} \qquad \text{for} \quad \tilde{\varepsilon} > 0 \,, \tag{4.15}$$

$$\xi_{\mu}^{-} \equiv \frac{\tilde{\varepsilon}}{\mathcal{B}_{\mu}^{-}} \qquad \text{for} \quad \tilde{\varepsilon} < 0 \,, \tag{4.16}$$

$$\underset{\sim}{a}_{\mu}^{+}\big(\xi_{\mu}^{+}\big) \equiv \sqrt{\mathcal{B}_{\mu}^{+}}\, \underset{\sim}{a}_{\mu}(\tilde{\varepsilon}) \quad \text{for} \quad \tilde{\varepsilon} > 0 \,, \tag{4.17}$$

$$\underset{\sim}{a}_{\mu}^{-}\big(\xi_{\mu}^{-}\big) \equiv \sqrt{\mathcal{B}_{\mu}^{-}}\, \underset{\sim}{a}_{\mu}(\tilde{\varepsilon}) \quad \text{for} \quad \tilde{\varepsilon} < 0 \,. \tag{4.18}$$

The new states $\underset{\sim}{a}_{\mu}^{p}(\xi_{\mu}^{p})$ (with $p \equiv \pm$) are again properly normalized, i.e.,

$$\Big\{ \underset{\sim}{a}_{\mu}^{p}\big(\xi_{\mu}^{p}\big), \underset{\sim}{a}_{\nu}^{p'\dagger}\big(\zeta_{\nu}^{p'}\big) \Big\} = \delta\big(\xi_{\mu}^{p} - \zeta_{\mu}^{p}\big)\delta_{\mu\nu}\,\delta_{pp'} \,. \tag{4.19}$$

Using the above definitions and the normalization of the DOS from Eq. (4.7), the normalized electronic state to which the impurity spin directly couples can be written as:

$$\begin{aligned} \underset{\sim}{f}_{0\mu} \quad \equiv \quad & \int_{0}^{1} \mathrm{d}\xi_{\mu}^{+} \sqrt{\rho\big(\xi_{\mu}^{+}\mathcal{B}_{\mu}^{+} + \varepsilon_F - \mu h\big)\mathcal{B}_{\mu}^{+}}\; \underset{\sim}{a}_{\mu}^{+}\big(\xi_{\mu}^{+}\big) \\ & + \int_{-1}^{0} \mathrm{d}\xi_{\mu}^{-} \sqrt{\rho\big(\xi_{\mu}^{-}\mathcal{B}_{\mu}^{-} + \varepsilon_F - \mu h\big)\mathcal{B}_{\mu}^{-}}\; \underset{\sim}{a}_{\mu}^{-}\big(\xi_{\mu}^{-}\big) \,, \qquad (4.20) \\ & \text{with} \;\; \Big\{ \underset{\sim}{f}_{0\mu}, \underset{\sim}{f}_{0\nu}^{\dagger} \Big\} = \delta_{\mu\nu} \,. \qquad (4.21) \end{aligned}$$

The introduction of $\underset{\sim}{f}_{0\mu}$ leads to an equivalent expression for the energy representation $\underset{\sim}{H}_{\mathrm{d}\tilde{\varepsilon}}$ from Eq. (4.12):

$$
\begin{aligned}
\underset{\sim}{H}_{\mathrm{NRG}} &\equiv W \sum_{\mu} \left(\frac{\mathcal{B}_\mu^+}{W} \int_0^1 \mathrm{d}\xi_\mu^+ \, \xi_\mu^+ \, \underset{\sim}{a}_\mu^{+\dagger}(\xi_\mu^+) \underset{\sim}{a}_\mu^+(\xi_\mu^+) \right. \\
&\qquad \left. + \frac{\mathcal{B}_\mu^-}{W} \int_{-1}^0 \mathrm{d}\xi_\mu^- \, \xi_\mu^- \, \underset{\sim}{a}_\mu^{-\dagger}(\xi_\mu^-) \underset{\sim}{a}_\mu^-(\xi_\mu^-) \right) \\
&\quad + J \underset{\sim}{\boldsymbol{S}} \cdot \sum_{\mu,\nu} \underset{\sim}{f}_{0\mu}^\dagger \frac{\boldsymbol{\sigma}_{\mu\nu}}{2} \underset{\sim}{f}_{0\nu} + \underset{\sim}{H}_{\mathrm{imp}}(B) \qquad (4.22) \\
&= \underset{\sim}{H}_{\mathrm{d}\tilde{\varepsilon}} \, . \qquad (4.23)
\end{aligned}
$$

This representation is the starting point for an NRG treatment of the original Kondo Hamiltonian (2.15). We refer to $\underset{\sim}{H}_{\mathrm{NRG}}/W$ as a "dimensionless representation" since $\underset{\sim}{H}_{\mathrm{NRG}}/W$ only contains dimensionless quantities.

4.3. Example: One-dimensional tight-binding electrons

As an example, consider the following Hamiltonian:

$$
\underset{\sim}{H}_{\mathrm{1DTB}} \equiv t \sum_{\substack{i=1 \\ \mu}}^{L} \left(\underset{\sim}{c}_{i\mu}^\dagger \underset{\sim}{c}_{i+1\mu} + \underset{\sim}{c}_{i+1\mu}^\dagger \underset{\sim}{c}_{i\mu} \right) . \qquad (4.24)
$$

It describes non-interacting "tight-binding" electrons that can hop between adjacent sites of a one-dimensional periodic lattice (i.e., a ring with $\underset{\sim}{c}_{L+1\mu}^{(\dagger)} = \underset{\sim}{c}_{1\mu}^{(\dagger)}$) [EFG+05]. We assume that the nearest-neighbor hopping parameter t is positive. By employing the discrete Fourier transformation [EFG+05]

$$
\underset{\sim}{c}_{k\mu}^\dagger \equiv \frac{1}{\sqrt{L}} \sum_{j=1}^{L} \mathrm{e}^{2\pi \mathrm{i}\, kj/L} \underset{\sim}{c}_{j\mu}^\dagger \, , \qquad (4.25)
$$

where the shift quantum number k satisfies $k \in \{0, 1, ..., L-1\}$, and by introducing the dispersion relation

$$
\varepsilon_k \equiv 2t \cos(2\pi k/L) \, , \qquad (4.26)
$$

Hamiltonian (4.24) can be equivalently written as:

$$
\underset{\sim}{H}_{\mathrm{1DTB}} = \sum_{\substack{k=0 \\ \mu}}^{L-1} \varepsilon_k \underset{\sim}{c}_{k\mu}^\dagger \underset{\sim}{c}_{k\mu} \, . \qquad (4.27)
$$

For an even number of lattice sites L, this representation of the Hamiltonian is furthermore equivalent to

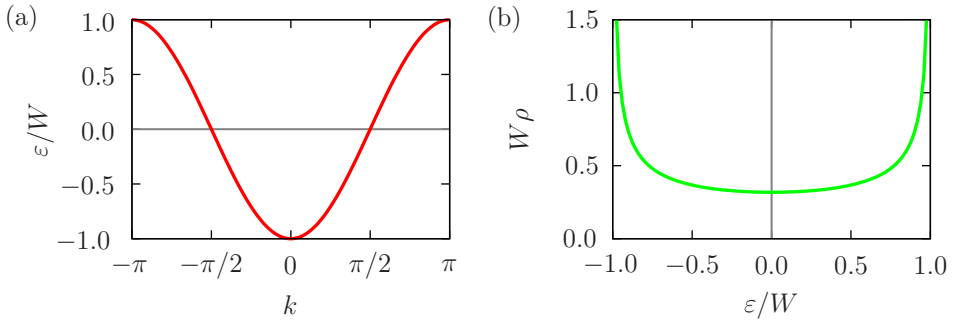

Figure 4.1.: (a) Dispersion relation $\varepsilon(k)$ from Eq. (4.30) and (b) corresponding density of states $\rho(\varepsilon)$ from Eq. (4.31) for one-dimensional tight-binding electrons described by Hamiltonian (4.24) with half-bandwidth $W = 2t$.

$$\underset{\sim}{H}_{\mathrm{1DTB}} = \sum_{\substack{q=-L/2 \\ \mu}}^{L/2-1} \varepsilon'_q \, \underset{\sim}{d}^\dagger_{q\mu} \underset{\sim}{d}_{q\mu} \; , \tag{4.28}$$

$$\text{with} \;\; \varepsilon'_q \equiv -2t \cos(2\pi q/L) \; , \tag{4.29}$$

because of translational invariance.

In the limit of an arbitrarily large lattice, i.e., for $L \gg 1$, we obtain the continuous dispersion relation

$$\boxed{\varepsilon(k) = -2t\cos(k) \quad \text{with} \quad k \in [-\pi, \pi) \; .} \tag{4.30}$$

According to the definition (4.6) of $\rho(\varepsilon)$, this dispersion relation leads to the following DOS per lattice site and per spin projection (using, e.g., the identity for the delta function from Eq. (4.138)):

$$\boxed{\rho(\varepsilon) = \frac{1}{2t\,\pi\sqrt{1-\left(\frac{\varepsilon}{2t}\right)^2}} \, \Theta\!\left(1 - \frac{|\varepsilon|}{2t}\right) \; .} \tag{4.31}$$

The half-bandwidth of the electrons is thus $W = 2t$. As required by the definition (4.6), the DOS (4.31) is normalized, i.e., $\int_{-W}^{W} \mathrm{d}\varepsilon \, \rho(\varepsilon) = 1$. The dispersion relation and the DOS are shown in Fig. 4.1.

4.4. Logarithmic discretization I: Standard discretization with z-averaging

In order to treat Hamiltonian (4.22) numerically, it is necessary to cast it into a discretized form. It turns out that this has to be done in a clever way if one intends to obtain results that are representative of the continuum limit of interest. The relevant low-energy scales for a quantum impurity model such as the Kondo model can be orders of magnitude smaller than, e.g., the bandwidth of the electrons. For this reason, a linear discretization of the continuum of electronic states does not constitute a practical approach since, in general, it would require an enormous amount of states in order to resolve the low-energy scales [BCP08]. Instead, a logarithmic discretization of the electron band is used. This allows to resolve low-energy features with a significantly reduced number of electronic states. Nevertheless, it is only one possible choice for the discretization and, as Wilson has remarked: "The only true justification for using the logarithmic division is that a successful calculation results." ([Wil75], p. 813) The original ("standard") implementation of the logarithmic discretization is discussed, e.g., in Refs. [Wil75, KmWW80a, KmWW80b].

Depending on the impurity problem, it might not be possible to use a logarithmic discretization mesh that is fine enough because of practical constraints. In this case, the obtained results might show obvious numerical artifacts such as artificial oscillations. A possibility of alleviating these artifacts is given by a method which is referred to as *z-averaging* since it involves averaging results for different discretization meshes that are determined by the so-called *twist parameter* z. Because these meshes are "interleaved" in a certain sense, the approach is also called the *interleaved method*. It was introduced in Ref. [YWO90] and further developed in Refs. [OO94, CPLO97].

4.4.1. Logarithmic discretization of the continuum of electronic states

For an accurate description of the low-energy and low-temperature properties of the considered quantum impurity model, NRG aims at a high energy resolution close to the Fermi energy, i.e., around $\xi = 0$ or, equivalently, $\varepsilon = \varepsilon_F$. We now introduce two numerical parameters, whose values are regarded as given in this subsection: the *discretization parameter* $\Lambda > 1$ and the *twist parameter* $z \in (0, 1]$. The meaning of the twist parameter and the idea of the related z-averaging are discussed in detail in the next section 4.4.2. If there are different "species" of electrons that are non-equivalent on the single-particle level (e.g., electrons with spin-up and spin-down in case of $h \neq 0$), the logarithmic discretization has to be carried out separately for each species.

In order to establish a logarithmic division of the integration ranges in Eq. (4.22), the following intervals are defined [YWO90]:

$$I_m^+(z) \;:\; \begin{cases} \Lambda^{-z} < \xi_\mu^+ \leq 1 & , \quad \text{for} \quad m = 0 \\ \Lambda^{-z-m} < \xi_\mu^+ \leq \Lambda^{-z-m+1} & , \quad \text{for} \quad m \geq 1 \end{cases} , \tag{4.32}$$

$$I_m^-(z) \;:\; \begin{cases} -1 \leq \xi_\mu^- < -\Lambda^{-z} & , \quad \text{for} \quad m = 0 \\ -\Lambda^{-z-m+1} \leq \xi_\mu^- < -\Lambda^{-z-m} & , \quad \text{for} \quad m \geq 1 \end{cases} . \tag{4.33}$$

In the special case $z = 1$, this division corresponds to the logarithmic discretization that has been proposed by Wilson [Wil75]. The logarithmic division is illustrated in Fig. 4.2 for $z = 1$ and three values of the discretization parameter Λ. Why is this division called logarithmic? The width of the intervals $I_m^\pm(z)$ for $m \geq 1$,

$$\Delta_m \equiv \Lambda^{-z-m+1} - \Lambda^{-z-m} = \mathrm{e}^{-m \ln \Lambda}\, \Lambda^{-z}(\Lambda - 1) \,, \tag{4.34}$$

exponentially decreases with growing interval index m. Since

$$\ln\bigl(\Lambda^{-z-m+1}\bigr) - \ln\bigl(\Lambda^{-z-m}\bigr) = \ln \Lambda = \text{const.} \,, \tag{4.35}$$

the interval definitions (4.32) and (4.33) correspond to an equipartition of the integration ranges in Hamiltonian (4.22) on a logarithmic scale.

In order to obtain a discrete representation of Hamiltonian (4.22), the infinite number of electronic states in each interval $I_m^p(z)$ ($p \equiv \pm$) has to be reduced to some finite number. In a typical NRG calculation, *one suitable state* is picked from each interval and all other electronic states are discarded. On each interval $I_m^p(z)$, there is actually only a single state which directly couples to the impurity spin. These states are kept to allow for a description of the interaction between electrons and impurity that is as good as possible. As illustrated by Fig. 4.2, the logarithmic discretization mesh becomes finer for smaller values of the discretization parameter Λ. In particular, the reduction of each interval to a single state becomes exact for $\Lambda \to 1$ and, in this limit, the continuum of electronic states is restored. $\Lambda \to 1$ corresponds to the continuum limit of the Kondo Hamiltonian that we are interested in.

Note that the selected states are linear combinations of the original single-particle states and thus mix different energies. On each interval, the chosen state can be interpreted as an element of a new basis. With respect to this new set of basis states, the purely electronic term in Hamiltonian (4.22) *cannot* be diagonal anymore. Although the interaction term can be represented exactly via the kept states, the reduction to one state per interval is thus necessarily an approximation for $\Lambda > 1$.

In case of a constant DOS, the new basis can be obtained by performing a Fourier expansion on each interval [Wil75, KmWW80a]. The kept state then corresponds to the respective zero mode. Since the Fourier expansion leads to explicit expressions for the neglected states, some additional analytical calculations become possible [Wil75, KmWW80a].

In order to simplify the notation, we henceforth drop indices and superscripts of integration variables where possible and introduce the following two abbreviations:

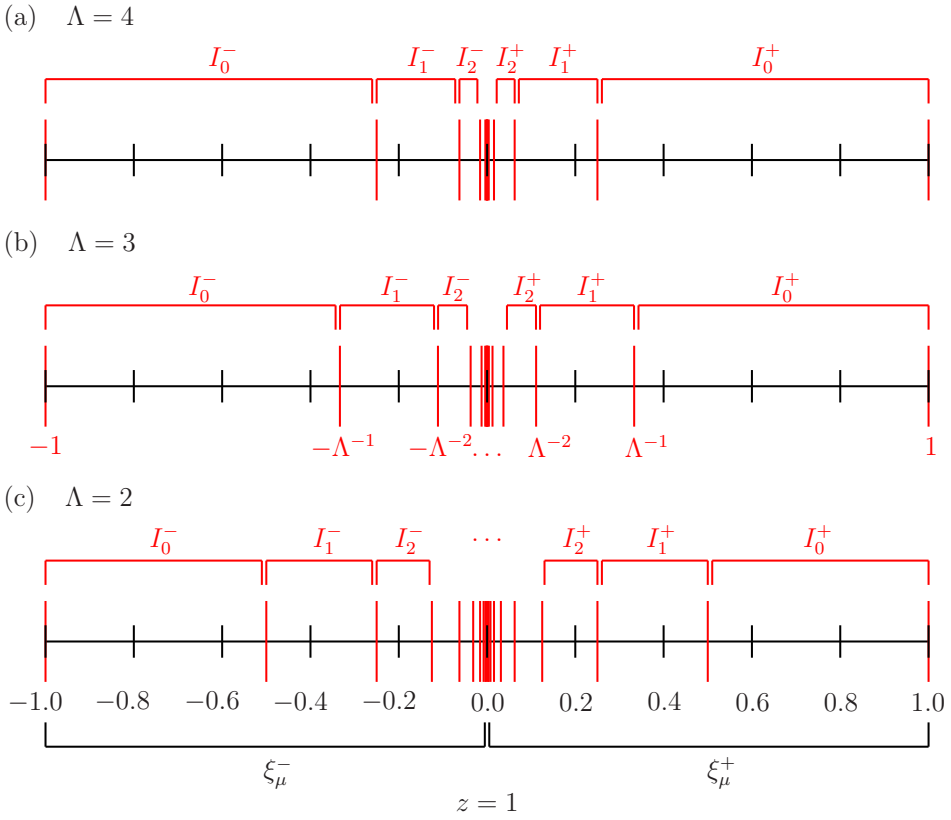

Figure 4.2.: Illustration of the logarithmic discretization according to Eqs. (4.32) and (4.33) for twist parameter $z = 1$ (i.e., as proposed by Wilson) and three values of the discretization parameter $\Lambda > 1$.

$$\boxed{\begin{aligned} \gamma_\mu^p(\xi) &\equiv \rho\big(\xi\mathcal{B}_\mu^p + \varepsilon_F - \mu h\big)\mathcal{B}_\mu^p \,, && (4.36)\\ \mathcal{W}_{m\mu}^p(z) &\equiv \int_{I_m^p(z)} \mathrm{d}\xi\, \rho\big(\xi\mathcal{B}_\mu^p + \varepsilon_F - \mu h\big) W \,. && (4.37) \end{aligned}}$$

The operator $\underset{\sim}{f}_{0\mu}$ from Eq. (4.20) can then be written as:

$$\underset{\sim}{f}_{0\mu} = \int_0^1 \mathrm{d}\xi\, \sqrt{\gamma_\mu^+(\xi)}\, \underset{\sim}{a}_\mu^+(\xi) \;+\; \int_{-1}^0 \mathrm{d}\xi\, \sqrt{\gamma_\mu^-(\xi)}\, \underset{\sim}{a}_\mu^-(\xi) \,. \tag{4.38}$$

Motivated by this representation of $\underset{\sim}{f}_{0\mu}$, we define the following zeroth "wave functions" $\varphi_{m0\mu}^p\big(z, \xi_\mu^p\big) = \big\langle \xi_\mu^p \big| \varphi_{m0\mu}^p(z) \big\rangle$ [CO05],

$$\boxed{\varphi_{m0\mu}^p(z,\xi) \;\equiv\; \begin{cases} \sqrt{\dfrac{\gamma_\mu^p(\xi)}{\int_{I_m^p(z)} \mathrm{d}\zeta\, \gamma_\mu^p(\zeta)}} & , \quad \text{for} \quad \xi \in I_m^p(z) \\ 0 & , \quad \text{otherwise} \end{cases}} \,, \tag{4.39}$$

which are properly normalized:

$$\big\langle \varphi_{m0\mu}^p(z) \big| \varphi_{m0\nu}^p(z) \big\rangle = \int_{I_m^p(z)} \mathrm{d}\xi\, \varphi_{m0\mu}^{p\,*}(z,\xi)\, \varphi_{m0\nu}^p(z,\xi) = \delta_{\mu\nu} \,. \tag{4.40}$$

Using $\big|\xi_\mu^p\big\rangle = \underset{\sim}{a}_\mu^{p\dagger}(\xi)|\Omega\rangle$ and $\big|\varphi_{m0\mu}^p(z)\big\rangle = \underset{\sim}{a}_{m0\mu}^{p\dagger}(z)|\Omega\rangle$ with the vacuum state $|\Omega\rangle$, the closure relation $\underset{\sim}{\mathbb{1}} = \sum_{p,m,\mu} \int_{I_m^p(z)} \mathrm{d}\xi_\mu^p \big|\xi_\mu^p\big\rangle\big\langle\xi_\mu^p\big|$ gives the expansions for the corresponding operators $\underset{\sim}{a}_{m0\mu}^p(z)$ in terms of the states $\underset{\sim}{a}_\mu^p(\xi)$:

$$\underset{\sim}{a}_{m0\mu}^p(z) \;=\; \int_{I_m^p(z)} \mathrm{d}\xi\, \varphi_{m0\mu}^{p\,*}(z,\xi)\, \underset{\sim}{a}_\mu^p(\xi) \,, \tag{4.41}$$

$$\big\{ \underset{\sim}{a}_{m0\mu}^p(z),\, \underset{\sim}{a}_{m'0\nu}^{p'\dagger}(z) \big\} \;=\; \delta_{pp'}\delta_{mm'}\delta_{\mu\nu} \,. \tag{4.42}$$

The new operators $\underset{\sim}{a}_{m0\mu}^p(z)$ allow for an exact representation of the state $\underset{\sim}{f}_{0\mu}$ from Eq. (4.38) (cf. Ref. [CO05]),

$$\boxed{\underset{\sim}{f}_{0\mu} = \sum_{p,m} \sqrt{\frac{\mathcal{B}_\mu^p}{W}\, \mathcal{W}_{m\mu}^p(z)}\, \underset{\sim}{a}_{m0\mu}^p(z) \,,} \tag{4.43}$$

and thus indeed correspond to those electronic states that directly couple to the impurity spin.

Next, starting with the function $\varphi_{m0\mu}^p(z,\xi)$, we formally construct a complete orthonormal set of functions $\varphi_{mn\mu}^p(z,\xi)$ on each interval $I_m^p(z)$ [CO05], i.e.,

$$\underset{\sim}{\mathbb{1}}_{I_m^p(z)} \;=\; \sum_{n,\mu} \big|\varphi^p_{mn\mu}(z)\big\rangle\big\langle\varphi^p_{mn\mu}(z)\big| \;, \tag{4.44}$$

$$\big\langle\varphi^p_{mn\mu}(z)\big|\varphi^p_{mn'\nu}(z)\big\rangle \;=\; \int_{I_m^p(z)} \mathrm{d}\xi\, \varphi^{p\,*}_{mn\mu}(z,\xi)\, \varphi^p_{mn'\nu}(z,\xi) \;=\; \delta_{nn'}\delta_{\mu\nu} \;, \tag{4.45}$$

with corresponding operators

$$\underset{\sim}{a}{}^p_{mn\mu}(z) = \int_{I_m^p(z)} \mathrm{d}\xi\, \varphi^{p\,*}_{mn\mu}(z,\xi)\, \underset{\sim}{a}{}^p_{\mu}(\xi) \;. \tag{4.46}$$

This allows us to set up the inverse transformation,

$$\underset{\sim}{a}{}^p_{\mu}(\xi) = \sum_n \varphi^p_{mn\mu}(z,\xi)\, \underset{\sim}{a}{}^p_{mn\mu}(z) \quad \text{for} \quad \xi \in I_m^p(z) \;, \tag{4.47}$$

and to express Hamiltonian (4.22) with respect to the new basis $\big\{\underset{\sim}{a}{}^p_{mn\mu}(z)\big\}$:

$$\begin{aligned} \underset{\sim}{H}_{\mathrm{NRG}} \;=\; & W \sum_{\substack{p,m\\ n,n'\\ \mu}} \frac{\mathcal{B}^p_\mu}{W} \mathcal{A}^p_{mnn'\mu}(z)\, \underset{\sim}{a}{}^{p\dagger}_{mn\mu}(z) \underset{\sim}{a}{}^p_{mn'\mu}(z) \\ & +\; J\underset{\sim}{\boldsymbol{S}} \cdot \sum_{\mu,\nu} \underset{\sim}{f}{}^\dagger_{0\mu} \frac{\boldsymbol{\sigma}_{\mu\nu}}{2} \underset{\sim}{f}_{0\nu} \;+\; \underset{\sim}{H}_{\mathrm{imp}}(B) \;, \end{aligned} \tag{4.48}$$

with

$$\mathcal{A}^p_{mnn'\mu}(z) \;\equiv\; \int_{I_m^p(z)} \mathrm{d}\xi\, \xi\, \varphi^{p\,*}_{mn\mu}(z,\xi)\, \varphi^p_{mn'\mu}(z,\xi) \;. \tag{4.49}$$

As expected, the electron term is non-diagonal with respect to the basis $\big\{\underset{\sim}{a}{}^p_{mn\mu}(z)\big\}$. For this reason, the states $\underset{\sim}{a}{}^p_{mn\mu}(z)$ with $n \neq 0$ indirectly couple to the impurity spin although the expansion (4.43) of $\underset{\sim}{f}_{0\mu}$ only involves the operators $\underset{\sim}{a}{}^p_{m0\mu}(z)$.

As one of the *central approximations of NRG*, the following replacement is now made [KmWW80a]:

$$\boxed{\mathcal{A}^p_{mnn'\mu}(z) \to \delta_{n0}\, \delta_{n'0}\, \mathcal{A}^p_{m00\mu}(z) \;.} \tag{4.50}$$

Starting with the definition (4.49), we find:

$$\boxed{\mathcal{A}^p_{m\mu}(z) \equiv \mathcal{A}^p_{m00\mu}(z) = \frac{\int_{I_m^p(z)} \mathrm{d}\xi\, \xi\, \gamma^p_\mu(\xi)}{\int_{I_m^p(z)} \mathrm{d}\zeta\, \gamma^p_\mu(\zeta)} \;.} \tag{4.51}$$

The substitution (4.50), along with $\underset{\sim}{a}{}^p_{m\mu}(z) \equiv \underset{\sim}{a}{}^p_{m0\mu}(z)$, leads to the desired *approximate* discrete representation of Hamiltonian (4.22) for the given twist parameter z:

$$
\begin{aligned}
\underset{\sim}{H}_{\mathrm{NRG}} \quad &\approx \quad W \sum_{\substack{p,m \\ \mu}} \mathcal{E}^p_{m\mu}(z)\, \underset{\sim}{a}^{p\dagger}_{m\mu}(z) \underset{\sim}{a}^{p}_{m\mu}(z) \\
&\qquad + \; J \underset{\sim}{\boldsymbol{S}} \cdot \sum_{\mu,\nu} \underset{\sim}{f}^{\dagger}_{0\mu} \frac{\boldsymbol{\sigma}_{\mu\nu}}{2} \underset{\sim}{f}_{0\nu} \; + \; \underset{\sim}{H}_{\mathrm{imp}}(B) \; , \qquad (4.52) \\
&\text{with} \\
\underset{\sim}{f}_{0\mu} \quad &= \quad \sum_{p,m} \sqrt{\frac{\mathcal{B}^p_\mu}{W} \mathcal{W}^p_{m\mu}(z)}\, \underset{\sim}{a}^{p}_{m\mu}(z) \; , \\
\mathcal{E}^p_{m\mu}(z) \quad &\equiv \quad \frac{\mathcal{B}^p_\mu}{W} \mathcal{A}^p_{m\mu}(z) \; = \; \frac{\mathcal{B}^p_\mu}{W} \frac{\int_{I^p_m(z)} \mathrm{d}\xi\, \xi\, \gamma^p_\mu(\xi)}{\int_{I^p_m(z)} \mathrm{d}\zeta\, \gamma^p_\mu(\zeta)} \; . \qquad (4.53)
\end{aligned}
$$

Eq. (4.53) is the "standard recipe" for determining the electron energies $W\mathcal{E}^p_{m\mu}(z)$ of the discretized Hamiltonian (cf. Ref. [BCP08]). Apart from the factor $\mathcal{B}^p_\mu/W$, it amounts to calculating the average "energy" on the interval $I^p_m(z)$ with respect to the "weight function" $\gamma^p_\mu(\xi)$ defined in Eq. (4.36).

This section might give the false impression that Hamiltonian (4.52) is the result of a strict derivation. In fact, the substitution (4.50) corresponds to an essentially uncontrolled approximation. For this reason, the energies that are assigned to the kept states $\underset{\sim}{a}^p_{m\mu}(z)$ are somewhat arbitrary (note, however, that the choice of the states $\underset{\sim}{a}^p_{m\mu}(z)$ is *not* arbitrary). It turns out that the definition (4.53) is not optimal. In particular, for larger values of Λ, the presented standard discretization cannot satisfactorily reproduce the density of states of the electrons (which appears in the weight function $\gamma^p_\mu(\xi)$). For a constant DOS, it has been found that the coupling parameter J (or, to be precise, each term involving the DOS) has to be *ad hoc* multiplied by a correction factor that depends on the discretization parameter Λ (cf. Ref. [BCP08]):

$$
A_\Lambda \equiv \frac{1}{2} \frac{\Lambda + 1}{\Lambda - 1} \ln \Lambda \; . \qquad (4.54)
$$

This factor appears, e.g., in Eq. (5.20) of Ref. [KmWW80a] and Eq. (3.36) of Ref. [KmWW80b]. In Ref. [CO05] it is shown for a constant DOS and for $\Lambda > 1$ that the correction factor A_Λ is necessary in order to correctly reproduce the spectral density of the operator $\underset{\sim}{f}_{0\mu}$, which is directly related to the DOS, after z-averaging (see below). However, for a general energy-dependent DOS, it is not known how the spectral density of $\underset{\sim}{f}_{0\mu}$ is affected and whether possible deviations can be corrected by a renormalization of coupling parameters. Superior choices for the energies $W\mathcal{E}^p_{m\mu}(z)$, which alleviate shortcomings of the standard discretization, are discussed in Secs. 4.5 and 4.7.

Since we are interested in the continuum limit $\Lambda \to 1$, it is in principle necessary to carry out calculations for decreasing values of the discretization parameter and to perform an extrapolation of the obtained results with respect to Λ. However, observables of typical quantum impurity models often display a rapid convergence

in Λ. Results for a discretization parameter that is not too large might therefore already be representative of the continuum limit [BCP08].

4.4.2. z-averaging ("interleaved method")

The parameter z is referred to as the *sliding parameter* [OO94] (see below) or the *twist parameter* (for the case of a linear discretization, a certain connection with the concept of "twisted" boundary conditions is established in [CO05]). The idea of the so-called z-averaging is the following: Choose a certain number N_z of z-values that are, e.g., uniformly distributed on the interval $(0, 1]$. N_z is typically small when calculating static quantities (e.g., $N_z = 2$ or $N_z = 4$), but can be considerably larger in calculations of spectral functions (see, e.g., [ŽP09]). For each value of z, i.e., for each discretization mesh, a separate NRG calculation is carried out and the desired observables are calculated. The results for the observables are then improved by averaging over all considered z-values for fixed temperature and magnetic field.

z-averaging is meant to attain a number of related goals:

- It is supposed to smooth or even eliminate artificial oscillations in the temperature dependence of observables at low temperature.
- Furthermore, the method aims at producing results that are more representative of the continuum limit $\Lambda \to 1$.
- In particular, NRG calculations with large values of Λ (i.e., $3 < \Lambda \leq 10$) shall become more accurate in order to produce meaningful results. Although a calculation with a large discretization parameter takes one further away from the continuum limit, it might still be desirable since it is numerically less demanding.

As regards the artificial oscillations, the influence of the logarithmic discretization on the temperature dependence of observables close to the low-temperature Fermi liquid fixed point of an Anderson impurity model has been investigated in detail for the impurity contributions to the magnetic susceptibility χ_{imp} [OO94] and the specific heat C_{imp} [CPLO97] (the concept of an impurity contribution is introduced in Sec. 4.13.1). It is found that the considered observables have an artificial component which oscillates as a function of the logarithmic temperature with period $\ln \Lambda$ and whose amplitude grows with Λ like $\exp(-\pi^2/\ln \Lambda)$. The prefactor of the artificial term depends, among other things, on the observable under consideration. Whereas the artifact vanishes in the continuum limit $\Lambda \to 1$, it becomes unacceptably large for $\Lambda \gtrsim 3$. In the case of an Anderson impurity model with $U = 0$, the artifact term $\widetilde{\chi}_{\mathrm{imp}}$ close to the low-temperature fixed point is proportional to [OO94]:

$$\widetilde{\chi}_{\mathrm{imp}} \;\propto\; \sum_{k=0}^{\infty} \alpha_k \,\cos\!\left(2\pi\left[z-\frac{1}{2}+\frac{\ln\bigl(2\pi[2k+1]\bigr)}{\ln\Lambda}+\frac{\ln\bigl(k_BT/D_N\bigr)}{\ln\Lambda}\right]\right) \tag{4.55}$$

$$\sim\; \sum_{k} \alpha_k \,\cos\bigl(2\pi x/\ln\Lambda+\delta(z,k)\bigr)\;, \tag{4.56}$$

with $x \equiv \ln\bigl(k_BT/D_N\bigr)$ and some energy scale D_N. Since the phase shift $\delta(z,k)$ is a linear function of the twist parameter and

$$\int_0^1 \mathrm{d}z\,\cos(\text{const.}+2\pi z) = 0\;, \tag{4.57}$$

an average over all z-values (or all phase shifts) removes the artifact term. Close to fixed points that can be described by a single-particle Hamiltonian, it is thus indeed possible to exactly restore the continuum limit by z-averaging [OO94]. Note, however, that in general z-averaging *cannot* reinstate the true continuum limit $\Lambda \to 1$ [BCP08]. One has to accept that NRG results might show systematic deviations that cannot be completely eliminated, neither by increasing N_z nor by reducing Λ [ŽP09]. Nevertheless, the quality of the discretization certainly affects the severity of the artifacts [ŽP09]. Ref. [Žit11b] suggests to use $N_z = 2^n$ in order to smooth higher-order oscillations with period up to $n\ln\Lambda$.

As a further illustration of the idea behind the z-averaging, we now discuss the effect of the "sliding parameter" z on the logarithmic discretization mesh defined by Eqs. (4.32) and (4.33). To this end, the z-dependence of the positive intervals $I_0^+(z)$, $I_m^+(z)$, and $I_{m-1}^+(z)$ is depicted in Fig. 4.3 (analogous conclusions apply to the negative integration range). As shown in Fig. 4.3 (a), the width of the outermost interval $I_0^+(z)$ shrinks to zero when z is decreased from one to zero. Furthermore, the intervals $I_m^+(z)$ with $m \geq 1$ move outwards upon decreasing z (see Fig. 4.3 (b)). In particular, we have

$$I_{m-1}^p(z=1) \;=\; I_m^p(z=0)\;. \tag{4.58}$$

The z-dependence of the discretization mesh as illustrated by Fig. 4.3 (b) is the reason why z-averaging is also referred to as the "interleaved method". It has important consequences for the parameters $\mathcal{A}_{m\mu}^p(z)$ that appear in the discretized Hamiltonian (4.52). In case of a constant DOS, the quantities

$$\mathcal{A}_{m\mu}^p(z)\Big|_{\rho\,=\,\mathrm{const.}} = \frac{\int_{I_m^p(z)}\mathrm{d}\xi\,\xi\,\gamma_\mu^p(\xi)}{\int_{I_m^p(z)}\mathrm{d}\zeta\,\gamma_\mu^p(\zeta)} = \frac{\int_{I_m^p(z)}\mathrm{d}\xi\,\xi\,\gamma_\mu^p}{\int_{I_m^p(z)}\mathrm{d}\zeta\,\gamma_\mu^p} = \bigl\langle\xi\bigr\rangle_{I_m^p(z)} \tag{4.59}$$

just correspond to the centers of the intervals $I_m^p(z)$. As Fig. 4.3 (c) demonstrates, the parameters $\mathcal{A}_{m\mu}^p(z)$ cover the whole integration range without overlap for continuous z-values from the interval $(0,1]$. z-averaging therefore represents a way

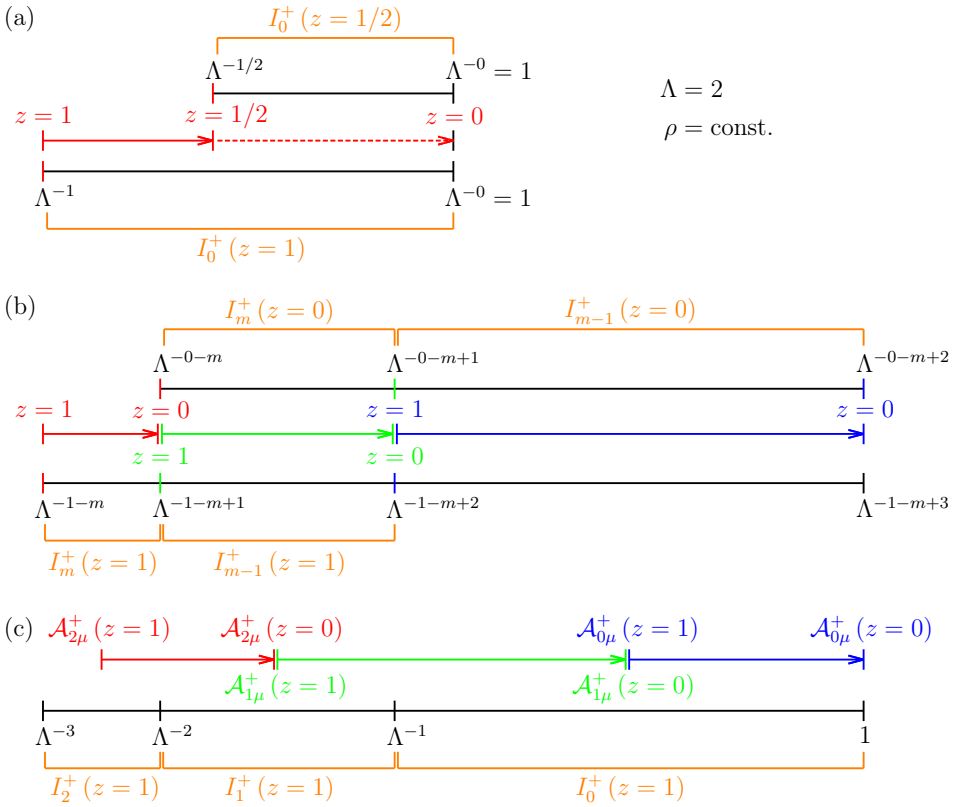

Figure 4.3.: Illustration of the effect of the "sliding parameter" z on the logarithmic discretization mesh defined by Eqs. (4.32) and (4.33). The interval widths are true to scale for discretization parameter $\Lambda = 2$. (a) z-dependence of the outermost positive interval $I_0^+(z)$. (b) z-dependence of two adjacent intervals $I_m^+(z)$ and $I_{m-1}^+(z)$. (c) z-dependence of the average "energies" $\mathcal{A}_{m\mu}^+(z)$ defined in Eq. (4.51), shown for the case of a constant density of states of the electrons, for the three outermost intervals $I_0^+(z)$, $I_1^+(z)$, and $I_2^+(z)$.

to sample electronic "energies" from the whole integration range by considering different "interleaved" discretization meshes.

In the case of non-interacting electrons with the Hamiltonian

$$\underset{\sim}{H} = \sum_k \varepsilon_k \underset{\sim}{c}_k^\dagger \underset{\sim}{c}_k \ , \tag{4.60}$$

the partition function is multiplicative and the thermodynamic potential thus additive with respect to the single-particle modes k. A thermodynamic observable O (as a derivative of the thermodynamic potential) can then also be written as the sum over contributions from the different modes:

$$O = \sum_k O_k \ . \tag{4.61}$$

In the non-interacting case, z-averaging effectively corresponds to a sampling of the sum on the right-hand side of Eq. (4.61) and can therefore, in principle, restore the continuum limit. However, for an interacting system, observables are in general non-additive with respect to single-particle states. Even a continuous z-averaging is therefore only an approximation and *cannot* fully reinstate the continuum limit.

4.5. Logarithmic discretization II: Improved discretization by Campo & Oliveira

Campo and Oliveira have proposed an alternative scheme for the logarithmic discretization in Ref. [CO04]. Their improved discretization is explained in detail in Ref. [CO05].

In the standard discretization as discussed in the previous section 4.4, the choice of the "energies" (4.53) for the states $\underset{\sim}{a}^p_{m\mu}(z)$ appearing in the discrete Hamiltonian (4.52) (i.e., the assignment of an energy to an interval $I^p_m(z)$) is somewhat arbitrary (the kept states, on the other hand, are determined by the form of the interaction between electrons and impurity spin according to Eqs. (4.22) and (4.43)). As already mentioned, the standard discretization leads to an erroneous representation of a *constant* density of states of the electrons that has to be "repaired" by a multiplication of the coupling parameter with the correction factor A_Λ from Eq. (4.54) [BCP08]. Even worse, such a renormalization factor is not available for the case of a general DOS. Furthermore, despite z-averaging, the standard discretization produces results with inferior convergence in Λ (see Fig. 1 of Ref. [CO05] and Fig. 11 of Ref. [ŽP09]), ruling out the use of large discretization parameters. A better logarithmic discretization of the continuum of electronic states is thus desirable. To this end, energies that differ from those defined in Eq. (4.53), and which turn out to be more suitable, are assigned to the intervals $I^p_m(z)$.

When using the improved discretization by Campo and Oliveira, everything is done as before, up to and including the definition of the zeroth "wave functions" $\varphi^p_{m0\mu}(z,\xi)$ in Eq. (4.39) with the corresponding operators $\underset{\sim}{a}^p_{m0\mu}(z)$ from

Eq. (4.41). The difference compared to the standard discretization is the way in which the new basis $\{\underset{\sim}{a}^p_{mn\mu}(z)\}$ is constructed on each interval $I^p_m(z)$. The first (zeroth) element $\underset{\sim}{a}^p_{m0\mu}(z)$ of this basis again corresponds to the function $\varphi^p_{m0\mu}(z,\xi)$. However, this time we demand that the complete set of functions $\varphi^p_{mn\mu}(z,\xi)$ be orthonormal with respect to a *modified scalar product* involving a (still unknown) positive weight function $g^p_{m\mu}(z,\xi)$ [CO05]:

$$\boxed{\int_{I^p_m(z)} \mathrm{d}\xi\, \varphi^{p\,*}_{mn\mu}(z,\xi)\, g^p_{m\mu}(z,\xi)\, \varphi^p_{mn'\mu}(z,\xi) = \delta_{nn'}\ .} \tag{4.62}$$

For a non-constant weight function, this relation implies that the wave functions $\varphi^p_{mn\mu}\big(z,\xi^p_\mu\big) = \big\langle \xi^p_\mu \big| \varphi^p_{mn\mu}(z)\big\rangle$ are no longer orthogonal with respect to the canonical scalar product that is used in the standard discretization. Furthermore, they are not properly normalized for $n \neq 0$. This means that the corresponding operators

$$\underset{\sim}{a}^p_{mn\mu}(z) = \int_{I^p_m(z)} \mathrm{d}\xi\, \varphi^{p\,*}_{mn\mu}(z,\xi)\, \underset{\sim}{a}^p_\mu(\xi) \tag{4.63}$$

do not satisfy standard fermionic anticommutation relations for $n \neq 0$. However, since the functions $\varphi^p_{m0\mu}(z,\xi)$ and thus also the operators $\underset{\sim}{a}^p_{m0\mu}(z)$ are unchanged, we still have $\big\{\underset{\sim}{a}^p_{m0\mu}(z), \underset{\sim}{a}^{p'\dagger}_{m'0\nu}(z)\big\} = \delta_{pp'}\delta_{mm'}\delta_{\mu\nu}$ as before. The orthonormality relation (4.62) and the expansion (4.63) give the corresponding inverse transformation [CO05],

$$\underset{\sim}{a}^p_\mu(\xi) = \sum_n g^p_{m\mu}(z,\xi)\, \varphi^p_{mn\mu}(z,\xi)\, \underset{\sim}{a}^p_{mn\mu}(z) \quad \text{for} \quad \xi \in I^p_m(z)\ , \tag{4.64}$$

which is then used to deduce the following exact representation of Hamiltonian (4.22) in terms of the new basis $\{\underset{\sim}{a}^p_{mn\mu}(z)\}$:

$$\begin{aligned} \underset{\sim}{H}_{\mathrm{NRG}} \;=\; & W \sum_{\substack{p,m\\ n,n'\\ \mu}} \frac{\mathcal{B}^p_\mu}{W} \widetilde{\mathcal{A}}^p_{mnn'\mu}(z)\, \underset{\sim}{a}^{p\dagger}_{mn\mu}(z) \underset{\sim}{a}^p_{mn'\mu}(z) \\ & +\; J\underset{\sim}{\boldsymbol{S}} \cdot \sum_{\mu,\nu} \underset{\sim}{f}^\dagger_{0\mu} \frac{\boldsymbol{\sigma}_{\mu\nu}}{2} \underset{\sim}{f}_{0\nu} \;+\; \underset{\sim}{H}_{\mathrm{imp}}(B)\ , \end{aligned} \tag{4.65}$$

with

$$\widetilde{\mathcal{A}}^p_{mnn'\mu}(z) \;\equiv\; \int_{I^p_m(z)} \mathrm{d}\xi\, \xi\, \varphi^{p\,*}_{mn\mu}(z,\xi)\, \varphi^p_{mn'\mu}(z,\xi)\, \big|g^p_{m\mu}(z,\xi)\big|^2\ . \tag{4.66}$$

The purely electronic term in $\underset{\sim}{H}_{\mathrm{NRG}}$ is again non-diagonal. The idea of the improved discretization scheme is to *choose* the weight functions $g^p_{m\mu}(z,\xi)$ in such

a way that the different states $\underset{\sim}{a}^p_{mn\mu}(z)$ on the same interval $I^p_m(z)$ are formally decoupled in the Hamiltonian [CO05], i.e., we need to have:

$$\widetilde{\mathcal{A}}^p_{mnn'\mu}(z) \propto \delta_{nn'} \; . \tag{4.67}$$

According to the definition (4.66) and the relation (4.62), the choice [CO05]

$$\boxed{g^p_{m\mu}(z,\xi) \equiv \frac{\widetilde{\mathcal{A}}^p_{m\mu}(z)}{\xi} \quad \text{for} \quad \xi \in I^p_m(z)} \tag{4.68}$$

produces the desired result, i.e.,

$$\widetilde{\mathcal{A}}^p_{mnn'\mu}(z) = \widetilde{\mathcal{A}}^p_{m\mu}(z)\, \delta_{nn'} \; . \tag{4.69}$$

Note that the parameters $\widetilde{\mathcal{A}}^p_{m\mu}(z)$ still have to be determined. With the definition (4.68), the expression (4.65) for the Hamiltonian is further simplified:

$$\begin{aligned} \underset{\sim}{H}_{\mathrm{NRG}} \;=\; & W \sum_{\substack{p,m \\ n,\mu}} \frac{\mathcal{B}^p_\mu}{W} \widetilde{\mathcal{A}}^p_{m\mu}(z)\, \underset{\sim}{a}^{p\dagger}_{mn\mu}(z) \underset{\sim}{a}^p_{mn\mu}(z) \\ & + \; J \underset{\sim}{\boldsymbol{S}} \cdot \sum_{\mu,\nu} \underset{\sim}{f}^\dagger_{0\mu} \frac{\boldsymbol{\sigma}_{\mu\nu}}{2} \underset{\sim}{f}_{0\nu} \; + \; \underset{\sim}{H}_{\mathrm{imp}}(B) \; . \end{aligned} \tag{4.70}$$

Although the electronic term in Hamiltonian (4.70) is *formally* diagonal on the operator level, one has to keep in mind that the chosen wave functions are not orthonormal with respect to the canonical scalar product. For this reason, the states $\underset{\sim}{a}^p_{mn\mu}(z)$ with $n \neq 0$ still indirectly couple to the impurity spin. As one of the *central approximations of NRG*, only the state with $n = 0$, i.e., $\underset{\sim}{a}^p_{m\mu}(z) \equiv \underset{\sim}{a}^p_{m0\mu}(z)$, is kept on each interval $I^p_m(z)$. Using the definition of $\varphi^p_{m0\mu}(z,\xi)$ from Eq. (4.39), the parameters $\widetilde{\mathcal{A}}^p_{m\mu}(z)$ are then determined by Eq. (4.62) with $n = n' = 0$ [CO05],

$$\int_{I^p_m(z)} \mathrm{d}\xi \left|\varphi^p_{m0\mu}(z,\xi)\right|^2 g^p_{m\mu}(z,\xi) \overset{(4.68)}{=} \widetilde{\mathcal{A}}^p_{m\mu}(z) \int_{I^p_m(z)} \frac{\mathrm{d}\xi}{\xi} \left|\varphi^p_{m0\mu}(z,\xi)\right|^2 = 1 \; , \tag{4.71}$$

which has the solution [CO04, CO05]:

$$\boxed{\widetilde{\mathcal{A}}^p_{m\mu}(z) = \frac{\int_{I^p_m(z)} \mathrm{d}\xi\, \gamma^p_\mu(\xi)}{\int_{I^p_m(z)} \frac{\mathrm{d}\zeta}{\zeta}\, \gamma^p_\mu(\zeta)} \; .} \tag{4.72}$$

This expression for the parameters is to be compared to the result (4.51) which is found in case of the standard discretization. Neglecting all states with $n \neq 0$ [CO05], the improved discretization scheme by Campo and Oliveira leads to the following *approximate* discrete representation of Hamiltonian (4.22) for the given twist parameter z:

$$
\begin{aligned}
\underset{\sim}{H}_{\mathrm{NRG}} \quad &\approx \quad W \sum_{\substack{p,m \\ \mu}} \widetilde{\mathcal{E}}^p_{m\mu}(z)\, \underset{\sim}{a}^{p\dagger}_{m\mu}(z) \underset{\sim}{a}^{p}_{m\mu}(z) \\
&\quad + \; J \underset{\sim}{\boldsymbol{S}} \cdot \sum_{\mu,\nu} \underset{\sim}{f}^{\dagger}_{0\mu} \frac{\boldsymbol{\sigma}_{\mu\nu}}{2} \underset{\sim}{f}_{0\nu} \; + \; \underset{\sim}{H}_{\mathrm{imp}}(B) \; , \qquad (4.73) \\
&\text{with} \\
\underset{\sim}{f}_{0\mu} \quad &= \quad \sum_{p,m} \sqrt{\frac{\mathcal{B}^p_\mu}{W} \mathcal{W}^p_{m\mu}(z)}\, \underset{\sim}{a}^{p}_{m\mu}(z) \; , \\
\widetilde{\mathcal{E}}^p_{m\mu}(z) \quad &\equiv \quad \frac{\mathcal{B}^p_\mu}{W} \widetilde{\mathcal{A}}^p_{m\mu}(z) \; = \; \frac{\mathcal{B}^p_\mu}{W} \frac{\int_{I^p_m(z)} \mathrm{d}\xi\, \gamma^p_\mu(\xi)}{\int_{I^p_m(z)} \frac{\mathrm{d}\zeta}{\zeta}\, \gamma^p_\mu(\zeta)} \; . \qquad (4.74)
\end{aligned}
$$

Compared to Eq. (4.52), which results from the standard discretization, different energies are assigned to the states $\underset{\sim}{a}^p_{m\mu}(z)$.

Using the standard discretization for a constant DOS, a complete set of orthonormal functions can be obtained by constructing a Fourier series in the variable ξ on each interval $I^p_m(z)$ [Wil75, KmWW80a]. In case of the improved discretization and a constant DOS, the relation (4.62) with the weight function (4.68) is instead fulfilled by a Fourier series in the variable $\ln \xi$ [CO05]. It can then be shown that the overlap of the zeroth mode $\varphi^p_{m0\mu}(z,\xi)$ and the remaining modes $\varphi^p_{mn\mu}(z,\xi)$ with $n \neq 0$ vanishes in the continuum limit $\Lambda \to 1$, so that the functions become orthogonal with respect to the canonical scalar product [CO05]. In particular, neglecting the states with $n \neq 0$ in Eq. (4.73) thus becomes exact for $\Lambda \to 1$.

For a constant DOS and arbitrary discretization parameter $\Lambda > 1$, the improved discretization by Campo and Oliveira gives, after z-averaging, the correct continuum result for the spectral density of the operator $\underset{\sim}{f}_{0\mu}$ over the whole energy range *without* the two intervals that directly border on the positive and negative band edge, respectively (see below) [CO05]. An *ad hoc* renormalization of coupling parameters as in the standard discretization is therefore not necessary. However, it has been found for a constant DOS that the spectral function of $\underset{\sim}{f}_{0\mu}$ is *not* correctly reproduced on the energy intervals $\big[W\big(1-\Lambda^{-1}\big)/\ln\Lambda, W\big]$ and $\big[-W, -W\big(1-\Lambda^{-1}\big)/\ln\Lambda\big]$ [ŽP09]. This shortcoming is finally solved by the latest discretization scheme proposed by Žitko and Pruschke [ŽP09, Žit09]. Their approach to the logarithmic discretization of the continuum of electronic states is described in Sec. 4.7.

For large values of the discretization parameter such as $\Lambda = 10$, the improved discretization has been found to give much better results than the standard discretization [CO04, CO05]. For example, the convergence of the results in Λ to the continuum limit $\Lambda \to 1$ is faster (see Fig. 11 of Ref. [ŽP09]) and fewer numerical artifacts are observed (for an extreme example, see Fig. 1 of Ref. [CO05]). However, different observables can have different requirements regarding the quality of the logarithmic discretization. For example, it is considered more difficult to obtain good results for the specific heat than, say, the magnetic susceptibility [CPLO97, CO05, BCP08].

4.6. Excursus: Continuum result for the spectral density of the operator $\underset{\sim}{f}_{0\mu}$

It turns out that the logarithmic discretization of the continuum of electronic states can be further improved by requiring that the discrete approximation to Hamiltonian (4.22) *without impurity* reproduces the spectral density of the operator $\underset{\sim}{f}_{0\mu}$ as good as possible with the chosen set of electronic states $\left\{\underset{\sim}{a}^p_{m\mu}(z)\right\}$ *after z-averaging.*

For this reason, we first introduce the concept of *spectral densities* (also called *spectral functions*) in this section and then derive the exact continuum result for the spectral density of the operator $\underset{\sim}{f}_{0\mu}$ from Eq. (4.20) (with respect to the *non-interacting electron part* of the full problem) by using the one-particle spectral function of the ideal fermionic quantum gas. The introduction to spectral densities is based on appendix B of the book [NR09].

4.6.1. Spectral densities

Let us consider the grand-canonical ensemble of statistical mechanics with the density operator

$$\underset{\sim}{\rho}_{\mathrm{GC}} \equiv \frac{\mathrm{e}^{-\beta \underset{\sim}{H}_{\mathrm{GC}}}}{Z_{\mathrm{GC}}} \,, \tag{4.75}$$

where we have introduced the partition function

$$Z_{\mathrm{GC}} \equiv \mathrm{tr}\left(\mathrm{e}^{-\beta \underset{\sim}{H}_{\mathrm{GC}}}\right) , \tag{4.76}$$

with $\underset{\sim}{H}_{\mathrm{GC}}$ defined in Eq. (2.16), and the standard abbreviation $\beta = 1/k_B T$. Thermodynamic expectation values are then calculated with respect to the density operator in the usual way:

$$\left\langle \underset{\sim}{A} \right\rangle \equiv \mathrm{tr}\left(\underset{\sim}{\rho}_{\mathrm{GC}}\, \underset{\sim}{A}\right) . \tag{4.77}$$

Measuring time in units of $\hbar$ (i.e., $\tau \equiv t/\hbar$), we furthermore define time-dependent operators in the Heisenberg picture [NR09]:

$$\underset{\sim}{A}(\tau) \equiv \mathrm{e}^{\mathrm{i}\tau \underset{\sim}{H}_{\mathrm{GC}}}\, \underset{\sim}{A}\, \mathrm{e}^{-\mathrm{i}\tau \underset{\sim}{H}_{\mathrm{GC}}} \,. \tag{4.78}$$

For the calculations, let us assume that we have a discrete orthonormal eigensystem of $\underset{\sim}{H}_{\mathrm{GC}}$:

$$\underset{\sim}{H}_{\mathrm{GC}}\,|E_n\rangle \;=\; E_n\,|E_n\rangle\;, \tag{4.79}$$

$$\langle E_n|E_m\rangle \;=\; \delta_{nm}\;, \tag{4.80}$$

$$\sum_n |E_n\rangle\langle E_n| \;=\; \underset{\sim}{\mathbb{1}}\;. \tag{4.81}$$

With these prerequisites, the *spectral density* (or *spectral function*) of two (fermionic) operators $\underset{\sim}{A}$ and $\underset{\sim}{B}$ is defined as [NR09]:

$$\boxed{\mathcal{S}_{AB}(\tau,\tau') \equiv \frac{1}{2\pi}\Big\langle \big\{\underset{\sim}{A}(\tau), \underset{\sim}{B}(\tau')\big\}\Big\rangle = \mathcal{S}_{AB}(\tau-\tau')\;.} \tag{4.82}$$

Here, we have assumed that the Hamiltonian does not explicitly depend on time. This causes the spectral density to be homogeneous in time. In the following, we are interested in the energy representation of the spectral density, which is obtained by means of a Fourier transformation [NR09]:

$$\boxed{\mathcal{S}_{AB}(E) \equiv \int\limits_{-\infty}^{\infty} \mathrm{d}(\tau-\tau')\,\mathcal{S}_{AB}(\tau-\tau')\,\mathrm{e}^{\mathrm{i}E(\tau-\tau')}\;.} \tag{4.83}$$

In order to illustrate the meaning and importance of $\mathcal{S}_{AB}$, which might be clouded by the abstract definition (4.82), we now derive the spectral representation of $\mathcal{S}_{AB}(E)$ with respect to the above eigensystem $\big\{|E_n\rangle\big\}$ of $\underset{\sim}{H}_{\mathrm{GC}}$. Using the identities (cf. Ref. [NR09])

$$Z_{\mathrm{GC}}\,\big\langle \underset{\sim}{A}(\tau)\underset{\sim}{B}(\tau')\big\rangle \;=\; \sum_{n,m} \mathrm{e}^{-\beta E_m}\big\langle E_n\big|\underset{\sim}{B}\big|E_m\big\rangle\big\langle E_m\big|\underset{\sim}{A}\big|E_n\big\rangle\,\mathrm{e}^{\mathrm{i}(E_m-E_n)(\tau-\tau')}\;, \tag{4.84}$$

$$Z_{\mathrm{GC}}\,\big\langle \underset{\sim}{B}(\tau')\underset{\sim}{A}(\tau)\big\rangle \;=\; \sum_{n,m} \mathrm{e}^{-\beta E_n}\big\langle E_n\big|\underset{\sim}{B}\big|E_m\big\rangle\big\langle E_m\big|\underset{\sim}{A}\big|E_n\big\rangle\,\mathrm{e}^{\mathrm{i}(E_m-E_n)(\tau-\tau')}\;, \tag{4.85}$$

and an integral representation of the delta function,

$$\delta(x) = \int\limits_{-\infty}^{\infty} \mathrm{d}\xi\,\mathrm{e}^{2\pi\mathrm{i}\,\xi x}\;, \tag{4.86}$$

Eqs. (4.82) and (4.83) can be combined to give the *spectral representation of the spectral density*:

$$\mathcal{S}_{AB}(E) = \frac{1}{Z_{\mathrm{GC}}}\sum_{n,m}\big\langle E_n\big|\underset{\sim}{B}\big|E_m\big\rangle\big\langle E_m\big|\underset{\sim}{A}\big|E_n\big\rangle\,\mathrm{e}^{-\beta E_n}\big(\mathrm{e}^{\beta E}+1\big)\,\delta\big(E-(E_n-E_m)\big)\;. \tag{4.87}$$

This equation simplifies in the limit $T \to 0$ or $\beta \to \infty$. With the energy E_0 of the groundstate and its degeneracy g_0, we obtain the following expressions for the *zero-temperature spectral density*, which might be more familiar than the definition (4.82):

$$\mathcal{S}_{AB}(T=0, E<0) = \frac{1}{g_0} \sum_{\substack{\{n_0\}, \\ m \notin \{n_0\}}} \langle E_{n_0} | \underset{\sim}{B} | E_m \rangle \langle E_m | \underset{\sim}{A} | E_{n_0} \rangle \, \delta\big(E - (E_{n_0} - E_m)\big) \,, \tag{4.88}$$

$$\mathcal{S}_{AB}(T=0, E>0) = \frac{1}{g_0} \sum_{\substack{\{m_0\}, \\ n \notin \{m_0\}}} \langle E_n | \underset{\sim}{B} | E_{m_0} \rangle \langle E_{m_0} | \underset{\sim}{A} | E_n \rangle \, \delta\big(E - (E_n - E_{m_0})\big) \,. \tag{4.89}$$

$\{m_0\}$ or $\{n_0\}$, respectively, is the set of indices labeling states with the groundstate energy E_0, i.e., $E_{n_0} = E_0$ and $E_{m_0} = E_0$.

As seen from the spectral representation (4.87), the spectral density is an important quantity since it contains information about all energy spacings in the spectrum of the Hamiltonian $\underset{\sim}{H}_{\mathrm{GC}}$ and about the matrix elements of the operators $\underset{\sim}{A}$ and $\underset{\sim}{B}$ with respect to the eigenstates of $\underset{\sim}{H}_{\mathrm{GC}}$. Combining the spectral representations of the correlation function from Eq. (4.85) and the spectral density from Eq. (4.87), the *spectral theorem* [NR09] is obtained:

$$\big\langle \underset{\sim}{B}(\tau') \underset{\sim}{A}(\tau) \big\rangle = \int_{-\infty}^{\infty} \mathrm{d}E \, \frac{\mathcal{S}_{AB}(E)}{\mathrm{e}^{\beta E} + 1} \, \mathrm{e}^{\mathrm{i}E(\tau' - \tau)} \,. \tag{4.90}$$

It shows that a suitable spectral density allows to calculate two-point correlation functions and (equal-time, i.e., $\tau = \tau'$) expectation values. In particular, the *one-electron spectral function* (note that the notation is simplified in the following by removing the redundant information about $\underset{\sim}{B} = \underset{\sim}{A}^\dagger$),

$$\mathcal{S}_{c_k}(E) \equiv \mathcal{S}_{c_k c_k^\dagger}(E) \,, \tag{4.91}$$

can be used to calculate $\big\langle \underset{\sim}{c}_k^\dagger \underset{\sim}{c}_k \big\rangle = \big\langle \underset{\sim}{n}_k \big\rangle$, which gives the Fermi-Dirac distribution.

4.6.2. One-electron spectral density of the ideal Fermi gas

We now derive the expression for the one-electron spectral density $\mathcal{S}_{c_k}(E)$ of the ideal (non-interacting) Fermi gas. Normally, one would use the formalism of Green's functions to calculate this quantity (see, e.g., App. B of Ref. [NR09]).

However, here we only use the definitions (4.82) and (4.83) in order to keep the discussion conceptually simple.

Let us consider "spinless" non-interacting fermions with the one-particle Hamiltonian

$$\underset{\sim}{H}_{\mathrm{GC}} = \sum_k (\varepsilon_k - \mu_{\mathrm{chem}}) \underset{\sim}{c}_k^\dagger \underset{\sim}{c}_k \; . \tag{4.92}$$

With the definitions

$$\left[\underset{\sim}{X}, \underset{\sim}{Y}\right]_m \equiv \left[\underset{\sim}{X}, \left[\underset{\sim}{X}, \underset{\sim}{Y}\right]_{m-1}\right] , \tag{4.93}$$

$$\left[\underset{\sim}{X}, \underset{\sim}{Y}\right]_0 \equiv \underset{\sim}{Y} , \tag{4.94}$$

and the identity

$$\left[\underset{\sim}{A}, \underset{\sim}{B}\,\underset{\sim}{C}\right] = \left\{\underset{\sim}{A}, \underset{\sim}{B}\right\} \underset{\sim}{C} - \underset{\sim}{B} \left\{\underset{\sim}{A}, \underset{\sim}{C}\right\} , \tag{4.95}$$

we find:

$$\left[\underset{\sim}{c}_k^\dagger \underset{\sim}{c}_k, \underset{\sim}{c}_k\right]_m = (-1)^m \underset{\sim}{c}_k \quad \text{for} \quad m \geq 0 \; . \tag{4.96}$$

The Hadamard lemma,

$$\mathrm{e}^{\underset{\sim}{X}} \underset{\sim}{Y} \mathrm{e}^{-\underset{\sim}{X}} = \sum_{m=0}^{\infty} \frac{1}{m!} \left[\underset{\sim}{X}, \underset{\sim}{Y}\right]_m , \tag{4.97}$$

then allows us to obtain the destruction operator in the Heisenberg picture:

$$\begin{aligned} \underset{\sim}{c}_k(\tau) &\equiv \mathrm{e}^{\mathrm{i}\tau \underset{\sim}{H}_{\mathrm{GC}}} \underset{\sim}{c}_k \mathrm{e}^{-\mathrm{i}\tau \underset{\sim}{H}_{\mathrm{GC}}} \\ &= \mathrm{e}^{\mathrm{i}\tau(\varepsilon_k - \mu_{\mathrm{chem}}) \underset{\sim}{c}_k^\dagger \underset{\sim}{c}_k} \underset{\sim}{c}_k \mathrm{e}^{-\mathrm{i}\tau(\varepsilon_k - \mu_{\mathrm{chem}}) \underset{\sim}{c}_k^\dagger \underset{\sim}{c}_k} \\ &= \underset{\sim}{c}_k \sum_{m=0}^{\infty} \frac{1}{m!} \big(- \mathrm{i}\tau(\varepsilon_k - \mu_{\mathrm{chem}}) \big)^m \\ &= \mathrm{e}^{-\mathrm{i}\tau(\varepsilon_k - \mu_{\mathrm{chem}})} \underset{\sim}{c}_k \; . \end{aligned} \tag{4.98}$$

From the last equation, it follows that

$$\left\{\underset{\sim}{c}_k(\tau), \underset{\sim}{c}_k^\dagger(\tau')\right\} = \mathrm{e}^{-\mathrm{i}(\varepsilon_k - \mu_{\mathrm{chem}})(\tau - \tau')} \; , \tag{4.99}$$

which directly gives the one-electron spectral density for arbitrary temperature $T \geq 0$:

$$\mathcal{S}_{c_k}(\tau - \tau') \equiv \frac{1}{2\pi} \left\langle \left\{\underset{\sim}{c}_k(\tau), \underset{\sim}{c}_k^\dagger(\tau')\right\} \right\rangle = \frac{1}{2\pi} \mathrm{e}^{-\mathrm{i}(\varepsilon_k - \mu_{\mathrm{chem}})(\tau - \tau')} \; . \tag{4.100}$$

With the integral representation (4.86) of the delta function and the identity $\delta(\alpha x) = \delta(x)/|\alpha|$, the energy representation of the one-electron spectral function for arbitrary temperature can be obtained by a Fourier transformation (cf. the result in App. B of Ref. [NR09]):

$$\boxed{\begin{aligned} \mathcal{S}_{c_k}(E) &= \int_{-\infty}^{\infty} \mathrm{d}x\, \frac{1}{2\pi}\, \mathrm{e}^{-\mathrm{i}(\varepsilon_k - \mu_{\mathrm{chem}})x}\, \mathrm{e}^{\mathrm{i}Ex} && (4.101) \\ &= \delta\big(E - (\varepsilon_k - \mu_{\mathrm{chem}})\big)\ . && (4.102) \end{aligned}}$$

4.6.3. Spectral density of $\underset{\sim}{f}_{0\mu}$

Let us now return to the original problem, i.e., to the calculation of the (non-interacting) spectral density of the operator $\underset{\sim}{f}_{0\mu}$ defined in Eq. (4.20):

$$\mathcal{S}_{f_{0\mu}}(\tau - \tau') = \frac{1}{2\pi} \Big\langle \big\{ \underset{\sim}{f}_{0\mu}(\tau), \underset{\sim}{f}^{\dagger}_{0\mu}(\tau') \big\} \Big\rangle\ . \tag{4.103}$$

By comparing the interaction terms in the Hamiltonians (4.22) and (2.17) (also note Eq. (2.14)), we see that, in the original discrete representation, the state $\underset{\sim}{f}_{0\mu}$ can be written as:

$$\boxed{\underset{\sim}{f}_{0\mu} = \frac{1}{\sqrt{L^d}} \sum_{\boldsymbol{k}} \underset{\sim}{c}_{\boldsymbol{k}\mu}\ .} \tag{4.104}$$

Generalizing the result (4.98) for the "spinless" Fermi gas to the spin-dependent case with the one-particle Hamiltonian

$$\underset{\sim}{H}_{\mathrm{GC}} = \sum_{\boldsymbol{k},\mu} (\varepsilon_{\boldsymbol{k}\mu} - \mu_{\mathrm{chem}}) \underset{\sim}{c}^{\dagger}_{\boldsymbol{k}\mu} \underset{\sim}{c}_{\boldsymbol{k}\mu}\ , \tag{4.105}$$

the operator $\underset{\sim}{f}_{0\mu}$ in the Heisenberg picture is obtained:

$$\underset{\sim}{f}_{0\mu}(\tau) = \frac{1}{\sqrt{L^d}} \sum_{\boldsymbol{k}} \underset{\sim}{c}_{\boldsymbol{k}\mu}(\tau) = \frac{1}{\sqrt{L^d}} \sum_{\boldsymbol{k}} \mathrm{e}^{-\mathrm{i}\tau(\varepsilon_{\boldsymbol{k}\mu} - \mu_{\mathrm{chem}})} \underset{\sim}{c}_{\boldsymbol{k}\mu}\ . \tag{4.106}$$

This result gives us the anticommutator,

$$\big\{ \underset{\sim}{f}_{0\mu}(\tau), \underset{\sim}{f}^{\dagger}_{0\mu}(\tau') \big\} = \frac{1}{L^d} \sum_{\boldsymbol{k}} \mathrm{e}^{-\mathrm{i}(\varepsilon_{\boldsymbol{k}\mu} - \mu_{\mathrm{chem}})(\tau - \tau')}\ , \tag{4.107}$$

and thereby the spectral function for arbitrary temperature:

$$\mathcal{S}_{f_{0\mu}}(\tau - \tau') = \frac{1}{2\pi\, L^d} \sum_{\boldsymbol{k}} \mathrm{e}^{-\mathrm{i}(\varepsilon_{\boldsymbol{k}\mu} - \mu_{\mathrm{chem}})(\tau - \tau')}\ . \tag{4.108}$$

Finally, by Fourier transformation and comparison with the definition (4.6) of the density of states $\rho(\varepsilon)$, we find the *exact continuum result* for the energy representation of the spectral density of the operator $\underset{\sim}{f}_{0\mu}$:

$$\begin{aligned} \mathcal{S}_{f_{0\mu}}(E) &= \frac{1}{L^d} \sum_{\boldsymbol{k}} \delta\big(E - (\varepsilon_{\boldsymbol{k}\mu} - \mu_{\mathrm{chem}})\big) \quad (4.109) \\ &= \rho(E - \mu h + \mu_{\mathrm{chem}}) \; . \quad (4.110) \end{aligned}$$

In an exact calculation, the *non-interacting* spectral function of the operator $\underset{\sim}{f}_{0\mu}$ is thus equal to the density of states of the conduction electrons for arbitrary temperature (taking into account the chemical potential and the magnetic field).

4.7. Logarithmic discretization III: "Optimal" discretization by Žitko & Pruschke

Compared to the standard discretization, the improved discretization by Campo and Oliveira [CO04, CO05] leads to results with a superior convergence in Λ. For a constant DOS [CO05] and a semi-elliptical DOS (see Fig. 6 of Ref. [ŽP09]), it has furthermore been shown analytically that an *ad hoc* renormalization of the coupling parameter is no longer necessary in order to give the correct value of the DOS at the Fermi level. However, even for a constant DOS, the improved discretization by Campo and Oliveira cannot correctly reproduce the spectral density of the operator $\underset{\sim}{f}_{0\mu}$ over the *whole* energy range (see Fig. 5 of Ref. [ŽP09]). In addition to numerical artifacts at low energies (see Fig. 4 b of Ref. [ŽP09]), there are in general pronounced *band edge artifacts* which appear at energies close to the half-bandwidth W.

In order to further improve the logarithmic discretization of the continuum of electronic states, Žitko and Pruschke [ŽP09] have introduced an alternative scheme for determining the energies that appear in the discrete approximation to Hamiltonian (4.22), which was subsequently extended by Žitko [Žit09]. Despite the "derivations" presented in the previous sections 4.4 and 4.5, the assignment of an energy to an interval according to the prescriptions of the standard and improved discretization is at least somewhat arbitrary. As a superior alternative, Žitko and Pruschke have proposed to *choose* certain energies in order to "optimally" describe the interaction between electrons and impurity spin using a discrete approximation to Hamiltonian (4.22). To this end, an energy is assigned to each interval in such a way that *after z-averaging* the exact result for the spectral function $\mathcal{S}_{f_{0\mu}}(\varepsilon)$ from Eq. (4.110) is reproduced as good as possible. This approach is intended to provide a discrete approximation that accurately describes the properties of the state $\underset{\sim}{f}_{0\mu}$ and thereby also the interaction between electrons and impurity. For an energy-dependent DOS, the logarithmic grid may now differ from the one defined by Eqs. (4.32) and (4.33). The full version of the new discretization scheme makes

use of an adaptive logarithmic grid that can be optimized to take into account the particular energy-dependence of the DOS [Žit09].

For the chosen twist parameter z and a given division of the integration ranges in Hamiltonian (4.22) into intervals, we proceed as before by selecting the known state $\underset{\sim}{a}^p_{m\mu}(z)$ from Eq. (4.41), using the weight function (4.39), on each interval $I^p_{m\mu}(z)$. Recall that the choice of these particular states is not arbitrary since they allow for an exact representation of the operator $\underset{\sim}{f}_{0\mu}$ according to Eq. (4.43). As one of the central NRG approximations, Hamiltonian (4.22) is then again reduced to the set of new states $\left\{\underset{\sim}{a}^p_{m\mu}(z)\right\}$ (cf. Eqs. (4.52) and (4.73)). However, now we want to *choose* the intervals $I^p_{m\mu}(z)$ and the energies $W\bar{\mathcal{E}}^p_{m\mu}(z)$ that are assigned to them in an "optimal" way.

For given twist parameter $z \in (0, 1]$, a discretization grid with intervals $I^p_{m\mu}(z)$ is defined by points $\Xi^p_{m\mu}(z)$ (cf. Fig. 4.2) [Žit09]:

$$\boxed{\begin{aligned} I^+_{m\mu}(z) &\equiv \left[\Xi^+_{m+1\mu}(z),\, \Xi^+_{m\mu}(z)\right] \quad \text{with} \quad m \geq 0\,, \qquad (4.111)\\ I^-_{m\mu}(z) &\equiv \left[\Xi^-_{m\mu}(z),\, \Xi^-_{m+1\mu}(z)\right] \quad \text{with} \quad m \geq 0\,. \qquad (4.112)\end{aligned}}$$

This discretization mesh has to satisfy some basic requirements [Žit09]:

$$\Xi^+_{0\mu}(z) \equiv 1\,, \qquad \Xi^+_{m+1\mu}(z) < \Xi^+_{m\mu}(z)\,, \qquad \lim_{m\to\infty} \Xi^+_{m\mu}(z) = 0\,, \tag{4.113}$$

$$\Xi^-_{0\mu}(z) \equiv -1\,, \quad \Xi^-_{m\mu}(z) \quad < \Xi^-_{m+1\mu}(z)\,, \quad \lim_{m\to\infty} \Xi^-_{m\mu}(z) = 0\,. \tag{4.114}$$

Since we still aim at an arbitrarily high energy resolution close to the point $\xi = 0$, i.e., around the Fermi energy, we introduce the discretization parameter $\Lambda > 1$ and require the *same asymptotic dependence* of the grid points on m as in the standard discretization (cf. Eqs. (4.32) and (4.33)) [Žit09]:

$$\boxed{\begin{aligned} \Xi^+_{m\mu}(z) &\sim \quad \Lambda^{-m} \quad \text{for} \quad m \gg 1\,, \qquad (4.115)\\ \Xi^-_{m\mu}(z) &\sim -\Lambda^{-m} \quad \text{for} \quad m \gg 1\,. \qquad (4.116)\end{aligned}}$$

As illustrated by Fig. 4.3, the following "continuity conditions" have to be additionally fulfilled to allow for a meaningful z-averaging [Žit09]:

$$\Xi^+_{0\mu}(z) \equiv 1 \quad \forall\, z\,, \qquad \Xi^+_{m+1\mu}(0) = \Xi^+_{m\mu}(1) \quad \forall\, m\,, \tag{4.117}$$

$$\Xi^-_{0\mu}(z) \equiv -1 \;\forall\, z\,, \qquad \Xi^-_{m\mu}(1) \quad = \Xi^-_{m+1\mu}(0) \;\forall\, m\,. \tag{4.118}$$

To each interval $I^p_{m\mu}(z)$ a (yet unknown) representative dimensionless parameter $\bar{\mathcal{A}}^p_{m\mu}(z)$ is assigned. For a meaningful z-averaging, these parameters have to cover the whole integration range in Hamiltonian (4.22) when the twist parameter is continuously varied between 0 and 1 (cf. Fig. 4.3 (c)) [Žit09]:

$$\bar{\mathcal{A}}^{+}_{0\mu}(0) \equiv 1 \,, \qquad \bar{\mathcal{A}}^{+}_{m+1\mu}(0) = \bar{\mathcal{A}}^{+}_{m\mu}(1) \quad \forall\, m \,, \tag{4.119}$$

$$\bar{\mathcal{A}}^{-}_{0\mu}(0) \equiv -1 \,, \qquad \bar{\mathcal{A}}^{-}_{m\mu}(1) \;\; = \bar{\mathcal{A}}^{-}_{m+1\mu}(0) \;\; \forall\, m \,. \tag{4.120}$$

Keeping the state $\underset{\sim}{a}^{p}_{m\mu}(z)$ defined by Eqs. (4.39) and (4.41) on each interval $I^{p}_{m\mu}(z)$ as before [ŽP09], we obtain the following discrete approximation to the conduction band Hamiltonian (cf. the terms appearing in Eqs. (4.52) and (4.73)):

$$\underset{\sim}{H}_{\mathrm{cb}}(z) \;\equiv\; W \sum_{\substack{p,m \\ \mu}} \frac{\mathcal{B}^{p}_{\mu}}{W} \bar{\mathcal{A}}^{p}_{m\mu}(z)\, \underset{\sim}{a}^{p\dagger}_{m\mu}(z) \underset{\sim}{a}^{p}_{m\mu}(z) \tag{4.121}$$

$$\equiv\; W \sum_{\substack{p,m \\ \mu}} \bar{\mathcal{E}}^{p}_{m\mu}(z)\, \underset{\sim}{a}^{p\dagger}_{m\mu}(z) \underset{\sim}{a}^{p}_{m\mu}(z) \,. \tag{4.122}$$

Furthermore, there is the special state from Eq. (4.43) that directly couples to the impurity spin. Defining

$$w^{p}_{m\mu}(z) \equiv \frac{\mathcal{B}^{p}_{\mu}}{W}\, \mathcal{W}^{p}_{m\mu}(z) \overset{(4.36)}{\underset{(4.37)}{=}} \int_{I^{p}_{m\mu}(z)} \mathrm{d}\xi\, \gamma^{p}_{\mu}(\xi) \,, \tag{4.123}$$

it has the following expansion [Žit09]:

$$\boxed{\underset{\sim}{f}_{0\mu} = \sum_{p,m} \sqrt{w^{p}_{m\mu}(z)}\, \underset{\sim}{a}^{p}_{m\mu}(z) \,.} \tag{4.124}$$

As the next step, the *z-averaged spectral density* of the operator $\underset{\sim}{f}_{0\mu}$ with respect to Hamiltonian (4.122) is calculated using results from the previous section 4.6:

$$\underset{\sim}{a}^{p}_{m\mu}(z,\tau) \;\equiv\; \mathrm{e}^{\mathrm{i}\tau \underset{\sim}{H}_{\mathrm{cb}}(z)}\, \underset{\sim}{a}^{p}_{m\mu}(z)\, \mathrm{e}^{-\mathrm{i}\tau \underset{\sim}{H}_{\mathrm{cb}}(z)} \tag{4.125}$$

$$\overset{(4.98)}{=}\; \mathrm{e}^{-\mathrm{i}\tau W \bar{\mathcal{E}}^{p}_{m\mu}(z)}\, \underset{\sim}{a}^{p}_{m\mu}(z) \,, \tag{4.126}$$

$$\big\{ \underset{\sim}{a}^{p}_{m\mu}(z,\tau), \underset{\sim}{a}^{p\dagger}_{m\mu}(z,\tau') \big\} \overset{(4.99)}{=}\; \mathrm{e}^{-\mathrm{i}W \bar{\mathcal{E}}^{p}_{m\mu}(z)[\tau-\tau']} \tag{4.127}$$

$$\overset{(4.100)}{=}\; 2\pi\, \mathcal{S}_{a^{p}_{m\mu}(z)}(\tau - \tau') \,. \tag{4.128}$$

Paying attention to the codomain of the energies $W\bar{\mathcal{E}}^{p}_{m\mu}(z)$, a Fourier transformation $\tau \to \tilde{\varepsilon}$ (cf. the definitions (4.8) of $\tilde{\varepsilon}$ and (4.14) of $\mathcal{B}^{p}_{\mu}$, and the result (4.102)) then gives:

$$\mathcal{S}_{a^{p}_{m\mu}(z)}(\tilde{\varepsilon}) = \delta\big(\tilde{\varepsilon} - W\bar{\mathcal{E}}^{p}_{m\mu}(z)\big) \,. \tag{4.129}$$

Using the representation (4.124) and the additivity of the contributions from the different states in the non-interacting case expressed by Eq. (4.109), we finally obtain:

$$\mathcal{S}_{f_{0\mu}}(z,\tilde{\varepsilon}) = \sum_{p,m} w^p_{m\mu}(z)\,\delta\big(\tilde{\varepsilon} - W\bar{\mathcal{E}}^p_{m\mu}(z)\big)\ . \tag{4.130}$$

For the one-particle Hamiltonian (4.122), a continuous z-averaging restores the continuum limit,

$$\boxed{\mathcal{S}_{f_{0\mu}}(\tilde{\varepsilon}) \equiv \int_0^1 \mathrm{d}z\,\mathcal{S}_{f_{0\mu}}(z,\tilde{\varepsilon}) = \int_0^1 \mathrm{d}z \sum_{p,m} w^p_{m\mu}(z)\,\delta\big(\tilde{\varepsilon} - W\bar{\mathcal{E}}^p_{m\mu}(z)\big)\ ,} \tag{4.131}$$

so that we can compare with the exact result for the spectral density from Eq. (4.110) (using $\mu_{\mathrm{chem}} \equiv \varepsilon_F$ as before):

$$\mathcal{S}^{\mathrm{exact}}_{f_{0\mu}}(\tilde{\varepsilon}) = \rho(\tilde{\varepsilon} - \mu h + \varepsilon_F)\ . \tag{4.132}$$

In order to make contact with the discretization grid introduced at the beginning of this section, let us go back to the variables ξ^+_μ and ξ^-_μ that appear in the dimensionless representation (4.22). For example, using the definition (4.15) and setting $\xi \equiv \xi^+_\mu$, we have for $\tilde{\varepsilon} > 0$:

$$\int_0^{W+\mu h-\varepsilon_F} \mathrm{d}\tilde{\varepsilon}\ \mathcal{S}^{\mathrm{exact}}_{f_{0\mu}}(\tilde{\varepsilon}) = \int_0^1 \mathrm{d}\xi\,\mathcal{B}^+_\mu\,\rho\big(\xi\mathcal{B}^+_\mu - \mu h + \varepsilon_F\big) \equiv \int_0^1 \mathrm{d}\xi\ \widetilde{\mathcal{S}}^{\mathrm{exact}}_{f_{0\mu}}(\xi)\ . \tag{4.133}$$

A comparison with the definition (4.36) shows that in an exact calculation the following equalities hold:

$$\boxed{\widetilde{\mathcal{S}}^{\mathrm{exact}}_{f_{0\mu}}(\xi) = \begin{cases} \mathcal{B}^+_\mu\,\rho\big(\xi\mathcal{B}^+_\mu - \mu h + \varepsilon_F\big) = \gamma^+_\mu(\xi) & ,\quad \text{for} \quad \xi > 0 \\ \mathcal{B}^-_\mu\,\rho\big(\xi\mathcal{B}^-_\mu - \mu h + \varepsilon_F\big) = \gamma^-_\mu(\xi) & ,\quad \text{for} \quad \xi < 0 \end{cases}\ .} \tag{4.134}$$

We are now ready to formulate the *central requirement* of the alternative discretization by Žitko and Pruschke: *After a continuous z-averaging*, the exact continuum result for the spectral density of the operator $\underset{\sim}{f}_{0\mu}$ shall be recovered [ŽP09, Žit09]:

$$\widetilde{\mathcal{S}}_{f_{0\mu}}(\xi) = \mathcal{B}_\mu^p \, \mathcal{S}_{f_{0\mu}}\big(\xi \mathcal{B}_\mu^p\big) \tag{4.135}$$

$$= \int_0^1 \mathrm{d}z \sum_{p,m} w_{m\mu}^p(z) \, \delta\big(\xi - \underbrace{W \bar{\mathcal{E}}_{m\mu}^p(z)/\mathcal{B}_\mu^p}_{= \bar{\mathcal{A}}_{m\mu}^p(z)}\big) \tag{4.136}$$

$$\stackrel{!}{=} \begin{cases} \gamma_\mu^+(\xi) & , \quad \text{for} \quad \xi > 0 \\ \gamma_\mu^-(\xi) & , \quad \text{for} \quad \xi < 0 \end{cases} . \tag{4.137}$$

By using an identity for the delta function,

$$\delta\big(f(x)\big) = \sum_i \frac{\delta(x - x_i)}{\left| \frac{\mathrm{d}f(x)}{\mathrm{d}x} \right|_{x = x_i}} , \tag{4.138}$$

which holds for a function $f(x)$ that only has simple roots x_i, the delta function can be eliminated from Eq. (4.136) (cf. Ref. [Žit09]):

$$\widetilde{\mathcal{S}}_{f_{0\mu}}(\xi) = \left. \frac{w_{m\mu}^p(z)}{\left((-p) \frac{\mathrm{d}\bar{\mathcal{A}}_{m\mu}^p(z)}{\mathrm{d}z}\right)} \right|_{\substack{p,m,z: \\ \xi = \bar{\mathcal{A}}_{m\mu}^p(z)}} . \tag{4.139}$$

Note the following two points:

- We have assumed that $\bar{\mathcal{A}}_{m\mu}^p(z)$ is monotonically decreasing (increasing) as a function of z for $p = +$ $(-)$. According to the basic requirements for the discretization grid from Eqs. (4.113) and (4.114), $\bar{\mathcal{A}}_{m\mu}^p(z)$ is furthermore monotonically decreasing (increasing) as a function of m for $p = +$ $(-)$.

- In combination with the continuity requirements from Eqs. (4.119) and (4.120), this means that the equation $\xi = \bar{\mathcal{A}}_{m\mu}^p(z)$ has a unique solution for all $\xi \in [-1, 1]$ (i.e., the indices p and m, and the twist parameter z, are uniquely determined).

For a solution of Eq. (4.137), it is convenient to change to a "continuous indexing" [ŽP09, Žit09]:

$$\boxed{x \equiv m + z \quad \Rightarrow \quad x \in (0, \infty) \, ,} \tag{4.140}$$

$$\Xi_{m\mu}^p(z) \; \to \; \Xi_\mu^p(x) \, , \quad \bar{\mathcal{A}}_{m\mu}^p(z) \; \to \; \bar{\mathcal{A}}_\mu^p(x) \, , \quad w_{m\mu}^p(z) \; \to \; w_\mu^p(x) \, . \tag{4.141}$$

According to the requirements formulated at the beginning of this section, the functions $\Xi_\mu^p(x)$ and $\bar{\mathcal{A}}_\mu^p(x)$ are assumed to be monotonically decreasing (increasing) for $p = +$ $(-)$, and they have to respect the following boundary conditions:

$$\Xi_\mu^+(x) = 1 \quad \text{for} \quad x \in (0,1] \,, \qquad \lim_{x\to\infty} \Xi_\mu^+(x) = 0 \,, \tag{4.142}$$

$$\Xi_\mu^-(x) = -1 \quad \text{for} \quad x \in (0,1] \,, \qquad \lim_{x\to\infty} \Xi_\mu^-(x) = 0 \,, \tag{4.143}$$

$$\lim_{x\to 0} \bar{\mathcal{A}}_\mu^+(x) = 1 \,, \qquad \lim_{x\to\infty} \bar{\mathcal{A}}_\mu^+(x) = 0 \,, \tag{4.144}$$

$$\lim_{x\to 0} \bar{\mathcal{A}}_\mu^-(x) = -1 \,, \quad \lim_{x\to\infty} \bar{\mathcal{A}}_\mu^-(x) = 0 \,. \tag{4.145}$$

Since the functions $\bar{\mathcal{A}}_\mu^p(x)$ are bijective, we may introduce (well-defined) inverse functions $\mathcal{R}_\mu^p\big(\xi_\mu^p\big)$ [Žit09]:

$$\mathcal{R}_\mu^p \;:\; \mathcal{R}_\mu^p\big(\bar{\mathcal{A}}_\mu^p(x)\big) = x \,, \tag{4.146}$$

$$\bar{\mathcal{A}}_\mu^p\big(\mathcal{R}_\mu^p\big(\xi_\mu^p\big)\big) = \xi_\mu^p \,, \tag{4.147}$$

$$\boxed{\bar{\mathcal{A}}_\mu^p(x) = \xi_\mu^p \quad \Longleftrightarrow \quad x = \mathcal{R}_\mu^p\big(\xi_\mu^p\big) \,.} \tag{4.148}$$

Using the continuous index x and the inverse functions $\mathcal{R}_\mu^p(\xi)$, Eq. (4.139) can be written as:

$$\widetilde{\mathcal{S}}_{f_{0\mu}}(\xi) = \left.\frac{w_\mu^p(x)}{\left((-p)\frac{\mathrm{d}\bar{\mathcal{A}}_\mu^p(x)}{\mathrm{d}x}\right)}\right|_{x\,=\,\mathcal{R}_\mu^p(\xi)} \,. \tag{4.149}$$

According to the requirement (4.137) for the spectral density, we thus have to find a solution $\bar{\mathcal{A}}_\mu^p(x)$, respecting the boundary conditions (4.144) or (4.145), respectively, to the following *ordinary differential equation (ODE)* (cf. Refs. [ŽP09] and [Žit09]):

$$\left.\frac{w_\mu^p(x)}{\left((-p)\frac{\mathrm{d}\bar{\mathcal{A}}_\mu^p(x)}{\mathrm{d}x}\right)}\right|_{x\,=\,\mathcal{R}_\mu^p(\xi)} = \gamma_\mu^p(\xi) \,, \tag{4.150}$$

with

$$w_\mu^p(x) \overset{(4.123)}{=} p \int_{\Xi_\mu^p(x+1)}^{\Xi_\mu^p(x)} \mathrm{d}\zeta\, \gamma_\mu^p(\zeta) \,. \tag{4.151}$$

By including the point $x = 0$, this ODE is then cast into the *final initial value problem* with an additional boundary condition for $x \to \infty$ [ŽP09, Žit09]:

$$\boxed{\begin{aligned} \frac{\mathrm{d}\bar{\mathcal{A}}^p_\mu(x)}{\mathrm{d}x} &= \frac{\int\limits_{\Xi^p_\mu(x)}^{\Xi^p_\mu(x+1)} \mathrm{d}\zeta\, \gamma^p_\mu(\zeta)}{\gamma^p_\mu\big(\bar{\mathcal{A}}^p_\mu(x)\big)} \quad \text{for} \quad x \in [0,\infty)\ , \\ &\text{with} \quad \bar{\mathcal{A}}^p_\mu(0) \equiv p \quad \text{and} \quad \lim_{x\to\infty} \bar{\mathcal{A}}^p_\mu(x) = 0\ . \end{aligned}} \tag{4.152}$$

Before Eq. (4.152) can be solved, we need a solution for the discretization grid $\Xi^p_\mu(x)$ for $x > 1$. The standard grid with $\Xi^p_{0\mu}(z) = p$ and $\Xi^p_{m\mu}(z) = p\,\Lambda^{1-m-z}$ for $m \geq 1$ (cf. Eqs. (4.32) and (4.33)) corresponds to the following solution for $\Xi^p_\mu(x)$:

$$\boxed{\Xi^p_\mu(x) = \Xi^p(x) = \begin{cases} p & , \quad \text{for} \quad x \in (0,1] \\ p\,\Lambda^{1-x} & , \quad \text{for} \quad x \in (1,\infty) \end{cases}\ .} \tag{4.153}$$

Because of the desired asymptotic behavior of the grid, we use the ansatz [Žit09]

$$\Xi^p_\mu(x) \equiv f^p_\mu(x)\,\Lambda^{1-x} \quad \text{for} \quad x \in [1,\infty)\ , \tag{4.154}$$

and require for the corresponding ODE [Žit09]:

$$\frac{\mathrm{d}\Xi^p_\mu(x)}{\mathrm{d}x} = -\ln(\Lambda)\,\Lambda^{1-x}\,\Phi^p_\mu\big(x, \Xi^p_\mu(x), \Lambda\big)\ , \tag{4.155}$$

with a function Φ^p_μ *of our choice*. Since $\mathrm{d}\Lambda^{1-x}/\mathrm{d}x = -\ln(\Lambda)\,\Lambda^{1-x}$, the desired asymptotic behavior of $\Xi^p_\mu(x)$ is obtained if

$$\lim_{\substack{x\to\infty \\ \Xi^p_\mu\to 0}} \Phi^p_\mu\big(x, \Xi^p_\mu, \Lambda\big) = \text{const.} \begin{cases} > 0 & , \quad \text{for} \quad p = + \\ < 0 & , \quad \text{for} \quad p = - \end{cases}\ . \tag{4.156}$$

Possible choices for the function $\Phi^p_\mu\big(x, \Xi^p_\mu, \Lambda\big)$ are:

1. $\Phi^p_\mu\big(x, \Xi^p_\mu, \Lambda\big) \equiv p$ leads to the standard discretization grid (4.153).

2. For an *adaptive discretization grid*, we may use [Žit09]

$$\Phi^p_\mu\big(x, \Xi^p_\mu, \Lambda\big) \equiv \frac{\alpha^p_\mu}{\gamma^p_\mu\big(\Xi^p_\mu\big)}\ , \tag{4.157}$$

   with a constant α^p_μ. The idea behind this ansatz is the following: If $\gamma^p_\mu\big(\Xi^p_\mu\big)$ is small (i.e., if the density of states is low), $\big|\Phi^p_\mu\big|$ and thus also $\big|\mathrm{d}\Xi^p_\mu/\mathrm{d}x\big|$ become large. As a consequence, there is a fast decrease of $\big|\Xi^p_\mu(x)\big|$ for increasing x, which leads to larger intervals $I^p_{m\mu}(z)$, and therefore a coarser discretization, in energy regimes with low density of states. The choice (4.157) for Φ^p_μ results in the following differential equation for the discretization grid:

$$\frac{\mathrm{d}\Xi^p_\mu(x)}{\mathrm{d}x} = -\ln(\Lambda)\,\Lambda^{1-x}\frac{\alpha^p_\mu}{\gamma^p_\mu\big(\Xi^p_\mu(x)\big)} \quad \text{for} \quad x \in (1,\infty)\ . \tag{4.158}$$

Separation of variables and integration of $\gamma_\mu^p\big(\Xi_\mu^p\big)\mathrm{d}\Xi_\mu^p = -\alpha_\mu^p \ln(\Lambda)\,\Lambda^{1-x}\,\mathrm{d}x$ gives (cf. the result in Ref. [Žit09]):

$$\alpha_\mu^p = \int_0^p \mathrm{d}\xi\,\gamma_\mu^p(\xi)\;. \tag{4.159}$$

For a constant DOS, the choice (4.157) therefore corresponds to the first possibility, i.e., $\Phi_\mu^p\big(x,\Xi_\mu^p,\Lambda\big) \equiv p$.

For actually solving the differential equation (4.152), it is convenient to use an ansatz for $\bar{\mathcal{A}}_\mu^p(x)$ analogous to Eq. (4.154) [ŽP09, Žit09]:

$$\bar{\mathcal{A}}_\mu^p(x) \equiv g_\mu^p(x)\,\Lambda^{1-x} \quad \text{for} \quad x \in [0,\infty)\;. \tag{4.160}$$

Inserting the definitions (4.154) and (4.160) into the corresponding ODE, the following two initial value problems are obtained (cf. Ref. [Žit09]):

$$\begin{aligned}\frac{\mathrm{d}f_\mu^p(x)}{\mathrm{d}x} &= \ln(\Lambda)\Big(f_\mu^p(x) - \Phi_\mu^p\big(x, f_\mu^p(x)\Lambda^{1-x},\Lambda\big)\Big) \quad \text{for} \quad x \in [1,\infty)\\ &\text{with} \quad f_\mu^p(1) \equiv p\;,\end{aligned} \tag{4.161}$$

$$\begin{aligned}\frac{\mathrm{d}g_\mu^p(x)}{\mathrm{d}x} &= \ln(\Lambda)\,g_\mu^p(x) + \frac{\int_{\Xi_\mu^p(x)}^{\Xi_\mu^p(x+1)} \mathrm{d}\zeta\,\gamma_\mu^p(\zeta)}{\Lambda^{1-x}\,\gamma_\mu^p\big(g_\mu^p(x)\Lambda^{1-x}\big)} \quad \text{for} \quad x \in [0,\infty)\\ &\text{with} \quad g_\mu^p(0) \equiv p\,\Lambda^{-1}\;.\end{aligned} \tag{4.162}$$

In a numerical solution, it has to be taken into account that the differential equations for $f_\mu^p(x)$ and $g_\mu^p(x)$ are stiff [Žit09, ŽP09].

In summary, the alternative discretization by Žitko and Pruschke leads to the following discrete *approximation* to Hamiltonian (4.22) for the given twist parameter z:

$$\underset{\sim}{H}_{\mathrm{NRG}} \approx W \sum_{\substack{p,m \\ \mu}} \bar{\mathcal{E}}^p_{m\mu}(z)\, \underset{\sim}{a}^{p\dagger}_{m\mu}(z) \underset{\sim}{a}^{p}_{m\mu}(z) + J \underset{\sim}{\boldsymbol{S}} \cdot \sum_{\mu,\nu} \underset{\sim}{f}^{\dagger}_{0\mu} \frac{\boldsymbol{\sigma}_{\mu\nu}}{2} \underset{\sim}{f}_{0\nu} + \underset{\sim}{H}_{\mathrm{imp}}(B)\,, \tag{4.163}$$

with

$$\underset{\sim}{f}_{0\mu} = \sum_{p,m} \sqrt{\frac{\mathcal{B}^p_\mu}{W} \mathcal{W}^p_{m\mu}(z)}\, \underset{\sim}{a}^{p}_{m\mu}(z)\,,$$

$$\bar{\mathcal{E}}^p_{m\mu}(z) = \frac{\mathcal{B}^p_\mu}{W} \bar{\mathcal{A}}^p_{m\mu}(z)\,,$$

and

$\bar{\mathcal{A}}^p_{m\mu}(z)$ as obtained from the solution $\bar{\mathcal{A}}^p_\mu(x)$ of Eq. (4.152) for the chosen grid $\Xi^p_\mu(x)$ (using $x = m + z$).

Note that the use of the "optimal discretization" does not make NRG an exact method (to begin with, it is not possible to carry out the continuous z-averaging that is done in Eq. (4.131) in an actual calculation). The obtained results will therefore still suffer from artifacts. However, the alternative discretization by Žitko and Pruschke can be expected to alleviate them [ŽP09, Žit09]. For example, the non-interacting spectral densities of $\underset{\sim}{f}_{0\mu}$ in case of a constant DOS (see Fig. 7 of Ref. [ŽP09]) and a semi-elliptical DOS (see Fig. 9 of Ref. [ŽP09]) are significantly better reproduced. Furthermore, the discretization by Žitko and Pruschke leads to even better convergence in Λ than the improved discretization by Campo and Oliveira (as, e.g., demonstrated in Fig. 11 of Ref. [ŽP09]).

If the DOS features large and rapid variations, it might be a good idea to use an adaptive discretization grid [Žit09]. The problems in reproducing the spectral density of $\underset{\sim}{f}_{0\mu}$ are apparently especially severe if the DOS is small or even zero over an extended energy range (see Figs. 1 and 2 of Ref. [Žit09]). For a further improvement of the obtained results, one can try to optimize the discretization mesh through the choice of the function Φ^p_μ (for a few ideas, see Ref. [Žit09]). It might also be possible to remove some of the remaining artifacts by averaging over results for different values of the discretization parameter Λ (this has been done in Ref. [CO04], as stated in Ref. [CO05]).

4.8. Parameters of the logarithmically discretized Hamiltonian for a constant density of states

In case of a constant DOS (i.e., $\rho(\varepsilon) \equiv \rho$), the expression for the "weight function" $\gamma_\mu^p(\xi)$ from Eq. (4.36) simplifies:

$$\boxed{\gamma_\mu^p(\xi) = \gamma_\mu^p = \rho\, \mathcal{B}_\mu^p\ .} \tag{4.164}$$

In the standard discretization, the parameters $\mathcal{A}_{m\mu}^p(z)$ appearing in the logarithmically discretized Hamiltonian are calculated according to Eq. (4.51). For a constant DOS, this equation reads as

$$\mathcal{A}_{m\mu}^p(z) = \mathcal{A}_m^p(z) = \frac{\int_{I_m^p(z)} \mathrm{d}\xi\, \xi}{\int_{I_m^p(z)} \mathrm{d}\zeta} \tag{4.165}$$

and leads to the following results (cf. Ref. [YWO90]):

$$\boxed{\begin{aligned} \mathcal{A}_0^+(z) = -\mathcal{A}_0^-(z) &= \frac{1}{2}\big(1+\Lambda^{-z}\big)\ , && (4.166)\\ \mathcal{A}_m^+(z) = -\mathcal{A}_m^-(z) &= \frac{1}{2}\big(1+\Lambda^{-1}\big)\,\Lambda^{1-z-m} \quad \text{for} \quad m \geq 1\ . && (4.167) \end{aligned}}$$

On the other hand, when using the improved discretization by Campo and Oliveira, the parameters $\widetilde{\mathcal{A}}_{m\mu}^p(z)$ are obtained from Eq. (4.72). In case of a constant DOS, this equation simplifies to

$$\widetilde{\mathcal{A}}_{m\mu}^p(z) = \widetilde{\mathcal{A}}_m^p(z) = \frac{\int_{I_m^p(z)} \mathrm{d}\xi}{\int_{I_m^p(z)} \frac{\mathrm{d}\zeta}{\zeta}}\ , \tag{4.168}$$

giving (cf. Ref. [CO05]):

$$\boxed{\begin{aligned} \widetilde{\mathcal{A}}_0^+(z) = -\widetilde{\mathcal{A}}_0^-(z) &= \frac{1-\Lambda^{-z}}{z\ln\Lambda}\ , && (4.169)\\ \widetilde{\mathcal{A}}_m^+(z) = -\widetilde{\mathcal{A}}_m^-(z) &= \frac{1-\Lambda^{-1}}{\ln\Lambda}\,\Lambda^{1-z-m} \quad \text{for} \quad m \geq 1\ . && (4.170) \end{aligned}}$$

Finally, in order to determine the parameters $\bar{\mathcal{A}}_{m\mu}^p(z)$ that are used in the alternative discretization scheme proposed by Žitko and Pruschke, we have to solve the differential equation

$$\frac{\mathrm{d}\bar{\mathcal{A}}_\mu^p(x)}{\mathrm{d}x} = \int_{\Xi_\mu^p(x)}^{\Xi_\mu^p(x+1)} \mathrm{d}\zeta = \Xi_\mu^p(x+1) - \Xi_\mu^p(x) \quad \text{for} \quad x \in [0,\infty)\ , \tag{4.171}$$

which results from Eq. (4.152) if the DOS is constant. Taking the solution $\Xi_\mu^p(x) = \Xi^p(x)$ for the standard discretization grid from Eq. (4.153), the following two differential equations are obtained:

$$\frac{\mathrm{d}\bar{\mathcal{A}}^p(x)}{\mathrm{d}x} = p\left(\Lambda^{-x} - 1\right) \qquad \text{for} \quad x \in [0,1]\,, \tag{4.172}$$

$$\frac{\mathrm{d}\bar{\mathcal{A}}^p(x)}{\mathrm{d}x} = p\,(1-\Lambda)\,\Lambda^{-x} \quad \text{for} \quad x \in [1,\infty)\,. \tag{4.173}$$

Both equations can be solved consecutively by separation of variables. With the initial values $\bar{\mathcal{A}}^p(0) \equiv p$ and $\bar{\mathcal{A}}^p(1) = p\left(1-\Lambda^{-1}\right)/\ln\Lambda$ (the latter is calculated from the solution of the first equation), we find:

$$\bar{\mathcal{A}}^p(x) = p\left(1 - x + \frac{1-\Lambda^{-x}}{\ln\Lambda}\right) \quad \text{for} \quad x \in [0,1]\,, \tag{4.174}$$

$$\bar{\mathcal{A}}^p(x) = p\,\frac{1-\Lambda^{-1}}{\ln\Lambda}\,\Lambda^{1-x} \qquad \text{for} \quad x \in [1,\infty)\,. \tag{4.175}$$

Replacing the continuous index $x = m+z$, these solutions correspond to the following parameters of the logarithmically discretized Hamiltonian (cf. Ref. [ŽP09]):

$$\bar{\mathcal{A}}_0^+(z) = -\bar{\mathcal{A}}_0^-(z) \;=\; \frac{1-\Lambda^{-z}}{\ln\Lambda} + 1 - z\,, \tag{4.176}$$

$$\bar{\mathcal{A}}_m^+(z) = -\bar{\mathcal{A}}_m^-(z) \;=\; \frac{1-\Lambda^{-1}}{\ln\Lambda}\,\Lambda^{1-z-m} \quad \text{for} \quad m \geq 1\,. \tag{4.177}$$

Compared to the improved discretization by Campo and Oliveira, only the parameters $\bar{\mathcal{A}}_0^p(z)$, which are assigned to the outermost intervals $I_0^p(z)$, are modified. This result seems plausible since the discretization by Campo and Oliveira already correctly reproduces the non-interacting spectral density $\widetilde{S}_{f_{0\mu}}(\xi)$ for a constant DOS and arguments $\xi \in \left[\widetilde{\mathcal{A}}_1^-(0), \widetilde{\mathcal{A}}_1^+(0)\right] = \left[\bar{\mathcal{A}}_1^-(0), \bar{\mathcal{A}}_1^+(0)\right]$ [CO05, ŽP09]. Moreover, note that the discretization schemes by Campo & Oliveira and Žitko & Pruschke lead to the same parameters in case of a constant DOS and $z = 1$.

4.9. Tridiagonalization of the discretized Hamiltonian: Mapping to the "Wilson chain"

With each of the approximations (4.52), (4.73), and (4.163) to the original Hamiltonian (4.22), we have a discrete model which could in principle be treated numerically by introducing a finite cutoff $m_{\max}$ for the interval index m. However, such a truncation would affect the expansion (4.43) of the operator $\underset{\sim}{f}_{0\mu}$ with respect to the states $\left\{\underset{\sim}{a}^p_{m\mu}(z)\right\}$ and therefore also the representation of the interaction term

in Hamiltonian (4.22) [YWO90]. The quality of the obtained results could then depend on the coupling strength J, too [YWO90].

For this reason, a standard NRG calculation (called "chain-NRG" [BLTV05]), takes a different approach. Instead of directly solving the discretized model, an additional step is introduced in which the discrete Hamiltonian is mapped to a semi-infinite tight-binding chain with nearest-neighbor interaction and the impurity at the closed end ([Wil75], cf. Ref. [BCP08]). The zeroth lattice site, to which the impurity spin couples, is identified with the state $\underset{\sim}{f}_{0\mu}$ in order to preserve an accurate (and hopefully coupling-strength-independent) description of the interaction between impurity and electrons. The resulting Hamiltonian is referred to as the *Wilson chain*. As discussed in Sec. 4.9.1, the parameters of the Wilson chain (i.e., the hopping parameters and on-site energies) have special properties that arise from the logarithmic discretization of the conduction band and are essential for a numerical solution of the model. From a mathematical point of view, the mapping onto the Wilson chain corresponds to a basis transformation for the electronic degrees of freedom which is *exact* and thus does not introduce any further approximations. In general, it is not possible to carry out the transformation analytically, but the calculation of the parameters of the Wilson chain can at least be made numerically exact. Once the parameters have been determined, the Wilson chain is approximately diagonalized by means of an iterative procedure that is discussed in detail in the next section 4.10. If we only consider a single spin-projection and impose a suitable ordering of basis states, the matrix representation of the transformed conduction band in the subspace with a single electron becomes tridiagonal. Hence, the basis transformation is also referred to as a *tridiagonalization*.

On the other hand, if the eigenvalue problem of the discretized Hamiltonian is directly solved (i.e., no tridiagonalization is performed), the method is referred to as "star-NRG" [BLTV05] (since the impurity spin couples to all modes $\left\{\underset{\sim}{a}^{p}_{m\mu}(z)\right\}$ via the state $\underset{\sim}{f}_{0\mu}$ in a star-shaped graph). In case of star-NRG, an iterative diagonalization of the discrete Hamiltonian similar to that of the Wilson chain in the conventional approach can be carried out. For a fermionic bath (corresponding to the conduction electrons), there are further arguments against using star-NRG [BLTV05]:

1. To begin with, chain-NRG is established and works well. Furthermore, it is not clear whether star-NRG has any advantages in case of a fermionic bath.

2. For a fermionic bath, there are positive and negative energies relative to the Fermi energy. In case of particle-hole symmetry, one would have to add two states ($\underset{\sim}{a}^{+}_{m\mu}(z)$ and $\underset{\sim}{a}^{-}_{m\mu}(z)$) in each step of an iterative diagonalization in order to preserve the symmetry. As a consequence, the Hilbert space would grow by a factor of 16 in each step (as opposed to a factor of 4 when using chain-NRG, see Sec. 4.10) so that the numerical cost of the iterative diagonalization would be significantly higher.

4.9.1. Derivation of recursion relations for the parameters of the Wilson chain

The hopping parameters and on-site energies of the Wilson chain can be calculated using a recursive scheme that was introduced for a bosonic bath in appendix A of Ref. [BLTV05] and later extended to the fermionic case in Ref. [BCP08].

The starting point for the derivation of recursion relations is the purely electronic term in one of the discrete approximations to $\underset{\sim}{H}_{\mathrm{NRG}}$ (cf. Eqs. (4.52), (4.73), and (4.163)) for the given twist parameter z:

$$\underset{\sim}{H}_{\mathrm{cb}}(z) \equiv W \sum_{\substack{p,m \\ \mu}} \mathcal{E}^p_{m\mu}(z)\, \underset{\sim}{a}^{p\dagger}_{m\mu}(z) \underset{\sim}{a}^{p}_{m\mu}(z) \,. \tag{4.178}$$

Note that here and in the following we use the same notation for the energies $W\mathcal{E}^p_{m\mu}(z)$ as in the standard discretization, regardless of the discretization scheme that is actually used in the calculation. We furthermore have the special state $\underset{\sim}{f}_{0\mu}$ from Eqs. (4.43) and (4.124),

$$\underset{\sim}{f}_{0\mu} = \sum_{p,m} \sqrt{\frac{\mathcal{B}^p_\mu}{W}\, \mathcal{W}^p_{m\mu}(z)}\, \underset{\sim}{a}^{p}_{m\mu}(z) = \sum_{p,m} \sqrt{w^p_{m\mu}(z)}\, \underset{\sim}{a}^{p}_{m\mu}(z) \,, \tag{4.179}$$

which is assigned to the zeroth site of the Wilson chain. To this end, it is chosen as the first element of the new basis $\left\{\underset{\sim}{f}_{n\mu}(z)\right\}$, whose construction is the topic of this section. Since $\underset{\sim}{f}_{0\mu}$ mixes electronic states of different energy, Hamiltonian (4.178) can no longer be diagonal with respect to the new basis. A nearest-neighbor interaction is thus "the next best thing".

The input to the tridiagonalization procedure consists of the energies $W\mathcal{E}^p_{m\mu}(z)$ and the coefficients $w^p_{m\mu}(z)$ that appear in the expansion of the state $\underset{\sim}{f}_{0\mu}$. After tridiagonalization, Hamiltonian (4.178) takes the form (cf. Ref. [BCP08])

$$\underset{\sim}{H}_{\mathrm{cb}}(z) = \sum_{\substack{n=0 \\ \mu}}^{\infty} \left[\epsilon_{n\mu}(z)\, \underset{\sim}{f}^\dagger_{n\mu}(z) \underset{\sim}{f}_{n\mu}(z) + t_{n\mu}(z) \Big(\underset{\sim}{f}^\dagger_{n\mu}(z) \underset{\sim}{f}_{n+1\mu}(z) + \underset{\sim}{f}^\dagger_{n+1\mu}(z) \underset{\sim}{f}_{n\mu}(z) \Big) \right] , \tag{4.180}$$

with the *on-site energies* $\epsilon_{n\mu}(z)$ and the *hopping parameters* $t_{n\mu}(z)$. Hamiltonian (4.180) corresponds to the electronic part of the semi-infinite *Wilson chain*. Starting with the energies $W\mathcal{E}^p_{m\mu}(z)$ and the coefficients $w^p_{m\mu}(z)$, the goal is now to determine the parameters $\epsilon_{n\mu}(z)$ and $t_{n\mu}(z)$. If states with different spin projection $\mu = \uparrow / \downarrow$ are *not* coupled, as in Hamiltonian (4.178), the tridiagonalization

can be carried out separately for each spin species. It corresponds to a (real) orthogonal transformation with the following representations for the new basis states [BCP08]:

$$\boxed{\underset{\sim}{f}_{n\mu}(z) \equiv \sum_{m=0,p}^{\infty} u^p_{nm\mu}(z)\, \underset{\sim}{a}^p_{m\mu}(z)\ .} \tag{4.181}$$

Comparing with Eq. (4.179) for $n = 0$, we directly obtain:

$$u^p_{0m\mu}(z) = \sqrt{w^p_{m\mu}(z)}\ . \tag{4.182}$$

The orthogonal transformations $\mathcal{U}^p_\mu(z)$ have the defining properties (compare Ref. [Wil75])

$$\big(\mathcal{U}^p_\mu(z)\big)^T \mathcal{U}^p_\mu(z) = \mathbb{1} \iff \sum_l u^p_{lk\mu}(z)\, u^p_{lm\mu}(z) = \delta_{km}\ , \tag{4.183}$$

$$\mathcal{U}^p_\mu(z) \big(\mathcal{U}^p_\mu(z)\big)^T = \mathbb{1} \iff \sum_l u^p_{kl\mu}(z)\, u^p_{ml\mu}(z) = \delta_{km}\ . \tag{4.184}$$

With $\bar{p} \equiv -p$, we furthermore require that [Wil75]

$$\begin{aligned}\big(\mathcal{U}^p_\mu(z)\big)^T \mathcal{U}^{\bar{p}}_\mu(z) = \mathcal{U}^p_\mu(z) \big(\mathcal{U}^{\bar{p}}_\mu(z)\big)^T = 0 \quad \Longleftrightarrow \\ \sum_l u^p_{lk\mu}(z)\, u^{\bar{p}}_{lm\mu}(z) = \sum_l u^p_{kl\mu}(z)\, u^{\bar{p}}_{ml\mu}(z) = 0\ .\end{aligned} \tag{4.185}$$

Using these properties, the inverse transformation to Eq. (4.181) is obtained as:

$$\boxed{\underset{\sim}{a}^p_{m\mu}(z) = \sum_{n=0}^{\infty} u^p_{nm\mu}(z)\, \underset{\sim}{f}_{n\mu}(z)\ .} \tag{4.186}$$

For each spin projection, we now make use of the desired equivalence between Hamiltonians (4.178) and (4.180) [BLTV05, BCP08]:

$$\begin{aligned}W \sum_{p,m} \mathcal{E}^p_{m\mu}(z)\, \underset{\sim}{a}^{p\dagger}_{m\mu}(z) \underset{\sim}{a}^p_{m\mu}(z) = \\ \sum_n \Big[\epsilon_{n\mu}(z)\, \underset{\sim}{f}^\dagger_{n\mu}(z) \underset{\sim}{f}_{n\mu}(z) \\ + t_{n\mu}(z) \Big(\underset{\sim}{f}^\dagger_{n\mu}(z) \underset{\sim}{f}_{n+1\mu}(z) + \underset{\sim}{f}^\dagger_{n+1\mu}(z) \underset{\sim}{f}_{n\mu}(z) \Big) \Big]\ .\end{aligned} \tag{4.187}$$

Inserting the expansion for $\underset{\sim}{a}^p_{m\mu}(z)$ leads to [BLTV05]

$$\sum_n W \sum_{p,m} \mathcal{E}^p_{m\mu}(z)\, u^p_{nm\mu}(z)\, \underset{\sim}{a}^{p\dagger}_{m\mu}(z) \underset{\sim}{f}_{n\mu}(z) \;=$$
$$\sum_n \Big[\epsilon_{n\mu}(z)\, \underset{\sim}{f}^\dagger_{n\mu}(z) \underset{\sim}{f}_{n\mu}(z) \;+\; t_{n\mu}(z)\Big(\underset{\sim}{f}^\dagger_{n\mu}(z) \underset{\sim}{f}_{n+1\mu}(z) + \underset{\sim}{f}^\dagger_{n+1\mu}(z) \underset{\sim}{f}_{n\mu}(z)\Big)\Big] \,, \tag{4.188}$$

so that, by equating coefficients for $n = 0$, we find [BLTV05]:

$$\boxed{W \sum_{p,m} \mathcal{E}^p_{m\mu}(z)\, u^p_{0m\mu}(z)\, \underset{\sim}{a}^{p\dagger}_{m\mu}(z) \;=\; \epsilon_{0\mu}(z) \underset{\sim}{f}^\dagger_{0\mu} + t_{0\mu}(z) \underset{\sim}{f}^\dagger_{1\mu}(z) \,.} \tag{4.189}$$

This identity, in combination with the expansion of $\underset{\sim}{f}_{0\mu}$ according to Eq. (4.181), allows us to determine the *zeroth on-site energy* [BLTV05]:

$$\epsilon_{0\mu}(z) \;=\; \Big\{\underset{\sim}{f}_{0\mu}, \epsilon_{0\mu}(z) \underset{\sim}{f}^\dagger_{0\mu} + t_{0\mu}(z) \underset{\sim}{f}^\dagger_{1\mu}(z)\Big\} \;=\; \ldots \tag{4.190}$$
$$= W \sum_{p,m} \mathcal{E}^p_{m\mu}(z) \big(u^p_{0m\mu}(z)\big)^2 \overset{(4.182)}{=} W \sum_{p,m} \mathcal{E}^p_{m\mu}(z)\, w^p_{m\mu}(z) \,. \tag{4.191}$$

Using the corresponding expansion for $\underset{\sim}{f}^\dagger_{0\mu}$, Eq. (4.189) can be furthermore rewritten as [BLTV05]:

$$t_{0\mu}(z) \underset{\sim}{f}^\dagger_{1\mu}(z) \;=\; W \sum_{p,m} \mathcal{E}^p_{m\mu}(z)\, u^p_{0m\mu}(z)\, \underset{\sim}{a}^{p\dagger}_{m\mu}(z) - \epsilon_{0\mu}(z) \underset{\sim}{f}^\dagger_{0\mu} \tag{4.192}$$
$$= \sum_{p,m} \big(W \mathcal{E}^p_{m\mu}(z) - \epsilon_{0\mu}(z)\big) u^p_{0m\mu}(z)\, \underset{\sim}{a}^{p\dagger}_{m\mu}(z) \,. \tag{4.193}$$

Comparing with the expansion of the state $\underset{\sim}{f}^\dagger_{1\mu}(z)$,

$$\underset{\sim}{f}^\dagger_{1\mu}(z) = \sum_{p,m} u^p_{1m\mu}(z)\, \underset{\sim}{a}^{p\dagger}_{m\mu}(z) \,, \tag{4.194}$$

we directly see that:

$$u^p_{1m\mu}(z) = \frac{1}{t_{0\mu}(z)} \big(W \mathcal{E}^p_{m\mu}(z) - \epsilon_{0\mu}(z)\big) u^p_{0m\mu}(z) \,. \tag{4.195}$$

With the expression for the operator $\underset{\sim}{f}_{1\mu}(z)$ corresponding to Eq. (4.194), we can then use Eq. (4.193) to calculate the *zeroth hopping parameter* [BLTV05]:

$$t_{0\mu}(z) = \left\{ \underset{\sim}{f}_{1\mu}(z),\, t_{0\mu}(z)\underset{\sim}{f}^{\dagger}_{1\mu}(z) \right\} = \ldots \tag{4.196}$$

$$= \frac{1}{t_{0\mu}(z)} \sum_{p,m} \left(W\mathcal{E}^{p}_{m\mu}(z) - \epsilon_{0\mu}(z) \right)^2 w^{p}_{m\mu}(z) \,, \tag{4.197}$$

or equivalently:

$$\left(t_{0\mu}(z)\right)^2 = W^2 \sum_{p,m} \left(\mathcal{E}^{p}_{m\mu}(z) - \frac{\epsilon_{0\mu}(z)}{W} \right)^2 w^{p}_{m\mu}(z) \,. \tag{4.198}$$

We have thus determined the parameters assigned to the zeroth site of the Wilson chain and thereby "initialized" the recursive procedure.

As the next step, it is shown how to calculate the parameters for lattice site n using the results for the previous site $n-1$. To this end, we go back to the equivalence (4.188) and equate coefficients for $n > 0$ [BLTV05]:

$$\begin{aligned} &W \sum_{p,m} \mathcal{E}^{p}_{m\mu}(z)\, u^{p}_{nm\mu}(z)\, \underset{\sim}{a}^{p\dagger}_{m\mu}(z) = \\ &\quad \epsilon_{n\mu}(z)\underset{\sim}{f}^{\dagger}_{n\mu}(z) + t_{n\mu}(z)\underset{\sim}{f}^{\dagger}_{n+1\mu}(z) + t_{n-1\mu}(z)\underset{\sim}{f}^{\dagger}_{n-1\mu}(z) \,. \end{aligned} \tag{4.199}$$

With the same approach as before, the *on-site energy for lattice site* n can then be determined [BLTV05]:

$$\epsilon_{n\mu}(z) = \left\{ \underset{\sim}{f}_{n\mu}(z),\, \epsilon_{n\mu}(z)\underset{\sim}{f}^{\dagger}_{n\mu}(z) + t_{n\mu}(z)\underset{\sim}{f}^{\dagger}_{n+1\mu}(z) + t_{n-1\mu}(z)\underset{\sim}{f}^{\dagger}_{n-1\mu}(z) \right\} \tag{4.200}$$

$$= \ldots = W \sum_{p,m} \mathcal{E}^{p}_{m\mu}(z) \left(u^{p}_{nm\mu}(z) \right)^2 . \tag{4.201}$$

In order to obtain an expression for the next group of elements of the orthogonal transformations $\mathcal{U}^{p}_{\mu}(z)$ (i.e., for index $n+1$, cf. Eq. (4.195)), Eq. (4.199) is rewritten as [BLTV05]:

$$t_{n\mu}(z)\underset{\sim}{f}^{\dagger}_{n+1\mu}(z) =$$

$$\sum_{p,m} W\mathcal{E}^{p}_{m\mu}(z)\, u^{p}_{nm\mu}(z)\, \underset{\sim}{a}^{p\dagger}_{m\mu}(z) - \epsilon_{n\mu}(z)\underset{\sim}{f}^{\dagger}_{n\mu}(z) - t_{n-1\mu}(z)\underset{\sim}{f}^{\dagger}_{n-1\mu}(z) = \tag{4.202}$$

$$\sum_{p,m} \left(W\mathcal{E}^{p}_{m\mu}(z)\, u^{p}_{nm\mu}(z) - \epsilon_{n\mu}(z)\, u^{p}_{nm\mu}(z) - t_{n-1\mu}(z)\, u^{p}_{n-1m\mu}(z) \right) \underset{\sim}{a}^{p\dagger}_{m\mu}(z) \,. \tag{4.203}$$

Analogous to the case $n = 0$, the result can be directly read off:

$$u^{p}_{n+1m\mu}(z) = \frac{1}{t_{n\mu}(z)} \left(\left(W\mathcal{E}^{p}_{m\mu}(z) - \epsilon_{n\mu}(z) \right) u^{p}_{nm\mu}(z) - t_{n-1\mu}(z)\, u^{p}_{n-1m\mu}(z) \right) . \tag{4.204}$$

Finally, we need to find the recursion relation for the *hopping parameter* $t_{n\mu}(z)$. To this end, we make use of Eq. (4.203) [BLTV05], the above result for $u^p_{n+1m\mu}(z)$, and the expression for $\epsilon_{n\mu}(z)$ from Eq. (4.201):

$$t_{n\mu}(z) = \left\{ \underset{\sim}{f}_{n+1\mu}(z),\, t_{n\mu}(z) \underset{\sim}{f}^{\dagger}_{n+1\mu}(z) \right\} = \dots \tag{4.205}$$

$$= \frac{1}{t_{n\mu}(z)} \left(\sum_{p,m} \left(W \mathcal{E}^p_{m\mu}(z)\, u^p_{nm\mu}(z) \right)^2 - \left(\epsilon_{n\mu}(z) \right)^2 - \left(t_{n-1\mu}(z) \right)^2 \right) , \tag{4.206}$$

or equivalently:

$$\left(t_{n\mu}(z) \right)^2 = W^2 \left(\sum_{p,m} \left(\mathcal{E}^p_{m\mu}(z)\, u^p_{nm\mu}(z) \right)^2 - \left(\frac{\epsilon_{n\mu}(z)}{W} \right)^2 - \left(\frac{t_{n-1\mu}(z)}{W} \right)^2 \right) . \tag{4.207}$$

This completes the derivation of the recursion relations for the parameters of the Wilson chain. Let us now summarize the obtained equations for the tridiagonalization of the logarithmically discretized conduction band Hamiltonian (4.178) (cf. Ref. [BCP08]):

Initialization for $n = 0$:

$$u^p_{0m\mu}(z) = \sqrt{\frac{\mathcal{B}^p_\mu}{W}\,\mathcal{W}^p_{m\mu}(z)}\,, \tag{4.208}$$

$$\frac{\epsilon_{0\mu}(z)}{W} = \sum_{p,m}\frac{\mathcal{B}^p_\mu}{W}\mathcal{A}^p_{m\mu}(z)\big(u^p_{0m\mu}(z)\big)^2\,, \tag{4.209}$$

$$\left(\frac{t_{0\mu}(z)}{W}\right)^2 = \sum_{p,m}\left(\frac{\mathcal{B}^p_\mu}{W}\mathcal{A}^p_{m\mu}(z) - \frac{\epsilon_{0\mu}(z)}{W}\right)^2\big(u^p_{0m\mu}(z)\big)^2\,, \tag{4.210}$$

$$u^p_{1m\mu}(z) = \frac{W}{t_{0\mu}(z)}\left(\frac{\mathcal{B}^p_\mu}{W}\mathcal{A}^p_{m\mu}(z) - \frac{\epsilon_{0\mu}(z)}{W}\right)u^p_{0m\mu}(z)\,. \tag{4.211}$$

Recursion relations for $n \geq 1$:

$$\frac{\epsilon_{n\mu}(z)}{W} = \sum_{p,m}\frac{\mathcal{B}^p_\mu}{W}\mathcal{A}^p_{m\mu}(z)\big(u^p_{nm\mu}(z)\big)^2\,, \tag{4.212}$$

$$\left(\frac{t_{n\mu}(z)}{W}\right)^2 = \sum_{p,m}\left(\frac{\mathcal{B}^p_\mu}{W}\mathcal{A}^p_{m\mu}(z)\,u^p_{nm\mu}(z)\right)^2 - \left(\frac{\epsilon_{n\mu}(z)}{W}\right)^2 - \left(\frac{t_{n-1\mu}(z)}{W}\right)^2\,, \tag{4.213}$$

$$u^p_{n+1m\mu}(z) = \frac{W}{t_{n\mu}(z)}\left[\left(\frac{\mathcal{B}^p_\mu}{W}\mathcal{A}^p_{m\mu}(z) - \frac{\epsilon_{n\mu}(z)}{W}\right)u^p_{nm\mu}(z) - \frac{t_{n-1\mu}(z)}{W}\,u^p_{n-1m\mu}(z)\right]. \tag{4.214}$$

For general input parameters, the on-site energies $\epsilon_{n\mu}(z)$ and hopping parameters $t_{n\mu}(z)$ have to be determined by numerically solving the recursion relations. For this purpose, suitable cutoffs $m_{\max}$ for the interval index m and $n_{\max}$ for the lattice site index n, respectively, have to be introduced. Since the parameters appearing in the recursion relations cover a wide range of values, a numerical solution suffers from instability so that at some point the recursion breaks down [BCP08]. For a maximal lattice site index $n_{\max}$ of, say, the order of 50, this can be avoided by using arbitrary precision arithmetics. In this way, it is also possible to obtain numerically exact (i.e., double precision) results for the parameters of the Wilson chain. Because of the instability, it is advisable to take a safe approach to the choice of numerical parameters and, preferably, to inspect the obtained on-site energies and hopping parameters. As discussed in Sec. 4.12, the value of $n_{\max}$ depends on the lowest temperature that is supposed to be reached in the NRG calculation and thereby also on the discretization parameter Λ. For larger Λ, a smaller value of $n_{\max}$ is necessary in order to "cool the system to the desired temperature".

In each step of the recursive solution, the elements $u^p_{n+1m\mu}(z)$ of the orthogonal transformations $\mathcal{U}^p_\mu(z)$ have to be determined. For given n, they can be interpreted as the components of a vector using the interval index m:

$$\mathbf{u}^p_{n+1\mu}(z) \equiv \left(u^p_{n+1,0\mu}(z),\, u^p_{n+1,1\mu}(z),\, u^p_{n+1,2\mu}(z),\, \ldots,\, u^p_{n+1,m_{\max}\mu}(z)\right) . \quad (4.215)$$

With the transformation property (4.184), we find:

$$\mathbf{u}^p_{n+1\mu}(z) \cdot \mathbf{u}^p_{n+1\mu}(z) = \sum_{m=0}^{m_{\max}} u^p_{n+1m\mu}(z)\, u^p_{n+1m\mu}(z) = \delta_{n+1,n+1} = 1 . \quad (4.216)$$

The vectors $\mathbf{u}^p_{n+1\mu}(z)$ are thus normalized to one, and it can certainly do no harm to explicitly enforce the normalization after each step of the recursive solution [BCP08].

For a particle-hole symmetric density of states (i.e., $\rho(\varepsilon) = \rho(-\varepsilon)$ with $\varepsilon_F = 0$) and $h = g_e \mu_B B = 0$, we have $\mathcal{B}^p = W$, $\mathcal{A}^+_m(z) = -\mathcal{A}^-_m(z)$ (cf. Eqs. (4.51), (4.72), and (4.152)), and $\mathcal{W}^+_m(z) = \mathcal{W}^-_m(z)$ according to the definition (4.37). With the ansatz $u^p_{nm}(z) = (-1)^n u^{\bar{p}}_{nm}(z)$ for the elements of the orthogonal transformations $\mathcal{U}^p(z)$ [Wil75], it can then be shown that all on-site energies $\epsilon_n(z)$ have to vanish. On the other hand, with the relations $\mathcal{E}^p_{m\mu}(z) = \mathcal{B}^p_\mu \mathcal{A}^p_{m\mu}(z)/W$ and $w^p_{m\mu}(z) = \mathcal{B}^p_\mu \mathcal{W}^p_{m\mu}(z)/W$, we obtain for $h > 0$:

$$w^p_{m\mu}(z) \;=\; w^{\bar{p}}_{m\bar{\mu}}(z) , \quad (4.217)$$

$$\mathcal{E}^p_{m\mu}(z) \;=\; -\,\mathcal{E}^{\bar{p}}_{m\bar{\mu}}(z) . \quad (4.218)$$

Using the ansatz $u^p_{nm\mu}(z) = (-1)^n u^{\bar{p}}_{nm\bar{\mu}}(z)$, it can be shown that in this case

$$\boxed{\epsilon_{n\uparrow}(z) = -\epsilon_{n\downarrow}(z) \quad \text{and} \quad t_{n\uparrow}(z) = t_{n\downarrow}(z) \quad \text{for all } n .} \quad (4.219)$$

In special cases, analytical solutions to the recursion relations have been obtained. For a constant DOS, $h = 0$, and $\epsilon_F = 0$, Wilson has found the following solution for the on-site energies and hopping parameters using the standard discretization with $z = 1$ (see p. 814 of Ref. [Wil75] and compare Ref. [BCP08]):

$$\boxed{\begin{aligned} \frac{\epsilon_n}{W} &= 0 && \text{for all } n , \quad (4.220)\\ \frac{t_n}{W} &= \frac{1}{2}\frac{\left(1+\Lambda^{-1}\right)\left(1-\Lambda^{-n-1}\right)}{\sqrt{1-\Lambda^{-2n-1}}\sqrt{1-\Lambda^{-2n-3}}}\,\Lambda^{-\frac{n}{2}} && \text{with } n \geq 0 . \quad (4.221) \end{aligned}}$$

Because of the instability that a numerical solution of the recursion relations displays, Wilson's analytical solution is useful for a check of the numerical code. A further analytical solution exists for a particle-hole-symmetric "pseudo-gap" density of states (i.e., $\rho(\varepsilon) \propto |\varepsilon|^r$ with $r > 0$), again for the standard discretization with $z = 1$ [BPH97].

Asymptotically, the hopping parameters $t_{n\mu}(z)$ of the Wilson chain decrease exponentially with increasing lattice site index n. In particular, Wilson's analytical solution has the following asymptotical dependence on n:

$$t_n/W \sim \Lambda^{-n/2} = \mathrm{e}^{\ln \Lambda^{-n/2}} = \mathrm{e}^{-\frac{n}{2}\ln\Lambda} \quad \text{for} \quad n \gg 1 \,. \tag{4.222}$$

The discretization parameter Λ thus determines how fast the hopping parameters decline along the chain. Note that the exponential decrease of the hopping parameters is crucial for the iterative diagonalization of the Wilson chain, which is discussed in the next section 4.10. Experience shows that the on-site energies, if they are unequal to zero, fall off even faster with increasing n than the hopping parameters.

In the case of a constant DOS and $\varepsilon_F = 0$, the following analytical expressions for the on-site energies of the zeroth site of the Wilson chain are obtained:

Standard discretization: (4.223)

$$W\epsilon_{0\mu}(z) = W\epsilon_{0\mu} = \frac{1}{4}\Big[\big(\mathcal{B}_\mu^+\big)^2 - \big(\mathcal{B}_\mu^-\big)^2\Big] \,.$$

Discretization by Campo and Oliveira: (4.224)

$$W\epsilon_{0\mu}(z) = \Big[\big(\mathcal{B}_\mu^+\big)^2 - \big(\mathcal{B}_\mu^-\big)^2\Big]\frac{1}{2\ln\Lambda}\left(\frac{\big(1-\Lambda^{-z}\big)^2}{z} + \frac{1-\Lambda^{-1}}{1+\Lambda^{-1}}\,\Lambda^{-2z}\right) \,.$$

Discretization by Žitko and Pruschke: (4.225)

$$W\epsilon_{0\mu}(z) = \Big[\big(\mathcal{B}_\mu^+\big)^2 - \big(\mathcal{B}_\mu^-\big)^2\Big]\frac{1}{2\ln\Lambda}\left(\big(1-\Lambda^{-z}\big)^2 + (1-z)\big(1-\Lambda^{-z}\big)\ln\Lambda + \frac{1-\Lambda^{-1}}{1+\Lambda^{-1}}\,\Lambda^{-2z}\right) \,.$$

Eqs. (4.224) and (4.225) give the same result for $z = 1$.

After tridiagonalization, we have an alternative approximation to the original Hamiltonian (4.22) for the given twist parameter z (note, however, that the tridiagonalization does not involve any new approximations compared to the logarithmically discretized model):

$$\underset{\sim}{H}_{\mathrm{NRG}} \approx \underset{\sim}{H}_{\mathrm{Wilson}}(z) \,. \tag{4.226}$$

The Hamiltonian of the Wilson chain is given by:

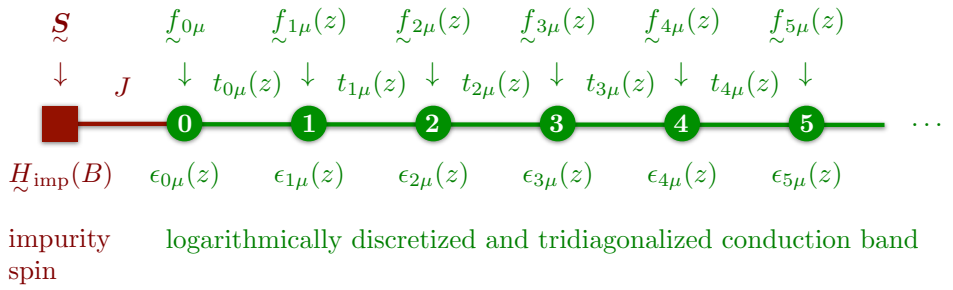

Figure 4.4.: Visualization of the Hamiltonian (4.227) which corresponds to the semi-infinite *Wilson chain*. The impurity spin $\underset{\sim}{\boldsymbol{S}}$ couples to the electron spin at the zeroth lattice site that is expressed via the operators $\underset{\sim}{f}_{0\mu}$.

$$
\begin{aligned}
\underset{\sim}{H}_{\mathrm{Wilson}}(z) \;\equiv\; & \sum_{n=0,\mu}^{\infty} \Big[\epsilon_{n\mu}(z)\, \underset{\sim}{f}^{\dagger}_{n\mu}(z) \underset{\sim}{f}_{n\mu}(z) \\
& \qquad + t_{n\mu}(z) \Big(\underset{\sim}{f}^{\dagger}_{n\mu}(z) \underset{\sim}{f}_{n+1\mu}(z) + \underset{\sim}{f}^{\dagger}_{n+1\mu}(z) \underset{\sim}{f}_{n\mu}(z) \Big) \Big] \\
& + J \underset{\sim}{\boldsymbol{S}} \cdot \sum_{\mu,\nu} \underset{\sim}{f}^{\dagger}_{0\mu} \frac{\boldsymbol{\sigma}_{\mu\nu}}{2} \underset{\sim}{f}_{0\nu} \;+\; \underset{\sim}{H}_{\mathrm{imp}}(B)\,, \qquad (4.227)
\end{aligned}
$$

$$
\text{with} \quad \Big\{ \underset{\sim}{f}_{n\mu}(z), \underset{\sim}{f}^{\dagger}_{n'\nu}(z) \Big\} = \delta_{nn'} \delta_{\mu\nu} \qquad (4.228)
$$

and the parameters $\epsilon_{n\mu}(z)$ and $t_{n\mu}(z)$ as solutions of the Eqs. (4.208) to (4.214) .

4.10. Iterative diagonalization of the Wilson chain, basis truncation, and Renormalization Group aspect

The Wilson chain is a semi-infinite system because it has a beginning in form of the impurity part, but no end (cf. Fig. 4.4). Since no analytical solution for the eigenvalue problem of the full Wilson chain is available ([Wil75], p. 816), an approximate numerical diagonalization is instead used. Such a diagonalization is, however, only possible for a system of finite size. For this reason, the Wilson chain has to be truncated by introducing a maximal lattice site index $n_{\max}$ and removing all sites with $n > n_{\max}$. At the moment, it is not obvious of what use the resulting finite part of the chain is and how physically meaningful results can be obtained

from it. If the value of $n_{\max}$ is too large, even the truncated Wilson chain cannot be diagonalized exactly anymore since the dimension of the associated total Hilbert space grows like $D_{\mathrm{imp}} 4^{n_{\max}+1}$ (with D_{imp} being the Hilbert space dimension for the impurity part of the chain). Because of the exponential growth, this "critical" value of $n_{\max}$ is quickly reached and an *approximate* numerical treatment of the finite chain fragment becomes necessary. To this end, one has to identify and keep the "important" states which "faithfully" reproduce the physical properties of the *full* Wilson chain in certain energy regimes. By discarding all the other less important states, the exponential growth of the total Hilbert space size is counteracted and it becomes possible (at least in principle) to numerically investigate truncated Wilson chains of arbitrary length.

In a NRG calculation, the Wilson chain is *iteratively diagonalized* until the maximal length determined by $n_{\max}$ is reached (as it turns out, observables can be calculated for lower temperatures if a larger value of $n_{\max}$ is used). The iterative construction of the Wilson chain is done by adding one lattice site at a time: After the chain has been (approximately) diagonalized up to and including site $N-1$, site N is added and the resulting enlarged fragment is diagonalized again. When a certain value of N is reached (which is of the order of 5), less important states have to be discarded by applying a suitable selection criterion in order to keep the number of considered states small and approximately constant.

4.10.1. Iterative construction of the Wilson chain and rescaling of the truncated Hamiltonians

Before the approximate diagonalization of the Wilson chain can be carried out, the iterative algorithm has to be initialized once by providing all the required information for one chain fragment (the type of information needed from the previous step in order to perform the calculations in the next step is described in Sec. 4.11). Typically, the fragment used for the initialization comprises the impurity part and the zeroth site of the chain (cf. Fig. 4.5 (a)). In order to obtain the necessary initial data, the corresponding part of the Wilson-chain Hamiltonian (4.227),

$$\boxed{\frac{\underset{\sim}{H}^{(0)}_{\mathrm{Wilson}}(z)}{W} \equiv \sum_{\mu} \frac{\epsilon_{0\mu}(z)}{W}\, \underset{\sim}{f}^{\dagger}_{0\mu} \underset{\sim}{f}_{0\mu} + \frac{J}{W} \underset{\sim}{\boldsymbol{S}} \cdot \sum_{\mu,\nu} \underset{\sim}{f}^{\dagger}_{0\mu} \frac{\boldsymbol{\sigma}_{\mu\nu}}{2} \underset{\sim}{f}_{0\nu} + \frac{\underset{\sim}{H}_{\mathrm{imp}}(B)}{W}\,,} \tag{4.229}$$

is diagonalized exactly (either analytically or numerically, see App. A).

In the first step of the iterative diagonalization, the first site of the Wilson chain is added (see Fig. 4.5 (b)) and, with the information from the previous (zeroth) step, the complete eigenvalue problem of the enlarged chain fragment is numerically solved. The couplings $t_{0\mu}(z)$ to the first lattice site cause the energy levels of Hamiltonian (4.229) to split up. In particular, the order of magnitude of the splitting between the groundstate and the first excited state of the enlarged fragment (i.e., the groundstate gap) is given by the hopping parameters that connect

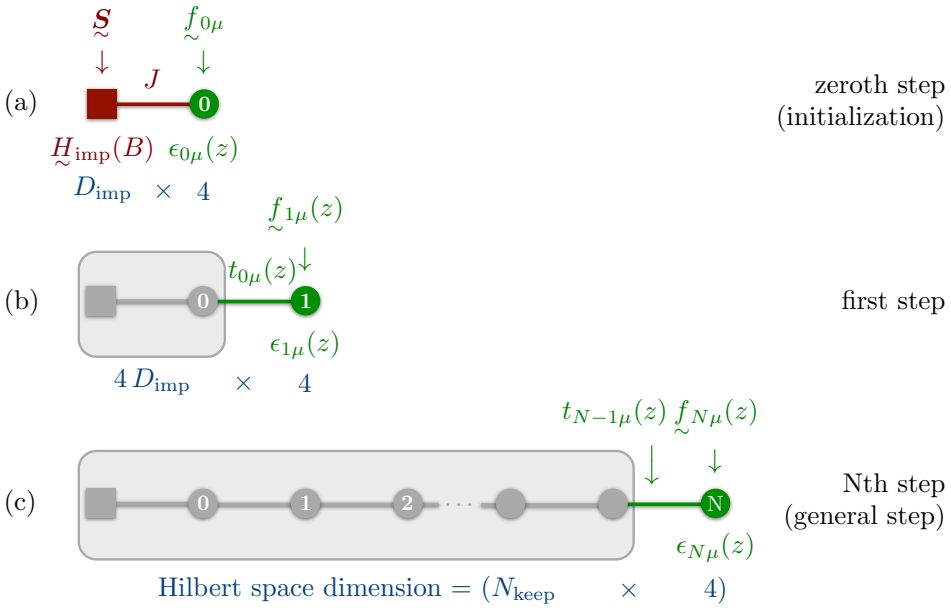

Figure 4.5.: Illustration of the iterative construction of the Wilson chain (cf. Fig. 4.4). D_{imp} denotes the dimension of the impurity Hilbert space and, as long as all states of the chain fragments are retained, the size of the total Hilbert space grows by a factor of four every time a new site is added. N_{keep} is the number of states that are kept after each step of the iterative diagonalization once states have to be discarded (see Sec. 4.10.2).

the newly added site to the existing part of the Wilson chain (cf. p. 816 of Ref. [Wil75], p. 1007 f. of Ref. [KmWW80a], and p. 406 of Ref. [BCP08]). In a NRG calculation, it is common to rescale the Hamiltonians for the finite fragments of the Wilson chain in such a way that the (dimensionless) groundstate gap becomes of order 1 (see p. 84 of Ref. [Hew93] and p. 408 of Ref. [BCP08]), which also makes the gap similar in each step of the iterative diagonalization. Such a rescaling is achieved when the truncated Hamiltonian $\underset{\sim}{H}^{(N)}_{\mathrm{Wilson}}(z)$ in the Nth step (cf. Fig. 4.5 (c)) is divided by the hopping parameter $t_{N-1}(z)$ that attaches the outermost lattice site N. If the hopping parameters depend on the spin projection μ, one can, e.g., use the average value $\big(t_{N-1\downarrow}(z) + t_{N-1\uparrow}(z)\big)/2$ for the rescaling. In the following, let τ_{N-1} be the (appropriately chosen) *dimensionless rescaling factor* in the Nth step of the iterative diagonalization:

$$\boxed{\tau_{N-1} \equiv \text{ dimensionless rescaling factor in step N .}} \tag{4.230}$$

From a strictly technical point of view, a rescaling is *not* necessary for the iterative diagonalization to work. However, since the hopping parameters decrease exponentially along the Wilson chain (cf. Eq. (4.222)), the rescaling ought to be beneficial to the numerics. Note that the truncated Hamiltonians have to be rescaled if one intends to investigate the fixed points of the considered model (in a Renormalization Group sense, see Sec. 4.10.5) by studying the *renormalization flow* of the calculated energy levels (as originally done in Refs. [Wil75, KmWW80a, KmWW80b], cf. p. 406 f. of Ref. [BCP08]). In this case, the "correct" choice of the rescaling factor (4.230) ultimately depends on the fixed point properties of the studied model (see p. 404 of Ref. [BCP08]).

As indicated by the chosen notation, the hopping parameters $t_{n\mu}(z)$ in general depend on the value of the twist parameter z. If they are used for the rescaling, the rescaling factor τ_{N-1} thus also becomes z-dependent. A z-averaging, however, is technically simpler if τ_{N-1} does not depend on z (cf. p. 411 of Ref. [BCP08]). We will expand on this point when discussing the role of temperature in a NRG calculation in Sec. 4.12.1. Instead of rescaling with the actual values $t_{n\mu}(z)$ that result from the tridiagonalization procedure, one can, e.g., use Wilson's analytical solutions (4.221) for the hopping parameters as z-independent rescaling factors. Note that z-averaging is a method for the optimization of static and dynamic observables (cf. Sec. 4.4.2). The introduction of a twist parameter is of limited use when investigating the renormalization flow of the calculated energy levels since there is no meaningful z-average for an energy spectrum (see p. 41 f. of Ref. [Žit07]).

Let us now introduce a *rescaled dimensionless Hamiltonian* $\underset{\sim}{\mathcal{H}}^{(1)}_{\mathrm{Wilson}}(z)$ for the

first step, illustrated in Fig. 4.5 (b), of the iterative diagonalization:

$$\begin{aligned}
\underset{\sim}{\mathcal{H}}^{(1)}_{\text{Wilson}}(z) &\equiv \tau_0^{-1}\,\frac{\underset{\sim}{H}^{(1)}_{\text{Wilson}}(z)}{W} \\
&\equiv \tau_0^{-1}\left[\frac{\underset{\sim}{H}^{(0)}_{\text{Wilson}}(z)}{W} + \sum_\mu \frac{\epsilon_{1\mu}(z)}{W}\,\underset{\sim}{f}^\dagger_{1\mu}(z)\underset{\sim}{f}_{1\mu}(z)\right. \\
&\qquad\left. + \sum_\mu \frac{t_{0\mu}(z)}{W}\left(\underset{\sim}{f}^\dagger_{0\mu}\underset{\sim}{f}_{1\mu}(z) + \underset{\sim}{f}^\dagger_{1\mu}(z)\underset{\sim}{f}_{0\mu}\right)\right].
\end{aligned} \tag{4.231}$$

In the Nth step (depicted in Fig. 4.5 (c)), in which lattice site N is added to the existing fragment of the Wilson chain, we analogously define a rescaled truncated Hamiltonian $\underset{\sim}{\mathcal{H}}^{(N)}_{\text{Wilson}}(z)$:

$$\begin{aligned}
\underset{\sim}{\mathcal{H}}^{(N)}_{\text{Wilson}}(z) &\equiv \tau_{N-1}^{-1}\,\frac{\underset{\sim}{H}^{(N)}_{\text{Wilson}}(z)}{W} \\
&\equiv \tau_{N-1}^{-1}\left[\frac{\underset{\sim}{H}^{(N-1)}_{\text{Wilson}}(z)}{W} + \sum_\mu \frac{\epsilon_{N\mu}(z)}{W}\,\underset{\sim}{f}^\dagger_{N\mu}(z)\underset{\sim}{f}_{N\mu}(z)\right. \\
&\qquad\left. + \sum_\mu \frac{t_{N-1\mu}(z)}{W}\left(\underset{\sim}{f}^\dagger_{N-1\mu}(z)\underset{\sim}{f}_{N\mu}(z) + \underset{\sim}{f}^\dagger_{N\mu}(z)\underset{\sim}{f}_{N-1\mu}(z)\right)\right] \\
&= \frac{\tau_{N-2}}{\tau_{N-1}}\,\underset{\sim}{\mathcal{H}}^{(N-1)}_{\text{Wilson}}(z) + \tau_{N-1}^{-1}\left[\sum_\mu \frac{\epsilon_{N\mu}(z)}{W}\,\underset{\sim}{f}^\dagger_{N\mu}(z)\underset{\sim}{f}_{N\mu}(z)\right. \\
&\qquad\left. + \sum_\mu \frac{t_{N-1\mu}(z)}{W}\left(\underset{\sim}{f}^\dagger_{N-1\mu}(z)\underset{\sim}{f}_{N\mu}(z) + \underset{\sim}{f}^\dagger_{N\mu}(z)\underset{\sim}{f}_{N-1\mu}(z)\right)\right].
\end{aligned} \tag{4.232}$$

Accordingly, there is the following relation between the Hamiltonians $\underset{\sim}{\mathcal{H}}^{(N)}_{\text{Wilson}}(z)$ and the Hamiltonian (4.227) of the semi-infinite Wilson chain:

$$\underset{\sim}{H}_{\text{Wilson}}(z) = \lim_{N\to\infty} W\tau_{N-1}\,\underset{\sim}{\mathcal{H}}^{(N)}_{\text{Wilson}}(z)\,. \tag{4.233}$$

It is common practice to reset the groundstate "energy" to zero after each step of the iterative diagonalization. Let ${}^0\underset{\sim}{\mathcal{H}}^{(N)}_{\text{Wilson}}(z)$ be the rescaled dimensionless Hamiltonian in step N with a groundstate of zero. From a technical point of view, the reset is again *not* necessary, but it prevents the energies from exponentially increasing along the Wilson chain (see p. 408 of Ref. [BCP08]). If the renormalization flow of the energy levels is supposed to be studied, the groundstate energy

has to be zeroed after each step so that excitations are automatically measured relative to the respective groundstate.

4.10.2. "Traditional" basis truncation

Irrespective of the criterion that is used to truncate the basis, it seems advisable to retain *all states* in the first few iterations [MWC12]. This way, a chain fragment of a certain length (comprising about five lattice sites) is diagonalized *exactly*. Apparently, the first few steps of the iterative diagonalization are crucial for a successful NRG calculation [Wei11].

When using the "traditional" basis truncation scheme, a number N_{keep} is defined that determines how many states are kept after each step once the beginning of the Wilson chain has been diagonalized exactly. The *criterion for selecting the "important" states* in each step that involves truncation is actually rather simple: One keeps a certain number of the lowest-lying energy levels so that the number of retained states is (approximately, see below) N_{keep} (we discuss in Sec. 4.10.4 why this truncation scheme works, i.e., why it produces states that accurately represent the properties of the full Wilson chain in certain energy regimes). Before the next lattice site is added to the existing chain fragment, all the remaining, higher-lying eigenstates are dropped (cf. Fig. 4.5 (c)). This way, the number of considered states is kept small (N_{keep} is typically of the order of a few thousands, see below) and approximately constant along the Wilson chain. Since the exponential growth of the total Hilbert space size is thus avoided, it becomes possible (at least in principle) to continue the iterative diagonalization up to arbitrary chain lengths. However, note that the accuracy of the obtained results decreases along the chain due to an accumulation of numerical errors. Depending on the precision used in the numerical calculations, the maximal length of the truncated Wilson chains for which reliable results can be obtained is therefore limited after all.

The energy levels of the finite chain fragments tend to be clustered (see p. 52 f. of Ref. [Žit07]). When truncating the basis, one should ensure that such a cluster is not accidentally split up since this might artificially break symmetries of the system. In order to prevent this, it is advisable to enforce an appropriate gap between the highest kept and the lowest discarded state ([Žit07], p. 53). Taking this precaution, the actual number of eigenstates that are retained after each step differs somewhat from the requested value N_{keep}.

The choice of N_{keep} depends, among other things, on the model under investigation, the observables to be calculated, and the value of the discretization parameter Λ. In case of a single-channel Kondo model with $S = 1/2$ and $\Lambda \approx 3$, one typically keeps a few thousand states for the calculation of thermodynamic observables [Wil75, Cos99, BCP08]. If a larger discretization parameter Λ is used, fewer states have to be retained in order to accurately describe the properties of the logarithmically discretized Hamiltonian (see Ref. [CPLO97], p. 405 of Ref. [BCP08], and Sec. 4.10.4). For larger Λ, however, the calculated observables should be expected to be less representative of the continuum limit $\Lambda \to 1$. In any case, N_{keep} needs to be large enough so that the obtained results can be considered as converged

(meaning that changes in the calculated quantities upon further increasing N_{keep} can be regarded as insignificant). Since we aim at producing results which reflect the properties of the studied model and not the numerical intricacies of the NRG algorithm, the effect of each of the numerical parameters on the calculated observables must be sufficiently small. If non-abelian symmetries are used, one should furthermore discern whether the specified number of kept states really refers to states or instead to multiplets (for complex symmetries, this can make a huge difference).

The basis truncation and the finite size of a chain fragment cause its energy spectrum to be only representative of the spectrum of the full Wilson chain on a particular energy or temperature scale (see Sec. 4.12).

4.10.3. "Modern" basis truncation

Let us denote the set of eigenvalues of ${}^{0}\underset{\sim}{\mathcal{H}}^{(N)}_{\mathrm{Wilson}}(z)$, the rescaled dimensionless Hamiltonian in step N with a groundstate of zero, by $\left\{\mathcal{E}_i^{(N)}(z)\right\}$. Instead of specifying how many states are to be kept once the basis is truncated, one can also define an *energy cutoff* $\mathcal{E}_{\mathrm{keep}} > 0$ in order to determine which eigenstates are retained (although this is a *single number*, the characteristic scales τ_{N-1} from Eq. (4.230) are correctly taken into account via the rescaling of the truncated Hamiltonians): After the enlarged chain fragment has been diagonalized, only those eigenstates of ${}^{0}\underset{\sim}{\mathcal{H}}^{(N)}_{\mathrm{Wilson}}(z)$ with eigenvalue $\mathcal{E}_i^{(N)}(z) \leq \mathcal{E}_{\mathrm{keep}}$ are kept. Depending on how dense the energy spectra in the different steps are, the actual number of retained states can vary significantly along the Wilson chain if this "modern" basis truncation scheme is used. Typical values of $\mathcal{E}_{\mathrm{keep}}$ for single-impurity single-channel Kondo models are $\mathcal{E}_{\mathrm{keep}} = 5 \ldots 15$ for $\Lambda \approx 3$ (see p. 817 of Ref. [Wil75], p. 87 of Ref. [Žit07], and Refs. [ŽPP08, Wei11]).

By using an energy cutoff instead of a fixed number of kept states, the computation time is supposed to be optimally divided between the different steps of the iterative diagonalization: A large number of the low-lying levels is only retained if this is really "necessary" (see p. 52 of Ref. [Žit07]). Furthermore, it is argued that the use of a cutoff is also beneficial to the quality of the obtained results [Wei11]. Keeping all states with $\mathcal{E} \leq \mathcal{E}_{\mathrm{keep}}$ produces a truncated energy spectrum of well-defined width. As discussed in Sec. 4.12.1, this should allow to *assign* certain temperatures to a particular step of the iterative diagonalization even more reliably.

4.10.4. Motivation for the energy-based truncation scheme

We still have to deal with the important question why it is *reasonable* to truncate the basis by simply keeping a certain number of the lowest-lying eigenstates after each step of the iterative diagonalization. Apparently, selecting states solely based on their energies only results in a successful calculation because the parameters of the Wilson chain have the special property of decreasing exponentially with

increasing lattice site index n (cf. p. 15 of Ref. [Cos99]). For a chain with uniform coupling, e.g., such a simple truncation scheme does not work well. In this case, a more elaborate criterion for the selection of "important" states is needed (e.g., via the spectra of reduced density matrices as in a Density Matrix Renormalization Group (DMRG) calculation; see Ref. [PKWH99]).

The non-interacting conduction electrons with their continuum of states do not possess a characteristic energy scale. In the Kondo model, they contribute to the physics on all energy scales (see p. 807 and 813 of Ref. [Wil75] and p. 78 of Ref. [Hew93]). Wilson's motivation for the logarithmic discretization was to establish a *separation of energy scales* ([Wil75], p. 813) that allows to consider the contributions of the different scales one after the other (in the spirit of an increasingly elaborate perturbation theory). *In a certain sense*, a lattice site that is added in the iterative diagonalization can indeed be regarded as a small perturbation of the existing chain fragment. On the one hand, because of the exponential decline of the hopping parameters, the prefactors $t_{N-1\mu}(z)/W\tau_{N-1}$ (with a value close to 1) of the terms in Eq. (4.232) connecting the newly added lattice site and the existing part of the Wilson chain are smaller than the ratio[1] $\tau_{N-2}/\tau_{N-1} > 1$ by which the Hamiltonian from the previous step is multiplied. On the other hand, Wilson has argued that the matrix elements of $\underset{\sim}{f}_{N-1\mu}(z)$ with respect to the eigenstates of $\underset{\sim}{\mathcal{H}}^{(N-1)}_{\mathrm{Wilson}}(z)$ are small if the two eigenstates are energetically well separated ([Wil75], p. 817). This means that the matrix elements of the coupling term $\underset{\sim}{f}^{\dagger}_{N-1\mu}(z)\underset{\sim}{f}_{N\mu}(z)+\underset{\sim}{f}^{\dagger}_{N\mu}(z)\underset{\sim}{f}_{N-1\mu}(z)$ with respect to the product basis in step N are also small if well separated states from step $N-1$ are involved. It *might* therefore be a good approximation for the low-energy spectrum in the current step if the high-energy states from the previous step are not taken into account at all and discarded right away ([Wil75], p. 817). In particular, the basis truncation is expected to work better for a larger discretization parameter Λ (cf. p. 11 and 15 of Ref. [Cos99]). In this case, the decrease of the hopping parameters along the Wilson chain is faster and, consequently, the relative importance of the newly added lattice site is lower. It turns out that for smaller values of Λ a larger number of the low-lying energy levels has to be retained in order to get converged results (see Ref. [CPLO97] and p. 405 of Ref. [BCP08]).

Note that the additional lattice site *cannot* be considered as a small perturbation in the sense that it is actually possible to treat it using perturbation theory. The reason is that the newly added site is *not* a small perturbation for the low-lying energy levels from the previous step (cf. p. 50 of Ref. [Žit07]). On account of this, it is necessary to completely diagonalize the enlarged chain fragment in each step. This way, NRG is also rendered non-perturbative with respect to all physical parameters (cf. p. 11 of Ref. [Cos99] and p. 396 of Ref. [BCP08]).

One should keep in mind that the basis truncation is an *approximation* whose quality has to be checked by varying the numerical parameters and observing the

[1] If Wilson's analytical solution for the hopping parameters is used for the rescaling (i.e., $\tau_N \equiv t_N/W$ with t_N/W from Eq. (4.221)), we have $\tau_{N-2}/\tau_{N-1} \approx \sqrt{\Lambda}$ for $N \gg 1$.

changes in the calculated quantities. In general, there are artifacts in the obtained results because of the neglect of high-energy states (see, e.g., Fig. 5 of Ref. [ŽP09]). By comparing with a fixed point Hamiltonian for $\Lambda = 2$ in the strong-coupling limit (i.e., for $n_{\max} \to \infty$; cf. Sec. 5.1.1), Wilson found that the relative deviation of the numerically calculated lowest energy levels is smaller than 10^{-5} (see p. 822 of Ref. [Wil75] and p. 15 of Ref. [Cos99]). For larger discretization parameter Λ, the error due to the basis truncation should be even smaller.

4.10.5. Renormalization Group aspect

Moving along the Wilson chain, the hopping parameters and on-site energies steadily decrease. As a result, the interaction between the conduction electrons and the impurity spin is effectively studied on increasingly small energy scales (cf. Sec. 4.12.1).

Before considering the Renormalization Group (RG) aspect of NRG, we try to summarize basic concepts of RG theory based on chapter 4.1 of the book [Hew93]. In a "standard" formulation of RG theory, one deals with a Hamiltonian of fixed structure whose parameters change under a RG transformation. For the Kondo model, Anderson's *poor man's scaling* [And70], which is briefly discussed in Sec. 5.1.1, is an example of such an approach. By means of the RG transformation, the original problem is considered on progressively larger length or smaller energy scales, respectively. In the course of this transition, degrees of freedom are eliminated and effectively absorbed into renormalized or "running" coupling parameters. The successive application of the RG transformation generates RG trajectories that describe the "flow" of the renormalized parameters upon reducing the energy scale on which the problem is studied. The RG transformation can possess *fixed points*, at which the running couplings are invariant. A fixed point can be *stable*, so that the RG trajectories are attracted to it, or *unstable*, meaning that the RG flow is eventually driven away from it. Close to a fixed point, it is useful to linearize and subsequently diagonalize the RG transformation. The obtained eigenvalues are then classified according to whether their powers (corresponding to a repeated application of the linearized RG transformation) increase or decrease. An eigenvalue is termed *relevant* (*irrelevant*) if it is larger (smaller) than 1. If there is at least one relevant eigenvalue, the corresponding fixed point is unstable. An eigenvalue that is equal to 1 is called *marginal*. If there are marginal eigenvalues (besides irrelevant ones), the linearized RG transformation alone is not sufficient in order to make a statement about the behavior of the trajectories in the vicinity of the fixed point and a more careful study becomes necessary.

Quantum impurity models can have fixed points with respect to a transformation that effectively lowers the energy scale. In practice, this means that there can be energy regimes in which it is possible to approximately replace the original model by some effective Hamiltonian (corresponding to a fixed point Hamiltonian with certain perturbations) whose parameters flow under the RG transformation. Such a fixed point can be unstable so that the system is eventually driven away from it if the energy scale is further reduced. Typically, there is some stable low-temperature fixed point.

A NRG calculation does not provide direct "access" to the effective Hamiltonians and their renormalized parameters (cf. p. 404 of Ref. [BCP08]). To begin with, only the energy levels obtained by diagonalizing the finite fragments of the Wilson chain are available. This way, however, one has a large set of "parameters" that can be analyzed using the RG formalism. If the truncated Hamiltonians are properly rescaled, it is possible to identify fixed points of the model by studying the *renormalization flow* of the energy levels (i.e., their dependence on the lattice site index n). Close to a fixed point, the lowest-lying eigenvalues depend only weakly on n (note that n has to be *either even or odd* as discussed below and compare, e.g., Fig. 6 of Ref. [Cos99] and Fig. 4 of Ref. [BCP08]). In this case, the numerically calculated energy spectra can be compared to the spectrum of a corresponding fixed point Hamiltonian with suitable corrections [Wil75, KmWW80a, KmWW80b].

In studies of impurity models, it is common to analyze the existence and the properties of fixed points in order to develop a consistent picture of the physical properties of the model on different energy scales. From a theoretical point of view, those fixed points may be considered as particularly interesting which cannot be effectively described by (interacting) fermionic quasiparticles (so-called "non-Fermi-liquids" as opposed to Fermi liquids; see Sec. 5.1.1). It is possible that apparently different models have, e.g., the same low-energy fixed point. In this sense, they can share *universal* properties (see Sec. 5.1.1).

The transition from ${}^0\underset{\sim}{\mathcal{H}}^{(N-1)}_{\mathrm{Wilson}}(z)$ to ${}^0\underset{\sim}{\mathcal{H}}^{(N)}_{\mathrm{Wilson}}(z)$ described by Eq. (4.232) (except for the reset of the groundstate energy) can be regarded as a *Renormalization Group transformation* $\mathcal{R}$ [Wil75, KmWW80a, Hew93, Cos99, BCP08]:

$$\boxed{{}^0\underset{\sim}{\mathcal{H}}^{(N)}_{\mathrm{Wilson}}(z) \equiv \mathcal{R}\left[{}^0\underset{\sim}{\mathcal{H}}^{(N-1)}_{\mathrm{Wilson}}(z)\right].} \tag{4.234}$$

For truncated Wilson chains (as for any other fermionic system of sufficiently small size), there is a pronounced even-odd effect, meaning that the properties of chain fragments with an even and odd number of lattice sites are different (cf. p. 406 of Ref. [BCP08]). As a result, the transformation $\mathcal{R}^2$ (but not $\mathcal{R}$) can have fixed points ([Hew93], p. 84). Furthermore, the fixed points for truncated chains with an even and odd number of sites in general differ (see p. 819 of Ref. [Wil75] and p. 409 of Ref. [BCP08]). Note that information is lost in each step of the iterative diagonalization in which the basis is truncated. For this reason, there is no inverse transformation to $\mathcal{R}$. Strictly speaking, we are therefore not dealing with a group, but with a semi-group ([Hew93], p. 72).

4.11. Implementation of the iterative diagonalization

In order to reduce the numerical cost of the iterative diagonalization, existing symmetries of the Wilson-chain Hamiltonian (4.227) should be taken into account as far as possible. The use of symmetries causes the Hamilton matrix, in each step, to be block-diagonal so that each block can be diagonalized separately. This speeds

up the calculation since the time required for a complete numerical diagonalization of a quadratic matrix of dimension N is of order $\mathcal{O}\big(N^3\big)$.

In the following, the simultaneous use of the two U(1) symmetries that are part of the SU(2) isospin symmetry (discussed in Sec. 2.4.1) and the SU(2) spin symmetry (considered in Sec. 2.4.2) is described. To this end, we work with basis states that have a charge quantum number Q and a magnetic quantum number M. U(1) symmetries have the advantage that they can be exploited simply via a standard product basis. In this sense, these symmetries are "free of charge". However, they do not offer the same computational gain as more complex symmetries do.

Appendix B of Ref. [KmWW80a] describes how to carry out the iterative diagonalization of the Wilson chain using the charge Q and the *full* SU(2) spin symmetry with quantum numbers S and M. The use of the two U(1) symmetries Q and M is also discussed in section 4.2 of Ref. [Hof00] ("NRG at broken rotational symmetry"). Furthermore, technical details regarding a NRG calculation *without* spin symmetry are considered in appendix B of Ref. [ŽP10].

4.11.1. Creating a matrix representation using quantum numbers Q and M

The eigenstates of the truncated and rescaled Hamiltonian $\underset{\sim}{\mathcal{H}}^{(N-1)}_{\text{Wilson}}(z)$, which is defined by Eq. (4.232), are labeled with the quantum numbers that are associated with the following two operators (note that the largest lattice site index appearing in $\underset{\sim}{\mathcal{H}}^{(N-1)}_{\text{Wilson}}(z)$ is $N-1$):

1. *Charge* $\underset{\sim}{Q}_{N-1}$, i.e., electron number relative to half-filling (cf. Eq. (2.53)):

$$\boxed{\underset{\sim}{Q}_{N-1} \equiv \sum_{n=0}^{N-1} \Big(\underset{\sim}{f}^{\dagger}_{n\uparrow}(z) \underset{\sim}{f}_{n\uparrow}(z) + \underset{\sim}{f}^{\dagger}_{n\downarrow}(z) \underset{\sim}{f}_{n\downarrow}(z) - 1 \Big) .} \tag{4.235}$$

   Let Q_{N-1} be the quantum number that is associated with the operator $\underset{\sim}{Q}_{N-1}$. Note that $\underset{\sim}{Q}_{N-1} = 2\underset{\sim}{\eta}^{z}_{N-1}$, with $\underset{\sim}{\eta}^{z}_{N-1}$ being the z-component of the total isospin introduced in Sec. 2.4.1. $\underset{\sim}{\eta}^{z}_{N-1}$ and thus also $\underset{\sim}{Q}_{N-1}$ change sign under a particle-hole transformation (see Eqs. (2.80) and (2.81)). This is the reason why $\underset{\sim}{Q}_{N-1}$ is referred to as "charge" (cf. p. 1008 f. of Ref. [KmWW80a]).

2. *z-component* $\underset{\sim}{S}^{z}_{N-1}$ *of the total spin* (cf. Eq. (2.65)):

$$\boxed{\underset{\sim}{S}^{z}_{N-1} \equiv \frac{1}{2} \sum_{n=0}^{N-1} \Big(\underset{\sim}{f}^{\dagger}_{n\uparrow}(z) \underset{\sim}{f}_{n\uparrow}(z) - \underset{\sim}{f}^{\dagger}_{n\downarrow}(z) \underset{\sim}{f}_{n\downarrow}(z) \Big) + \underset{\sim}{S}^{z} .} \tag{4.236}$$

   Let M_{N-1} be the quantum number that is associated with the operator $\underset{\sim}{S}^{z}_{N-1}$. The corresponding U(1) symmetry is part of the full SU(2) spin

symmetry discussed in Sec. 2.4.2. It should be noted that $\underset{\sim}{S}^z$ alone is no conserved quantity of $\underset{\sim}{\mathcal{H}}^{(N-1)}_{\text{Wilson}}(z)$. As usual, it is advisable to work with $2\underset{\sim}{S}^z_{N-1}$ in an actual numerical implementation since the corresponding quantum number only takes integer values (this is analogous to using $\underset{\sim}{Q}_{N-1}$ instead of $\underset{\sim}{\eta}^z_{N-1}$).

Let us now assume that the Hamiltonian $\underset{\sim}{\mathcal{H}}^{(N-1)}_{\text{Wilson}}(z)$ has been diagonalized so that a certain number of its eigenvalues and eigenstates are available (note that in the following subscripts of quantum numbers are omitted where possible in order to simplify the notation):

$$\boxed{\underset{\sim}{\mathcal{H}}^{(N-1)}_{\text{Wilson}}(z)\,\big|Q,M;(\mathcal{E},r)\big\rangle^{(N-1)}_{(z)} = \mathcal{E}^{(N-1)}_{(Q,M)}(z)\,\big|Q,M;(\mathcal{E},r)\big\rangle^{(N-1)}_{(z)}\ .} \tag{4.237}$$

r is an additional index that resolves all degeneracies, i.e., it numbers states with the same values of $\mathcal{E}^{(N-1)}_{(Q,M)}(z)$, Q_{N-1}, and M_{N-1}. Furthermore, the following matrix elements are supposed to be known:

$$\begin{aligned}
&{}^{(N-1)}_{(z)}\big\langle Q+1,M+1/2;(\mathcal{E},r)\big|\,\underset{\sim}{f}^\dagger_{N-1\uparrow}(z)\,\big|Q,M;(\mathcal{E}',r')\big\rangle^{(N-1)}_{(z)}\ ,\\
&{}^{(N-1)}_{(z)}\big\langle Q+1,M-1/2;(\mathcal{E},r)\big|\,\underset{\sim}{f}^\dagger_{N-1\downarrow}(z)\,\big|Q,M;(\mathcal{E}',r')\big\rangle^{(N-1)}_{(z)}\ .
\end{aligned} \tag{4.238}$$

Our goal is to create a matrix representation of the Hamiltonian $\underset{\sim}{\mathcal{H}}^{(N)}_{\text{Wilson}}(z)$ using Eq. (4.232), which relates $\underset{\sim}{\mathcal{H}}^{(N-1)}_{\text{Wilson}}(z)$ and $\underset{\sim}{\mathcal{H}}^{(N)}_{\text{Wilson}}(z)$. To this end, we first need a basis for the newly added lattice site N:

$$\boxed{\begin{aligned}
|\,0\,\rangle^{(N)} &\equiv |\,\Omega\,\rangle^{(N)}\ ,\\
|\,\uparrow\rangle^{(N)} &\equiv \underset{\sim}{f}^\dagger_{N\uparrow}(z)\,|\,\Omega\,\rangle^{(N)}\ ,\\
|\,\downarrow\rangle^{(N)} &\equiv \underset{\sim}{f}^\dagger_{N\downarrow}(z)\,|\,\Omega\,\rangle^{(N)}\ ,\\
|\,\uparrow\downarrow\rangle^{(N)} &\equiv \underset{\sim}{f}^\dagger_{N\uparrow}(z)\underset{\sim}{f}^\dagger_{N\downarrow}(z)\,|\,\Omega\,\rangle^{(N)}\ .
\end{aligned}} \tag{4.239}$$

Here, $|\,\Omega\,\rangle^{(N)}$ is the vacuum at lattice site N. Note that the ordering of the creation operators in the state $|\,\uparrow\downarrow\rangle^{(N)}$ is a convention. It would even be possible to choose a different ordering for each N. Having a basis for site N, we can construct a

product basis of the enlarged chain fragment that is described by $\underset{\sim}{\mathcal{H}}^{(N)}_{\mathrm{Wilson}}(z)$:

$$\begin{aligned}
\left|Q,M;(\mathcal{E},r)\right\rangle^{(N-1)}_{(z)} \otimes |\,0\,\rangle^{(N)} &\equiv |Q-1,M\quad\;\;;(\mathcal{E},r)_{N-1},1\rangle^{(N)}_{(z)}\,,\\
\left|Q,M;(\mathcal{E},r)\right\rangle^{(N-1)}_{(z)} \otimes |\uparrow\rangle^{(N)} &\equiv |Q\quad\;\;,M+1/2;(\mathcal{E},r)_{N-1},2\rangle^{(N)}_{(z)}\,,\\
\left|Q,M;(\mathcal{E},r)\right\rangle^{(N-1)}_{(z)} \otimes |\downarrow\rangle^{(N)} &\equiv |Q\quad\;\;,M-1/2;(\mathcal{E},r)_{N-1},3\rangle^{(N)}_{(z)}\,,\\
\left|Q,M;(\mathcal{E},r)\right\rangle^{(N-1)}_{(z)} \otimes |\uparrow\downarrow\rangle^{(N)} &\equiv |Q+1,M\quad\;\;;(\mathcal{E},r)_{N-1},4\rangle^{(N)}_{(z)}\,.
\end{aligned} \tag{4.240}$$

Note that the quantum numbers on the left-hand side refer to the operators $\underset{\sim}{Q}_{N-1}$ and $\underset{\sim}{S}^z_{N-1}$, whereas those on the right-hand side refer to $\underset{\sim}{Q}_N$ and $\underset{\sim}{S}^z_N$. Since lattice site N is described by four states, each eigenstate $\left|Q,M;(\mathcal{E},r)\right\rangle^{(N-1)}_{(z)}$ from the previous step $N-1$ appears in four product basis states $|Q',M';(\mathcal{E},r)_{N-1},i\rangle^{(N)}_{(z)}$ of the enlarged chain fragment.

In order to use the symmetries of $\underset{\sim}{\mathcal{H}}^{(N)}_{\mathrm{Wilson}}(z)$, we have to set up matrix representations in invariant subspaces characterized by quantum numbers (Q_N,M_N). For this purpose, Eqs. (4.240) are formally "inverted" (cf. p. 57 of Ref. [Hof00]):

$$\boxed{\begin{aligned}
|Q,M;(\mathcal{E},r)_{N-1},1\rangle^{(N)}_{(z)} &= |Q+1,M\quad\;\;;(\mathcal{E},r)\rangle^{(N-1)}_{(z)} \otimes |\,0\,\rangle^{(N)}\,,\\
|Q,M;(\mathcal{E},r)_{N-1},2\rangle^{(N)}_{(z)} &= |Q\quad\;\;,M-1/2;(\mathcal{E},r)\rangle^{(N-1)}_{(z)} \otimes |\uparrow\rangle^{(N)}\,,\\
|Q,M;(\mathcal{E},r)_{N-1},3\rangle^{(N)}_{(z)} &= |Q\quad\;\;,M+1/2;(\mathcal{E},r)\rangle^{(N-1)}_{(z)} \otimes |\downarrow\rangle^{(N)}\,,\\
|Q,M;(\mathcal{E},r)_{N-1},4\rangle^{(N)}_{(z)} &= |Q-1,M\quad\;\;;(\mathcal{E},r)\rangle^{(N-1)}_{(z)} \otimes |\uparrow\downarrow\rangle^{(N)}\,.
\end{aligned}} \tag{4.241}$$

According to Eqs. (4.240), there are *up to four* ways in which a state with quantum numbers $(Q_N,M_N,(\mathcal{E},r)_{N-1})$ can be created. For arbitrary (possible) quantum numbers $(Q_N,M_N,(\mathcal{E},r)_{N-1})$, not all of the states (4.241) necessarily exist. This, however, is completely irrelevant for the following discussion, which only aims at establishing rules for the calculation of matrix elements involving states of a certain type.

In a subspace with the quantum numbers (Q_N,M_N), the following matrix elements have to be determined in order to obtain the desired Hamilton matrix (cf.

the recursion relation (4.232)):

$$\begin{aligned}
&{}^{(N)}_{(z)}\langle Q,M;(\mathcal{E},r)_{N-1},i|\,\underset{\sim}{\mathcal{H}}^{(N)}_{\text{Wilson}}(z)\,|Q,M;(\mathcal{E}',r')_{N-1},j\rangle^{(N)}_{(z)} \;=\\
&\quad\frac{\tau_{N-2}}{\tau_{N-1}}\,\langle\dots|\,\underset{\sim}{\mathcal{H}}^{(N-1)}_{\text{Wilson}}(z)\,|\dots\rangle_{\boldsymbol{A}} \;+\\
&\quad\tau_{N-1}^{-1}\sum_{\mu}\frac{\epsilon_{N\mu}(z)}{W}\,\langle\dots|\,\underset{\sim}{f}^{\dagger}_{N\mu}(z)\underset{\sim}{f}_{N\mu}(z)\,|\dots\rangle_{\boldsymbol{B}} \;+\\
&\quad\tau_{N-1}^{-1}\sum_{\mu}\frac{t_{N-1\mu}(z)}{W}\,\Big\langle\dots\Big|\Big(\underset{\sim}{f}^{\dagger}_{N-1\mu}(z)\underset{\sim}{f}_{N\mu}(z)+\underset{\sim}{f}^{\dagger}_{N\mu}(z)\underset{\sim}{f}_{N-1\mu}(z)\Big)\Big|\dots\Big\rangle_{\boldsymbol{C}}\;.
\end{aligned}\tag{4.242}$$

The Hamiltonian $\underset{\sim}{\mathcal{H}}^{(N-1)}_{\text{Wilson}}(z)$ only gives a contribution on the diagonal,

$$\begin{aligned}
&\langle\dots|\,\underset{\sim}{\mathcal{H}}^{(N-1)}_{\text{Wilson}}(z)\,|\dots\rangle_{\boldsymbol{A}} \;=\\
&{}^{(N)}_{(z)}\langle Q,M;(\mathcal{E},r)_{N-1},i|\,\underset{\sim}{\mathcal{H}}^{(N-1)}_{\text{Wilson}}(z)\,|Q,M;(\mathcal{E}',r')_{N-1},j\rangle^{(N)}_{(z)} \;=\\
&{}^{(N)}_{(z)}\langle Q,M;(\mathcal{E},r)_{N-1},i|\,\underset{\sim}{\mathcal{H}}^{(N-1)}_{\text{Wilson}}(z)\,|Q,M;(\mathcal{E},r)_{N-1},i\rangle^{(N)}_{(z)}\;\delta_{\mathcal{E}\mathcal{E}'}\,\delta_{rr'}\,\delta_{ij}\;,
\end{aligned}\tag{4.243}$$

and the four types of matrix elements simply correspond to eigenvalues from the previous step $N-1$:

$$\begin{aligned}
{}^{(N)}_{(z)}\langle Q,M;(\mathcal{E},r)_{N-1},1|\,\underset{\sim}{\mathcal{H}}^{(N-1)}_{\text{Wilson}}(z)\,|Q,M;(\mathcal{E},r)_{N-1},1\rangle^{(N)}_{(z)} &= \mathcal{E}^{(N-1)}_{(Q+1,M)}(z)\;,\\
{}^{(N)}_{(z)}\langle Q,M;(\mathcal{E},r)_{N-1},2|\,\underset{\sim}{\mathcal{H}}^{(N-1)}_{\text{Wilson}}(z)\,|Q,M;(\mathcal{E},r)_{N-1},2\rangle^{(N)}_{(z)} &= \mathcal{E}^{(N-1)}_{(Q,M-1/2)}(z)\;,\\
{}^{(N)}_{(z)}\langle Q,M;(\mathcal{E},r)_{N-1},3|\,\underset{\sim}{\mathcal{H}}^{(N-1)}_{\text{Wilson}}(z)\,|Q,M;(\mathcal{E},r)_{N-1},3\rangle^{(N)}_{(z)} &= \mathcal{E}^{(N-1)}_{(Q,M+1/2)}(z)\;,\\
{}^{(N)}_{(z)}\langle Q,M;(\mathcal{E},r)_{N-1},4|\,\underset{\sim}{\mathcal{H}}^{(N-1)}_{\text{Wilson}}(z)\,|Q,M;(\mathcal{E},r)_{N-1},4\rangle^{(N)}_{(z)} &= \mathcal{E}^{(N-1)}_{(Q-1,M)}(z)\;.
\end{aligned}\tag{4.244}$$

The particle-number operators for lattice site N, $\underset{\sim}{n}_{N\mu}(z)\equiv\underset{\sim}{f}^{\dagger}_{N\mu}(z)\underset{\sim}{f}_{N\mu}(z)$, also have diagonal matrix representations,

$$\begin{aligned}
&\langle\dots|\,\underset{\sim}{n}_{N\mu}(z)\,|\dots\rangle_{\boldsymbol{B}} \;=\\
&{}^{(N)}_{(z)}\langle Q,M;(\mathcal{E},r)_{N-1},i|\,\underset{\sim}{n}_{N\mu}(z)\,|Q,M;(\mathcal{E}',r')_{N-1},j\rangle^{(N)}_{(z)} \;=\\
&{}^{(N)}_{(z)}\langle Q,M;(\mathcal{E},r)_{N-1},i|\,\underset{\sim}{n}_{N\mu}(z)\,|Q,M;(\mathcal{E},r)_{N-1},i\rangle^{(N)}_{(z)}\;\delta_{\mathcal{E}\mathcal{E}'}\,\delta_{rr'}\,\delta_{ij}\;,
\end{aligned}\tag{4.245}$$

and, for the chosen numbering of the states in Eqs. (4.241), we directly obtain:

$$\underset{\sim}{n}_{N\uparrow}(z):\begin{pmatrix} 1 & 2 & 3 & 4 & \boldsymbol{j/i} \\ 0 & 0 & 0 & 0 & 1 \\ 0 & \mathbb{1} & 0 & 0 & 2 \\ 0 & 0 & 0 & 0 & 3 \\ 0 & 0 & 0 & \mathbb{1} & 4 \end{pmatrix}, \quad \underset{\sim}{n}_{N\downarrow}(z):\begin{pmatrix} 1 & 2 & 3 & 4 & \boldsymbol{j/i} \\ 0 & 0 & 0 & 0 & 1 \\ 0 & 0 & 0 & 0 & 2 \\ 0 & 0 & \mathbb{1} & 0 & 3 \\ 0 & 0 & 0 & \mathbb{1} & 4 \end{pmatrix}. \tag{4.246}$$

Lastly, the matrix elements of the hopping term have to be determined:

$$\Big\langle \dots \Big| \underbrace{\left(\underset{\sim}{f}^{\dagger}_{N-1\mu}(z)\underset{\sim}{f}_{N\mu}(z) + \underset{\sim}{f}^{\dagger}_{N\mu}(z)\underset{\sim}{f}_{N-1\mu}(z)\right)}_{\equiv \underset{\sim}{F}_{N\mu}(z)} \Big| \dots \Big\rangle_{\boldsymbol{C}} \quad = \tag{4.247}$$

$$\overset{(N)}{(z)}\langle Q, M; (\mathcal{E}, r)_{N-1}, i \big| \, \underset{\sim}{F}_{N\mu}(z) \, \big| Q, M; (\mathcal{E}', r')_{N-1}, j \rangle^{(N)}_{(z)} \ .$$

The states of lattice site N can be "eliminated" from the product basis states (4.241) by using the corresponding matrix representations of the operators $\underset{\sim}{f}^{(\dagger)}_{N\mu}(z)$:

$$\underset{\sim}{f}^{\dagger}_{N\uparrow}(z) \quad : \quad \begin{pmatrix} |\,0\rangle & |\uparrow\rangle & |\downarrow\rangle & |\uparrow\downarrow\rangle & \boldsymbol{(N)} \\ 0 & 0 & 0 & 0 & \langle 0\,| \\ 1 & 0 & 0 & 0 & \langle\uparrow\,| \\ 0 & 0 & 0 & 0 & \langle\downarrow\,| \\ 0 & 0 & 1 & 0 & \langle\uparrow\downarrow\,| \end{pmatrix}, \tag{4.248}$$

$$\underset{\sim}{f}_{N\uparrow}(z) = \left(\underset{\sim}{f}^{\dagger}_{N\uparrow}(z)\right)^{\dagger}: \quad \begin{pmatrix} |\,0\rangle & |\uparrow\rangle & |\downarrow\rangle & |\uparrow\downarrow\rangle & \boldsymbol{(N)} \\ 0 & 1 & 0 & 0 & \langle 0\,| \\ 0 & 0 & 0 & 0 & \langle\uparrow\,| \\ 0 & 0 & 0 & 1 & \langle\downarrow\,| \\ 0 & 0 & 0 & 0 & \langle\uparrow\downarrow\,| \end{pmatrix}, \tag{4.249}$$

$$\underset{\sim}{f}^{\dagger}_{N\downarrow}(z) \quad : \quad \begin{pmatrix} |\,0\rangle & |\uparrow\rangle & |\downarrow\rangle & |\uparrow\downarrow\rangle & \boldsymbol{(N)} \\ 0 & 0 & 0 & 0 & \langle 0\,| \\ 0 & 0 & 0 & 0 & \langle\uparrow\,| \\ 1 & 0 & 0 & 0 & \langle\downarrow\,| \\ 0 & -1 & 0 & 0 & \langle\uparrow\downarrow\,| \end{pmatrix}, \tag{4.250}$$

$$\underset{\sim}{f}_{N\downarrow}(z) = \left(\underset{\sim}{f}^{\dagger}_{N\downarrow}(z)\right)^{\dagger}: \quad \begin{pmatrix} |\,0\rangle & |\uparrow\rangle & |\downarrow\rangle & |\uparrow\downarrow\rangle & \boldsymbol{(N)} \\ 0 & 0 & 1 & 0 & \langle 0\,| \\ 0 & 0 & 0 & -1 & \langle\uparrow\,| \\ 0 & 0 & 0 & 0 & \langle\downarrow\,| \\ 0 & 0 & 0 & 0 & \langle\uparrow\downarrow\,| \end{pmatrix}. \tag{4.251}$$

This way, the matrix elements $\boldsymbol{C}$ can be expressed via matrix elements with respect to the eigenstates from the previous step $N-1$ (note that the operators $\underset{\sim}{F}_{N\mu}(z)$ are Hermitian and compare p. 57 of Ref. [Hof00]):

$$\underset{\sim}{F}_{N\uparrow}(z): \begin{pmatrix} 1 & 2 & 3 & 4 & \boldsymbol{j/i} \\ 0 & \mathcal{A} & 0 & 0 & 1 \\ \mathcal{A}^\dagger & 0 & 0 & 0 & 2 \\ 0 & 0 & 0 & \mathcal{B} & 3 \\ 0 & 0 & \mathcal{B}^\dagger & 0 & 4 \end{pmatrix}, \quad \underset{\sim}{F}_{N\downarrow}(z): \begin{pmatrix} 1 & 2 & 3 & 4 & \boldsymbol{j/i} \\ 0 & 0 & \mathcal{C} & 0 & 1 \\ 0 & 0 & 0 & \mathcal{D} & 2 \\ \mathcal{C}^\dagger & 0 & 0 & 0 & 3 \\ 0 & \mathcal{D}^\dagger & 0 & 0 & 4 \end{pmatrix}, \tag{4.252}$$

with

$$\begin{aligned}
\mathcal{A}_{(\mathcal{E},r)(\mathcal{E}',r')} &= {}^{(N)}_{(z)}\langle Q,M;(\mathcal{E},r)_{N-1},1|\,\underset{\sim}{F}_{N\uparrow}(z)\,|Q,M;(\mathcal{E}',r')_{N-1},2\rangle^{(N)}_{(z)} = \\
&\quad {}^{(N-1)}_{(z)}\langle Q+1,M;(\mathcal{E},r)\,|\,\underset{\sim}{f}^\dagger_{N-1\uparrow}(z)\,|Q,M-1/2;(\mathcal{E}',r')\rangle^{(N-1)}_{(z)}\,, \\
\mathcal{B}_{(\mathcal{E},r)(\mathcal{E}',r')} &= {}^{(N)}_{(z)}\langle Q,M;(\mathcal{E},r)_{N-1},3|\,\underset{\sim}{F}_{N\uparrow}(z)\,|Q,M;(\mathcal{E}',r')_{N-1},4\rangle^{(N)}_{(z)} = \\
&\quad \overset{!}{-}{}^{(N-1)}_{(z)}\langle Q,M+1/2;(\mathcal{E},r)|\,\underset{\sim}{f}^\dagger_{N-1\uparrow}(z)\,|Q-1,M;(\mathcal{E}',r')\,\rangle^{(N-1)}_{(z)}\,, \\
\mathcal{C}_{(\mathcal{E},r)(\mathcal{E}',r')} &= {}^{(N)}_{(z)}\langle Q,M;(\mathcal{E},r)_{N-1},1\,|\,\underset{\sim}{F}_{N\downarrow}(z)\,|Q,M;(\mathcal{E}',r')_{N-1},3\rangle^{(N)}_{(z)} = \\
&\quad {}^{(N-1)}_{(z)}\langle Q+1,M;(\mathcal{E},r)\,|\,\underset{\sim}{f}^\dagger_{N-1\downarrow}(z)\,|Q,M+1/2;(\mathcal{E}',r')\rangle^{(N-1)}_{(z)}\,, \\
\mathcal{D}_{(\mathcal{E},r)(\mathcal{E}',r')} &= {}^{(N)}_{(z)}\langle Q,M;(\mathcal{E},r)_{N-1},2|\,\underset{\sim}{F}_{N\downarrow}(z)\,|Q,M;(\mathcal{E}',r')_{N-1},4\rangle^{(N)}_{(z)} = \\
&\quad {}^{(N-1)}_{(z)}\langle Q,M-1/2;(\mathcal{E},r)|\,\underset{\sim}{f}^\dagger_{N-1\downarrow}(z)\,|Q-1,M;(\mathcal{E}',r')\,\rangle^{(N-1)}_{(z)}\,.
\end{aligned} \tag{4.253}$$

Assuming that the matrix elements (4.238) of the creation operators $\underset{\sim}{f}^\dagger_{N-1\mu}(z)$ are available, a matrix representation of the Hamiltonian $\underset{\sim}{\mathcal{H}}^{(N)}_{\text{Wilson}}(z)$ can now be calculated in all invariant subspaces (Q_N, M_N) by inserting the matrix elements $\boldsymbol{A}$, $\boldsymbol{B}$, and $\boldsymbol{C}$ into Eq. (4.242). A complete numerical diagonalization of the Hamilton matrix in each subspace then gives the eigenvalues $\left\{\mathcal{E}^{(N)}_{(Q,M)}(z)\right\}$ and the eigenstates $\left\{|Q,M;(\mathcal{E},r)\rangle^{(N)}_{(z)}\right\}$. Since the obtained energy eigenvalues are used in order to determine the states to keep, the basis can be truncated only after the Hamiltonian has been diagonalized in *all* subspaces (Q_N, M_N).

If the iterative diagonalization of the Wilson chain needs to be continued (i.e., the enlarged chain fragment including site $N+1$ has to be diagonalized), the following matrix elements with respect to the eigenstates *that are retained in step* N must be determined (compare the matrix elements (4.238) which are necessary

for the calculation of the matrix elements $\boldsymbol{C}$):

$$\boxed{\begin{array}{l} {}^{(N)}_{(z)}\big\langle Q+1, M+1/2; (\mathcal{E}, r)\big| \underset{\sim}{f}^{\dagger}_{N\uparrow}(z) \big|Q, M; (\mathcal{E}', r')\big\rangle^{(N)}_{(z)} \,, \\ {}^{(N)}_{(z)}\big\langle Q+1, M-1/2; (\mathcal{E}, r)\big| \underset{\sim}{f}^{\dagger}_{N\downarrow}(z) \big|Q, M; (\mathcal{E}', r')\big\rangle^{(N)}_{(z)} \,. \end{array}} \tag{4.254}$$

It is possible to calculate these matrix elements by explicit summation using the vector representations of the eigenstates $\big|Q, M; (\mathcal{E}, r)\big\rangle^{(N)}_{(z)}$ with respect to the product basis $\Big\{|Q, M; (\mathcal{E}, r)_{N-1}, i\rangle^{(N)}_{(z)}\Big\}$ (see p. 58 of Ref. [Hof00]). As regards numerical efficiency, however, this approach does not seem to be optimal. As an alternative, the required matrix elements can be determined via matrix-matrix multiplications, for which highly-optimized numerical routines are available. We will return to this point in Sec. 4.11.3 after a short excursus.

4.11.2. Excursus: Transforming to the eigenbasis of the Hamiltonian

Let us assume that we have an orthonormal basis $\big\{|\Phi_i\rangle\big\}$ of the Hilbert space with standard properties,

$$\begin{aligned} \langle\Phi_i|\Phi_j\rangle &= \delta_{ij} \,, \\ \sum_i |\Phi_i\rangle\langle\Phi_i| &= \underset{\sim}{\mathbb{1}} \,, \end{aligned} \tag{4.255}$$

and the (trivial) vector representations

$$|\Phi_i\rangle = \sum_j \delta_{ji} |\Phi_j\rangle \,. \tag{4.256}$$

With respect to this basis, the Hamiltonian $\underset{\sim}{H}$ has the matrix representation $\mathcal{H}$:

$$\underset{\sim}{H} = \sum_{i,j} \mathcal{H}_{ij} |\Phi_i\rangle\langle\Phi_j| \quad \text{with} \quad \mathcal{H}_{ij} \equiv \big\langle\Phi_i\big|\underset{\sim}{H}\big|\Phi_j\big\rangle \,. \tag{4.257}$$

Furthermore, let $\big\{|E_\mu\rangle\big\}$ be the orthonormal eigenbasis of $\underset{\sim}{H}$, i.e.:

$$\begin{aligned} \underset{\sim}{H}\,|E_\mu\rangle &= E_\mu |E_\mu\rangle \,, \\ \langle E_\mu|E_\nu\rangle &= \delta_{\mu\nu} \quad\;\; , \\ \sum_\mu |E_\mu\rangle\langle E_\mu| &= \underset{\sim}{\mathbb{1}} \quad\;\; . \end{aligned} \tag{4.258}$$

The eigenstates have certain vector representations with respect to the old basis:

$$|E_\mu\rangle = \sum_i \langle\Phi_i|E_\mu\rangle |\Phi_i\rangle \equiv \sum_i \mathcal{U}_{i\mu} |\Phi_i\rangle \,. \tag{4.259}$$

$\mathcal{U}$ is a unitary matrix whose columns contain the vector representations of the eigenstates $|E_\mu\rangle$ with respect to the original basis $\{|\Phi_i\rangle\}$. It is obtained as part of a complete numerical diagonalization of the Hamilton matrix $\mathcal{H}$.

The matrix $\mathcal{U}$ can be used, e.g., to transform to the spectral (diagonal) representation $\mathcal{D}$ of $\underset{\sim}{H}$:

$$\underset{\sim}{H} = \sum_{\mu,\nu} \mathcal{D}_{\mu\nu} |E_\mu\rangle\langle E_\nu| \;, \tag{4.260}$$

with

$$\begin{aligned} \mathcal{D}_{\mu\nu} \;\equiv\; E_\mu \delta_{\mu\nu} \;&=\; \big\langle E_\mu \big| \underset{\sim}{H} \big| E_\nu \big\rangle \\ &=\; \sum_{i,j} \langle E_\mu|\Phi_i\rangle \mathcal{H}_{ij} \langle \Phi_j|E_\nu\rangle \\ &=\; \sum_{i,j} \mathcal{U}^\dagger_{\mu i}\, \mathcal{H}_{ij}\, \mathcal{U}_{j\nu} \;. \end{aligned} \tag{4.261}$$

Note that this system of equations corresponds to a *matrix equation*:

$$\boxed{\mathcal{D} = \mathcal{U}^\dagger \mathcal{H} \mathcal{U} \;.} \tag{4.262}$$

Completely analogous to Eqs. (4.261), the old matrix representation $\mathcal{O}$ of an arbitrary operator $\underset{\sim}{O}$ is transformed to the eigenbasis of the Hamiltonian, resulting in the matrix $\widetilde{\mathcal{O}}$:

$$\widetilde{\mathcal{O}}_{\mu\nu} = \sum_{i,j} \mathcal{U}^\dagger_{\mu i}\, \mathcal{O}_{ij}\, \mathcal{U}_{j\nu} \;, \tag{4.263}$$

or, in the form of a matrix equation:

$$\boxed{\widetilde{\mathcal{O}} = \mathcal{U}^\dagger \mathcal{O} \mathcal{U} \;.} \tag{4.264}$$

Having the matrix representation $\mathcal{O}$ with respect to the original basis and the transformation matrix $\mathcal{U}$, we can thus calculate the matrix representation $\widetilde{\mathcal{O}}$ with respect to the eigenbasis of the Hamiltonian by taking the conjugate transpose of $\mathcal{U}$ and performing two matrix-matrix multiplications using suitable numerical routines. It should be noted that the operator $\underset{\sim}{O}$ might not have the same symmetry properties as the Hamilton operator $\underset{\sim}{H}$. In this case, $\underset{\sim}{O}$ can "connect" different subspaces that are invariant with regard to $\underset{\sim}{H}$ (the existing connections can then be described by what is known as *selection rules*).

4.11.3. Calculating the matrix representations of the creation operators for the next step

We now return to the calculation of the matrix elements (4.254). In contrast to the Hamiltonian $\underset{\sim}{\mathcal{H}}^{(N)}_{\mathrm{Wilson}}(z)$, the creation operators $\underset{\sim}{f}^\dagger_{N\mu}(z)$ connect subspaces with different values of Q_N and M_N (the corresponding selection rules are illustrated in Fig. 4.6).

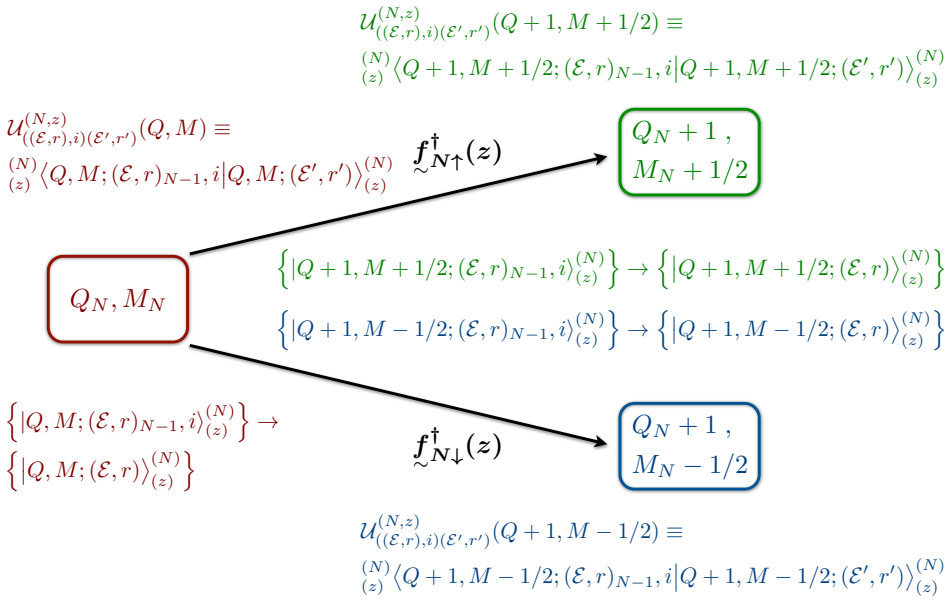

Figure 4.6.: Illustration of the selection rules, regarding the quantum numbers Q_N and M_N, for the matrix elements of the creation operators $\underset{\sim}{f}^{\dagger}_{N\mu}(z)$ with respect to the eigenbasis of the Hamiltonian in step N. In each subspace (Q_N, M_N), the numerical diagonalization of the matrix representation of $\underset{\sim}{\mathcal{H}}^{(N)}_{\mathrm{Wilson}}(z)$ with respect to the corresponding product basis $\left\{|Q,M;(\mathcal{E},r)_{N-1},i\rangle^{(N)}_{(z)}\right\}$ gives the matrix of eigenvectors $\mathcal{U}^{(N,z)}(Q,M)$.

According to the general result (4.264), the matrix elements of $\underset{\sim}{f}^{\dagger}_{N\uparrow}(z)$ that are required for the next step of the iterative diagonalization can be calculated in the following way:

$$\begin{aligned}
&{}^{(N)}_{(z)}\big\langle Q+1, M+1/2; (\mathcal{E},r)\big|\, \underset{\sim}{f}^{\dagger}_{N\uparrow}(z)\,\big|Q, M; (\mathcal{E}',r')\big\rangle^{(N)}_{(z)} \\
&\quad = \sum_{\substack{((\mathcal{V},q),i)\\((\mathcal{V}',q'),j)}} \Big[\Big(\mathcal{U}^{(N,z)}(Q+1, M+1/2)\Big)^{\dagger}_{(\mathcal{E},r)((\mathcal{V},q),i)} \times \\
&\qquad\quad {}^{(N)}_{(z)}\big\langle Q+1, M+1/2; (\mathcal{V},q)_{N-1}, i\big|\, \underset{\sim}{f}^{\dagger}_{N\uparrow}(z)\,\big|Q, M; (\mathcal{V}',q')_{N-1}, j\big\rangle^{(N)}_{(z)} \times \\
&\qquad\quad \mathcal{U}^{(N,z)}_{((\mathcal{V}',q'),j)(\mathcal{E}',r')}(Q, M)\Big] .
\end{aligned} \tag{4.265}$$

The matrix elements of $\underset{\sim}{f}^{\dagger}_{N\downarrow}(z)$ are obtained in an analogous manner:

$$\begin{aligned}
&{}^{(N)}_{(z)}\big\langle Q+1, M-1/2; (\mathcal{E},r)\big|\, \underset{\sim}{f}^{\dagger}_{N\downarrow}(z)\,\big|Q, M; (\mathcal{E}',r')\big\rangle^{(N)}_{(z)} \\
&\quad = \sum_{\substack{((\mathcal{V},q),i)\\((\mathcal{V}',q'),j)}} \Big[\Big(\mathcal{U}^{(N,z)}(Q+1, M-1/2)\Big)^{\dagger}_{(\mathcal{E},r)((\mathcal{V},q),i)} \times \\
&\qquad\quad {}^{(N)}_{(z)}\big\langle Q+1, M-1/2; (\mathcal{V},q)_{N-1}, i\big|\, \underset{\sim}{f}^{\dagger}_{N\downarrow}(z)\,\big|Q, M; (\mathcal{V}',q')_{N-1}, j\big\rangle^{(N)}_{(z)} \times \\
&\qquad\quad \mathcal{U}^{(N,z)}_{((\mathcal{V}',q'),j)(\mathcal{E}',r')}(Q, M)\Big] .
\end{aligned} \tag{4.266}$$

As input information, we thus need the matrix representations of $\underset{\sim}{f}^{\dagger}_{N\mu}(z)$ with respect to the product bases of the two connected subspaces (which are, in general, non-quadratic since the dimensions of the invariant subspaces vary) and the corresponding transformation matrices $\mathcal{U}^{(N,z)}(Q, M)$ (cf. Fig. 4.6).

Let us take a closer look at the matrix elements

$${}^{(N)}_{(z)}\big\langle Q, M; (\mathcal{V},q)_{N-1}, i\big|\, \underset{\sim}{f}^{\dagger}_{N\mu}(z)\,\big|Q', M'; (\mathcal{V}',q')_{N-1}, j\big\rangle^{(N)}_{(z)} . \tag{4.267}$$

The index i of a product basis state $|Q, M; (\mathcal{V},q)_{N-1}, i\rangle^{(N)}_{(z)}$ indicates how this state has been created (cf. Eq. (4.241)), i.e., which subspace (Q_{N-1}, M_{N-1}) of the previous step it comes from. Since the eigenstates $|Q, M; (\mathcal{V},q)\rangle^{(N-1)}_{(z)}$ obtained in step $N-1$ are orthonormal, the matrix elements (4.267) can only be non-zero if the left and right state originate from the same subspace (Q_{N-1}, M_{N-1}) and, furthermore, they are proportional to $\delta_{\mathcal{V}\mathcal{V}'}\,\delta_{qq'}$. As a result, the matrix

representations of the creation operators $\underset{\sim}{f}^{\dagger}_{N\mu}(z)$ with respect to the product basis states each contain two non-zero blocks, which are equal to $\pm\mathbb{1}$ (two blocks are non-zero because there are two possibilities for matching the charge and magnetic quantum numbers of the left and right product basis state in each case):

$$\boxed{\begin{aligned}\underset{\sim}{f}^{\dagger}_{N\uparrow}(z):&\quad\begin{pmatrix} 1 & 2 & 3 & 4 & \boldsymbol{j/i} \\ 0 & 0 & 0 & 0 & 1 \\ \mathbb{1} & 0 & 0 & 0 & 2 \\ 0 & 0 & 0 & 0 & 3 \\ 0 & 0 & \mathbb{1} & 0 & 4 \end{pmatrix}, \\ \underset{\sim}{f}^{\dagger}_{N\downarrow}(z):&\quad\begin{pmatrix} 1 & 2 & 3 & 4 & \boldsymbol{j/i} \\ 0 & 0 & 0 & 0 & 1 \\ 0 & 0 & 0 & 0 & 2 \\ \mathbb{1} & 0 & 0 & 0 & 3 \\ 0 & -\mathbb{1} & 0 & 0 & 4 \end{pmatrix}.\end{aligned}} \tag{4.268}$$

An additional minus sign appears in case of $\underset{\sim}{f}^{\dagger}_{N\downarrow}(z)$ since ${}^{(N)}\langle\uparrow\downarrow|\,\underset{\sim}{f}^{\dagger}_{N\downarrow}(z)\,|\uparrow\rangle^{(N)} = -1$. The matrix-matrix multiplications that correspond to Eq. (4.266) are illustrated in Fig. 4.7.

4.12. Temperature in a NRG calculation

Unfortunately, a solution of the eigenvalue problem of the full semi-infinite Wilson chain, described by Hamiltonian (4.227), is not available. Instead, the iterative diagonalization results in approximations to the *low-energy spectrum* of chain fragments of increasing length. The quality of this approximation critically depends on the number of kept states. If the low-energy spectra are sufficiently accurate (i.e., if enough states are retained), they can be used to calculate thermodynamic expectation values that are representative of the properties of the full Wilson chain *in certain temperature intervals*. To this end, one or several suitable temperature values are *assigned* to each step of the iterative diagonalization.

When choosing the temperatures for which observables are calculated in a certain step, there a two major aspects to consider:

1. In the course of the iterative diagonalization, high-energy states are discarded in order to allow for the approximate treatment of large chain fragments. As a consequence, only a relatively small number of approximate eigenstates of the Hamiltonian $\underset{\sim}{\mathcal{H}}^{(N)}_{\mathrm{Wilson}}(z)$ is available in step N. When calculating thermodynamic expectation values, the discarded high-energy states would appear with certain pre-factors (depending on the studied observable) and certain weights (depending on the considered temperature). In order to produce results that accurately reflect the properties of the chain fragment

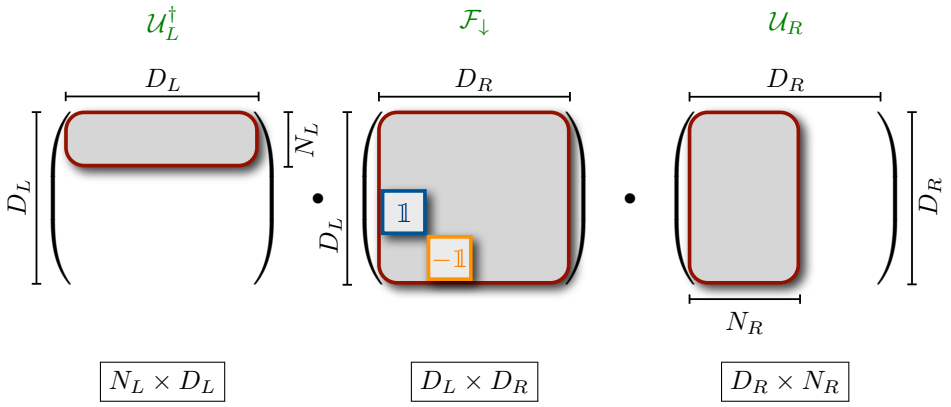

Figure 4.7.: Illustration of the matrix-matrix multiplications that correspond to Eq. (4.266). $\mathcal{U}_{L(R)}$ is the matrix of eigenvectors (in ascending order with respect to the calculated eigenvalues) for the left (right) subspace, and $\mathcal{F}_\downarrow$ denotes the matrix representation (4.268) of $\underset{\sim}{f}^\dagger_{N\downarrow}(z)$. The dimensions of the left and right subspace are D_L and D_R, respectively, and N_L (N_R) eigenstates are kept after basis truncation. The resulting matrix thus has dimensions $N_L \times N_R$. Because of the simple structure of $\mathcal{F}_\downarrow$, the calculation produces a lot of zeros. If performance is insufficient, one should investigate whether the memory layout of the matrices allows for optimization.

in step N, the temperature has to be chosen *sufficiently low* so that the contribution of the high-lying, non-existing states would be small and can be safely neglected. Because of the pre-factors, certain observables such as the specific heat (see p. 409 f. of Ref. [BCP08]) are more susceptible to truncation errors than others and thus, in general, more difficult to calculate.

2. Only finite chain fragments are (approximately) diagonalized. As a result, information about the lowest energy scales (encoded in the hopping parameters and on-site energies of the remaining part of the Wilson chain) is missing from the energy spectrum obtained in step N. Since this mainly affects the low-energy part of the spectrum ([BCP08], p. 408), the temperature has to be *so high* that the structure of the lowest-lying levels is thermally washed out and the importance of the missing details sufficiently reduced. The inaccuracy of the calculated observables because of the truncation of the Wilson chain can be estimated using perturbation theory (see the next section 4.12.1).

In practice, it might not be possible to simultaneously fulfill both requirements equally well. In this case, some kind of trade-off is necessary when assigning temperatures to the different steps of the iterative diagonalization.

4.12.1. Assigning temperatures to the different steps of the iterative diagonalization

The energy spectra of the truncated and rescaled Hamiltonians ${}^0\underset{\sim}{\mathcal{H}}^{(N)}_{\mathrm{Wilson}}(z)$ are characterized by the lowest excitation "energy" $\mathcal{E}^{(N)}_{\mathrm{min}}(z) > 0$ and the "energy" $\mathcal{E}^{(N)}_{\mathrm{max}}(z)$ of the highest kept state. In his calculations, Wilson found the lowest excitation energy to be usually smaller than 1 ([Wil75], p. 817). $\mathcal{E}^{(N)}_{\mathrm{max}}(z)$ is either directly determined by the chosen cutoff $\mathcal{E}_{\mathrm{keep}}$ (and the enforced energy gap, cf. Sec. 4.10.2) or it results from the requested number N_{keep} of retained states and the value of the discretization parameter Λ (which controls how dense the energy spectra are [CPLO97]). Typical values are $\mathcal{E}^{(N)}_{\mathrm{max}}(z) \approx 5 \ldots 10$ (see p. 817 of Ref. [Wil75], p. 15 of Ref. [Cos99], and p. 406 of Ref. [BCP08]).

In order to assign a temperature to each step of the iterative diagonalization, a dimensionless parameter $\bar{\beta}$ ([BCP08], p. 408) corresponding to an inverse thermal energy β is introduced (it is also possible to define a set $\{\bar{\beta}_i\}$ of such values, see below). Since the rescaling factors (4.230) depend on N and render the lowest excitation energy similar for all N, $\bar{\beta}$ can be chosen to be independent of N. A similar quantity called $\bar{\beta}$ already appears in Refs. [Wil75] (see p. 826 and table XI) and [KmWW80a] (see Eq. (2.41)). According to the two requirements discussed at the beginning of section 4.12, one now tries to choose $\bar{\beta}$ in such a way that the

following inequalities hold:

$$\boxed{\mathcal{E}_{\min}^{(N)}(z) \ll \bar{\beta}^{-1} \ll \mathcal{E}_{\max}^{(N)}(z) \;\Leftrightarrow\; \underbrace{\left[\mathcal{E}_{\min}^{(N)}(z)\right]^{-1}}_{>1} \gg \bar{\beta} \gg \underbrace{\left[\mathcal{E}_{\max}^{(N)}(z)\right]^{-1}}_{\sim 0.1} .} \tag{4.269}$$

In the simplest case, $\bar{\beta}$ is also taken to be independent of the twist parameter z. Through $\mathcal{E}_{\max}^{(N)}(z)$, the choice of $\bar{\beta}$ depends on the discretization parameter Λ if a fixed number of states is kept in each step (cf. p. 408 of Ref. [BCP08]). The inequalities (4.269) leave a certain (limited) freedom when defining $\bar{\beta}$. Because of the typical values of $\mathcal{E}_{\min}^{(N)}(z)$ and $\mathcal{E}_{\max}^{(N)}(z)$ quoted above, a reasonable choice of $\bar{\beta}$ usually is (cf. table XI of Ref. [Wil75], p. 1010 f. of Ref. [KmWW80a], p. 1045 of Ref. [KmWW80b], and p. 408 of Ref. [BCP08]):

$$\boxed{\bar{\beta} \in [0.4, 1] \, .} \tag{4.270}$$

By undoing the rescaling of the truncated Hamiltonians (cf. Eq. (4.233)), the physical temperature T_N (or inverse thermal energy β_N) in step N of the iterative diagonalization is found to be:

$$\boxed{k_B T_N = \frac{1}{\beta_N} = \frac{W \tau_{N-1}}{\bar{\beta}} \, .} \tag{4.271}$$

Because of the N-dependence of the rescaling factors τ_{N-1}, the temperature also becomes dependent on the maximal lattice site index N of the chain fragment in step N. As a result, we effectively assign a certain temperature to a chain fragment of a certain length. Since the rescaling factors are related to the exponentially declining hopping parameters (i.e., $\tau_{N-1} \sim t_{N-1\mu}/W$), Eq. (4.271) implies that the effective temperature also decreases exponentially along the Wilson chain towards the open end. The choice of the maximal lattice site index $n_{\max}$ of the considered chain fragments thus determines the lowest temperature for which observables can be calculated.

If the rescaling factors τ_{N-1} were contingent on the twist parameter z, then T_N would also depend on z according to Eq. (4.271) (unless $\bar{\beta}$ was chosen in such a way as to compensate the z-dependence of τ_{N-1}). z-averaging, however, aims at taking the mean value of observables calculated for different z-values *at fixed temperature* ([BCP08], p. 411). z-independent rescaling factors thus technically simplify a z-averaging because one has the same set of temperatures $\{T_N\}$ for all considered z-values. Nevertheless, using some kind of interpolation, it would still be possible to perform a meaningful z-averaging in case of z-dependent (i.e., possibly optimized) effective temperatures. Since the condition (4.269) still leaves a certain freedom when choosing $\bar{\beta}$ (i.e., when assigning a temperature T_N to a step N), the question remains as to whether such an "optimized" z-averaging leads to any appreciable improvement of the results.

What happens if $\bar{\beta}$ is chosen incorrectly?

1. If $\bar{\beta}$ is taken *too large*, i.e., if the temperature is effectively too low, observables calculated for a single z-value can be expected to show pronounced oscillations as a function of temperature, even for discretization parameters as "small" as, e.g., $\Lambda = 3$.

2. If $\bar{\beta}$ is chosen *too small*, i.e., if the temperature is effectively too high, observables can deviate significantly from the correct result because of the missing high-energy states. Without the exact result, however, this might not be obvious so that it could be more dangerous to take $\bar{\beta}$ too small.

As long as the above condition (4.269) is fulfilled, there is no reason not to assign *several* temperatures to a single step of the iterative diagonalization via a set of values $\left\{\bar{\beta}_i\right\}$ (cf. p. 1045 of Ref. [KmWW80b]). On the contrary, this can help to ensure that the temperature in a certain step is chosen correctly (i.e., neither too low nor too high): As with all other numerical parameters, the calculated observables should only weakly depend on $\bar{\beta}$. In this particular case, this means that the data points obtained from a set of values $\left\{\bar{\beta}_i\right\}$ all have to lie on the same smooth curve.

There is an estimate for the error that results from neglecting the semi-infinite remainder of the Wilson chain. It is obtained by treating the coupling term that connects the considered and neglected part of the chain in perturbation theory. For the magnetic susceptibility, such a calculation shows that the error is of order $\mathcal{O}(\bar{\beta}/\Lambda)$ (see p. 1010 and appendix F of Ref. [KmWW80a]). It thus becomes smaller for higher effective temperature (washing out the low-energy spectrum that is significantly modified by the remaining part of the Wilson chain) and larger discretization parameter (reducing the relative strength of the coupling term).

4.13. Calculation of thermodynamic observables

Having identified a set of suitable temperatures $\left\{T_N^i\right\}$, we can use the approximate energy spectrum obtained in step N, which comprises a relatively small number of eigenvalues of the order of a few thousand, for the calculation of thermodynamic observables. These are meant to resemble the quantities that would result for the considered temperatures $\left\{T_N^i\right\}$ in a hypothetical calculation taking into account the *full* Wilson chain. As a reminder, thermodynamic expectation values are determined with respect to the grand-canonical ensemble for the chosen value of the chemical potential μ_{chem}. Since the chemical potential is absorbed into the Hamiltonian according to the definition (2.16), the eigenvalues $\left\{\mathcal{E}_{(Q,M)}^{(N)}(z)\right\}$ of $\underset{\sim}{\mathcal{H}}_{\text{Wilson}}^{(N)}(z)$ already include the effect of the term $-\mu_{\text{chem}}\underset{\sim}{N}$.

4.13.1. The concept of an "impurity contribution"

When defining observables, there are at least three important aspects to consider:

1. The interaction between impurity and conduction electrons is *not* negligibly small. The two subsystems are therefore *not* weakly coupled. As a result, certain observables such as the entropy are not additive, i.e., the total entropy is not simply the sum of entropies of the subsystems. In this sense, there is no "entropy of the impurity".

2. We are interested in a system with an arbitrarily large number of lattice sites L that is mapped onto the semi-infinite Wilson chain. Unless observables are properly normalized (e.g., by considering the contribution per lattice site) or suitable differences are calculated, the limit $L \to \infty$ is, in general, not well defined.

3. In an experimental study of, e.g., magnetic ions in a metallic host, it might be difficult or even impossible to directly measure properties of the impurity atoms. However, for, e.g., atoms and molecules deposited on a suitable substrate, certain impurity properties are directly measurable (see the introduction of the paper included in chapter 8).

It is for these reasons that one usually takes a pragmatic approach by considering "impurity contributions to thermodynamic observables". The *impurity contribution* $O_{\mathrm{imp}}(T,B)$ *to an observable* $O(T,B)$ is defined in the following way:

$$\boxed{O_{\mathrm{imp}}(T,B) \equiv O_{\mathrm{total}}^{\text{with impurity}}(T,B) - O_{\mathrm{total}}^{\text{without impurity}}(T,B)\ .} \tag{4.272}$$

Such a quantity is meant to reflect the changes in an observable due to the presence of the impurity. Conceptually, one would have to perform two measurements: one for a system with impurities (whose mutual interaction has to be sufficiently small so that a description using a single-impurity model is possible) and one for a comparable "clean" system. The results would then be subtracted in order to compare them with the corresponding impurity contribution. In principle, the quantity $O_{\mathrm{total}}^{\text{w/o impurity}}(T,B)$ can be calculated analytically since the system without impurity is non-interacting. However, it is more convenient to determine this quantity numerically, too, by using NRG and removing the impurity part from the Wilson chain. This could even improve the quality of the obtained results since there is the prospect that similar numerical errors cancel when calculating the difference (4.272) (cf. p. 56 of Ref. [Žit07]). Note that it is necessary to determine $O_{\mathrm{total}}^{\text{w/o impurity}}(T,B)$ for each value of the magnetic field B if the g-factor of the electrons is non-zero (on the other hand, for $g_e = 0$, the quantity does not depend on B at all).

In principle, all impurity contributions can be calculated by taking suitable derivatives of the *impurity contribution to the free energy* F_{imp} (or, equivalently,

the grand-canonical potential[2]):

$$\boxed{F_{\mathrm{imp}}(T,B) \equiv -k_B T \ln\left(\frac{Z^{\text{with impurity}}(T,B)}{Z^{\text{w/o impurity}}(T,B)}\right).} \tag{4.273}$$

Here, $Z(T,B)$ is the grand-canonical partition function. Although it seems to be a good idea to consider alternatives before calculating numerical derivatives ([BCP08], p. 408), determining impurity contributions by numerical differentiation of F_{imp} is nevertheless possible (see, e.g., [MWC12]).

Note that thermodynamic expectation values of impurity operators can also be calculated using NRG (as an example, we discuss the calculation of the impurity magnetization in Sec. 4.13.4). Such *local observables* are valuable since they directly reflect the properties of the impurity in contact with the conduction electrons.

4.13.2. Definitions of the considered observables

For the calculation of thermodynamic expectation values, we introduce the grand-canonical *partition function*,

$$Z(T,B) \equiv \mathrm{tr}\left[\mathrm{e}^{-\beta\left(\underset{\sim}{H}(B)-\mu_{\mathrm{chem}}\underset{\sim}{N}\right)}\right], \tag{4.274}$$

and the grand-canonical *density operator*:

$$\underset{\sim}{\rho}(T,B) \equiv \frac{\mathrm{e}^{-\beta\left(\underset{\sim}{H}(B)-\mu_{\mathrm{chem}}\underset{\sim}{N}\right)}}{Z(T,B)}\,. \tag{4.275}$$

In this thesis, the following thermodynamic observables with standard definitions are considered:

1. *Entropy* $S(T,B)$:

$$\boxed{\begin{aligned} S(T,B) &\equiv -\left.\frac{\partial F(T,B)}{\partial T}\right|_B \\ &= -k_B\left\langle \ln \underset{\sim}{\rho}(T,B)\right\rangle = -k_B\,\mathrm{tr}\left[\underset{\sim}{\rho}(T,B)\ln\underset{\sim}{\rho}(T,B)\right] \\ &= \ldots = k_B\beta\left\langle \underset{\sim}{H}(B)-\mu_{\mathrm{chem}}\underset{\sim}{N}\right\rangle + k_B \ln Z(T,B)\,. \end{aligned}} \tag{4.276}$$

[2] As the grand-canonical potential, F depends on the chemical potential μ_{chem}, i.e., $F = F(T,B,\mu_{\mathrm{chem}})$. Since the particle-hole symmetric case is exclusively considered in this thesis (i.e., the chemical potential is always assumed to be zero), we omit the dependency on μ_{chem} in the following.

2. *Total magnetization* $M(T,B)$:

$$\boxed{\begin{aligned} M(T,B) &\equiv -\left.\frac{\partial F(T,B)}{\partial B}\right|_T \\ &= \ldots = -\mu_B \left\langle g_e \underset{\sim}{S}^z_{\text{total}} + g_S \underset{\sim}{S}^z \right\rangle \\ &\overset{g_e = g_S}{=} -g_S \mu_B \left\langle \underset{\sim}{S}^z_{\text{total}} \right\rangle . \end{aligned}} \tag{4.277}$$

As an alternative, one can introduce a *magnetization operator* (cf. p. 9 of Ref. [NR09]),

$$\underset{\sim}{M} \equiv -\frac{\partial \underset{\sim}{H}(B)}{\partial B} , \tag{4.278}$$

and take its thermodynamic expectation value:

$$\boxed{M(T,B) = \left\langle \underset{\sim}{M} \right\rangle .} \tag{4.279}$$

On the one hand, the total magnetization thus reflects how the free energy changes upon a variation of the magnetic field and, on the other hand, it is the average magnetic moment of the system for given T and B. Note that the magnetization operator and therefore also the magnetization are additive quantities, making it possible to define an *impurity magnetization* (see Sec. 4.13.4).

3. *Magnetic susceptibility* $\chi(T,B)$:

$$\boxed{\begin{aligned} \chi(T,B) &\equiv \left.\frac{\partial M(T,B)}{\partial B}\right|_T = -\left.\frac{\partial^2 F(T,B)}{\partial B^2}\right|_T \\ &\overset{g_e = g_S}{=} \ldots = (g_S \mu_B)^2 \beta \Big[\left\langle \left(\underset{\sim}{S}^z_{\text{total}} \right)^2 \right\rangle - \left\langle \underset{\sim}{S}^z_{\text{total}} \right\rangle^2 \Big] . \end{aligned}} \tag{4.280}$$

For vanishing magnetic field, the expression obtained for equal g-factors is a special case of the *fluctuation-dissipation theorem* (see, e.g., p. 23 of Ref. [NR09]), which relates the response to an external perturbation (in this case, the magnetic field) to unperturbed random fluctuations of the system (here, to fluctuations of $\underset{\sim}{S}^z_{\text{total}}$). Since the average magnetic moment in zero field vanishes, a simplified equation holds for the zero-field susceptibility:

$$\chi(T, B=0) \overset{g_e = g_S}{=} (g_S \mu_B)^2 \beta \left\langle \left(\underset{\sim}{S}^z_{\text{total}} \right)^2 \right\rangle . \tag{4.281}$$

4. *Effective magnetic moment* $\mu_{\text{eff}}(T,B)$:

$$\mu^2_{\text{eff}}(T,B) \equiv k_B T \chi(T,B) . \tag{4.282}$$

In particular, for a free spin $\underset{\sim}{\boldsymbol{S}}$, we have the following result, which corresponds to the well-known *Curie law*:

$$\begin{aligned}\mu_{\mathrm{eff}}^2(T, B=0) &= \mu_{\mathrm{eff}}^2 \\ &= (g_S\mu_B)^2\big\langle\big(\underset{\sim}{S}^z\big)^2\big\rangle = (g_S\mu_B)^2\big\langle\underset{\sim}{\boldsymbol{S}}^2\big\rangle/3 = (g_S\mu_B)^2 S(S+1)/3\,.\end{aligned} \tag{4.283}$$

Note that in case of equal g-factors the above observables can all be calculated solely by using the quantum numbers $\mathcal{E}^{(N)}_{(Q,M)}(z)$ and M_N of the eigenstates of $\underset{\sim}{\mathcal{H}}^{(N)}_{\mathrm{Wilson}}(z)$.

4.13.3. Calculating impurity contributions

To begin with, we need to determine the *partition function in step N* for the temperatures $\{T_N^i\}$ that result from the set of values $\{\bar{\beta}_i\}$ according to Eq. (4.271). As an approximation to the "true" partition function (describing the properties of the full semi-infinite Wilson chain), that can be used when calculating either impurity contributions or local observables, the following quantity is considered:

$$\boxed{\begin{aligned}Z^{(N)}(T_N^i, B; z) &\equiv \mathrm{tr}\Big[\mathrm{e}^{-\beta_N^i \underset{\sim}{H}^{(N)}_{\mathrm{Wilson}}(z)}\Big] = \mathrm{tr}\Big[\mathrm{e}^{-W\tau_{N-1}\beta_N^i \underset{\sim}{H}^{(N)}_{\mathrm{Wilson}}(z)/W\tau_{N-1}}\Big] \\ &= \mathrm{tr}\Big[\mathrm{e}^{-\bar{\beta}_i \underset{\sim}{\mathcal{H}}^{(N)}_{\mathrm{Wilson}}(z)}\Big] \;\approx\; \sum_{\substack{Q_N, M_N;\\ (\mathcal{E},r)_N}} \mathrm{e}^{-\bar{\beta}_i \mathcal{E}^{(N)}_{(Q,M)}(z)}\,.\end{aligned}} \tag{4.284}$$

Note that the Hamiltonian of the Wilson chain $\underset{\sim}{H}_{\mathrm{Wilson}}(z)$ from Eq. (4.227) implicitly depends on the magnetic field B (via the hopping parameters and on-site energies) so that all quantities derived from it, such as $Z^{(N)}(T_N^i, B; z)$, also become dependent on B.

One possibility is to calculate thermodynamic expectation values only with those eigenstates of $\underset{\sim}{\mathcal{H}}^{(N)}_{\mathrm{Wilson}}(z)$ that are kept after basis truncation (cf. p. 406 and 409 f. of Ref. [BCP08] and p. 18 of Ref. [Cos99]). As an alternative, one can also use *all* eigenstates obtained in step N. In case of those thermodynamic observables that are solely determined by the quantum numbers of the eigenstates, this would not even significantly increase the numerical cost. However, if matrix representations of impurity operators are required, which first have to be transformed to the eigenbasis in step N (see Sec. 4.13.4), the calculation becomes more expensive. Whether it is beneficial to use all eigenstates when investigating the thermodynamics, ought to depend on how well the condition (4.269) is fulfilled if only the retained states are taken into account.

Resetting the groundstate energy to zero after each step of the iterative diagonalization does not affect thermodynamic expectation values. We may thus use ${}^0\underset{\sim}{\mathcal{H}}^{(N)}_{\mathrm{Wilson}}(z)$ instead of $\underset{\sim}{\mathcal{H}}^{(N)}_{\mathrm{Wilson}}(z)$. This is even preferable since all eigenvalues of

${}^0\underset{\sim}{\mathcal{H}}^{(N)}_{\mathrm{Wilson}}(z)$ are non-negative so that the occurrence of exponentials with large positive arguments, which can cause a numerical overflow, is avoided when evaluating traces.

According to the definitions (4.276) to (4.280), the approximate eigenstates of $\underset{\sim}{\mathcal{H}}^{(N)}_{\mathrm{Wilson}}(z)$ are used to calculate the following *provisional approximations* to the total entropy, the total magnetization, and the total susceptibility, respectively:

$$\begin{aligned}
&\frac{S(T_N^i,B;z)}{k_B} \approx \\
&\qquad \frac{\bar\beta_i}{Z^{(N)}(T_N^i,B;z)} \sum_{\substack{Q_N,M_N;\\(\mathcal{E},r)_N}} \mathcal{E}^{(N)}_{(Q,M)}(z)\,\mathrm{e}^{-\bar\beta_i \mathcal{E}^{(N)}_{(Q,M)}(z)} + \ln\Big(Z^{(N)}(T_N^i,B;z)\Big)\,, \\
&\frac{M(T_N^i,B;z)}{g_S\mu_B} \overset{g_e=g_S}{\approx} \\
&\qquad -\frac{1}{Z^{(N)}(T_N^i,B;z)} \sum_{\substack{Q_N,M_N;\\(\mathcal{E},r)_N}} M_N\,\mathrm{e}^{-\bar\beta_i \mathcal{E}^{(N)}_{(Q,M)}(z)}\,, \\
&\frac{k_B T_N^i \chi(T_N^i,B;z)}{(g_S\mu_B)^2} \overset{g_e=g_S}{\approx} \\
&\qquad \frac{1}{Z^{(N)}(T_N^i,B;z)} \sum_{\substack{Q_N,M_N;\\(\mathcal{E},r)_N}} M_N^2\,\mathrm{e}^{-\bar\beta_i \mathcal{E}^{(N)}_{(Q,M)}(z)} - \left(\frac{M(T_N^i,B;z)}{g_S\mu_B}\right)^2 .
\end{aligned} \tag{4.285}$$

Note that the above quantities can all be determined without requiring the actual value of T_N^i or β_N^i. For the calculation of $\chi(T_N^i,B;z)$, however, one would need the temperature T_N^i that follows from Eq. (4.271) for the respective $\bar\beta_i$.

The truncated Wilson chains display an even-odd effect, i.e., their properties depend on whether the number of lattice sites is even or odd. As a consequence, observables calculated as a function of temperature for a single z-value show oscillations. In order to smooth these oscillations, an *even-odd average* for the given twist parameter z can be performed using, e.g., a linear interpolation (see p. 409 of Ref. [BCP08]):

$$\begin{aligned}
O_{\mathrm{even+odd}}(T_N^i,B;z) \equiv \frac{1}{2}\Bigg[&O(T_N^i,B;z) + O(T_{N-1}^i,B;z) \\
&+ \frac{O(T_{N+1}^i,B;z) - O(T_{N-1}^i,B;z)}{T_{N+1}^i - T_{N-1}^i}\big(T_N^i - T_{N-1}^i\big)\Bigg].
\end{aligned} \tag{4.286}$$

If more than one temperature is assigned to a single step of the iterative diagonalization, one could also use some higher-order interpolation between even and odd

lattice sites. An improved value of $\chi(T_N^i, B; z)$ can be obtained by first optimizing $k_B T_N^i \chi(T_N^i, B; z)$, which contains only $\bar{\beta}_i$ according to Eqs. (4.285), and then dividing the result by $k_B T_N^i$.

After calculating the desired quantities for all N_z considered values of the twist parameter z (both for the system with and without impurity), the *final NRG approximation for the impurity contribution* $O_{\mathrm{imp}}(T_N^i, B)$ is determined as:

$$\boxed{O_{\mathrm{imp}}(T_N^i, B) \equiv \frac{1}{N_z} \sum_{\{z\}} \left[O_{\text{even+odd}}^{\text{with impurity}}(T_N^i, B; z) - O_{\text{even+odd}}^{\text{w/o impurity}}(T_N^i, B; z) \right] .} \tag{4.287}$$

Note that, in general, some observables are more difficult to calculate than others. For example, numerical parameters that are sufficient for determining χ_{imp} might not allow to obtain a satisfactory result for the impurity contribution to the specific heat (see p. 409 f. of Ref. [BCP08]).

4.13.4. Calculating local observables: The impurity magnetization

Analogous to Eqs. (4.278) and (4.279), we define the *impurity magnetization* $\mathcal{M}(T, B)$ (compare the definition (2.52) of the impurity Hamiltonian $\underset{\sim}{H}_{\mathrm{imp}}(B)$),

$$\boxed{\mathcal{M}(T, B) \equiv -\left\langle \frac{\partial \underset{\sim}{H}_{\mathrm{imp}}(B)}{\partial B} \right\rangle = -g_S \mu_B \left\langle \underset{\sim}{S}^z \right\rangle ,} \tag{4.288}$$

which is related to the total magnetization $M(T, B)$ according to Eqs. (4.277):

$$M(T, B) = \mathcal{M}(T, B) - g_e \mu_B \left\langle \underset{\sim}{s}^z_{\mathrm{total}} \right\rangle . \tag{4.289}$$

Since the impurity operator $\underset{\sim}{S}^z$ alone is no conserved quantity of the Kondo Hamiltonian, the calculation of the impurity magnetization $\mathcal{M}$ in step N of the iterative diagonalization requires matrix elements of $\underset{\sim}{S}^z$ with respect to the eigenstates of $\underset{\sim}{\mathcal{H}}^{(N)}_{\mathrm{Wilson}}(z)$:

$$\boxed{\frac{\mathcal{M}(T_N^i, B; z)}{g_S \mu_B} \approx - \sum_{\substack{Q_N, M_N; \\ (\mathcal{E}, r)_N}} {}^{(N)}_{(z)}\!\left\langle Q, M; (\mathcal{E}, r) \right| \underset{\sim}{S}^z \left| Q, M; (\mathcal{E}, r) \right\rangle^{(N)}_{(z)} \frac{\mathrm{e}^{-\bar{\beta}_i \mathcal{E}^{(N)}_{(Q,M)}(z)}}{Z^{(N)}(T_N^i, B; z)} .} \tag{4.290}$$

The *final NRG approximation for a local observable* such as the impurity magnetization is obtained in a similar way as for an impurity contribution (cf. Eq. (4.287)):

$$\boxed{\mathcal{M}(T_N^i, B) \equiv \frac{1}{N_z} \sum_{\{z\}} \mathcal{M}_{\text{even+odd}}(T_N^i, B; z) .} \tag{4.291}$$

Calculations for a system without impurity are, of course, not necessary in this case.

How to determine the required matrix elements

If the calculation of a thermodynamic expectation value requires matrix elements of an impurity operator (such as $\underset{\sim}{S}^z$) with respect to the eigenstates of the Hamiltonians $\underset{\sim}{\mathcal{H}}^{(N)}_{\text{Wilson}}(z)$, they have to be determined in each step N of the iterative diagonalization using information from the previous step $N-1$.

Let us assume that the following matrix elements of $\underset{\sim}{S}^z$ with regard to the eigenstates from step $N-1$ are known for all combinations of the quantum numbers (Q_{N-1}, M_{N-1}):

$$\overset{(N-1)}{(z)}\!\left\langle Q, M; (\mathcal{E}, r)\right| \underset{\sim}{S}^z \left|Q, M; (\mathcal{E}', r')\right\rangle^{(N-1)}_{(z)} .$$

Only these matrix elements can be non-zero since $\underset{\sim}{S}^z$ shares the symmetry properties of the Hamiltonian $\underset{\sim}{\mathcal{H}}^{(N-1)}_{\text{Wilson}}(z)$, i.e., $\left[\underset{\sim}{S}^z, \underset{\sim}{S}^z_{N-1}\right] = \left[\underset{\sim}{S}^z, \underset{\sim}{Q}_{N-1}\right] = 0$. We now want to calculate the matrix elements required in step N:

$$\boxed{\overset{(N)}{(z)}\!\left\langle Q, M; (\mathcal{E}, r)\right| \underset{\sim}{S}^z \left|Q, M; (\mathcal{E}', r')\right\rangle^{(N)}_{(z)} .} \tag{4.292}$$

Basically, this is done in the same way as for the creation operators $\underset{\sim}{f}^\dagger_{N\mu}(z)$ (see Sec. 4.11.3). However, there are two differences:

1. Since $\underset{\sim}{S}^z$ "respects" the U(1) symmetries of the Hamiltonian, the calculations are carried out in subspaces (Q_N, M_N).

2. For the calculation of the matrix representation with respect to the product basis $\left\{|Q, M; (\mathcal{E}, r)_{N-1}, i\rangle^{(N)}_{(z)}\right\}$ in step N, we need matrix elements with regard to the eigenstates $\left|Q, M; (\mathcal{E}, r)\right\rangle^{(N-1)}_{(z)}$ *from the previous step.*

Because an impurity operator does not affect the newly added lattice site, we have

$$\begin{aligned}&\overset{(N)}{(z)}\!\left\langle Q, M; (\mathcal{E}, r)_{N-1}, i\right| \underset{\sim}{S}^z \left|Q, M; (\mathcal{E}', r')_{N-1}, j\right\rangle^{(N)}_{(z)} \quad = \\ &\overset{(N)}{(z)}\!\left\langle Q, M; (\mathcal{E}, r)_{N-1}, i\right| \underset{\sim}{S}^z \left|Q, M; (\mathcal{E}', r')_{N-1}, i\right\rangle^{(N)}_{(z)} \delta_{ij} ,\end{aligned} \tag{4.293}$$

and, with the definition (4.241) of the product basis states, the potentially non-zero

matrix elements are obtained as:

$$\begin{aligned}
\mathcal{S}^{11}_{(\mathcal{E},r)(\mathcal{E}',r')} &= {}^{(N)}_{(z)}\langle Q,M;(\mathcal{E},r)_{N-1},1|\,\underset{\sim}{S}^{z}\,|Q,M;(\mathcal{E}',r')_{N-1},1\rangle^{(N)}_{(z)} = \\
&\quad {}^{(N-1)}_{(z)}\langle Q+1,M;(\mathcal{E},r)\;\;|\,\underset{\sim}{S}^{z}\,|Q+1,M;(\mathcal{E}',r')\;\;\rangle^{(N-1)}_{(z)}\;, \\
\mathcal{S}^{22}_{(\mathcal{E},r)(\mathcal{E}',r')} &= {}^{(N)}_{(z)}\langle Q,M;(\mathcal{E},r)_{N-1},2|\,\underset{\sim}{S}^{z}\,|Q,M;(\mathcal{E}',r')_{N-1},2\rangle^{(N)}_{(z)} = \\
&\quad {}^{(N-1)}_{(z)}\langle Q,M-1/2;(\mathcal{E},r)|\,\underset{\sim}{S}^{z}\,|Q,M-1/2;(\mathcal{E}',r')\rangle^{(N-1)}_{(z)}\;, \\
\mathcal{S}^{33}_{(\mathcal{E},r)(\mathcal{E}',r')} &= {}^{(N)}_{(z)}\langle Q,M;(\mathcal{E},r)_{N-1},3|\,\underset{\sim}{S}^{z}\,|Q,M;(\mathcal{E}',r')_{N-1},3\rangle^{(N)}_{(z)} = \\
&\quad {}^{(N-1)}_{(z)}\langle Q,M+1/2;(\mathcal{E},r)|\,\underset{\sim}{S}^{z}\,|Q,M+1/2;(\mathcal{E}',r')\rangle^{(N-1)}_{(z)}\;, \\
\mathcal{S}^{44}_{(\mathcal{E},r)(\mathcal{E}',r')} &= {}^{(N)}_{(z)}\langle Q,M;(\mathcal{E},r)_{N-1},4|\,\underset{\sim}{S}^{z}\,|Q,M;(\mathcal{E}',r')_{N-1},4\rangle^{(N)}_{(z)} = \\
&\quad {}^{(N-1)}_{(z)}\langle Q-1,M;(\mathcal{E},r)\;\;|\,\underset{\sim}{S}^{z}\,|Q-1,M;(\mathcal{E}',r')\;\;\rangle^{(N-1)}_{(z)}\;.
\end{aligned} \tag{4.294}$$

The matrix representation of $\underset{\sim}{S}^{z}$ with respect to the product basis in a subspace (Q_N, M_N) thus has the following block-diagonal form:

$$\underset{\sim}{S}^{z}: \begin{pmatrix}
1 & 2 & 3 & 4 & \boldsymbol{j/i} \\
\mathcal{S}^{11} & 0 & 0 & 0 & 1 \\
0 & \mathcal{S}^{22} & 0 & 0 & 2 \\
0 & 0 & \mathcal{S}^{33} & 0 & 3 \\
0 & 0 & 0 & \mathcal{S}^{44} & 4
\end{pmatrix}. \tag{4.295}$$

Each block $\mathcal{S}^{ii}$ is symmetric since $\underset{\sim}{S}^{z}$ is Hermitian with real-valued matrix elements. As discussed for the creation operators $\underset{\sim}{f}^{\dagger}_{N\mu}(z)$, the matrices of kept eigenvectors $\mathcal{U}^{(N,z)}(Q,M)$ are used to transform the representations (4.295) to the retained part of the eigenbasis of $\underset{\sim}{\mathcal{H}}^{(N)}_{\mathrm{Wilson}}(z)$ (compare Eqs. (4.265) and (4.266), as well as Fig. 4.7), in order to determine the required matrix elements (4.292). For the evaluation of traces, only the diagonal elements (i.e., $\mathcal{E} = \mathcal{E}'$ and $r = r'$) are necessary. Setting up the matrix representations (4.295) *in the next step*, however, also requires the non-diagonal elements from the current step.

Note that an "update" of the corresponding matrix representation, which has been illustrated in this section using the example of $\underset{\sim}{S}^{z}$, has to be separately carried out for each impurity operator for which thermodynamic expectation values are supposed to be calculated.

5. Application: The single-impurity Kondo model in zero magnetic field

As a first application of the NRG method described in detail in chapter 4, we now study the temperature dependence of typical impurity contributions to thermodynamic observables (such as entropy and magnetic susceptibility) for the single-channel single-impurity Kondo model *without* external magnetic field. The exchange-isotropic Kondo model with impurity spin $S = 1/2$ was considered by Wilson when he introduced the Numerical Renormalization Group [Wil75] (also compare Ref. [KmWW75]).

After discussing the special case of a spin-1/2 impurity (which is completely screened by a single conduction electron channel at zero temperature) in Sec. 5.1, we investigate Kondo models with larger impurity spin in Sec. 5.2. For $S > 1/2$, so-called *underscreening* occurs: The impurity spin is only partially compensated by a single electron channel and there is a non-zero magnetic moment at $T = 0$ corresponding to a *residual spin* $S - 1/2$.

The temperature dependence of the observables considered for the Kondo model with $S = 1/2$ is used to illustrate the meaning of the *Kondo temperature* and the associated concept of *universality* (see Sec. 5.1.1). In Sec. 5.1.2, as a test of the NRG calculations for $S = 1/2$, we furthermore compare with quasi-exact results for the entropy and magnetic susceptibility in the *universal (or scaling) regime* that have been obtained as part of the Bethe ansatz solution of the Kondo problem. Finally, generalizations of the Kondo Hamiltonian involving either additional potential scattering or exchange anisotropy of XXZ-type are studied in Secs. 5.1.3 and 5.1.4, respectively. Both modifications are known to lead to the same low-temperature strong-coupling fixed point which is found for the standard exchange-isotropic Kondo model. We consider them here since they are related to an effective pseudo-spin-1/2 Kondo model that is used in the paper included in chapter 8.

5.1. Complete screening of an impurity spin $S = 1/2$

Let us begin with a discussion of the temperature-dependent properties of the Kondo model with impurity spin $S = 1/2$ and antiferromagnetic exchange coupling $J > 0$ in zero magnetic field B. Note that in this thesis only the case of a conduction band with a *constant* density of states is considered. We comment on

the choice of a constant DOS at the end of Sec. 5.1.2. In order to be properly normalized in accordance with the definition (4.6), a constant DOS has to take the value $\rho \equiv 1/2W$, with W being the half-bandwidth of the electrons. Furthermore, we implicitly assume that the g-factors of electrons g_e and impurity spin g_S are equal. Since the magnetic field vanishes, the value of g_e does not appear in the actual calculations and thus does not change the results. Nevertheless, the quantity that is calculated according to the last line of Eqs. (4.280) can only be interpreted as the total magnetic susceptibility if the g-factors are equal.

Fig. 5.1 shows the impurity contributions (introduced in Sec. 4.13.1) to the entropy S_{imp}, the effective magnetic moment[1] $k_B T \chi_{\mathrm{imp}}$, and the magnetic susceptibility χ_{imp} as a function of temperature for three values of the coupling strength $\rho J \ll 1$. $S_{\mathrm{imp}}(T)/k_B$ is a measure of the effective number of degrees of freedom which the impurity spin possesses at the temperature T. As illustrated for a free spin by Eq. (4.283), $k_B T \chi_{\mathrm{imp}}(T)$ provides information about the temperature-dependent "effective magnetic moment" of the impurity. Lastly, the zero-field susceptibility $\chi_{\mathrm{imp}}(T)$ describes the linear response of the impurity contribution to the magnetization, which is studied in chapter 8, to an applied magnetic field (compare the definition of $\chi(T, B)$ in Eq. (4.280)).

At high temperature, electrons and impurity progressively decouple. In accordance with the definition (4.272) of an impurity contribution, the entropy $S_{\mathrm{imp}}(T)/k_B$, which is presented in Fig. 5.1 (a), hence approaches the corresponding high-temperature value of a free spin $S = 1/2$ (i.e., $\ln(2S+1) = \ln 2$) for $k_B T/W \to \infty$. Below a characteristic temperature, which can be identified with the *Kondo temperature* T_K as demonstrated in Sec. 5.1.2, the impurity contribution to the entropy enters the "low-temperature" regime. The characteristic temperature scale depends on the coupling strength and decreases for smaller values of ρJ. In the limit of zero temperature, S_{imp}/k_B vanishes. This result indicates that the impurity effectively has no remaining degrees of freedom at $T = 0$. We thus say that the conduction electrons have *screened* the impurity spin.

Fig. 5.1 (b) shows $k_B T \chi_{\mathrm{imp}}(T)/(g_S \mu_B)^2$. For temperatures that are large compared to the Kondo temperature, the effective magnetic moment tends to the respective (temperature-independent) value of a free spin-1/2 (i.e., 1/4 according to the Curie law expressed by Eq. (4.283)), again because of the increasing decoupling of electrons and impurity. Note, however, that this limiting value is only asymptotically reached since there are slowly declining logarithmic corrections (see Sec. 5.1.1 and, in particular, Eq. (5.2)). As already observed for the impurity contribution to the entropy, a crossover occurs at a certain temperature that depends on the coupling strength. In particular, $k_B T \chi_{\mathrm{imp}}$ vanishes for $T \to 0$, revealing that the impurity is no longer magnetic at zero temperature because its magnetic moment is screened by the conduction electrons. This interpretation is consistent with the zero-temperature limit of S_{imp}/k_B as discussed above.

The impurity contribution to the magnetic susceptibility plotted in Fig. 5.1 (c)

[1] Note that in the following we also refer to $k_B T \chi_{\mathrm{imp}}$ as the "effective magnetic moment" of the impurity even though, strictly speaking, it is the square of the effective moment according to the definition (4.282).

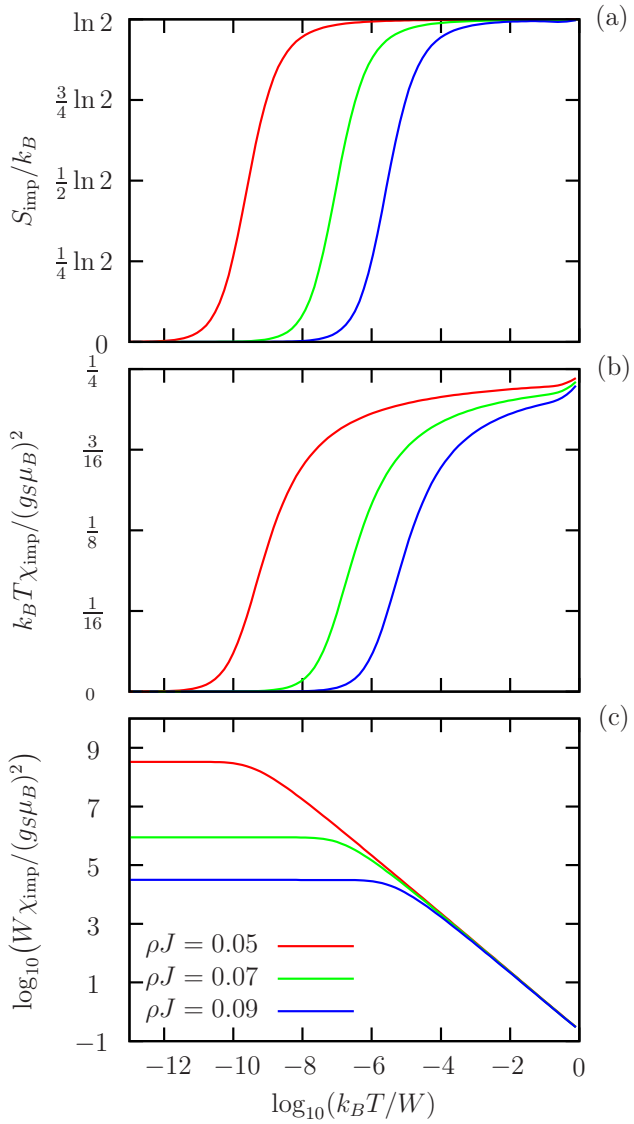

Figure 5.1.: Impurity contribution to (a) the entropy, (b) the effective magnetic moment, and (c) the magnetic susceptibility as a function of temperature for impurity spin $S = 1/2$, $B = 0$, a constant density of states $\rho \equiv 1/2W$, and three values of the coupling strength $\rho J > 0$. The curves are the result of a spline interpolation through the numerically obtained data points. Calculations have been carried out using the discretization scheme by Žitko and Pruschke with an enforced energy gap of 0.01 and the following parameters: $\Lambda = 3$, $N_{\mathrm{keep}} = 5000$, $\bar{\beta} = 0.7$, and $z = 0.25, 0.5, 0.75, 1$.

goes to a finite and non-zero value for temperatures below T_K. This limiting value depends on the coupling strength and increases upon reducing ρJ. A free spin is described by a zero-field susceptibility that diverges for $T \to 0$ and is thus completely polarized by any non-zero magnetic field at $T = 0$. In contrast, *even at zero temperature*, the impurity contribution to the magnetization $M_{\mathrm{imp}}(T, B)$ grows linearly with increasing (small) magnetic field (see chapter 8). According to the definition (4.280), the slope of $M_{\mathrm{imp}}(T = 0, B \to 0)$ is given by the limiting value $\chi_{\mathrm{imp}}(T \to 0, B = 0)$, which is larger if the coupling strength, and thus also the Kondo temperature, is smaller. In particular, this slope diverges in the limit $\rho J \to 0$ and the Curie behavior of a free spin with $S = 1/2$ is recovered. Furthermore, at temperatures that are large compared to the Kondo temperature, the Curie law describing a free spin-1/2 is also asymptotically restored and, as a consequence, $\chi_{\mathrm{imp}}(T)$ vanishes for $k_B T/W \to \infty$.

5.1.1. Kondo temperature, universality, and Fermi liquid theory

For a flat conduction band with a constant DOS $\rho(\varepsilon) \equiv \rho$ and $\varepsilon \in [-W, W]$, the usual estimate for the *order of magnitude* of the *Kondo temperature* T_K in case of small coupling strength $\rho J \ll 1$ is given by (see p. 835 of Ref. [Wil75], Ref. [KmWW75], and p. 1025 of Ref. [KmWW80a]):

$$\boxed{k_B T_K/W \approx \sqrt{\rho J}\, \mathrm{e}^{-1/\rho J}\ .} \tag{5.1}$$

According to this expression, the dependence of T_K on the dimensionless quantity ρJ is non-analytic for $\rho J = 0$.

The result (5.1) can, e.g., be obtained by carrying out a perturbative Renormalization-Group-based approach for the weak coupling regime $\rho J \ll 1$, known as Anderson's *poor man's scaling* [And70], to third order in ρJ (see p. 58 ff. and appendix D of the book [Hew93]). In second order, one gets the less accurate estimate $k_B T_K/W \approx \mathrm{e}^{-1/\rho J}$ ([Hew93], p. 62). In a poor-man's-scaling calculation, the Kondo model is *approximately* mapped onto an effective model of the same structure, which is valid on a reduced energy scale, with a renormalized or "running" exchange parameter $\widetilde{J}$ (cf. p. 58, 61, and 64 of Ref. [Hew93]). A stepwise perturbative elimination of electronic states near the upper and lower band edge results in a certain *scaling equation* that describes the renormalization flow of $\widetilde{J}$ when the energy scale is lowered. It turns out that in the weak-coupling regime the scaling trajectories of the Kondo model are fully characterized by a single *scaling invariant* which is identified with the Kondo temperature (see Ref. [And70] and p. 62 of Ref. [Hew93]). This is a statement of *universality*: The parameters of the original Hamiltonian (i.e., W, ρ, and J) are absorbed into the energy scale $k_B T_K$ (note that the parameter dependence of T_K has to be established for each particular problem, see Secs. 5.1.3 and 5.1.4), which then uniquely determines the low-energy properties of the model ([Hew93], p. 62 and 64). In particular, thermodynamic observables in the weak-coupling (or scaling) regime are described by *universal functions* of the variable T/T_K (cf. p. 332 of Ref.

[AFL83] and p. 62 of Ref. [Hew93]). Certain generalizations of the Kondo Hamiltonian are known to preserve the universal properties so that the thermodynamic behavior in the scaling regime is still given by the same universal functions (in this sense, the "universality class" of the Kondo model is unchanged). This is, e.g., true for additional potential scattering (discussed in Sec. 5.1.3) and for an exchange-anisotropic interaction (see Sec. 5.1.4 and note that Anderson originally studied the exchange-anisotropic Kondo Hamiltonian [And70]). In case of isotropic *ferromagnetic* coupling, the poor man's scaling can be continued to arbitrarily small energy scales, with the result that the renormalized coupling $\widetilde{J}$ vanishes in this limit ([Hew93], p. 64). In contrast, for *antiferromagnetic* interaction $0 < \rho J \ll 1$, $\widetilde{J}$ eventually increases upon further reducing the energy scale so that at some point the running coupling can no longer be considered as small and the perturbative scaling loses its justification ([Hew93], p. 61 f.). In a calculation to second order, the renormalized exchange interaction even diverges at the energy $k_B T_K$ (the "true" scaling trajectories, however, ought to give a finite value of $\widetilde{J}$ for any non-zero energy; cf. p. 64 f. of Ref. [Hew93]).

The Kondo temperature can also be related to perturbative weak-coupling expansions of thermodynamic observables such as the impurity contribution to the zero-field magnetic susceptibility $\chi_{\mathrm{imp}}(T)$. As shown by the poor-man's-scaling approach, it is only possible to treat the coupling strength ρJ as small in the regime of high temperature. For this reason, a perturbation series in ρJ for $\rho J \ll 1$ effectively corresponds to a high-temperature expansion (see p. 64 of Ref. [Hew93]). This becomes evident by the appearance of terms that logarithmically depend on the temperature and lead to a breakdown of perturbation theory for $T \to 0$ (see p. 811 of Ref. [Wil75] and p. 47 ff. of Ref. [Hew93]). Furthermore, a summation of logarithmically divergent terms in leading order produces singularities at a non-zero temperature $k_B T/W \approx \mathrm{e}^{-1/\rho J}$, which is to be compared to Eq. (5.1) ([Hew93], p. 49). In his original article, Wilson managed to extend existing second-order results for the weak-coupling expansion of $\chi_{\mathrm{imp}}(T)$ (see, e.g., p. 47 of Ref. [Hew93]) to fourth order in ρJ ([Wil75], p. 830). Such a calculation also allows to obtain the above estimate (5.1) for T_K (see below and also compare p. 835 of Ref. [Wil75]).

The Kondo temperature as the *high-temperature perturbative scale* can be precisely defined by requiring that the high-temperature expansion of the susceptibility does not contain terms of order $1/\ln^2(T/T_K)$ (see Ref. [FL82], p. 333 of Ref. [AFL83], and p. 88 f. of Ref. [Hew93]). With this "normalization condition", one finds the following *asymptotic series* for $\chi_{\mathrm{imp}}(T)$ (see Refs. [AL81, FL82], p. 333 and 364 of Ref. [AFL83], p. 459 and 494 of Ref. [TW83], and p. 88 of Ref. [Hew93]):

$$\boxed{\begin{aligned}&\chi_{\mathrm{imp}}(T \gg T_K, B = 0; S = 1/2) = \\ &\frac{(g_S \mu_B)^2}{4\, k_B T}\left(1 - \frac{1}{\ln(T/T_K)} - \frac{\ln\ln(T/T_K)}{2\ln^2(T/T_K)} + \ldots\right).\end{aligned}} \tag{5.2}$$

This equation describes how the impurity spin becomes asymptotically free for $T/T_K \to \infty$ so that its susceptibility $\chi_{\rm imp}(T, B = 0)$ approaches the Curie law for a free spin-1/2 (i.e., $k_B T \chi_{\rm imp}(T, B = 0)/(g_S \mu_B)^2 = \left\langle \left(\underset{\sim}{S}^z\right)^2 \right\rangle = 1/4$). Wilson's great achievement was to come up with an approximate numerical method for the investigation of the Kondo model in the regime $T < T_K$ [Wil75], which is not accessible by perturbation theory. The invention of NRG made it possible for the first time to calculate thermodynamic observables over the whole temperature range. In particular, Wilson was able to relate the Kondo temperature T_K as appearing in the high-temperature expansion (5.2) to the low-temperature limit of the susceptibility (cf. Fig. 5.1 (c)), which reflects the strong-coupling behavior of the Kondo model (see p. 835 of Ref. [Wil75] and p. 89 of Ref. [Hew93]):

$$\boxed{\chi_{\rm imp}(T \ll T_K, B = 0; S = 1/2) = \frac{(g_S \mu_B)^2 w}{4\, k_B T_K}\ .} \tag{5.3}$$

Here, w is a universal number with the numerical value 0.4128 ± 0.002 ([Wil75], p. 835), which has been named *Wilson number* ([Hew93], p. 90). Eq. (5.3) is sometimes also referred to as "Wilson's definition of the Kondo temperature".

Later, an exact expression for w could be derived in the context of the Bethe ansatz solution of the Kondo model (cf. Sec. 5.1.2). In case of impurity spin $S = 1/2$, the Kondo temperature can also be defined as the *strong-coupling (or low-temperature) scale* in the spirit of Eq. (5.3) (note that this is not possible for $S > 1/2$ as discussed in Sec. 5.2). Let us call this quantity T_L. As possible definitions of T_L (modulo the additional factor 1/2) we then have (see p. 579 and 590 of Ref. [TW83], and compare the scale T_0 in Refs. [AL81, FL82] and on p. 333 and 355 of Ref. [AFL83])

$$\boxed{\chi_{\rm imp}(T = 0, B = 0; S = 1/2) \equiv \frac{1}{2} \frac{(g_S \mu_B)^2}{\pi\, k_B T_L}\ ,} \tag{5.4}$$

or ([Hew93], p. 155)

$$\chi_{\rm imp}(T = 0, B = 0; S = 1/2) \equiv \frac{(g_S \mu_B)^2}{4\, k_B T_L}\ . \tag{5.5}$$

With the latter definition (5.5), the Wilson number w is the universal ratio of the two scales T_K and T_L,

$$w = \frac{T_K}{T_L}\ , \tag{5.6}$$

and is given by (see Refs. [AL81, FL82], p. 368 f. of Ref. [AFL83], p. 591 f. of Ref. [TW83], and p. 155 of Ref. [Hew93]):

$$w = \frac{\mathrm{e}^{\gamma + 1/4}}{\pi^{3/2}}\ . \tag{5.7}$$

Here, $\gamma \approx 0.577216$ is Euler's constant, yielding a numerical value $w \approx 0.41071$ that is consistent with Wilson's NRG result quoted above.

For small antiferromagnetic couplings ρJ, there is an implicit equation with a certain universal function $\Phi(y)$ that relates the zero-field susceptibility to a quantity called *effective bandwidth* $\widetilde{W}(\rho J)$ for thermal energies much smaller than the bandwidth W, but much larger than the Kondo scale $k_B T_K$ (see p. 830 of Ref. [Wil75], and also compare Ref. [KmWW75], p. 1025 of Ref. [KmWW80a], and p. 501 of Ref. [TW83]):

$$\Phi\big(4\,k_B T \chi_{\mathrm{imp}}(T)/(g_S \mu_B)^2 - 1\big) = \Phi(\rho J) + \ln\big(k_B T/\widetilde{W}(\rho J)\big) \tag{5.8}$$

$$\equiv \ln\big(T/T_K(\rho J)\big)\ , \tag{5.9}$$

with the Kondo temperature (cf. p. 835 of Ref. [Wil75]):

$$\boxed{k_B T_K(\rho J) = \widetilde{W}(\rho J)\exp\big(-\Phi(\rho J)\big)\ .} \tag{5.10}$$

The effective bandwidth divided by W has a *non-universal* power-series expansion in ρJ [Wil75, KmWW75, KmWW80a]. Furthermore, for small arguments, there is the following approximation for the function $\Phi(y)$ [Wil75, KmWW80a, TW83]:

$$\boxed{\Phi(y) = \frac{1}{y} - \frac{1}{2}\ln|y| + \mathcal{O}(y)\ .} \tag{5.11}$$

Inserting the expansion (5.11) into the expression (5.10) for T_K and using $\widetilde{W}(\rho J) \approx W$, we obtain the standard estimate for the Kondo temperature from Eq. (5.1).

At low temperatures $T \ll T_K$ close to the strong-coupling fixed point, the physical properties of the spin-1/2 Kondo model are captured by an effective theory proposed by Nozières [Noz74]. This description takes for granted that the effective exchange coupling between electrons and impurity becomes infinitely large at the strong-coupling fixed point so that the impurity spin is frozen in a singlet with an electron at the zeroth site of the Wilson chain (cf. Ref. [Wil75] and p. 87 of Ref. [Hew93]). Although for non-zero temperature $0 < T \ll T_K$ (or finite effective coupling) this singlet is still expected to be very stable, certain virtual excitations become possible [Noz74]. This renders the singlet "polarizable" and causes it to act as a local scattering center for the remaining conduction electrons, thereby mediating effective interactions between them [Noz74]. In order to formalize this physical picture, a variant of *Landau's Fermi liquid theory* can be used. A Fermi liquid description rests on the assumption that there is a direct relation between the low-lying excitations of the interacting system and the excitations of the same system when the interaction is switched off (cf. Ref. [Noz74] and p. 103 of Ref. [Hew93]). From a technical point of view, the energies of excited states of the interacting system can be expressed as series expansions in the "occupation numbers of quasiparticles" ([Hew93], p. 103). Since the scattering with the singlet induces interactions between the remaining conduction electrons, these expansions have to

include at least the leading non-linear (i.e., quadratic) term. The expansions of the excitation energies comprise free coefficients (whose number can typically be restricted by symmetry considerations) which characterize the quasiparticles and have to be suitably parameterized ([Hew93], p. 104 f.). This makes the whole approach phenomenological. Physical quantities such as the free energy are defined as functionals of the occupation numbers of quasiparticles, which are regarded as variational parameters ([Hew93], p. 104). Minimizing the free energy with respect to these occupation numbers gives access to the low-temperature thermodynamics so that observables such as the specific heat and the magnetic susceptibility can be calculated for $T \ll T_K$. In particular, χ_{imp} is found to be constant (compare Fig. 5.1 (c), and see Ref. [Noz74], p. 505 of Ref. [TW83], and p. 107 of Ref. [Hew93]). In his original article, Nozières characterized the quasiparticles by an energy and an elastic-scattering phase shift (for a Fermi liquid, in contrast to a *non-Fermi-liquid*, the inelastic-scattering cross section vanishes at the Fermi level [MAC$^+$05]). The free parameters of the theory were then determined by a comparison with Wilson's numerical results. In summary, the low-energy excitations of the spin-1/2 Kondo model correspond to fermionic quasiparticles with relatively weak interactions ([Hew93], p. 105 and 109) that form a *local Fermi liquid* [BCP08].

5.1.2. Comparison with the Bethe ansatz solution

The isotropic Kondo Hamiltonian (with arbitrary impurity spin) can be exactly diagonalized by a method based on the so-called *Bethe ansatz* [TW83, AFL83, Hew93]. A brief overview of the approach and its restrictions is given in chapter 7. For the moment, note that conduction electrons and impurity are assumed to have the same g-factor and that the Bethe ansatz solution is concerned with the *scaling* or *universal regime* in which all relevant energy scales (such as thermal energy and Zeeman energy) are small compared to the bandwidth of the conduction electrons. This regime is characterized by a single energy scale (corresponding to the Kondo temperature T_K) and the temperature dependence of impurity contributions to thermodynamic observables in zero magnetic field is described by *universal functions* of the variable T/T_K (see p. 332 of Ref. [AFL83]).

In case of zero temperature, the Bethe ansatz approach yields an exact solution for the field-dependent magnetization in closed form (see chapter 7). Moreover, the exact solution for the eigensystem of the Kondo Hamiltonian allows for the derivation of a system of equations determining the impurity contribution to the free energy F_{imp} at non-zero temperature and thus, in principle, the whole thermodynamics [RLA82, TW83, AFL83]. In general, these equations have to be solved numerically. Results for the entropy $S_{\mathrm{imp}}(T/T_K)/k_B$ (for impurity spin $S = 1/2$) and for the magnetic susceptibility $k_B T_K \chi_{\mathrm{imp}}(T/T_K)/(g_S \mu_B)^2$ (for $S = 1/2, 1, 3/2$) are tabulated in Ref. [DS82] and on p. 626 of Ref. [TW83], respectively. Furthermore, the original NRG results for the effective magnetic moment $k_B T \chi_{\mathrm{imp}}(T/T_K)/(g_S \mu_B)^2$ can be found on p. 1025 of Ref. [KmWW80a].

Fig. 5.2 displays the data shown in Fig. 5.1 in a different way. For each value

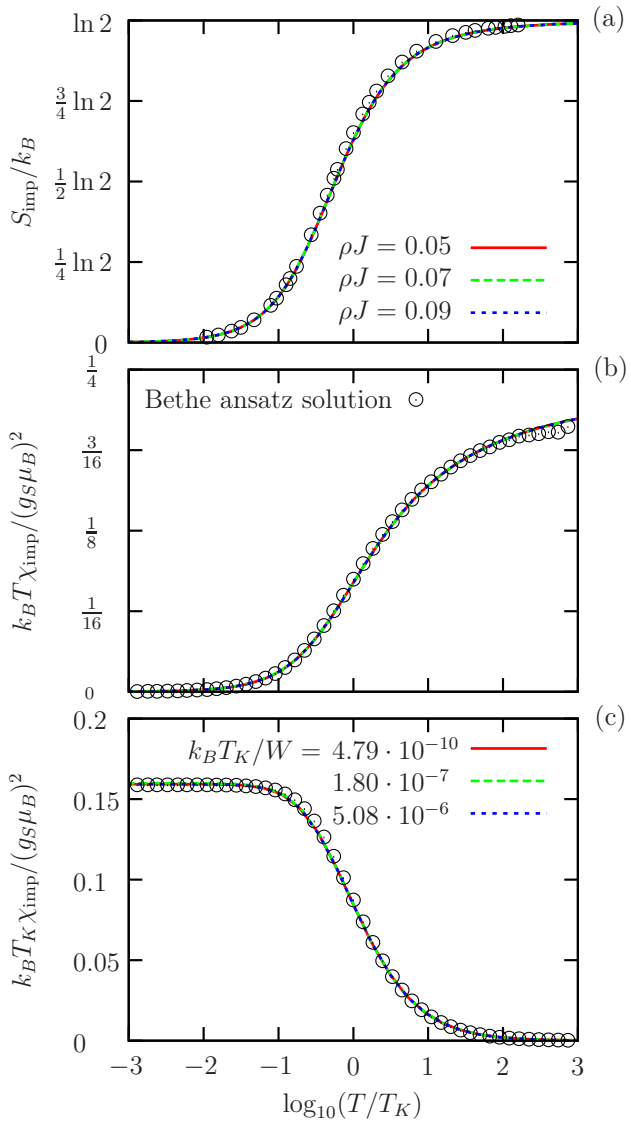

Figure 5.2.: Impurity contribution to (a) the entropy, (b) the effective magnetic moment, and (c) the magnetic susceptibility as a function of the rescaled temperature T/T_K for impurity spin $S = 1/2$. These are the same results as shown in Fig. 5.1 and the Bethe ansatz solutions are taken from Ref. [DS82] (S_{imp}) and p. 626 of Ref. [TW83] (χ_{imp}). Note that the definition (5.4) of the Kondo temperature is used and that the values of T_K have been *calculated* according to equation (13) of Ref. [HS13] (i.e., $T_H = \sqrt{2\pi/\mathrm{e}}\,T_K$, cf. chapter 8) by taking the corresponding values of the temperature scale T_H (discussed in chapter 7) from table I of Ref. [HS13].

of the coupling strength ρJ, the corresponding Kondo temperature[2] T_K has been determined as described in the caption. The obtained values of T_K are used to rescale the temperature axis, allowing the impurity contributions to the entropy, the effective magnetic moment, and the susceptibility to be plotted as functions of T/T_K (note that χ_{imp} is additionally multiplied by $k_B T_K$). After the rescaling, the curves calculated for the different coupling parameters ρJ are nearly indistinguishable in the plots of Fig. 5.2. This result illustrates the universality discussed in the previous section 5.1.1. The curves presented in Fig. 5.2 furthermore show that the crossover to the strong-coupling regime occurs at the temperature $T \approx T_K$ for all three considered observables. Having determined the respective Kondo temperatures, the NRG results for small coupling strength $\rho J \ll 1$ can be compared to the Bethe ansatz solutions that are obtained in the scaling regime. We find the agreement of the NRG and Bethe ansatz results to be quite convincing.

Having illustrated the universal thermodynamic properties of the spin-1/2 Kondo model for a constant density of states, we now briefly discuss the case of an energy-dependent DOS $\rho(\varepsilon)$. To this end, it is assumed that $\rho(\varepsilon)$ can be expanded in powers of ε about the Fermi energy ε_F (as an example, consider the DOS (4.31) of one-dimensional tight-binding electrons which is plotted in Fig. 4.1 (b)). For the single-impurity Anderson model (which is related to the spin-1/2 Kondo model as discussed in Sec. 2.2.1), it is found that the energy-dependent non-constant terms in an expansion of $\rho(\varepsilon)$ correspond to irrelevant perturbations (in a Renormalization-Group sense) about the so-called local-moment fixed point of the model (see p. 1013 and 1030 of Ref. [KmWW80a] and p. 1080 of Ref. [KmWW80b]). For the Kondo model, we may therefore expect that the approach to the low-temperature fixed point for $\rho(\varepsilon) \neq$ const. is similar to the case with a constant DOS. In particular, a comparable temperature dependence of observables should be obtained in the scaling regime. Using Eq. (5.1) in order to estimate the Kondo temperature in case of an energy-dependent DOS, the constant ρ can be replaced by the value $\rho(\varepsilon_F)$ of the DOS at the Fermi energy. Note, however, that the energy dependence of $\rho(\varepsilon)$ in general affects the non-universal expansion of the effective bandwidth $\widetilde{W}(\rho J)$, and thereby also the value of T_K (compare Eq. (5.10), and see p. 1080 of Ref. [KmWW80b] and p. 104 of Ref. [Žit07]).

5.1.3. Effect of additional potential scattering

Let us consider the following variant of the Kondo Hamiltonian, which includes *potential scattering* K at the zeroth site of the Wilson chain (cf. Eqs. (4.20) and (4.22) with $B = 0$, $\varepsilon_F = 0$, $\rho(\varepsilon) \equiv \rho = \text{const.}$, and $\underset{\sim}{H}_{\mathrm{imp}} = 0$):

[2] We would like to avoid confusion, but the "Kondo temperature" appearing in Fig. 5.2 actually corresponds to the low-temperature scale T_L defined in Eq. (5.4). However, since we have used the symbol T_K for this quantity in Ref. [HS13] (cf. chapter 8), we do the same at this point. Furthermore, the scale denoted by T_L is also referred to as T_K in, e.g., Ref. [TW83].

$$\underset{\sim}{H}_{\mathrm{K}} \equiv W \Bigg[\sum_{\mu} \Bigg(\int_{-1}^{1} \mathrm{d}\xi\, \xi\, \underset{\sim}{a}^{\dagger}_{\mu}(\xi) \underset{\sim}{a}_{\mu}(\xi) + \underbrace{\rho K \int_{-1}^{1} \mathrm{d}\xi \int_{-1}^{1} \mathrm{d}\xi'\, \underset{\sim}{a}^{\dagger}_{\mu}(\xi) \underset{\sim}{a}_{\mu}(\xi')}_{= \frac{K}{W} \underset{\sim}{f}^{\dagger}_{0\mu} \underset{\sim}{f}_{0\mu}} \Bigg)$$
$$+\ \rho J\, \underset{\sim}{\boldsymbol{S}} \cdot \sum_{\mu,\nu} \int_{-1}^{1} \mathrm{d}\xi \int_{-1}^{1} \mathrm{d}\xi'\, \underset{\sim}{a}^{\dagger}_{\mu}(\xi) \frac{\boldsymbol{\sigma}_{\mu\nu}}{2} \underset{\sim}{a}_{\nu}(\xi') \Bigg] . \tag{5.12}$$

As discussed in Sec. 2.2.1, a Kondo model with additional potential scattering appears as a limiting case of the asymmetric (i.e., $\delta \neq 0$) single-impurity Anderson model according to Eq. (2.26). The electronic part of $\underset{\sim}{H}_{\mathrm{K}}$ can be diagonalized by performing a unitary transformation to *scattering states* $\underset{\sim}{c}_{\mu}(\zeta)$ (see Refs. [Kon68, CL79b] and appendix C of Ref. [KmWW80b]):

$$\underset{\sim}{a}_{\mu}(\xi) = \int_{-1}^{1} \mathrm{d}\zeta\, u(\xi,\zeta) \underset{\sim}{c}_{\mu}(\zeta) , \tag{5.13}$$

with a complicated generalized function $u(\xi,\zeta)$. Using this transformation, one can derive the identity [KmWW80b]

$$\int_{-1}^{1} \mathrm{d}\xi\, \underset{\sim}{a}_{\mu}(\xi) = \int_{-1}^{1} \mathrm{d}\zeta\, \frac{\sin\delta(\zeta)}{\pi\rho K}\, \underset{\sim}{c}_{\mu}(\zeta) , \tag{5.14}$$

where the phase shift $\delta(\zeta)$ is defined by ($\mathcal{P}$ denotes the Cauchy principal value):

$$\pi \cot\delta(\zeta) + \mathcal{P} \int_{-1}^{1} \frac{\mathrm{d}\xi}{\zeta - \xi} = \frac{1}{\rho K} . \tag{5.15}$$

Applying transformation (5.13) to $\underset{\sim}{H}_{\mathrm{K}}$, the scattering term is eliminated at the price of a more complicated interaction term [KmWW80b]:

$$\underset{\sim}{H}_{\mathrm{K}} = W \Bigg[\sum_{\mu} \int_{-1}^{1} \mathrm{d}\zeta\, \zeta\, \underset{\sim}{c}^{\dagger}_{\mu}(\zeta) \underset{\sim}{c}_{\mu}(\zeta)$$
$$+\ \rho J\, \underset{\sim}{\boldsymbol{S}} \cdot \sum_{\mu,\nu} \int_{-1}^{1} \mathrm{d}\zeta \int_{-1}^{1} \mathrm{d}\zeta'\, \frac{\sin\delta(\zeta)}{\pi\rho K} \frac{\sin\delta(\zeta')}{\pi\rho K}\, \underset{\sim}{c}^{\dagger}_{\mu}(\zeta) \frac{\boldsymbol{\sigma}_{\mu\nu}}{2} \underset{\sim}{c}_{\nu}(\zeta') \Bigg] . \tag{5.16}$$

From a Renormalization-Group point of view, non-constant terms in an expansion of $\delta(\zeta)$ about $\zeta = 0$ lead to the appearance of irrelevant operators about

the low-temperature fixed point [KmWW80a, KmWW80b] (compare the remark regarding the choice of a constant DOS at the end of the last section 5.1.2). As an approximation, one may therefore replace the phase shift by its value $\delta(0)$ at the Fermi energy and use:

$$\left(\frac{\sin\delta(0)}{\pi\rho K}\right)^2 = \left(\frac{1}{\pi\rho K}\sin\operatorname{arccot}\left(\frac{1}{\pi\rho K} + \frac{1}{\pi}\underbrace{\mathcal{P}\int_{-1}^{1}\frac{\mathrm{d}\xi}{\xi}}_{=0}\right)\right)^2 \tag{5.17}$$

$$= \frac{1}{1+(\pi\rho K)^2}\,. \tag{5.18}$$

The substitution $\delta(\zeta) \to \delta(0)$ results in a Kondo Hamiltonian with an energy-independent interaction term and an effective coupling strength ρJ_{eff} (cf. Refs. [Kon68, TC69, KKH11]):

$$\boxed{\begin{aligned}\underset{\sim}{H}_{\mathrm{K}} \approx W\Bigg[&\sum_{\mu}\int_{-1}^{1}\mathrm{d}\zeta\,\zeta\,\underset{\sim}{c}^{\dagger}_{\mu}(\zeta)\underset{\sim}{c}_{\mu}(\zeta)\\ &+\underbrace{\frac{\rho J}{1+(\pi\rho K)^2}}_{\equiv\rho J_{\mathrm{eff}}}\underset{\sim}{\boldsymbol{S}}\cdot\sum_{\mu,\nu}\int_{-1}^{1}\mathrm{d}\zeta\int_{-1}^{1}\mathrm{d}\zeta'\,\underset{\sim}{c}^{\dagger}_{\mu}(\zeta)\frac{\boldsymbol{\sigma}_{\mu\nu}}{2}\underset{\sim}{c}_{\nu}(\zeta')\Bigg]\,.\end{aligned}} \tag{5.19}$$

The effective coupling strength can then be used to estimate the order of magnitude of the Kondo temperature according to Eq. (5.1):

$$\boxed{k_B T_K/W \approx \sqrt{\rho J_{\mathrm{eff}}}\,\mathrm{e}^{-1/\rho J_{\mathrm{eff}}}\,.} \tag{5.20}$$

Note that the effective bandwidth $\widetilde{W}$ introduced in Eq. (5.8) and appearing in the expression (5.10) for the Kondo temperature in general depends on the neglected non-constant components of $\delta(\zeta)$ and thereby on ρK (see p. 1080 of Ref. [KmWW80b] and compare Sec. 5.1.2).

In Fig. 5.3, NRG results for the impurity contributions to the entropy and the effective magnetic moment of a spin-1/2 Kondo model with isotropic exchange interaction $\rho J = 0.07$ are presented for several values of the scattering parameter $\rho K > 0$. Because of the approximation (5.19) for the Kondo Hamiltonian with additional potential scattering, we expect that identical results would be obtained for negative values of ρK. Plots (a) and (c) of Fig. 5.3 demonstrate that the crossover to the strong-coupling behavior occurs at lower temperature if ρK is larger. Furthermore, plot (a) reveals that there is a dip in $S_{\mathrm{imp}}(T)/k_B$ for thermal energies close to the band edge (i.e., for $k_B T \lesssim W$). This dip becomes more pronounced for larger scattering parameter. A similar effect, though less noticeable,

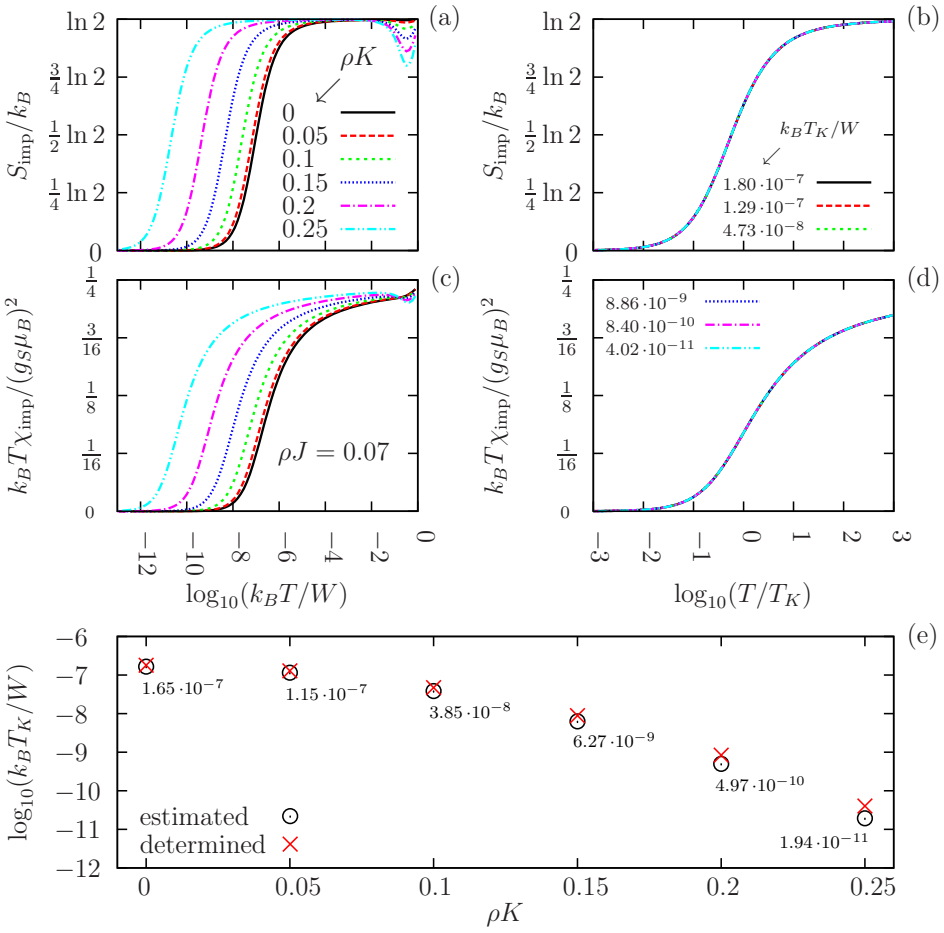

Figure 5.3.: Impurity contribution to (a) the entropy and (c) the effective magnetic moment as a function of temperature for impurity spin $S = 1/2$, isotropic coupling $\rho J = 0.07$, and several values of the scattering parameter $\rho K > 0$. Plots (b) and (d) show the same data as a function of the rescaled temperature T/T_K. The Kondo temperatures have been determined as described in appendix D of Ref. [HS13] (by fitting to an entropy curve with known value of T_K; see main text and chapter 8) and, as in Fig. 5.2, correspond to the definition (5.4). In plot (e), the obtained values of $k_B T_K/W$ are compared with the estimates given by Eq. (5.20). For the numerical parameters used in the calculations, see the caption of Fig. 5.1.

is also observed in the temperature dependence of the effective magnetic moment. For each value of ρK, as indicated in the caption, the result for $S_{\mathrm{imp}}(T)/k_B$ has been fitted to the entropy curve with $\rho J = 0.07$ and $k_B T_K/W \approx 1.80 \cdot 10^{-7}$ shown in Fig. 5.2, using the Kondo temperature as a fit parameter. In particular, this means that the definition of T_K corresponds to Eq. (5.4) as before. Using the obtained Kondo temperatures, the temperature axis is rescaled and the considered observables are plotted as a function of T/T_K. After the rescaling, the curves for the different scattering parameters shown in plots (b) and (d) are virtually indistinguishable. This demonstrates that additional potential scattering preserves the universal properties of the spin-1/2 Kondo model in the scaling regime, in accordance with the form of the approximate Hamiltonian (5.19). The determined Kondo temperatures decrease with increasing scattering parameter ρK and can be compared with the estimates given by Eq. (5.20). As illustrated by plot (e), the approximate expression (5.20) underestimates the obtained values of $k_B T_K/W$, with better agreement for smaller values of ρK.

5.1.4. Effect of exchange anisotropy

We now study the thermodynamic properties of the Kondo model (2.17) with impurity spin $S = 1/2$ and exchange anisotropy of XXZ-type (i.e., $J_\perp \equiv J^x \equiv J^y$, $J_\parallel \equiv J^z$, and $J_\perp \neq J_\parallel$). For a spin-1/2 impurity, a single conduction electron channel, $J_\perp > 0$, and $J_\parallel > -J_\perp$, exchange anisotropy is known to correspond to an irrelevant perturbation about the strong-coupling fixed point that is found for isotropic exchange interaction $J_\perp = J_\parallel$ (see Refs. [And70, SDL08], p. 594 of Ref. [TW83], and p. 61 f. of Ref. [Hew93]). An estimate for the Kondo temperature T_K in the exchange-anisotropic case has been obtained by a poor-man's-scaling calculation to second order [RWHS06b]. For $J_\perp \geq J_\parallel > 0$, we have [ŽPP08]:

$$\boxed{\begin{aligned} k_B T_K/W &\approx \exp\left(-\frac{\alpha}{\rho J_\parallel}\right), \\ \alpha &\equiv \frac{\arctan\gamma}{\gamma}, \\ \gamma &\equiv \sqrt{\left(\frac{J_\perp}{J_\parallel}\right)^2 - 1}\,. \end{aligned}} \tag{5.21}$$

Using $\arctan(\mathrm{i}x)/\mathrm{i} = \operatorname{arctanh}(x)$, the expression for the case $0 < J_\perp \leq J_\parallel$ thus

reads as [ŽPP08]:

$$\boxed{\begin{aligned} k_B T_K/W &\approx \exp\left(-\frac{\widetilde{\alpha}}{\rho J_\parallel}\right), \\ \widetilde{\alpha} &\equiv \frac{\operatorname{arctanh}\widetilde{\gamma}}{\widetilde{\gamma}}, \\ \widetilde{\gamma} &\equiv \sqrt{1-\left(\frac{J_\perp}{J_\parallel}\right)^2}. \end{aligned}} \tag{5.22}$$

In the isotropic limit $J \equiv J_\perp \equiv J_\parallel$, we find $\gamma = \widetilde{\gamma} = 0$, $\alpha = \widetilde{\alpha} = 1$, and hence $k_B T_K/W \approx \exp(-1/\rho J)$, which is the perturbative estimate for the Kondo temperature to second order in ρJ (cf. Sec. 5.1.1).

Fig. 5.4 displays NRG results for the impurity contributions to the entropy and the effective magnetic moment of a spin-1/2 Kondo model (now again *without* potential scattering) with fixed longitudinal coupling $\rho J_\parallel = 0.07$ and varying transverse coupling $\rho J_\perp$. The concept of this figure is similar to that of Fig. 5.3 so that the presented results can be interpreted in the same way. After rescaling the temperature axis using the determined Kondo temperatures, the entropy curves for the different transverse coupling parameters $\rho J_\perp$ shown in plot (b) are impossible to distinguish. In case of the effective magnetic moment depicted in plot (d), we observe slight deviations from the curve with $J_\perp = J_\parallel$ for $T \gg T_K$. The obtained results are consistent with the known conclusion that an exchange-anisotropic interaction with $J_\perp \neq J_\parallel$ corresponds to an irrelevant perturbation about the strong-coupling (low-temperature) fixed point of the isotropic Kondo model. The Kondo temperatures, which have been determined in the same way as for the curves shown in Fig. 5.3, increase with the transverse coupling strength $\rho J_\perp$. In plot (e), they are compared with the estimates given by Eqs. (5.21) for $J_\perp \geq J_\parallel$ and by Eqs. (5.22) for $J_\perp \leq J_\parallel$, respectively. One should keep in mind that these approximate expressions for T_K are the result of a second-order perturbative calculation. For this reason, the obtained approximations should be expected to be less accurate compared to a third-order estimate (such as the one for the isotropic case $J_\perp = J_\parallel$ given by Eq. (5.1)). We find that the expressions (5.21) and (5.22) overestimate the determined values of $k_B T_K/W$.

5.2. Underscreening of an impurity spin $S > 1/2$

A single conduction electron channel can only partially screen an isotropic impurity spin with $S > 1/2$. This results in what is known as the *underscreened Kondo effect*. At zero temperature, one degree of freedom of the impurity is quenched by the conduction electrons so that a non-zero magnetic moment corresponding to a reduced spin $S - 1/2$ remains [Mat67, CL79a]. This *residual spin* displays a ferromagnetic interaction with the electron bath that scales to zero in the limit of vanishing temperature [GCA92], albeit very slowly [MAC+05]. At low tempera-

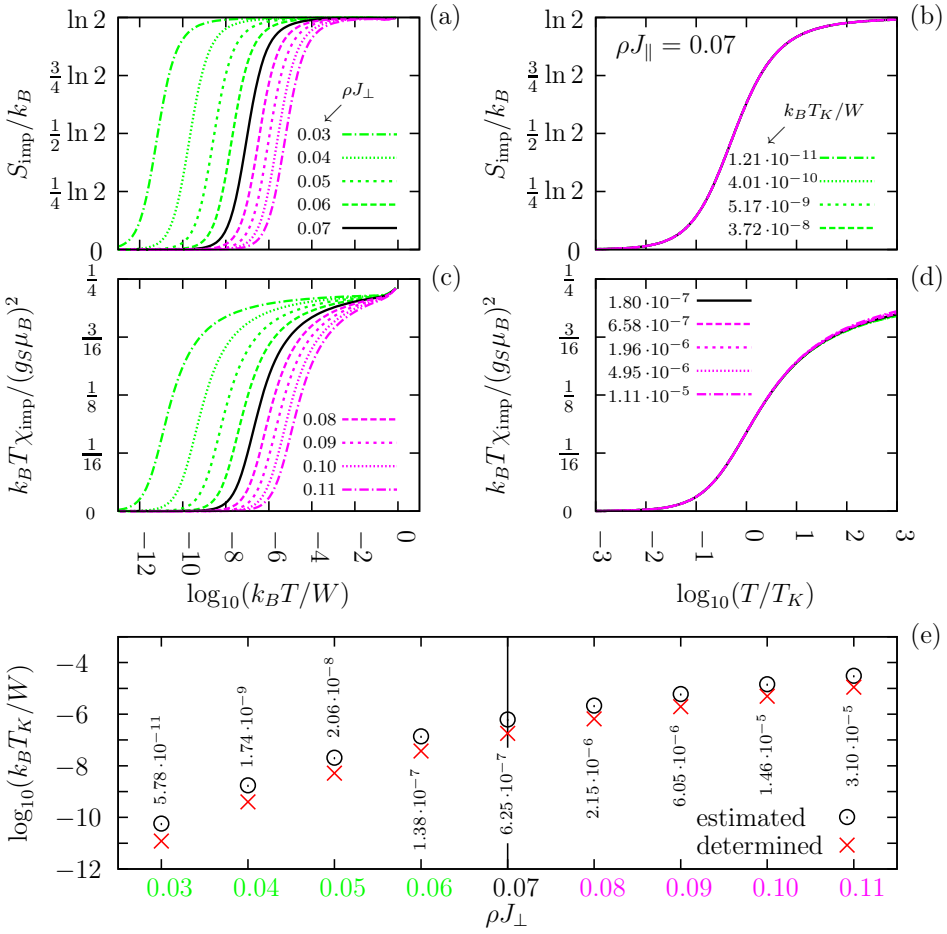

Figure 5.4.: Impurity contribution to (a) the entropy and (c) the effective magnetic moment as a function of temperature for impurity spin $S = 1/2$, $\rho K = 0$, fixed longitudinal coupling $\rho J_\parallel = 0.07$, and several values of the transverse coupling strength $\rho J_\perp$. Plots (b) and (d) show the same data as a function of the rescaled temperature T/T_K. The Kondo temperatures have been determined as described in the caption of Fig. 5.3. In plot (e), the obtained values of k_BT_K/W are compared with the second-order estimates given by Eqs. (5.21) for $J_\perp \geq J_\parallel$ and by Eqs. (5.22) for $J_\perp \leq J_\parallel$, respectively. For the numerical parameters used in the calculations, see the caption of Fig. 5.1.

ture, the residual spin thus progressively decouples from the conduction electrons and becomes asymptotically free for $T \to 0$ [GCA92, CP03]. This property is reminiscent of the *spin-1/2* Kondo model with ferromagnetic interaction [MAC$^+$05] (cf. p. 158 of Ref. [Hew93]). A poor-man's-scaling calculation for the exchange-isotropic ferromagnetic Kondo model with $S = 1/2$ can be carried out to arbitrarily small energy scales and it is found that the running coupling parameter scales to zero in the limit of vanishing temperature [And70] (cf. p. 64 of Ref. [Hew93]).

In case of zero magnetic field, the strong-coupling fixed point of the underscreened Kondo model differs from the low-temperature Fermi-liquid fixed point that a system with a completely screened spin-1/2 impurity is attracted to [Noz74]. This modified fixed point has been termed a *singular* (as opposed to a *regular*) *Fermi liquid* since, e.g., the quasiparticle density of states diverges at zero energy [CP03, MAC$^+$05]. A characteristic feature of a singular Fermi liquid is the extremely slow approach to the corresponding fixed point [CL79a, MAC$^+$05]. Note that a non-zero magnetic field restores regular-Fermi-liquid behavior at low temperature [CP03, MAC$^+$05].

The high-temperature expansion of the impurity contribution to the susceptibility for arbitrary impurity spin S is simply a generalization of the result (5.2) for the case $S = 1/2$ (see Ref. [FW81a] and p. 370 and 378 of Ref. [AFL83]):

$$\boxed{\begin{aligned}&\chi_{\mathrm{imp}}(T \gg T_K, B = 0; S) = \\ &\frac{(g_S\mu_B)^2 S(S+1)}{3\,k_B T}\left(1 - \frac{1}{\ln(T/T_K)} - \frac{\ln\ln(T/T_K)}{2\ln^2(T/T_K)} + \dots\right).\end{aligned}} \tag{5.23}$$

In the limit $T/T_K \to \infty$, $\chi_{\mathrm{imp}}(T, B = 0)$ approaches the Curie law for a free spin S (i.e., $k_B T\chi(T, B = 0)/(g_S\mu_B)^2 = \langle (\underset{\sim}{S}^z)^2 \rangle = \langle \underset{\sim}{\boldsymbol{S}}^2 \rangle/3 = S(S+1)/3$) with slowly declining logarithmic corrections. In other words, the impurity becomes asymptotically free at high temperature.

For impurity spin $S \geq 1$, the low-temperature expansion of χ_{imp} is analogous to Eq. (5.23) if substituting $S \to S - 1/2$ (see again Ref. [FW81a] and p. 370 and 378 of Ref. [AFL83]):

$$\boxed{\begin{aligned}&\chi_{\mathrm{imp}}(T \ll T_K, B = 0; S \geq 1) = \\ &\frac{(g_S\mu_B)^2 (S^2 - 1/4)}{3\,k_B T}\left(1 - \frac{1}{\ln(T/T_K)} - \frac{\ln|\ln(T/T_K)|}{2\ln^2(T/T_K)} + \dots\right).\end{aligned}} \tag{5.24}$$

At low temperature $T \ll T_K$, the impurity contribution to the susceptibility more and more shows a temperature dependence according to the Curie law for a free spin $S - 1/2$ (i.e., $k_B T\chi(T, B = 0)/(g_S\mu_B)^2 = (S - 1/2)(S + 1/2)/3 = (S^2 - 1/4)/3$). The appearance of logarithmic terms in the expansion (5.24) is a sign of the ferromagnetic interaction between the residual spin $S-1/2$ and the conduction electrons and corresponds to a concrete realization of the very slow approach to the low-temperature fixed point that is characteristic of a singular Fermi liquid (see above).

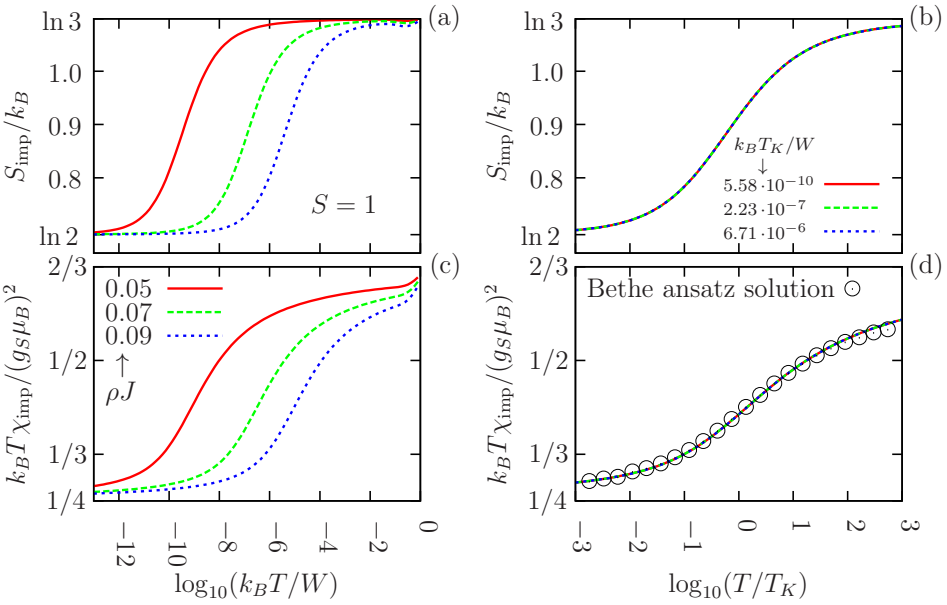

Figure 5.5.: Impurity contribution to (a) the entropy and (c) the effective magnetic moment as a function of temperature for impurity spin $S = 1$, $B = 0$, and three values of the coupling strength ρJ (for $S = 3/2$, see Fig. 5.6). Plots (b) and (d) show the same data as a function of the rescaled temperature T/T_K. The Kondo temperatures have been determined as described in the caption of Fig. 5.2 (cf. main text), and the Bethe ansatz solution for $\chi_{\rm imp}(T/T_K)$ is taken from p. 626 of Ref. [TW83]. Apart from $N_{\rm keep} = 6000$, the numerical parameters used in the NRG calculations are those given in the caption of Fig. 5.1.

Note the absence of terms of order $1/\ln^2(T/T_K)$ in both the high- and low-temperature expansions ([AFL83], p. 378). This "normalization condition" gives meaning to the Kondo temperature for arbitrary impurity spin S.[3] Furthermore, it is found that with this definition k_BT_K is the same energy scale both in the regime of high and low temperature ([AFL83], p. 370 and 378). For a non-zero magnetic field, there is another energy scale k_BT_H that is defined in a similar manner via the low- and high-field expansions of the zero-temperature impurity contribution to the magnetization (see Sec. 7.2).

In Figs. 5.5 and 5.6, we present NRG results for the impurity contributions to the entropy and the effective magnetic moment for impurity spin $S = 1$ and

[3] For impurity spin $S \geq 1$, T_K cannot be defined via the low-temperature limit of the impurity contribution to the susceptibility as in the case of $S = 1/2$ (see, e.g., Eq. (5.3)) since $\chi_{\rm imp}(T, B = 0)$ diverges for $T \to 0$ according to the Curie law for the residual spin $S - 1/2$.

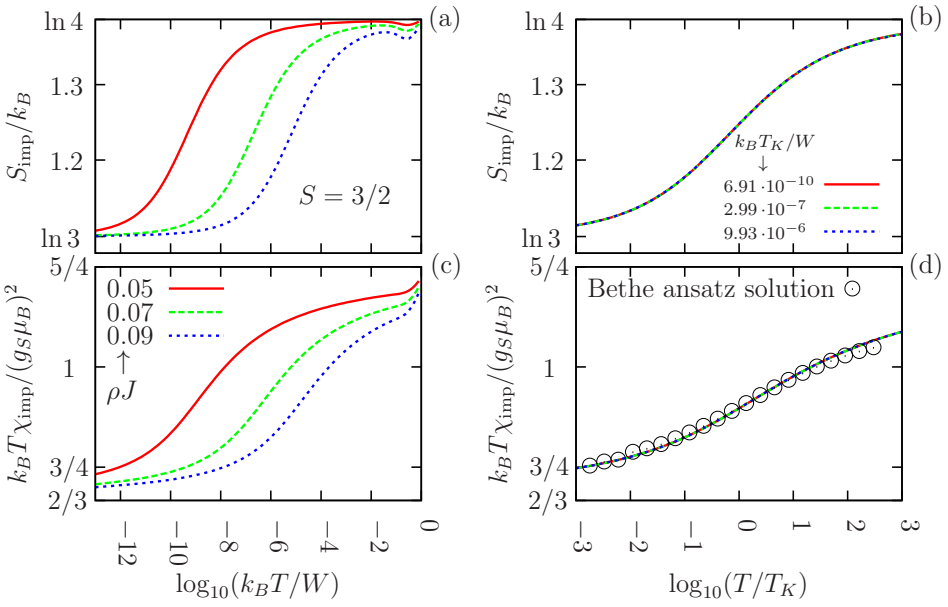

Figure 5.6.: Impurity contribution to (a) the entropy and (c) the effective magnetic moment as a function of temperature for impurity spin $S = 3/2$, zero magnetic field, and three values of the coupling strength ρJ (compare the results for $S = 1$ in Fig. 5.5). In plots (b) and (d), the same data is presented as a function of the rescaled temperature T/T_K. The Kondo temperatures have been determined as described in the caption of Fig. 5.2 (cf. main text), and the Bethe ansatz solution for $\chi_{\rm imp}(T/T_K)$ is again taken from p. 626 of Ref. [TW83]. This time, $N_{\rm keep} = 7000$ has been used in the NRG calculations. For the remaining numerical parameters, see the caption of Fig. 5.1.

$S = 3/2$, respectively, and the same three values of the coupling strength ρJ as before. According to the above discussion of the underscreened Kondo effect, $S_{\mathrm{imp}}(T)/k_B$ tends to $\ln(2S+1)$ for $k_BT/W \to \infty$ and takes the value $\ln(2[S-1/2]+1) = \ln(2S)$ in the limit $k_BT/W \to 0$. Both at high and low temperature, the magnetic susceptibility is described more and more by a Curie law. As per Eq. (5.23), the high-temperature limit of $k_BT\chi_{\mathrm{imp}}/(g_S\mu_B)^2$ is $S(S+1)/3$. At low temperature, on the other hand, the value $(S^2-1/4)/3$ is approached, in accordance with the asymptotic expansion (5.24). For each coupling strength ρJ, the Kondo temperature has been calculated by taking the corresponding value of the temperature scale T_H from table I of Ref. [HS13] (see chapter 8) and using the relation (compare the caption of Fig. 5.2)

$$T_K = \sqrt{\frac{\mathrm{e}}{2\pi}}\, T_H \ . \tag{5.25}$$

The rescaled curves for the different coupling parameters $\rho J \ll 1$ are virtually indistinguishable in the presented plots. This result demonstrates that the exchange-isotropic single-channel Kondo model displays universal behavior in the scaling regime also for impurity spin $S > 1/2$. The effective magnetic moment as a function of the rescaled temperature T/T_K can be compared with the corresponding Bethe ansatz solution as tabulated in Ref. [TW83]. Excluding the regime $T \gg T_K$, we again find convincing agreement between NRG and Bethe ansatz results.

The way in which we have determined the "Kondo temperature" for each exchange coupling ρJ requires a brief explanation. Eq. (5.25) relates the quantity T_H to the low-temperature scale T_L which we have decided to also denote by T_K. T_L is defined in Eq. (5.4) *for impurity spin $S = 1/2$*. However, T_K *cannot* be associated with the zero-temperature limit of the impurity contribution to the magnetic susceptibility for impurity spin $S > 1/2$ since $\chi_{\mathrm{imp}}(T \to 0, B = 0)$ is divergent in this case (compare footnote 3). If the Kondo temperature is instead interpreted as the perturbative high-temperature scale in terms of Eq. (5.23), the relation between T_K and T_H is given by (for impurity spin $S = 1/2$, see, e.g., p. 591 of Ref. [TW83] and p. 369 of Ref. [AFL83]):

$$T_K = 2\beta \mathrm{e}^{\gamma - 7/4}\, T_H \ . \tag{5.26}$$

Here, $\gamma \approx 0.577216$ is Euler's constant and β is another constant (not to be confused with the inverse thermal energy) with the numerical value $\ln\beta \approx 0.662122$. As pointed out in Ref. [DZ05], and in contrast to the statements in the original literature (see Ref. [FL82] and p. 379 of Ref. [AFL83]), Eq. (5.26) should hold for arbitrary impurity spin S. Using the identity (see p. 62 of Ref. [And94] and note the typo in equation (4) of Ref. [DZ05])

$$\ln\beta = \ln\left(\frac{\mathrm{e}^{5/2}}{2\pi}\right) \approx 0.6621229 \ , \tag{5.27}$$

the following relation, which is to be compared to Eq. (5.25), is obtained:

$$\boxed{T_K = \frac{\mathrm{e}^{\gamma+3/4}}{\pi}\, T_H \ .} \tag{5.28}$$

The chosen "normalization"[4] of the Kondo temperature is, however, not crucial for the discussion of the universal temperature dependence of observables. In his original paper ([Wil75], p. 835), Wilson observed the following point: If T_K is multiplied by an arbitrary constant that is independent of ρJ, the effective magnetic moment $k_B T \chi_{\mathrm{imp}}(T)$ still only depends on the value of T/T_K in the scaling regime. Note, however, that the value of $\chi_{\mathrm{imp}}(T/T_K)$ for a certain ratio T/T_K *is* determined by the chosen definition of the Kondo temperature (in fact, this is the normalization).

[4]The scale T_H is normalized as discussed in Sec. 7.2. If the relation (5.28) is used, then T_K should be normalized as described above, in the paragraph following Eq. (5.24). On the other hand, if T_K is determined from T_H according to Eq. (5.25) *for* $S > 1/2$, a certain ratio to T_H, expressed by Eq. (5.25), is instead enforced as the normalization condition.

Part III.

The single-channel single-impurity Kondo model with and without uniaxial anisotropy in non-zero magnetic field

6. The isotropic single-impurity Kondo model in non-zero magnetic field

We now consider the case of a non-zero external magnetic field B and study the thermodynamic properties of the *isotropic* single-channel single-impurity Kondo model as a function of temperature and magnetic field. To this end, NRG calculations of the impurity contributions to the entropy $S_{\mathrm{imp}}(T,B)$ and the effective magnetic moment $k_BT\chi_{\mathrm{imp}}(T,B)$ are presented for impurity spin $S=1/2,1,3/2$. The Bethe ansatz solution for the zero-temperature field-dependent impurity contribution to the magnetization is discussed in chapter 7 and compared to NRG results in Ref. [HS13] (see chapter 8). There, also the impurity magnetization $\mathcal{M}(T,B)$, which is defined in Eq. (4.288), is investigated. At the moment, we are only concerned with the case of equal g-factors of electrons g_e and impurity spin g_S. The influence of the ratio g_e/g_S on the magnetic properties of the Kondo model is studied in Ref. [HS13] (see chapter 8).

For the case of impurity spin $S=1/2$, it is demonstrated in the following that a magnetic field has basically no effect on S_{imp} and $k_BT\chi_{\mathrm{imp}}$ if $g_S\mu_BB<k_BT_K$. This result reflects the complete screening of the impurity's magnetic moment by the conduction electrons that occurs in the limit $T\ll T_K$ for $B=0$ (cf. Fig. 5.2). Note, however, that any non-zero magnetic field leads to a non-zero magnetization. *In this sense*, even a fully-screened spin-1/2 impurity at zero temperature acts magnetic for $B>0$. In case of $S>1/2$, a magnetic field with $g_S\mu_BB>k_BT$ always significantly affects the impurity, irrespective of the value of the Kondo temperature, since a residual spin with non-zero magnetic moment is formed for $T\ll T_K$ (cf. Figs. 5.5 and 5.6). The impurity thus stays magnetic on energy scales smaller than k_BT_K and corresponding effects of a field $g_S\mu_BB>k_BT$ are observed in the impurity contributions to the entropy and the effective magnetic moment.

For a number of constant magnetic fields, the temperature dependence of the impurity contributions to the specific heat, the entropy, the magnetization, and the magnetic susceptibility of the single-channel single-impurity Kondo model with $S\leq 7/2$ has been studied in Ref. [SS89]. The results presented in this article were obtained by numerically solving the corresponding thermodynamic Bethe ansatz equations (cf. chapter 7). Later, also the thermodynamic properties of the multi-channel single-impurity Kondo model in an applied magnetic field were investigated [SS91].

6.1. Thermodynamics of an impurity spin $S = 1/2$

Fig. 6.1 shows NRG calculations of $S_{\mathrm{imp}}(T, B)$ and $k_B T \chi_{\mathrm{imp}}(T, B)$ for impurity spin $S = 1/2$, both as a function of temperature (for a number of positive magnetic fields) and magnetic field (for several temperature values). As illustrated by plots (a) and (c), both observables are linear functions of the temperature for $T \ll T_K$ in case of zero field.[1] If $g_S \mu_B B \gg k_B T_K$, a swift drop of S_{imp} and $k_B T \chi_{\mathrm{imp}}$ is observed below the thermal energy $k_B T \approx g_S \mu_B B$, followed by a linear decline for $k_B T \ll g_S \mu_B B$. For Zeeman energies of the order of the Kondo energy scale $k_B T_K$, the calculated curves are nearly identical to those obtained in case of zero field. The temperature dependencies of the impurity contributions to the entropy and the effective magnetic moment are thus basically unaffected by a magnetic field satisfying $g_S \mu_B B < k_B T_K$.

The role of an external magnetic field in the spin-1/2 Kondo model can be further illuminated by looking at the field dependencies of the considered observables as displayed in plots (b) and (d). Starting from the zero-field value of S_{imp} or $k_B T \chi_{\mathrm{imp}}$, respectively, which is determined by the ratio T/T_K (cf. Fig. 5.2), the effect of an applied magnetic field only becomes noticeable if the Zeeman energy exceeds $\max(k_B T_K, k_B T)$. This insensitivity of the spin-1/2 Kondo model to a field satisfying $g_S \mu_B B \ll k_B T_K$ reflects the complete screening of the impurity's magnetic moment that occurs for temperatures $T \ll T_K$. In the limit $g_S \mu_B B / W \to \infty$, the impurity contributions to both the entropy and the effective magnetic moment tend to zero. The limit of large magnetic field (like the limit of high temperature) can be related to the well-known behavior of a free spin. Note that such a reasoning is again only meaningful in an asymptotic sense. This point is exemplified by the asymptotic high-field expansion of the zero-temperature impurity contribution to the magnetization, which is discussed in Sec. 7.2 and given by Eq. (7.5). The degeneracy of the multiplet associated with a free spin is completely lifted by a non-zero magnetic field. At a temperature that is sufficiently low in order to resolve the groundstate gap or, vice versa, for a sufficiently large field, the free spin is thus effectively reduced to a single level. According to their definitions (cf. Eqs. (4.276) and (4.280)), both the entropy and the effective magnetic moment are then approximately zero.

6.2. Thermodynamics of an impurity spin $S > 1/2$

In Figs. 6.2 and 6.3, we present NRG calculations of the impurity contributions to the entropy and the effective magnetic moment for impurity spin $S = 1$ and $S = 3/2$, respectively, again both as a function of temperature and magnetic field. As a point of reference, the temperature dependencies of the two considered observables are also shown for $g_S \mu_B B / W \approx 0$, illustrating once again the previously discussed

[1] This result agrees with the constant non-zero value that $\chi_{\mathrm{imp}}(T, B = 0)$ approaches for $T \ll T_K$ (cf. Fig. 5.2 (c)) and, respectively, with the linear temperature dependence of the zero-field specific heat for $T \ll T_K$ (see, e.g., p. 828 f. and 835 of Ref. [Wil75] and Ref. [DS82]).

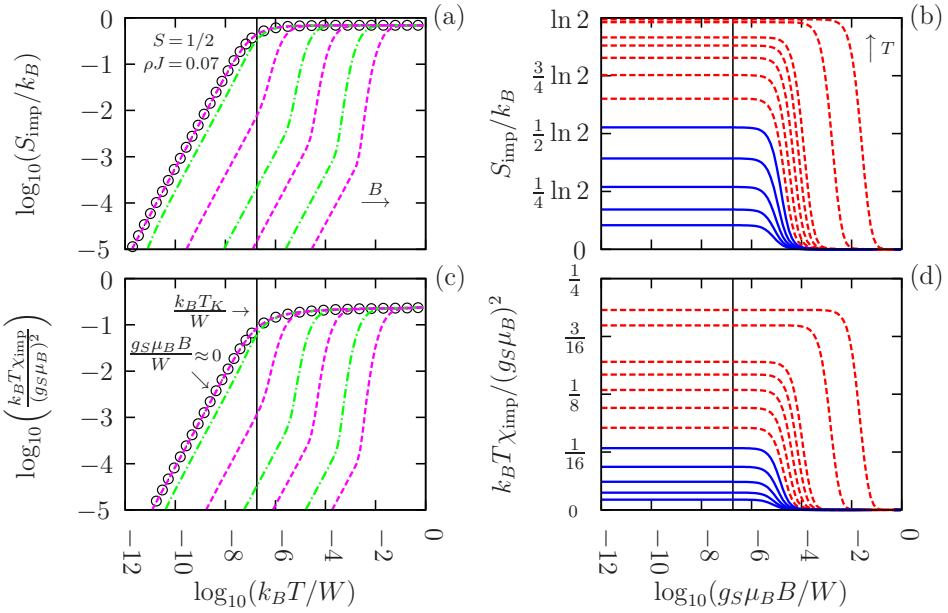

Figure 6.1.: Impurity contributions to the entropy and the effective magnetic moment for impurity spin $S = 1/2$ with $g_e = g_S$ and isotropic coupling $\rho J = 0.07$, as a function of temperature for non-zero magnetic field [plots (a) and (c)] and as a function of magnetic field for non-zero temperature [plots (b) and (d)]. The vertical lines indicate the thermal energy or Zeeman energy, respectively, that equals $k_B T_K \approx 1.80{\cdot}10^{-7} W$. In plots (a) and (c), the value of $g_S \mu_B B/W$ increases from left to right: $1.00{\cdot}10^{-15}$ (open symbols), $1.43{\cdot}10^{-6}$, $1.09{\cdot}10^{-5}$, $1.24{\cdot}10^{-4}$, $1.41{\cdot}10^{-3}$, $1.07 \cdot 10^{-2}$, $1.22 \cdot 10^{-1}$, and $9.28 \cdot 10^{-1}$. Note that $g_S \mu_B B > k_B T_K$ for all curves. In plots (b) and (d), the value of $k_B T/W$ increases from bottom to top: $1.28 \cdot 10^{-8}$, $2.21 \cdot 10^{-8}$, $3.83 \cdot 10^{-8}$, $6.64 \cdot 10^{-8}$, $1.15 \cdot 10^{-7}$, $1.99 \cdot 10^{-7}$, $3.45 \cdot 10^{-7}$, $5.97 \cdot 10^{-7}$, $1.03 \cdot 10^{-6}$, $1.79 \cdot 10^{-6}$, $2.79 \cdot 10^{-5}$, and $4.35 \cdot 10^{-4}$. Whereas T is smaller than T_K for the blue curves, we have $T > T_K$ for the red curves. For the numerical parameters used in the NRG calculations, see the caption of Fig. 5.1.

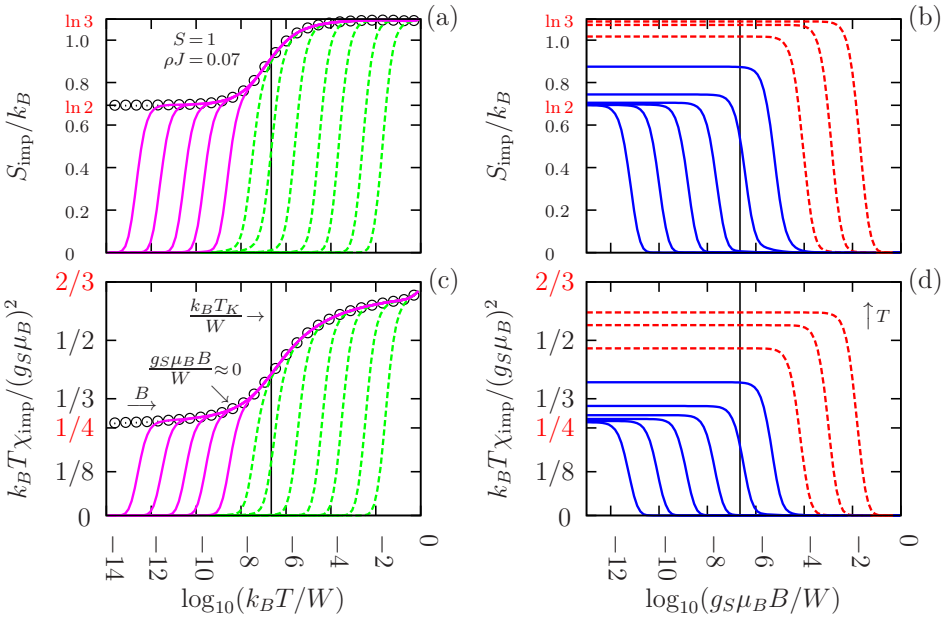

Figure 6.2.: Impurity contributions to the entropy and the effective magnetic moment for impurity spin $S = 1$ (for $S = 3/2$, see Fig. 6.3) with $g_e = g_S$ and isotropic coupling $\rho J = 0.07$, as a function of temperature for non-zero magnetic field [plots (a) and (c)] and as a function of magnetic field for non-zero temperature [plots (b) and (d)]. The vertical lines mark the thermal energy or Zeeman energy, respectively, that equals $k_BT_K \approx 2.23 \cdot 10^{-7}W$. In plots (a) and (c), the value of $g_S\mu_BB/W$ increases from left to right: $1.00 \cdot 10^{-15}$ (open symbols), $1.12 \cdot 10^{-11}$, $1.28 \cdot 10^{-10}$, $1.46 \cdot 10^{-9}$, $1.11 \cdot 10^{-8}$, $1.26 \cdot 10^{-7}$, $1.43 \cdot 10^{-6}$, $1.09 \cdot 10^{-5}$, $1.24 \cdot 10^{-4}$, $1.41 \cdot 10^{-3}$, $1.07 \cdot 10^{-2}$, $1.22 \cdot 10^{-1}$, and $9.28 \cdot 10^{-1}$. For the green curves, $g_S\mu_BB$ is larger than k_BT_K. In contrast, the Zeeman energy satisfies $g_S\mu_BB < k_BT_K$ for the magenta curves. In plots (b) and (d), the value of k_BT/W increases from bottom to top: $1.25 \cdot 10^{-13}$, $1.95 \cdot 10^{-12}$, $3.03 \cdot 10^{-11}$, $4.73 \cdot 10^{-10}$, $7.37 \cdot 10^{-9}$, $1.15 \cdot 10^{-7}$, $1.79 \cdot 10^{-6}$, $2.79 \cdot 10^{-5}$, and $4.35 \cdot 10^{-4}$. Whereas T is smaller than T_K for the blue curves, we have $T > T_K$ for the red curves. The NRG calculations have been carried out using the numerical parameters given in the caption of Fig. 5.5.

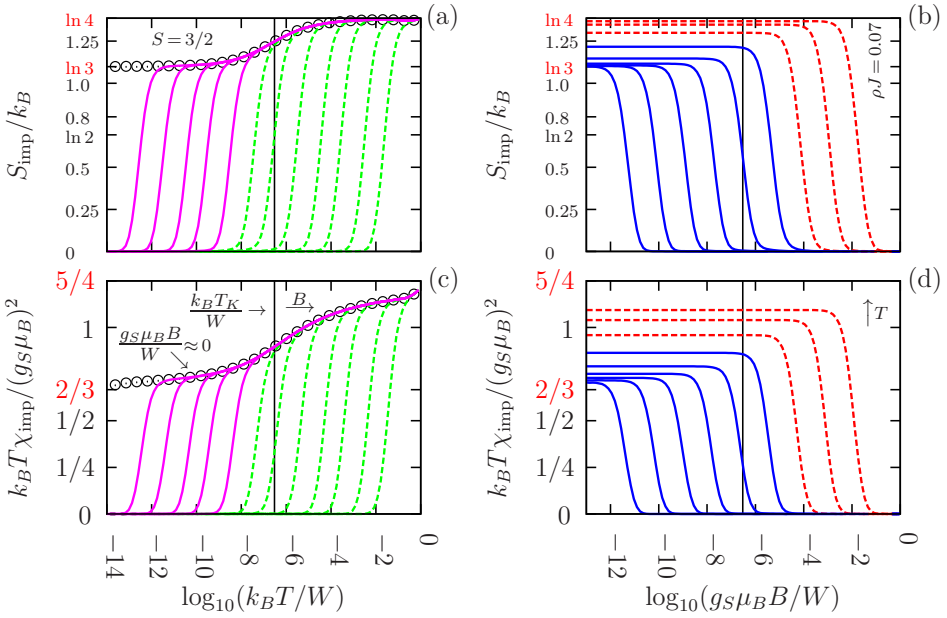

Figure 6.3.: Impurity contributions to the entropy and the effective magnetic moment for impurity spin $S = 3/2$ (compare the results for $S = 1$ shown in Fig. 6.2) with $g_e = g_S$ and isotropic coupling $\rho J = 0.07$, as a function of temperature for non-zero magnetic field [plots (a) and (c)] and as a function of magnetic field for non-zero temperature [plots (b) and (d)]. The vertical lines indicate the thermal energy or Zeeman energy, respectively, that matches the Kondo energy scale $k_BT_K \approx 2.99 \cdot 10^{-7}W$. For the constant magnetic fields in plots (a) and (c) and for the constant temperatures in plots (b) and (d), respectively, the same values are used as in Fig. 6.2. Furthermore, the colors of the curves have the same meaning as before. The results have been calculated using the numerical parameters described in the caption of Fig. 5.6.

underscreened Kondo effect (cf. Figs. 5.5 and 5.6). A non-zero magnetic field lifts the remaining effective degeneracy of the impurity and hence leads to a sharp decrease of S_{imp} and $k_B T \chi_{\mathrm{imp}}$ for thermal energies below $k_B T \approx g_S \mu_B B$. This drop is followed by a linear decline to zero for $k_B T \ll g_S \mu_B B$, as demonstrated for impurity spin $S = 1/2$ and $g_S \mu_B B \gg k_B T_K$ in Figs. 6.1 (a) and 6.1 (c). In contrast to the spin-1/2 Kondo model, the temperature dependencies of the impurity contributions to the entropy and the effective magnetic moment for $S > 1/2$ are thus always affected by a non-zero external magnetic field.

The curves $S_{\mathrm{imp}}(T > 0, B)$ and $k_B T \chi_{\mathrm{imp}}(T > 0, B)$ shown in the respective plots (b) and (d) of Figs. 6.2 and 6.3 further demonstrate that an impurity spin $S > 1/2$ stays magnetic on energy scales smaller than $k_B T_K$. The limit of zero field in plots (b) and (d) is to be compared with the results presented in the corresponding plots (a) and (c). The field dependencies of the two considered observables illustrate that an applied magnetic field becomes relevant if the Zeeman energy exceeds the thermal energy. This is true irrespective of the value of the Kondo temperature since the residual spin $S - 1/2$, which is formed for temperatures $T \ll T_K$, has a non-zero magnetic moment and therefore also responds to an external field. As discussed for the case $S = 1/2$ in the previous section 6.1, the impurity spin is effectively reduced to a single level in the limit $g_S \mu_B B / W \to \infty$, causing both the entropy and the effective magnetic moment to approach zero.

7. The Bethe ansatz solution for the universal impurity contribution to the magnetization of the isotropic single-impurity Kondo model

The exact diagonalization of the isotropic Kondo model with arbitrary impurity spin S goes back to Hans Bethe's analytic solution [Bet31] of the antiferromagnetic one-dimensional spin-1/2 Heisenberg model with nearest-neighbor interaction from 1931 [TW83, AFL83, Hew93]. Bethe succeeded in constructing the exact eigenstates of the Hamiltonian using a particular function which has subsequently been termed *the Bethe ansatz* (cf. p. 524 of Ref. [TW83]). Calculating the energy spectrum of the model then corresponds to finding a solution of certain *Bethe ansatz equations* ([TW83], p. 538). Hamiltonians that can be diagonalized using the Bethe ansatz possess special symmetry properties which restrict their dynamics and render them "integrable" (see p. 525 of Ref. [TW83] and p. 334 of Ref. [AFL83]).

In order to apply the Bethe ansatz to the Kondo model, some additional *assumptions* are necessary:

1. The dispersion relation $\varepsilon(\boldsymbol{k})$ of the conduction electrons has to be linear for all wavevectors (corresponding to a constant density of states) [AFL83, Hew93]:
$$\varepsilon(\boldsymbol{k}) \propto |\boldsymbol{k}| \; . \tag{7.1}$$

2. The properties of the model are studied in the *scaling* or *universal regime* in which all relevant energy scales (e.g., due to non-zero temperature or magnetic field) are small compared to either the finite bandwidth of the conduction electrons or the cutoff imposed on the electron spectrum. The cutoff (or bandwidth) may then be viewed as arbitrarily large and details of the cutoff procedure are expected to only affect the parameter dependence of the Kondo temperature T_K, but not the obtained universal properties expressed via T_K ([AFL83], p. 332).

3. The g-factors of electrons g_e and impurity g_S have to be taken as equal so that a non-zero magnetic field couples to the z-component of the total spin (cf. p. 332 and 352 of Ref. [AFL83]). There has been an attempt at treating the general case $g_e \neq g_S$ within the framework of the Bethe ansatz in Ref. [Low84].

In the actual calculations, the Kondo Hamiltonian is first converted to a one-dimensional real-space representation by means of a Fourier transformation and then cast into first-quantized form by deriving a Schrödinger equation for its eigenfunctions [AFL83, Hew93]. In order to solve this equation, one has to impose some boundary conditions, which are typically chosen to be periodic [TW83, AFL83, Hew93]. The wave functions are then determined using one of the variants of the Bethe ansatz approach.

Having obtained the eigenstates of the Hamiltonian, it becomes possible to study the thermodynamic properties of the model in the thermodynamic limit. To this end, one considers the impurity contribution to the free energy F_{imp}, from which, in principle, all thermodynamic observables can be derived by differentiating. F_{imp} is determined by a set of functions which are solutions of an infinite system of coupled non-linear integral equations (see p. 540 of Ref. [TW83], p. 357 of Ref. [AFL83], and Refs. [RLA82, Hew93]), that are also referred to as *thermodynamic Bethe ansatz equations* [EFG$^+$05]. In general, these equations have to be solved numerically (cf. p. 334 of Ref. [AFL83] and Ref. [Hew93]). To this end, the infinite system of coupled equations is truncated to some finite number. This, of course, introduces a certain error and thus determines the obtainable precision of the results [RLA82]. The equations are then, e.g., cast into the form of matrix equations and iterated until convergence is achieved [RLA82].

7.1. The closed expressions for the zero-temperature impurity contribution to the magnetization

In case of zero temperature, the Bethe ansatz provides closed expressions for the universal field-dependent impurity contribution to the magnetization M_{imp} for arbitrary impurity spin S. These results have been used to calculate the M_{imp}-curves of the Kondo model without uniaxial anisotropy in the paper included in chapter 8. The Bethe ansatz solutions involve a certain energy scale $k_B T_H$ whose ratio to the Kondo scale $k_B T_K$ is a universal number[1] (see p. 590 ff. of Ref. [TW83], p. 356, 369 f., and 378 f. of Ref. [AFL83], and p. 155 of Ref. [Hew93]) and whose meaning is clarified in the next section 7.2.

For large magnetic fields $g_S \mu_B B > k_B T_H$, there is an integral representation of the impurity contribution to the magnetization for arbitrary impurity spin S (see p. 183 of Ref. [FW81a] and p. 581 of Ref. [TW83], and also compare Refs.

[1] Note that the ratio of T_H to T_K, interpreted as the high-temperature perturbative scale, was found to depend on S in Refs. [FL82] and [AFL83] (p. 379), whereas a similar calculation in Ref. [DZ05] led to the conclusion that it is actually independent of S (see Eq. (5.28), and also compare Ref. [BK04]).

[AL81, FL82] as well as p. 355 and 375 of Ref. [AFL83]):

$$\boxed{\begin{aligned}&M_{\mathrm{imp}}(T=0, g_S\mu_B B > k_B T_H; S)/g_S\mu_B = \\ &S - \frac{1}{2\pi^{3/2}} \int\limits_0^\infty \mathrm{d}\omega\, \frac{\sin(2\pi S\omega)}{\omega}\, \Gamma(1/2+\omega) \Big(\frac{\omega}{\mathrm{e}}\Big)^{-\omega} \mathrm{e}^{-2\omega \ln(g_S\mu_B B/k_B T_H)} \,.\end{aligned}} \tag{7.2}$$

In case of small fields $g_S\mu_B B < k_B T_H$, one has to distinguish between impurity spin $S = 1/2$, which is completely screened by the conduction electrons at $B = 0$ and $T = 0$, and impurity spin $S > 1/2$, for which only partial Kondo screening occurs (leaving a residual spin $S - 1/2$). For $S = 1/2$, the following series can be used to calculate M_{imp} (see Refs. [FW81b, FW81a] and p. 582 of Ref. [TW83], and also compare Ref. [AL81] and p. 355 of Ref. [AFL83]):

$$\boxed{\begin{aligned}&M_{\mathrm{imp}}(T=0, g_S\mu_B B < k_B T_H; S=1/2)/g_S\mu_B = \\ &\frac{1}{2\sqrt{\pi}} \sum_{n=0}^{\infty} \left(\frac{n+1/2}{\mathrm{e}}\right)^{n+1/2} \frac{(-1)^n}{n!\,(n+1/2)} \left(\frac{g_S\mu_B B}{k_B T_H}\right)^{2n+1} .\end{aligned}} \tag{7.3}$$

For very small magnetic fields $g_S\mu_B B \ll k_B T_H$, M_{imp} is thus linear in B with a prefactor that is inversely proportional to T_H. The impurity contribution to the magnetization for arbitrary impurity spin is given by a sum of an integral and a series [FW81a] that apparently ought to read as (cf. p. 582 of Ref. [TW83]):

$$\boxed{\begin{aligned}&M_{\mathrm{imp}}(T=0, g_S\mu_B B < k_B T_H; S)/g_S\mu_B = S - 1/2 + \\ &\frac{1}{2\pi^{3/2}} \int\limits_0^\infty \mathrm{d}\omega\, \frac{\sin\big(2\pi(S-1/2)\omega\big)}{\omega}\, \Gamma(1/2-\omega) \Big(\frac{\omega}{\mathrm{e}}\Big)^{\omega} \mathrm{e}^{-2\omega\, |\ln(g_S\mu_B B/k_B T_H)|} + \\ &\frac{1}{2\sqrt{\pi}} \sum_{n=0}^{\infty} \left(\frac{n+1/2}{\mathrm{e}}\right)^{n+1/2} \frac{(-1)^n}{n!\,(n+1/2)} \cos\big(2\pi(S-1/2)(n+1/2)\big) \left(\frac{g_S\mu_B B}{k_B T_H}\right)^{2n+1} .\end{aligned}} \tag{7.4}$$

The representation (7.4) consistently reduces to Eq. (7.3) for impurity spin $S = 1/2$. Replacing S with $S - 1/2$, note the similarity between the solution (7.2) for $g_S\mu_B B > k_B T_H$ and the integral appearing in Eq. (7.4).

7.2. Asymptotic field dependencies of the zero-temperature impurity contribution to the magnetization

For very large magnetic fields $g_S\mu_B B \gg k_B T_H$ and for arbitrary impurity spin, the impurity contribution to the magnetization at zero temperature can be written

as a perturbation series (see Refs. [AL81, FL82], p. 592 of Ref. [TW83], p. 333 and 375 of Ref. [AFL83], as well as p. 146 and 157 of Ref. [Hew93]):

$$\boxed{\begin{aligned}&M_{\mathrm{imp}}(T=0, g_S\mu_B B \gg k_B T_H; S)/g_S\mu_B = \\ &S\left(1 - \frac{1}{2\ln(g_S\mu_B B/k_B T_H)} - \frac{\ln\ln(g_S\mu_B B/k_B T_H)}{4\ln^2(g_S\mu_B B/k_B T_H)} + \ldots\right) .\end{aligned}} \tag{7.5}$$

In the limit $g_S\mu_B B/k_B T_H \to \infty$, M_{imp} thus tends to the saturation magnetization $g_S\mu_B S$ of a free spin S. Note, however, that the impurity spin only becomes asymptotically free for large fields because of the slowly declining logarithmic corrections.

In case of $S = 1/2$, the behavior for very small fields $g_S\mu_B B \ll k_B T_H$ is described by the series (7.3). On the other hand, for impurity spin $S > 1/2$, we have the following asymptotic expansion of the impurity contribution to the magnetization, which is again similar to Eq. (7.5) if substituting $S \to S - 1/2$ (see p. 375 of Ref. [AFL83] and p. 157 of Ref. [Hew93]):

$$\boxed{\begin{aligned}&M_{\mathrm{imp}}(T=0, g_S\mu_B B \ll k_B T_H; S \geq 1)/g_S\mu_B = \\ &(S-1/2)\left(1 - \frac{1}{2\ln(g_S\mu_B B/k_B T_H)} - \frac{\ln|\ln(g_S\mu_B B/k_B T_H)|}{4\ln^2(g_S\mu_B B/k_B T_H)} + \ldots\right) .\end{aligned}} \tag{7.6}$$

According to this result, M_{imp} approaches the saturation magnetization $g_S\mu_B(S-1/2)$ of a free spin $S-1/2$ in the limit $k_B T_H/g_S\mu_B B \to \infty$, once again with slowly vanishing logarithmic contributions. This asymptotic behavior is another sign of the ferromagnetic coupling between the residual spin $S-1/2$, which remains after the partial Kondo screening, and the conduction electrons (see p. 158 of Ref. [Hew93] and compare Sec. 5.2).

The high-field scale $k_B T_H$ is chosen in such a way that the perturbative expansion (7.5) does not contain terms of order $1/\ln^2(g_S\mu_B B/k_B T_H)$ (see p. 333, 355 f., 370, and 375 of Ref. [AFL83], as well as p. 146 and 157 of Ref. [Hew93]). In particular, this "normalization" allows to define T_H for any impurity spin S. With an analogous requirement for the low-field asymptotic series (7.6), it turns out that the energy scale $k_B T_H$ is the same for small and large magnetic fields (see p. 370 of Ref. [AFL83] and p. 157 of Ref. [Hew93]). Note the similarity between this definition of T_H and the definition of the Kondo temperature T_K via the low- and high-temperature expansions of the zero-field impurity contribution to the susceptibility (cf. Sec. 5.2).

8. "Numerical Renormalization Group calculations of the magnetization of Kondo impurities with and without uniaxial anisotropy"

As the *main result of this thesis*, this chapter contains a comprehensive manuscript submitted to Physical Review B that has been accepted for publication (in a revised version) as Ref. [HS13].

The paper presents a detailed NRG study of the Kondo Hamiltonian (2.15) with the impurity part (2.52) (which includes *uniaxial anisotropy* D) in non-zero magnetic field B for different ratios g_e/g_S of electron and impurity g-factor. The three cases $D = 0$ (isotropic impurity), $D < 0$ (*easy axis* anisotropy), and $D > 0$ (*hard axis* anisotropy) are analyzed, extending existing results for $B = 0$ from Ref. [ŽPP08] to the situation with non-zero field. Throughout the investigation, we focus on the field dependence at low temperature of the impurity magnetization $\mathcal{M} = -g_S\mu_B\langle \underset{\sim}{S}^z \rangle$ (introduced in Eq. (4.288)) and the impurity contribution to the magnetization M_{imp}. In case of $D = 0$, the obtained NRG results for $M_{\mathrm{imp}}(B, T \approx 0)$ are compared with the corresponding zero-temperature Bethe ansatz solutions discussed in chapter 7.

The published version also cites a study of the single-impurity Anderson model (2.19) reported in Ref. [MWC12]. In particular, this paper presents an investigation of the relationship between the impurity contributions to the zero-field susceptibility for $g_e = 0$ and $g_e = g_S$. The two susceptibilities are found to be close to identical for all considered temperatures as expected from the *Clogston-Anderson compensation theorem* (see p. 299 of Ref. [Hew93]).

Our NRG calculations are motivated by the question as to how the magnetic properties of a deposited magnetic molecule are modified by the interaction with a non-magnetic metallic substrate (cf. Sec. 2.3.2). The field-dependent magnetic moment of deposited atoms and molecules can be measured (as an ensemble average) using, e.g., X-ray magnetic circular dichroism (XMCD). In recent years, it has also become possible to obtain time-averaged magnetization curves of individual atoms (and suitable molecules) on non-magnetic metallic surfaces by means of spin-polarized scanning tunneling spectroscopy (SP-STS). We refer the reader to the introduction of the manuscript for references to corresponding experiments.

Numerical Renormalization Group calculations of the magnetization of Kondo impurities with and without uniaxial anisotropy

Martin Höck and Jürgen Schnack

We study a Kondo impurity model with additional uniaxial anisotropy D in a non-zero magnetic field B using the Numerical Renormalization Group (NRG). The ratio g_e/g_S of electron and impurity g-factor is regarded as a free parameter and, in particular, the special cases of a "local" ($g_e = 0$) and "bulk" ($g_e = g_S$) field are considered. For a bulk field, the relationship between the impurity magnetization $\mathcal{M}$ and the impurity contribution to the magnetization M_{imp} is investigated. Furthermore, we study how the value of g_e affects the impurity magnetization curves. In case of an impurity with $D = 0$ and $g_e = g_S$, it is demonstrated that at zero temperature $\mathcal{M}(B)$, unlike $M_{\mathrm{imp}}(B)$, does *not* display universal behavior. With additional "easy axis" anisotropy, the impurity magnetization for non-zero temperature is well described by a shifted and rescaled Brillouin function on energy scales that are small compared to $|D|$. In case of "hard axis" anisotropy, the magnetization curves can feature steps which are due to field-induced pseudo-spin-1/2 Kondo effects. For large hard axis anisotropy and a local field, these screening effects are described by an exchange-anisotropic spin-1/2 Kondo model with an additional scattering term that is spin-dependent (in contrast to ordinary potential scattering). Our study is motivated by the question how the magnetic properties of a deposited magnetic molecule are modified by the interaction with a non-magnetic metallic surface.

I. INTRODUCTION

Magnetic molecules offer the prospect of encoding and storing information in their magnetic state. The latter point applies, in particular, to bistable molecules such as single molecule magnets (SMMs).[1–4] The possibility to store, e.g., one bit of information in the state of a single molecule would constitute an enormous miniaturization and could lead to data storage technologies with significantly increased areal density.[5] However, to make a (potentially elusive) technological application feasible, the molecules need to be individually addressable so that their magnetic state can be probed and manipulated on a molecule-by-molecule basis. In the last years, there has been an increasing interest in the question whether this functionality can be achieved by a controlled deposition of magnetic molecules on suitable substrates.[5–8] While such an approach might solve the problem of addressability, it can introduce new complications due to interactions between the molecules and the surface. Depending on details such as the molecule's ligands, the presence of an additional decoupling layer, and, of course, the characteristics of the surface, the interaction with the substrate might alter the magnetic properties of the molecule in an important (and possibly adverse) way. Thus, even if the magnetic response of the isolated molecule is well understood (e.g., through a description by a suitable spin model[9]), its magnetic properties in contact with the surface have to be reinvestigated.

In this article, we study a single-channel Kondo impurity model with non-zero magnetic field and additional uniaxial anisotropy $D(\underset{\sim}{S}^z)^2$ for the impurity spin operator $\underset{\sim}{\boldsymbol{S}}$. Such an anisotropy term (along with transverse anisotropy $E[(\underset{\sim}{S}^x)^2 - (\underset{\sim}{S}^y)^2]$) is a common part of a pure spin model for the description of isolated magnetic molecules (in particular, for representing SMMs).[9] The quantum impurity model is intended to serve as a minimal representation of an anisotropic magnetic molecule on a non-magnetic metallic substrate and, with transverse anisotropy E, has already been used to describe SMMs interacting with metallic electrodes.[10–12] Furthermore, it has been found that the above uniaxial and transverse anisotropy terms are also appropriate to model the surface-induced anisotropy of a single magnetic atom on a metallic substrate with a decoupling layer.[13–15] To investigate how the interaction with the electrons affects the magnetic properties of the impurity, we carry out Numerical Renormalization Group[16–18] (NRG) calculations and focus on the magnetic field dependence of the impurity magnetization.

Regarding the experimental situation, the magnetic moment of deposited molecules (or atoms)[15] can be measured using methods such as X-ray magnetic circular dichroism (XMCD).[7,19–27] XMCD is an element-specific technique of high sensitivity based on the absorption of circularly polarized X-rays and can be used to obtain an ensemble-averaged result for the magnetic field dependent molecule magnetization.[28–30] In principle, it is also possible to extract information about different contributions to the observed magnetic moment (such as the orbital and spin contribution) from the XMCD data using, e.g., sum rules.[7,21,22,24,27] In the last years, magnetization curves of magnetic atoms on non-magnetic metallic surfaces could also be recorded using spin-polarized scanning tunneling spectroscopy (SP-STS).[15,31–35] In contrast to XMCD, this method provides a time-average of the field-dependent magnetic moment of a single atom. It has been demonstrated that SP-STS can also be applied to (suitable) deposited magnetic molecules.[36–38]

The static magnetization of Kondo impurity models (including related models such as the single-impurity Anderson model) has been investigated by a number of techniques. Among these are Green's-function methods,[39,40] the Bethe Ansatz,[41–52] and NRG[53–55] (including density matrix based extensions). By now, there are also several

studies of the time-dependence of the magnetization in non-equilibrium situations (e.g., after a quantum quench or with a non-zero voltage bias).[56–60] In particular, non-equilibrium spin dynamics of impurity models can be investigated by using a generalization of NRG called time-dependent NRG (TD-NRG).[12,61,62]

The present article extends existing NRG results for the Kondo model with uniaxial anisotropy[63] to the case of non-zero magnetic field. The system with non-zero field (with a focus on the properties of spectral functions) has been previously studied in Refs. 64 and 65. Furthermore, magnetization curves for isotropic Kondo impurities and for a Kondo impurity featuring both longitudinal and transverse anisotropy have been calculated in Ref. 55. We would like to stress, however, that our investigation places emphasis on different aspects of the problem and is thus complementary to Ref. 55.

The remainder of this article is organized as follows. In Sec. II, the quantum impurity model is introduced and transformed to a representation that is suitable for further numerical treatment. Sec. III provides information about our use of the NRG method and contains definitions of the considered observables. In Sec. IV, we study the magnetic field dependence of the impurity magnetization and the impurity contribution to the magnetization for an isotropic system (i.e., with anisotropy parameter $D = 0$) and analyze the relation between both quantities. After an investigation of the Kondo model with additional "easy axis" anisotropy ($D < 0$) in Sec. V, the case of "hard axis" anisotropy ($D > 0$) is considered in Sec. VI. In order to describe the field-induced pseudo-spin-1/2 Kondo effects that are observed in the magnetization curves for large hard axis anisotropy, an effective model is derived and its properties are studied. We conclude this article with a summary of the results in Sec. VII. Appendix A contains a brief description of the technical details of an NRG calculation with non-zero magnetic coupling of the conduction electrons. The remaining appendices are concerned with the coupling strength dependence of the magnetization for $D = 0$ (App. B), the effect of a non-zero magnetic coupling of the conduction electrons on the impurity magnetization curves (App. C), and certain technical aspects relevant to the study of the effective model (App. D).

II. MODEL

A. Hamiltonian

In this work, we study a Hamilton operator $\underset{\sim}{H}$ consisting of three parts:

$$\underset{\sim}{H} = \underset{\sim}{H}_{\text{electrons}} + \underset{\sim}{H}_{\text{coupling}} + \underset{\sim}{H}_{\text{impurity}} \,. \tag{1}$$

The first term $\underset{\sim}{H}_{\text{electrons}}$ represents non-interacting tight-binding electrons whose hopping between two sites i and j of a periodic lattice with L sites is described by the corresponding hopping parameter t_{ij}:

$$\underset{\sim}{H}_{\text{electrons}} = \sum_{i\neq j,\,\sigma} t_{ij}\, \underset{\sim}{d}^{\dagger}_{i\sigma}\, \underset{\sim}{d}_{j\sigma} + g_e \mu_B B \underset{\sim}{\mathcal{S}}^z \,. \tag{2}$$

Here, $\underset{\sim}{d}^{(\dagger)}_{i\sigma}$ is a destruction (creation) operator for an electron with spin projection $\sigma = \pm 1/2 \mathrel{\widehat{=}} \uparrow / \downarrow$ at lattice site i. The effect of an external magnetic field B is taken into account by a Zeeman term with electron g-factor g_e, Bohr magneton μ_B, and the z-component of the total spin of the electrons $\underset{\sim}{\mathcal{S}}^z = \frac{1}{2}\sum_i (\underset{\sim}{n}_{i\uparrow} - \underset{\sim}{n}_{i\downarrow})$ with $\underset{\sim}{n}_{i\sigma} = \underset{\sim}{d}^{\dagger}_{i\sigma}\underset{\sim}{d}_{i\sigma}$. Using a discrete Fourier transformation, $\underset{\sim}{c}^{\dagger}_{\boldsymbol{k}\sigma} = (1/\sqrt{L})\sum_j e^{i\boldsymbol{k}\cdot\boldsymbol{R}_j}\, \underset{\sim}{d}^{\dagger}_{j\sigma}$, Hamiltonian (2) can be equivalently written in the more common form

$$\underset{\sim}{H}_{\text{electrons}} = \sum_{\boldsymbol{k},\sigma} \underbrace{(\varepsilon_{\boldsymbol{k}} + \sigma g_e \mu_B B)}_{=\varepsilon_{\boldsymbol{k}\sigma}(B)}\, \underset{\sim}{c}^{\dagger}_{\boldsymbol{k}\sigma}\, \underset{\sim}{c}_{\boldsymbol{k}\sigma} \,, \tag{3}$$

with a dispersion relation $\varepsilon_{\boldsymbol{k}\sigma}(B)$, assigning an energy ε to a wavevector $\boldsymbol{k}$, that now depends on spin projection and magnetic field. In general, the spin-independent dispersion relation $\varepsilon_{\boldsymbol{k}}$ is anisotropic in $\boldsymbol{k}$-space.

For the interaction term in Eq. (1), we use a standard isotropic Kondo coupling,

$$\underset{\sim}{H}_{\text{coupling}} = J \underset{\sim}{\boldsymbol{S}} \cdot \underset{\sim}{\boldsymbol{s}}_0 \,, \tag{4}$$

and assume that the impurity spin $\underset{\sim}{\boldsymbol{S}}$ couples antiferromagnetically ($J > 0$) to the electronic spin at the origin, which is given by $\underset{\sim}{\boldsymbol{s}}_0 = (1/2L)\sum_{\boldsymbol{k},\boldsymbol{k}',\mu,\nu} \underset{\sim}{c}^{\dagger}_{\boldsymbol{k}\mu}\boldsymbol{\sigma}_{\mu\nu}\underset{\sim}{c}_{\boldsymbol{k}'\nu}$ with the vector of Pauli matrices $\boldsymbol{\sigma}$.

Finally, the impurity part of Hamiltonian (1) represents a localized spin with quantum number S which couples to the external magnetic field with g-factor g_S and possesses an additional uniaxial anisotropy D:

$$\underset{\sim}{H}_{\text{impurity}} = D(\underset{\sim}{S}^z)^2 + g_S \mu_B B \underset{\sim}{S}^z \,. \tag{5}$$

With the chosen convention, the impurity spin has an "easy axis" for $D < 0$ and a "hard axis" or an "easy plane" for $D > 0$. A further transverse anisotropy $E[(\underset{\sim}{S}^x)^2 - (\underset{\sim}{S}^y)^2]$ is *not* considered in this article. $\underset{\sim}{H}_{\text{impurity}}$ can be seen as a minimal representation of a magnetic molecule with a single magnetic center or as a "giant spin approximation" for an SMM.[9,66]

Hamiltonian (1) corresponds to an exchange-isotropic single-channel Kondo impurity model with additional uniaxial anisotropy and non-zero external magnetic field. The special choices $g_e = 0$ and $g_e = g_S$ for the electron g-factor are referred to as a "local" and "bulk" magnetic field, respectively. Regarding the modeling of a deposited

magnetic molecule, it has to be emphasized that Hamiltonian (1) suffers from a number of simplifications. For example, there is no orbital contribution to the magnetism, and no charge fluctuations between molecule and surface are possible. In this article, we only consider the effect of the Kondo coupling on the magnetic properties of the impurity spin.

B. Transformation to an energy representation

In order to treat Hamiltonian (1) using NRG, $\underset{\sim}{H}_{\text{electrons}}$ and $\underset{\sim}{H}_{\text{coupling}}$ are expressed via a continuous energy representation for the electronic degrees of freedom. To this end, we first take a standard continuum limit in $\boldsymbol{k}$-space (i.e., we consider a lattice of dimension d with $L \gg 1$).[17] By adapting the corresponding expression for the two-impurity Kondo model from Ref. 67 to the single-impurity case (see also Ref. 68), we then define those states with energy ε to which the localized spin *directly* couples:

$$\underset{\sim}{a}_{\varepsilon\mu} = \frac{1}{\sqrt{(2\pi)^d \rho(\varepsilon-\mu h)}} \int \mathrm{d}\boldsymbol{k}\, \delta(\varepsilon - \varepsilon_\mu(\boldsymbol{k}, B))\, \underset{\sim}{c}_{\boldsymbol{k}\mu}\ , \quad (6)$$

where we have introduced the abbreviation $h = g_e \mu_B B$ and the normalized density of states (DOS) per spin projection and lattice site $\rho(\varepsilon) = (1/L)\sum_{\boldsymbol{k}} \delta(\varepsilon - \varepsilon_{\boldsymbol{k}})$. Denoting the half-width of the conduction band by W, the allowed energies ε for spin projection μ span the interval $[-W+\mu h,\, W+\mu h]$. The new operators $\underset{\sim}{a}_{\varepsilon\mu}$ are properly normalized because of the pre-factor involving the DOS.

If we are only interested in impurity properties, then all other electronic states different from those defined in Eq. (6) can be safely discarded without introducing any approximation.[17] This leads to the desired continuous energy representation of Hamiltonian (1):

$$\begin{aligned} \underset{\sim}{H} \to \sum_\mu \int_{-W+\mu h}^{W+\mu h} \mathrm{d}\varepsilon\, \varepsilon\, \underset{\sim}{a}^\dagger_{\varepsilon\mu} \underset{\sim}{a}_{\varepsilon\mu} \qquad (7) \\ + J \underset{\sim}{\boldsymbol{S}} \cdot \sum_{\mu,\nu} \left(\int_{-W+\mu h}^{W+\mu h} \mathrm{d}\varepsilon\, \sqrt{\rho(\varepsilon-\mu h)}\, \underset{\sim}{a}^\dagger_{\varepsilon\mu} \right) \frac{\boldsymbol{\sigma}_{\mu\nu}}{2} \times \\ \left(\int_{-W+\nu h}^{W+\nu h} \mathrm{d}\varepsilon'\, \sqrt{\rho(\varepsilon'-\nu h)}\, \underset{\sim}{a}_{\varepsilon'\nu} \right) + \underset{\sim}{H}_{\text{impurity}}\,. \end{aligned}$$

For $h = 0$, i.e., for $B = 0$ or $g_e = 0$, Eq. (7) reduces to the well-known expression for the energy representation of the Kondo model.[69] In the following, we consider the case of a constant DOS: $\rho(\varepsilon) = 1/2W = \rho$.

III. METHOD AND OBSERVABLES

A. Method: NRG

Approximate eigenvalues and eigenvectors of Hamiltonian (7) for the calculation of impurity properties can be obtained with the Numerical Renormalization Group[16–18] (NRG). However, the procedure leading to the parameters of the Wilson chain has to be slightly modified if $h \neq 0$ (see App. A for a brief discussion of the required changes).

Both a non-zero magnetic field and an additional uniaxial anisotropy break the full SU(2)-symmetry in spin space of Hamiltonian (1). For this reason, we label eigenstates of $\underset{\sim}{H}$ only with the charge quantum number Q and the magnetic quantum number S^z_{total} of the z-component of the total spin. Except for one example in App. D, all NRG calculations are carried out using the improved discretization scheme proposed by Žitko and Pruschke[70,71] with averaging over four z-values that are equidistantly spaced on the interval $(0, 1]$. The Hamiltonians describing the truncated Wilson chain are always rescaled by employing Wilson's analytical solution for the hopping parameters for the case of the standard discretization with $z = 1$.[16,18] Observables are computed using only those states that are kept after truncation and results are averaged over even and odd sites of the Wilson chain according to the prescription of Ref. 18. We use a discretization parameter $\Lambda = 3$, a dimensionless inverse temperature $\bar{\beta} = 0.7$, and a fixed number of kept states of the order of 5000 to achieve convergence for all considered observables within the resolution of the presented plots. Nevertheless, at $\Lambda > 1$ there might still be slight systematic deviations for non-zero temperature, which can for example be demonstrated by setting $J = 0$ and comparing the NRG results with the analytical solution for a free spin. It is necessary to perform a separate NRG calculation for each value of the magnetic field. If curves are shown in a plot, they are thus the result of a spline interpolation through the numerically obtained data points.

B. Observables

In our calculations we focus on the impurity magnetization which is defined as the thermodynamic expectation value of the impurity magnetization operator:

$$\mathcal{M}(T,B) = -\left\langle \frac{\partial \underset{\sim}{H}_{\text{impurity}}}{\partial B} \right\rangle = -g_S \mu_B \langle \underset{\sim}{S}^z \rangle\ . \quad (8)$$

Furthermore, we consider the impurity contribution to the entropy, magnetization, and magnetic susceptibility. The impurity contribution to some quantity $\mathcal{O}$ is defined in the usual way:[18]

$$\mathcal{O}_{\rm imp} = \mathcal{O}_{\rm total}^{\rm with\ impurity} - \mathcal{O}_{\rm total}^{\rm w/o\ impurity} \ . \qquad (9)$$

The observable $\mathcal{O}_{\rm total}^{\rm w/o\ impurity}$ for the system without impurity is also calculated using NRG by removing the impurity part from the Wilson chain. For the entropy $S(T,B)$, the magnetization $M(T,B)$, and the susceptibility $\chi(T,B)$, we use the standard definitions $S(T,B) = -\partial\Omega(T,B)/\partial T$, $M(T,B) = -\partial\Omega(T,B)/\partial B$, and $\chi(T,B) = \partial M(T,B)/\partial B$, with $\Omega(T,B)$ being the grand-canonical potential. According to the definitions (8) and (9), the impurity contribution to the magnetization $M_{\rm imp}$ can be written as:

$$M_{\rm imp} = \mathcal{M} + M_{\rm electrons}^{\rm with\ impurity} - M_{\rm electrons}^{\rm w/o\ impurity} \ . \qquad (10)$$

If the electron g-factor is zero or if impurity and electrons decouple (which happens for $J \to 0$ or $T \to \infty$), we thus have the special case $M_{\rm imp}(T,B) = \mathcal{M}(T,B)$.

In the grand-canonical calculations the chemical potential is assumed to be zero. For a symmetric DOS, $\rho(\varepsilon) = \rho(-\varepsilon)$, the free electron band is thus on average half-filled for arbitrary magnetic field and temperature.

IV. IMPURITIES WITH $D = 0$

Let us first consider the case of an isotropic impurity with $D = 0$ in Hamiltonian (5) and study the impurity contribution to the magnetization $M_{\rm imp}$ and the impurity magnetization $\mathcal{M}$, both as function of temperature and magnetic field. For the moment, we are only concerned with the special case of equal g-factors of impurity and electrons (corresponding to a bulk magnetic field). Recalling the motivation given in the introduction, $\mathcal{M}$ as the expectation value of the impurity magnetization operator should be the observable that is more closely related to experimental magnetization data obtained by methods such as XMCD.

A. Field-dependence of the magnetization

In case of the Kondo model with $D = 0$, $g_e = g_S$, and arbitrary impurity spin S, the Bethe Ansatz (BA) allows for the derivation of a closed expression for the impurity contribution to the magnetization at zero temperature.[41–44,46,47] $M_{\rm imp}(B, T = 0)$ is known to display universal behavior in the so-called scaling regime, in which all relevant energy scales are small compared to the energy cutoff (or the finite bandwidth).[47] "Bare" parameters of the model can then be absorbed into a certain energy scale $k_B T_H$ so that the field-dependence of $M_{\rm imp}$ at zero temperature is described by a universal function $f_S(x)$ (see Eq. (5.1.33) of Ref. 46), with x being the rescaled magnetic field: $x = g_S\mu_B B/k_B T_H$. For each value of S, the energy scale $k_B T_H$ is chosen in such a way that the asymptotic high-field (i.e., $g_S\mu_B B \gg k_B T_H$) expansion for $f_S(x)$ does not contain terms of order $1/\ln^2(g_S\mu_B B/k_B T_H)$.[47,72] With this choice, the asymptotic low-field (i.e., $g_S\mu_B B \ll k_B T_H$) expansion for $S \geq 1$ does not include such terms either.[72] In case of impurity spin $S = 1/2$, we adopt the convention of Ref. 46 according to which the Kondo temperature T_K is identified with the strong coupling scale (as opposed to the high-temperature scale)[47] and defined as:

$$\frac{\chi_{\rm imp}(T=0,B=0)}{(g_S\mu_B)^2} = \frac{1}{2\pi\, k_B T_K} \ . \qquad (11)$$

The relation between T_H and T_K for $S = 1/2$ is then given by:[46]

$$T_H = \sqrt{\frac{2\pi}{e}}\, T_K \ . \qquad (12)$$

Note that in the remainder of this article results for the energy scales $k_B T_H$ and $k_B T_K$ always refer to either the corresponding situation with $D = 0$ or a comparable situation with $D = 0$.

In Fig. 1 we plot the universal BA solution for $M_{\rm imp}(T = 0)$ for three different impurity spins $S = 1/2, 1$, and $3/2$.[73] $f_S(x)$ is a strictly monotonically increasing function of x and approaches the saturation magnetization of a free spin, $g_S\mu_B S$, for $x \to \infty$ with slowly decaying logarithmic corrections.[46,47,72] The behavior in the limit $x \to 0$ depends on the value of S: In case of $S = 1/2$, $f_{1/2}(x) \propto x$ for small x, whereas for $S \geq 1$ the function $f_S(x)$ goes to the saturation magnetization of a reduced spin with $S-1/2$, again with logarithmic corrections.[46,47,72] This low-field behavior mirrors the Kondo screening which, for vanishing magnetic field, reduces the impurity spin S to a residual spin $S - 1/2$ in the limit $T/T_K \ll 1$.[74,75] The magnetic properties of the impurity are furthermore markedly different from that of a free spin as the magnetization of a free spin at $T = 0$ saturates for any positive magnetic field.

Using NRG, we have calculated $M_{\rm imp}(B, T \approx 0)$ for several values of the coupling strength ρJ and have fitted the obtained curves to the respective universal BA curve by employing T_H as a fit parameter (see Fig. 1). The nice agreement with the BA solution demonstrates the universal field-dependence that $M_{\rm imp}$ displays for small ρJ and allows us to reliably determine the value of T_H for all considered impurity spins. However, note that for very large magnetic fields (i.e., for $g_S\mu_B B \lesssim W$), we leave the scaling regime and the rescaled $M_{\rm imp}$-curves, as calculated by NRG, start to drop below the universal BA curves (this is not shown in Fig. 1). The determined approximate values of $k_B T_H/W$ are given in Table I. We find that the fitted values of T_H increase with the impurity spin for fixed coupling strength and, furthermore, that the relative deviation between the results for different S decreases when ρJ is reduced. However, even for the smallest considered coupling strength

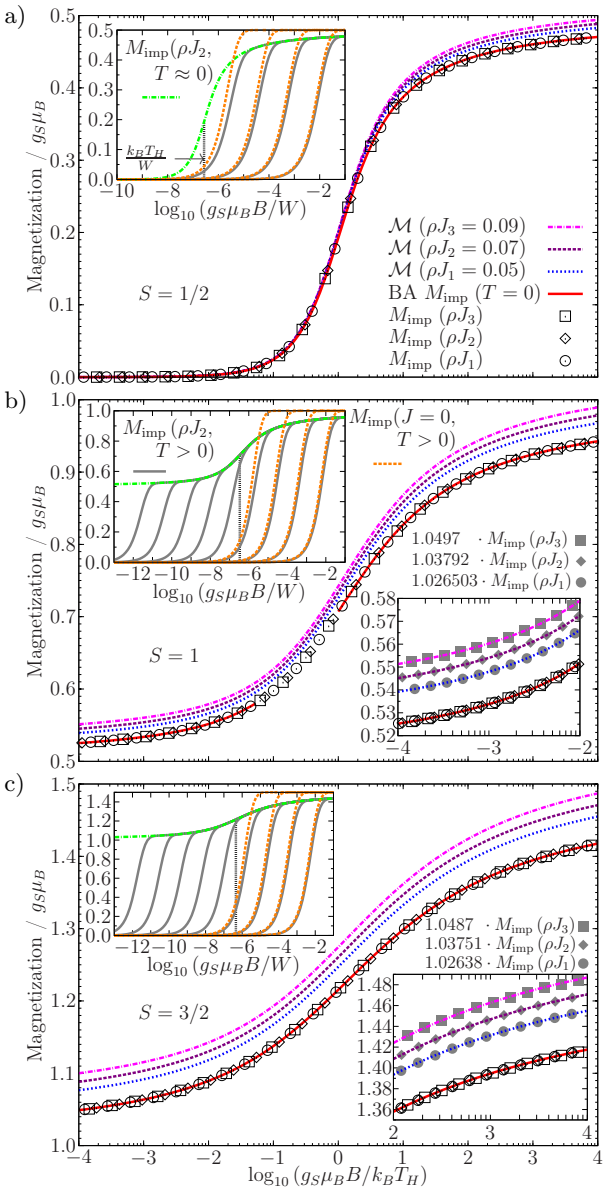

FIG. 1. (Color online) **Main plots:** Impurity contribution to the magnetization $M_{\rm imp}$ and impurity magnetization $\mathcal{M}$ as function of magnetic field for $g_e = g_S$, three different couplings ρJ, and for impurity spin a) $S = 1/2$, b) $S = 1$, and c) $S = 3/2$. The temperature is $k_B T/W \approx 1.54 \cdot 10^{-15} \approx 0$ and the field is rescaled using $k_B T_H$. In case of $S = 1$, part of the universal BA solution for $M_{\rm imp}(x, T = 0)$ is missing in the regime $g_S\mu_B B \lesssim k_B T_H$. **Upper left insets** show NRG results for $M_{\rm imp}(B)$ at $T \approx 0$ and finite temperature as a function of magnetic field, now expressed in units of W. $M_{\rm imp}(B)$ for $J = 0$ is also computed using NRG and resembles the magnetization of the free spin. Thermal energies increase from left to right and range from $1.79 \cdot 10^{-6} W$ (plot a) or $1.95 \cdot 10^{-12} W$ (plots b and c) to $6.79 \cdot 10^{-3} W$. Results for adjacent temperatures are calculated using truncated Wilson chains whose lengths differ by five lattice sites. **Lower right insets** show a close-up of the magnetization curves for b) low fields and c) high fields along with data points for $M_{\rm imp}$ that are multiplied by a coupling-dependent constant $\gtrsim 1$.

($\rho J = 0.05$), the values of T_H for $S = 1/2$ and $S = 3/2$ still deviate by about 44 %. According to Eqs. (11) and (12), the values of T_H for $S = 1/2$ reported in Table I correspond to the following Kondo temperatures: $k_B T_K/W \approx 4.79 \cdot 10^{-10}$ ($\rho J = 0.05$), $1.80 \cdot 10^{-7}$ (0.07), and $5.08 \cdot 10^{-6}$ (0.09). For comparison, the standard estimate for the Kondo temperature,[16,17]

$$k_B T_K'/W \approx \sqrt{\rho J} \exp(-1/\rho J) , \qquad (13)$$

gives $k_B T_K'/W \approx 4.61 \cdot 10^{-10}$ ($\rho J = 0.05$), $1.65 \cdot 10^{-7}$ (0.07), and $4.48 \cdot 10^{-6}$ (0.09). As a further check, we have determined the Kondo temperature for $S = 1/2$ and $\rho J = 0.07$ by fitting the zero-field BA solution for the impurity contribution to the susceptibility from Ref. 46 and the impurity contribution to the entropy from Ref. 76 (the specified low-temperature limit of the impurity contribution to the specific heat shows that their definition of T_K corresponds to Eq. (11)). In both cases a value of $k_B T_K/W \approx 1.79 \cdot 10^{-7}$ is obtained, which is quite similar to the one following from Table I.

The upper left insets of Fig. 1 show finite temperature NRG results for $M_{\rm imp}(T, B)$ with a coupling strength $\rho J = 0.07$. While the Bethe Ansatz provides a closed expression for the field-dependence of $M_{\rm imp}$ at zero temperature, a calculation for non-zero temperature leads to so-called thermodynamic BA equations that, at least in general, have to be solved numerically.[45,77] Hence, finite temperature results for the magnetization are not easily available. As a reference point, we replot the zero-temperature magnetization curves that cross over to the strong coupling regime in the vicinity of $g_S\mu_B B \approx k_B T_H$. As long as the thermal energy is small compared to the Zeeman energy, the magnetization always closely follows the respective zero-temperature curve. On the other hand, if the thermal energy is not negligibly small compared to the Zeeman energy, we have to distinguish between complete screening and underscreening of the impurity spin. For $S \geq 1$, non-zero temperature is always important as it also affects the residual spin. On the energy scale $g_S\mu_B B \approx k_B T$ there is a swift drop of $M_{\rm imp}(B)$ that is eventually followed by a linear decay for small fields $g_S\mu_B B \ll k_B T$. In the special case $S = 1/2$, however, non-zero temperature has little effect if $T \ll T_K$ and the magnetization already displays a linear dependence on the magnetic field for $g_S\mu_B B \approx k_B T$ due to the Kondo screening. In the upper left insets of Fig. 1 we also compare the results for $M_{\rm imp}(T, B)$ with NRG calculations for vanishing coupling $J = 0$. This comparison is meant to illustrate the effect of a non-zero value of J.[78] At high temperatures (compared to T_H), the impurity spin is progressively decoupled from the electronic system and its magnetization hence resembles the result for $J = 0$ more closely. However, note that the impurity only becomes asymptotically free for high temperatures.

In addition to the impurity contribution to the magnetization $M_{\rm imp}$, we also plot the impurity magnetization $\mathcal{M}(B)$ for the same values of the coupling ρJ and

TABLE I. Approximate values of k_BT_H/W as used in Fig. 1, obtained by fitting the universal Bethe Ansatz solution for $M_{\rm imp}(x, T = 0)$, and proportionality factors $\alpha(\rho J)$ relating $\mathcal{M}$ and $M_{\rm imp}$ according to Eq. (14). The results for α have been averaged over magnetic fields $g_S\mu_B B/W \in [10^{-13}, 10^{-1}]$ for $k_BT/W \approx 1.54 \cdot 10^{-15} \approx 0$. Numbers in parentheses give the corresponding standard deviation for the last decimal place. For Zeeman energies close to the band edge (i.e., for $g_S\mu_B B \lesssim W$), which have not been considered for the average, α noticeably decreases (increases) for $S = 1/2$ ($S = 1, 3/2$).

	$S = 1/2$		$S = 1$		$S = 3/2$	
ρJ	k_BT_H/W	α	k_BT_H/W	α	k_BT_H/W	α
0.05	$7.29 \cdot 10^{-10}$	1.02659(1)	$8.49 \cdot 10^{-10}$	1.026503(7)	$1.05 \cdot 10^{-9}$	1.02638(2)
0.07	$2.74 \cdot 10^{-7}$	1.03822(2)	$3.39 \cdot 10^{-7}$	1.03792(3)	$4.55 \cdot 10^{-7}$	1.03751(6)
0.09	$7.72 \cdot 10^{-6}$	1.05048(3)	$1.02 \cdot 10^{-5}$	1.04970(8)	$1.51 \cdot 10^{-5}$	1.0487(2)

negligible temperature in Fig. 1. The magnetic field is again rescaled by k_BT_H using the values from Table I. We find that $\mathcal{M}$ and $M_{\rm imp}$ differ for all considered magnetic fields with $\mathcal{M}(B)$ being larger than $M_{\rm imp}(B)$ for given B. This means, in particular, that for large magnetic fields $\mathcal{M}$ comes closer to the saturation magnetization of a free spin than $M_{\rm imp}$ does and, according to Eq. (10), that the magnetization of the conduction electrons is reduced due to the interaction with the impurity spin. Upon decreasing ρJ at constant rescaled field x, we observe that the impurity magnetization becomes smaller and thus approaches the universal curve for $M_{\rm imp}(x)$. A comparison of the NRG results for $\mathcal{M}$ and $M_{\rm imp}$ shows that both quantities are proportional to each other *for fixed coupling strength* ρJ, i.e.,

$$\mathcal{M}(B, T \approx 0) = \alpha(\rho J)\, M_{\rm imp}(B, T \approx 0)\ , \qquad (14)$$

with a proportionality factor $\alpha > 1$ that depends on ρJ (see Table I for a list of the calculated values of $\alpha(\rho J)$). With the accuracy indicated in Table I, relation (14) holds for Zeeman energies that are small compared to the half-bandwidth W. It is illustrated for the case of small magnetic fields (for $S = 1$) and large magnetic fields (for $S = 3/2$) in the lower right insets of Fig. 1. While the obtained values for $\alpha(\rho J)$ decrease with increasing impurity spin S, the values for different S differ by less than 0.2 % according to Table I. Since impurity and electrons progressively decouple at high temperatures, we expect α to be temperature dependent with $\alpha \to 1$ for $k_BT/W \gg 1$ (cf. Eq. (10)). The results presented in Fig. 1 show that the magnetic field cannot be rescaled by k_BT_H or any energy scale proportional to it so as to produce a universal curve for the field-dependent impurity magnetization $\mathcal{M}$. This conclusion applies although the field-dependence of $M_{\rm imp}$ is given by a universal function and $\mathcal{M}(B) \propto M_{\rm imp}(B)$ for fixed coupling strength ρJ, since the proportionality factor in Eq. (14) depends on the value of ρJ.

To elucidate our findings, we refer to one of the original Bethe Ansatz investigations of the Kondo model.[49] With the assumptions of a BA calculation (including an arbitrarily large energy cutoff $\mathscr{D}$), it is found that $\mathcal{M} = M_{\rm imp}$. To study the influence of the cutoff scheme, a comparison with perturbation theory is carried out showing that $\mathcal{M}$ has leading corrections of order $1/\ln(\mathscr{D})$, whereas the corrections of $M_{\rm imp}$ vanish like $1/\mathscr{D}$ and thus much faster.[49] The regime in which all relevant energy scales are negligibly small compared to the cutoff *in a logarithmic sense*, e.g. $\ln(\mathscr{D}/g_S\mu_B B) \gg 1$, is termed "extreme scaling limit".[49]

With this background we reach the following interpretation of the NRG results for $\mathcal{M}(B)$ and $M_{\rm imp}(B)$: For the chosen values of the coupling strength ρJ, the half-bandwidth W (basically serving as the unit of energy) can be regarded as very large compared to all relevant energy scales $\mathcal{E}$ so that corrections of order $\mathcal{E}/W$ can be expected to be small. It is for this reason that we find nice agreement with the universal BA solution for $M_{\rm imp}(x, T = 0)$ as long as the Zeeman energy is small compared to W. On the other hand, corrections of order $1/\ln(W/\mathcal{E})$ are not necessarily negligible for a finite value of W. This appears to be an adequate explanation for our NRG results showing that $\mathcal{M} \neq M_{\rm imp}$. Moreover, a decrease of ρJ corresponds to an increase of the bandwidth and thus bandwidth-related corrections should become smaller. Accordingly, $\mathcal{M}(B)$ approaches $M_{\rm imp}(B)$ for smaller coupling strength at constant magnetic field B. These observations might also bear some importance for experimental situations: While experimental parameters are certainly suitable to consider the scaling regime (in case the system exhibits universal behavior), it is less clear whether an experimental system can be placed in the extreme scaling regime.

The difference between $M_{\rm imp}$ and $\mathcal{M}$ is further investigated in App. B by studying the coupling strength dependence of both quantities.

V. IMPURITIES WITH EASY AXIS ANISOTROPY

We now deal with the case of an impurity with additional easy axis anisotropy (i.e., with anisotropy parameter $D < 0$ in Eq. (5)). In this section, emphasis is placed on the field-dependence of the impurity magnetization $\mathcal{M}$, again for the case of equal g-factors. Before considering the full impurity model given by Eq. (1), let us briefly recapitulate the magnetic properties of a free spin with easy axis anisotropy that is described by

Hamiltonian (5).

For negative anisotropy parameter D and vanishing magnetic field, the groundstate of a spin $S \geq 1$ is a doublet composed of the states with magnetic quantum number $M = \pm S$. In the special case $S = 1/2$, the anisotropy term $D(\underset{\sim}{S}^z)^2$ evaluates to a constant and is thus insignificant for the thermodynamics. The first excited state is a singlet with $M = 0$ for $S = 1$ and a doublet with $M = \pm(S-1)$ for all larger spins. It follows that the energy gap between groundstate and first excited state is given by $|D|(2S-1)$. For thermal energies that are small compared to this gap, the zero-field magnetic susceptibility approximately obeys a Curie law with Curie constant $\langle(\underset{\sim}{S}^z)^2\rangle = S^2$ (instead of $S(S+1)/3$ for an isotropic spin).

What do we expect for the full impurity model if there is an additional easy axis anisotropy? Since the groundstate doublet of the free spin with easy axis anisotropy has $|\Delta M| = 2S > 1$, the two states it is comprised of are not connected by a single spinflip, which changes M by 1. Furthermore, for increasing values of $|D|$ the gap in the energy spectrum of the free spin with easy axis anisotropy progressively suppresses scattering processes connecting groundstate and first excited state. With the scattering picture in mind, one would thus assume that the Kondo effect is weakened by a negative value of D. This is in line with the simplified picture in the limit $|D| \to \infty$: The anisotropy term $D(\underset{\sim}{S}^z)^2$ then effectively acts as a projection operator onto the groundstate doublet of the impurity with $M = \pm S$ and hence asymptotically reduces the full Kondo interaction of Eq. (4) to an Ising-type coupling.[63] With respect to the impurity magnetization $\mathcal{M}$, there appears to be an even simpler argument: A larger absolute value of the anisotropy parameter D energetically lifts all excited states of the impurity, which have reduced magnetic moment in comparison to the groundstate doublet. At large $|D|$ one would thus expect that the excited states have less weight in the many-body groundstate of the full impurity model leading to an increased value of $\mathcal{M}$ at zero temperature for positive magnetic field.

A. Field-dependence of the impurity magnetization

In Fig. 2 low-temperature NRG results for the impurity magnetization $\mathcal{M}(B)$ for impurity spin $S = 1, 3/2, 2$ are presented. We start the discussion of the results at high magnetic fields and move from there to lower fields. If the Zeeman energy is much larger than the anisotropy parameter, i.e., if $g_S\mu_B B \gg |D|$, nearly isotropic behavior of $\mathcal{M}(B)$ is observed. At smaller fields $g_S\mu_B B \approx |D|$, the impurity magnetization for $D < 0$ begins to deviate from the curve for $D = 0$ and, for $g_S\mu_B B \ll |D|$, converges to a D-dependent value larger than $g_S\mu_B(S-1/2)$. In the limit of low fields, the impurity magnetization curves for $D < 0$ shown in Fig. 2 are well described by a linear field-dependence:

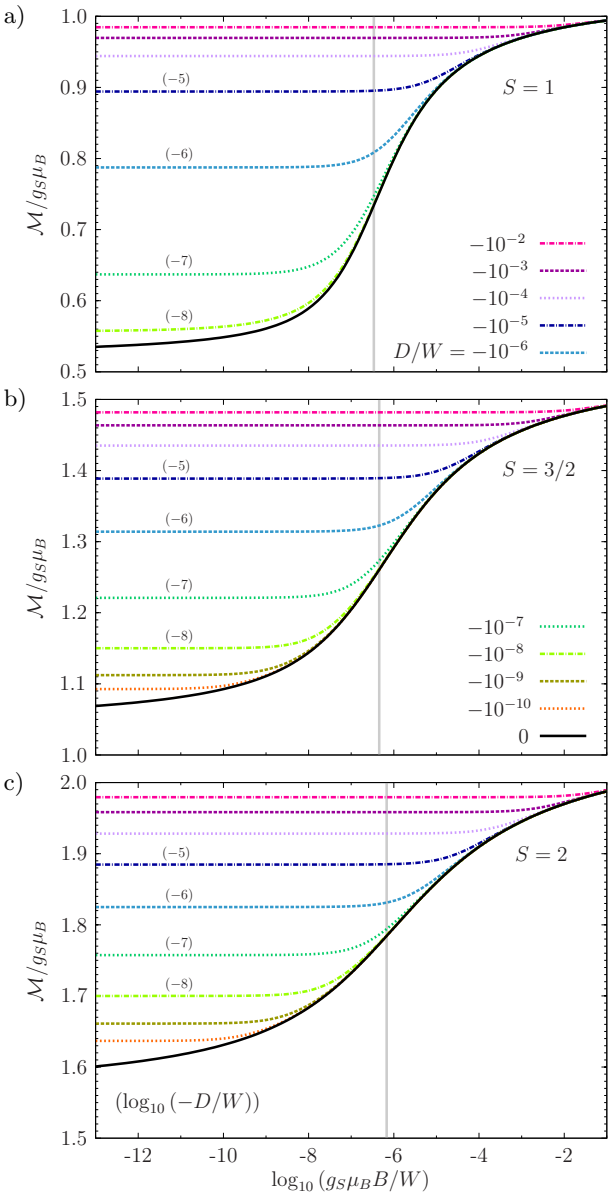

FIG. 2. (Color online) Impurity magnetization $\mathcal{M}$ for different anisotropy parameters $D < 0$ (easy axis anisotropy) as function of magnetic field for $k_BT/W \approx 1.54 \cdot 10^{-15} \approx 0$, coupling strength $\rho J = 0.07$, and impurity spin a) $S = 1$, b) $S = 3/2$, and c) $S = 2$. We compare with the magnetization of an impurity with $D = 0$ (solid line). As before, equal g-factors of electrons and impurity are assumed. Vertical lines mark the respective value of k_BT_H/W, which is determined by fitting the universal Bethe Ansatz solution for $M_{\rm imp}(T = 0)$ in case of $D = 0$. For $\rho J = 0.07$ and $S = 2$, we find $k_BT_H/W \approx 6.8 \cdot 10^{-7}$.

$$\mathcal{M}(B, T \approx 0) \approx \mathcal{M}_0(D) \; + \; \gamma(D) \cdot g_S\mu_B B/W \; . \quad (15)$$

$\mathcal{M}_0(D)$ thus corresponds to the impurity magnetization in the groundstate of Hamiltonian (1) for infinitesimal magnetic field. The low-field behavior for $D < 0$ as de-

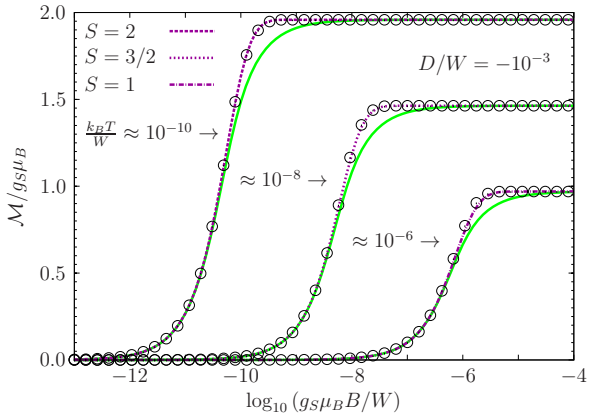

FIG. 3. (Color online) Impurity magnetization $\mathcal{M}$ as function of magnetic field for anisotropy $D/W = -10^{-3}$ and *non-zero* temperature $k_BT/W \approx 1.03 \cdot 10^{-6}$ for $S = 1$, $k_BT/W \approx 1.28 \cdot 10^{-8}$ for $S = 3/2$, and $k_BT/W \approx 1.58 \cdot 10^{-10}$ for $S = 2$. Note that $\mathcal{M}$ is *not* saturated for any field in the plot range (cf. the results for $k_BT/W \approx 0$ in Fig. 2). Open symbols represent fits using a rescaled and shifted Brillouin function, $\widetilde{B}_S(x) = \gamma B_S(\eta x)$, and solid (green) lines fits using a rescaled and shifted Langevin function, $\widetilde{L}(x) = \gamma L(\eta x)$.

scribed by Eq. (15) is different from that displayed by an isotropic impurity: For $D = 0$ and $S \geq 1$, the impurity contribution to the magnetization $M_{\rm imp}(B)$, which is proportional to $\mathcal{M}(B)$ according to Eq. (14), approaches the limit of zero magnetic field with slowly decaying logarithmic corrections.[46,47,72]

From the results presented in Fig. 2 we conclude that for non-zero magnetic field and $D < 0$ a larger value of $|D|$ leads to a larger impurity magnetization $\mathcal{M}$, with the upper bound for $|D| \to \infty$ given by the free saturation value $g_S\mu_B S$. This observation is in agreement with the expectations formulated at the beginning of this section. One might therefore say that an easy axis anisotropy stabilizes the impurity spin.

Taking another look at Fig. 2 and focusing on the regime of small magnetic fields with $g_S\mu_B B \ll |D|$, one could be misled to think that there is a saturation of the impurity magnetization $\mathcal{M}$ (this impression would not occur for an impurity with $D = 0$). This raises the question whether it is possible to approximately describe the field-dependence of $\mathcal{M}$ for $g_S\mu_B B \ll |D|$ and non-zero temperature $k_BT \ll |D|$ using a model for a free spin. In the simplest case, such a description could be provided by a Brillouin function $B_S(x)$, which gives the temperature- and field-dependence of the magnetization of a free and isotropic spin S. As demonstrated in Fig. 3 for one value of D, it is in fact possible to adequately fit the magnetization $\mathcal{M}(B, T > 0)$ for an impurity with easy axis anisotropy using a rescaled and shifted Brillouin function, $\widetilde{B}_S(x) = \gamma B_S(\eta x)$ with free parameters γ and η, as long as $k_BT \ll |D|$ and $g_S\mu_B B \ll |D|$. However, larger fields than those considered in Fig. 3 would reveal that $\mathcal{M}$ is actually not yet saturated (cf. Fig. 2). The ratio of $|D|$ and k_BT_H determines the "apparent saturation value" of $\mathcal{M}$ and thus the parameter γ. In contrast to a fit with a modified Brillouin function, a classical description using a rescaled and shifted Langevin function, $\widetilde{L}(x) = \gamma L(\eta x)$ with $L(x) = \lim_{S\to\infty} B_S(x)$, does not work well for magnetic fields close to the "saturation field" (cf. the solid lines in Fig. 3), as expected for a quantum mechanical system with low spin. Nevertheless, a fit using $\widetilde{L}(x)$ can produce reasonable results for fields that are small compared to the "saturation field".

The results depicted in Fig. 3 might be of importance for an experimental study of a system that is (approximately) described by Hamiltonian (1) with a strong easy axis anisotropy. It is then conceivable that a measurement of the magnetization for magnetic fields that can be realistically produced in an experiment (depending on the value of D, fields with $g_S\mu_B B \approx |D|$ might not be obtainable) does not allow to distinguish between the magnetic response of an impurity spin with easy axis anisotropy and that of a free spin. Such a scenario seems more likely if the experimental control over the g-factor and the absolute magnitude of the magnetization is limited, and if $|D|$ is large compared to k_BT_H so that the "apparent saturation value" of the impurity magnetization lies close to the free saturation value $g_S\mu_B S$.

B. Impurity contribution to the magnetization and the susceptibility

We have furthermore investigated the relationship between $M_{\rm imp}$ for non-zero magnetic field and the impurity contribution to the susceptibility $\chi_{\rm imp}$ at zero field. At low temperature $k_BT \ll |D|$, $\chi_{\rm imp}$ obeys a Curie law with a Curie constant interpolating between the free isotropic value of $S(S+1)/3$ for $|D| \to 0$ and the free anisotropic low-temperature value of S^2 for $|D| \to \infty$.[63] It turns out that there is a simple relation between the Curie constant and the low-temperature magnetization $M_{\rm imp}$ for small magnetic fields $g_S\mu_B B \ll |D|$:

$$\left.\frac{k_BT\chi_{\rm imp}}{(g_S\mu_B)^2}\right|_{B=0,\, k_BT\ll|D|} \cong \left.\left(\frac{M_{\rm imp}}{g_S\mu_B}\right)^2\right|_{\tilde{h}\ll|D|,\, k_BT\ll\tilde{h}}, \tag{16}$$

with $\tilde{h} = g_S\mu_B B$. The relative deviation between left hand and right hand side of Eq. (16), as determined by NRG calculations for all parameter combinations used in Fig. 2, is less than 1 ‰. The relationship between zero-field susceptibility and magnetization expressed by Eq. (16) is actually the same as for a doublet composed of states with magnetic quantum numbers $\pm M$. In particular, a free spin with easy axis anisotropy effectively reduces to such a doublet at low temperature $k_BT \ll |D|$, as discussed at the beginning of this section.

In summary, the following picture of the low-temperature properties of a Kondo impurity with easy axis anisotropy is obtained: The impurity effectively

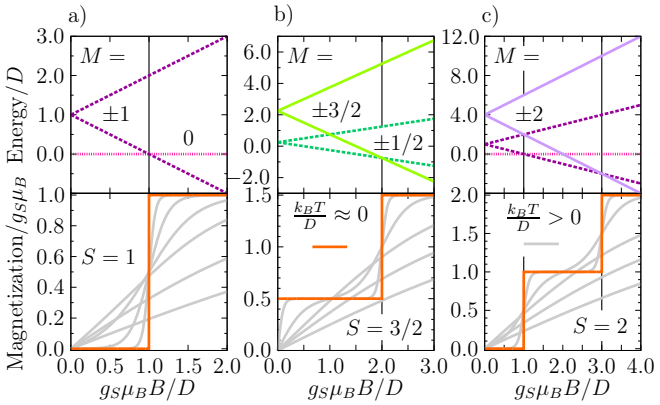

FIG. 4. (Color online) Energy levels with magnetic quantum numbers M (upper panels) and magnetization (lower panels) as function of magnetic field for an anisotropic spin, described by Hamiltonian (5) with $D > 0$ (hard axis anisotropy), with a) $S = 1$, b) $S = 3/2$, and c) $S = 2$. For the magnetization curves and fields larger than the respective saturation field, temperature increases from top to bottom.

acts as a two-level system with residual entropy $S_{\rm imp} = k_B \ln 2$,[63] that splits up in a small magnetic field (leading to $S_{\rm imp} = 0$) and displays an unusual groundstate magnetization indicative of a so-called "fractional spin"[63]. Despite this special property, the combination of $\chi_{\rm imp}$ and $M_{\rm imp}$ shows that the magnetic response at low temperature and field still resembles that of an ordinary magnetic doublet.

VI. IMPURITIES WITH HARD AXIS ANISOTROPY

We now investigate how an additional hard axis anisotropy ($D > 0$) affects the magnetic properties of the impurity spin. To lay the foundations for a study of the full impurity problem, we first discuss the magnetic field dependence of the magnetization for a free spin with hard axis anisotropy that is described by Hamiltonian (5) with $D > 0$.

For positive D and $B = 0$, the eigenvalues of Hamiltonian (5) are energetically ordered according to the absolute value of their magnetic quantum number M. Depending on the spin S, the groundstate is thus either a singlet with $M = 0$ (for integer S) or a doublet with $M = \pm 1/2$ (for half-integer S). In either case, the rest of the energy spectrum consists of doublets with magnetic quantum numbers $\pm M$ and $1/2 < M \leq S$. The energy gap $\Delta_{|M|}$ between a level with quantum number M and the next higher-lying doublet is given by $\Delta_{|M|} = (2|M| + 1)D$. As a consequence of the magnetic field dependence of the energy levels due to the Zeeman term in Eq. (5), n groundstate level crossings occur for positive magnetic fields, with $n = S$ for integer spin and $n = S - 1/2$ for half-integer spin. At the field $B_M = \Delta_{|M|}/g_S\mu_B$, the magnetic quantum number of the groundstate abruptly changes from $-M$ to $-(M+1)$ and hence the zero-temperature magnetization curve displays a discontinuous step. This connection is illustrated in Fig. 4 for spin $S = 1, 3/2$, and 2. Non-zero temperature smears out the magnetization steps and renders them continuous. As the low-energy situation is the same in the vicinity of each groundstate level crossing, so is the effect of moderate temperature (cf. Fig. 4 c).

Since the groundstate of a free spin with hard axis anisotropy in zero magnetic field differs for integer and half-integer spin, the properties of the full impurity model (1) with $D > 0$ and $B = 0$ also depend on the impurity spin S.[63] A simplified picture applies for large ratios $D/k_BT_H \gg 1$. In this case, little Kondo screening can occur for decreasing temperature before the anisotropy becomes effective on the energy scale $k_BT \approx D$ and higher-lying impurity states are frozen out.[63] The impurity spin is then approximately reduced to the groundstate of the corresponding free spin with $D > 0$.[63] For integer S, this is a non-magnetic singlet. In contrast, a doublet with $M \approxeq \pm 1/2$ is effectively formed for half-integer impurity spin. In Ref. 63 it is shown that this doublet undergoes pseudo-spin-1/2 Kondo screening at low temperature $k_BT \ll D$. The observed Kondo effect is described by an anisotropic exchange interaction which reflects that the effective doublet emerges from the original impurity spin multiplet.[63]

For a free spin with hard axis anisotropy in non-zero magnetic field, Fig. 4 demonstrates that the two energy levels which form the degenerate groundstate at a level crossing field have magnetic quantum numbers differing by $|\Delta M| = 1$. This means that the two levels are connected by a single spinflip. For the full impurity model (1) with $D/k_BT_H \gg 1$ we therefore expect that at certain magnetic fields and for low temperature $k_BT \lesssim D$ the impurity spin is effectively reduced to a doublet with $|\Delta M| \approxeq 1$ so that a "field-induced" pseudo-spin-1/2 Kondo effect can arise. In particular, the screening should be exchange-anisotropic as the impurity spin is again restricted to a subset of all its states for $k_BT \lesssim D$. Since all free spins with hard axis anisotropy display groundstate level crossings, these field-induced Kondo effects ought to be observable for arbitrary impurity spin $S \geq 1$ at $D/k_BT_H \gg 1$. Furthermore, for large D the number of field-induced Kondo effects is expected to match the number of groundstate level crossings that occur for the corresponding free spin with $D > 0$.

A. Magnetic field dependence of the impurity magnetization

We begin with a discussion of the magnetic field dependence of the impurity magnetization $\mathcal{M}(B)$ for equal g-factors and quasi-vanishing temperature $T \approx 0$. Magnetization curves for impurity spin $S = 1, 3/2$, and 2, and several values of the anisotropy parameter $D > 0$ are shown in Fig. 5. Since the coupling strength ρJ,

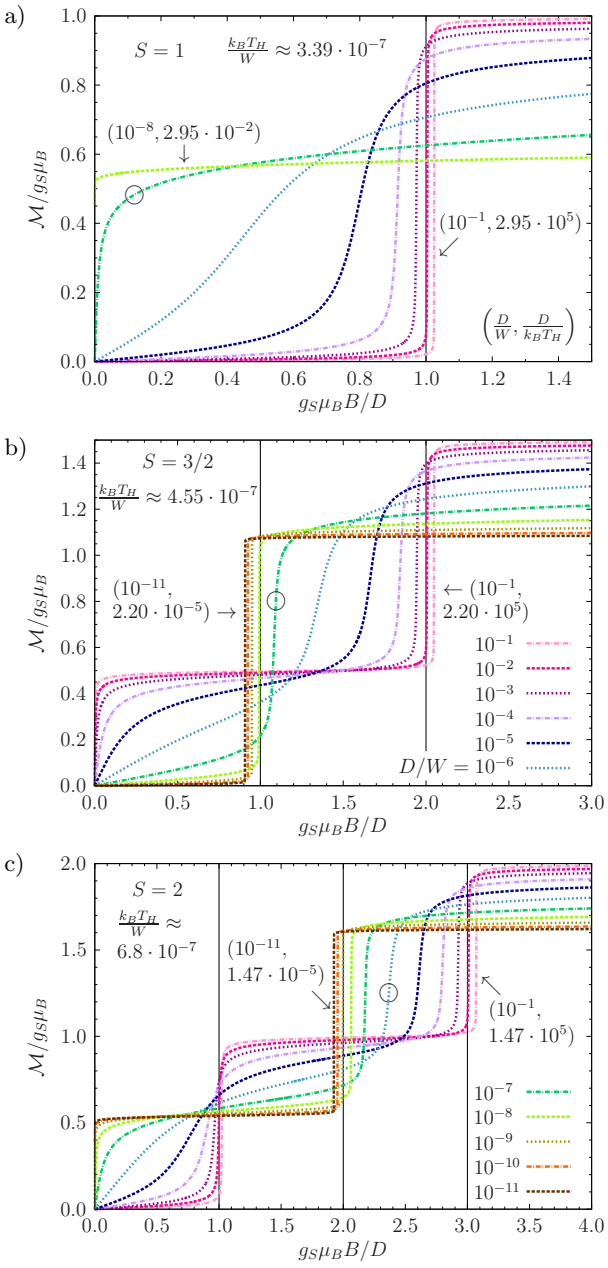

FIG. 5. (Color online) Impurity magnetization $\mathcal{M}$ for varying hard axis anisotropy $D > 0$ as function of magnetic field for temperature $k_BT/W \approx 1.54 \cdot 10^{-15} \approx 0$, coupling strength $\rho J = 0.07$, equal g-factors, and impurity spin a) $S = 1$, b) $S = 3/2$, and c) $S = 2$. The value of D increases from bottom to top or from left to right, respectively. Note the rescaling of the Zeeman energy $g_S\mu_BB$ by D. Circles indicate those magnetization curves for which $|(D - k_BT_H)/W|$ is minimal.

and thus the energy scale k_BT_H according to Table I, is kept constant, the ratio D/k_BT_H is varied. It turns out that this ratio determines the qualitative behavior of the impurity magnetization curves. Note that a linear magnetic field scale is used in Fig. 5 to allow for an easy comparison with the results for a free spin with hard axis anisotropy from Fig. 4.

For an interpretation of the results for $\mathcal{M}(B, T \approx 0)$, let us first consider the two limiting cases in which D is either small or large compared to k_BT_H. In the following, imagine that we move from large magnetic fields to lower fields. If D is large, then little Kondo screening can occur before the anisotropy becomes effective. As a *guideline*, we might thus think of the energy spectrum of a free spin S with hard axis anisotropy. On the other hand, for small D significant Kondo screening can take place before the magnetic field reaches the energy scale defined by the anisotropy, so that it eventually becomes more appropriate to think of the energy levels of a free spin $S - 1/2$ with hard axis anisotropy. As illustrated in Fig. 4, groundstate level crossings occur for a spin with hard axis anisotropy at certain fields and give rise to steps in the zero-temperature magnetization curve. For small and large anisotropy D, the impurity magnetization $\mathcal{M}(B, T \approx 0)$ also displays sharp, step-like features that are surrounded by magnetic field domains in which $\mathcal{M}$ only slowly increases with B ("pseudo-plateaus"). However, due to the energy continuum of electronic states, these sharp features remain continuous even in the limit of zero temperature. The number of steps and their position relative to the field $D/g_S\mu_B$ depends on the impurity spin S for large D and on the residual spin $S - 1/2$ for small D, respectively. The case $S = 1$ is special because the residual spin-1/2 cannot have uniaxial anisotropy. The single step which exists for $S = 1$ at large D therefore disappears for smaller values of D. With respect to the energy scale imposed by the anisotropy, the steps in the impurity magnetization curves become well-defined for small and large D (cf. Figs. 5 b and c). In addition, the pseudo-plateaus become flatter. Fig. 5 c furthermore suggests that the two steps appearing in $\mathcal{M}(B, T \approx 0)$ for $S = 2$ and large D have different width. We are going to discuss the aspect of step width in more detail in Sec. VI B. In particular, it will be shown that an impurity magnetization step is steeper if it occurs at larger field. It turns out that a standard z-averaging of the NRG results introduces artifacts into the magnetization steps for large anisotropy D. This problem is investigated in more detail in the context of an effective model in App. D. The plots shown in Fig. 5 are not visibly affected by this numerical shortcoming.

The position of the steps in the impurity magnetization curves for both small and large anisotropy D compared to k_BT_H seems interesting. Figs. 5 b and c show that for small D and impurity spin $S = 3/2$ and $S = 2$ a step occurs at a magnetic field which is smaller than the corresponding level crossing field for a free spin $S - 1/2$ with hard axis anisotropy (cf. Fig. 4). In contrast, for large D and all three impurity spins considered in Fig. 5, each impurity magnetization step is found at a field exceeding the corresponding level crossing field for a free spin S with $D > 0$. One might wonder whether the half-bandwidth W of the electrons has an impact on these two effects. To investigate this question for the case of small anisotropy,

we have calculated additional magnetization curves for impurity spin $S = 3/2$ and $S = 2$ with decreasing coupling strength ρJ (0.09, 0.07, and 0.05). Since $\rho = 1/2W$, a reduction of ρJ can be interpreted as an increase of the half-bandwidth W for constant J. For each value of the coupling strength the anisotropy parameter was chosen so as to give a constant ratio $D/k_BT_H = 10^{-3}$ according to Table I. With this choice of D, a reduction of ρJ leads to a shift of the step in the impurity magnetization curve towards smaller fields *relative to* $D/g_S\mu_B$. This suggests that the effect observed for small D is not bandwidth-related. The question at which fields impurity magnetization steps occur for large anisotropy is investigated in Sec. VI B.

The limiting cases of small and large anisotropy D compared to k_BT_H are connected by a regime with partial Kondo screening in which it is not possible to exclusively think in terms of the impurity spin S or an residual spin $S - 1/2$. Impurity magnetization steps are broadened in this regime with respect to the energy scale D and, upon reducing the anisotropy parameter, move towards lower fields relative to $D/g_S\mu_B$ (see Fig. 5 b). In addition, one step disappears for $D \approx k_BT_H$ in case of integer impurity spin (cf. Fig. 5 c). Kondo screening effectively changes the impurity spin S from integer to half-integer and vice versa.[63] Depending on the ratio D/k_BT_H and the resulting degree of Kondo screening, different behavior of the impurity magnetization is therefore observed, in particular for fields $g_S\mu_BB \lesssim D$: While there is little magnetic response for an effective integer spin (at zero temperature, there is none at all for a free integer spin with hard axis anisotropy as shown in Fig. 4), we have larger impurity magnetization $\mathcal{M} \approx g_S\mu_B/2$ for effective half-integer spin. However, in the latter case an additional pseudo-spin-1/2 Kondo effect occurs[63] which leads to a suppression of the impurity magnetization for magnetic fields $g_S\mu_BB \ll D$.

In order to study the three different anisotropy regimes ($D/k_BT_H \ll 1$, $D/k_BT_H \approx 1$, and $D/k_BT_H \gg 1$) in more detail, selected impurity magnetization curves from Fig. 5 are replotted using a logarithmic magnetic field scale (see Figs. 6, 7, and 8). This brings out pseudo-spin-1/2 Kondo effects more clearly and allows for a better comparison with the magnetization of an impurity with $D = 0$. Figs. 6, 7, and 8 furthermore demonstrate the effect of non-zero temperature on the impurity magnetization in case of hard axis anisotropy.

At large magnetic field $g_S\mu_BB \gg D$, the magnetization curve $\mathcal{M}(B, T \approx 0)$ for an impurity with hard axis anisotropy closely resembles the result for $D = 0$. For lower fields $g_S\mu_BB \gtrsim D$, the anisotropy eventually becomes effective and the impurity magnetization begins to deviate from the curve for $D = 0$. In this sense, an additional hard axis anisotropy prevents the Kondo screening, which would reduce the impurity spin S to an residual spin $S - 1/2$ in the limit $g_S\mu_BB/k_BT_H \to 0$ for $D = 0$, from completing. The ratio D/k_BT_H controls the extent of Kondo screening on the energy scale D. In particular,

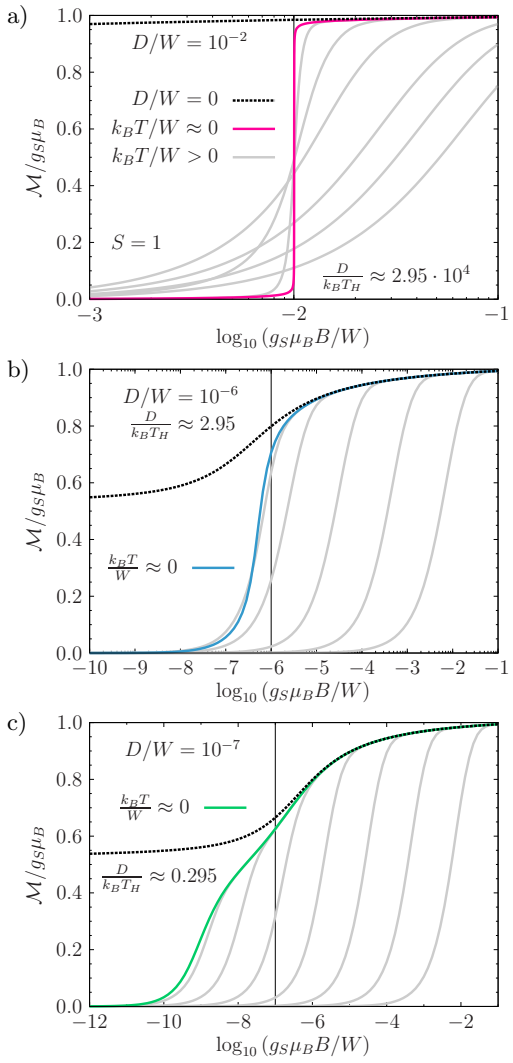

FIG. 6. (Color online) Impurity magnetization $\mathcal{M}$ as function of magnetic field for impurity spin $S = 1$ and anisotropy parameter a) $D/W = 10^{-2}$, b) $D/W = 10^{-6}$, and c) $D/W = 10^{-7}$ (solid lines, cf. Fig. 5). Dashed lines show $\mathcal{M}(B)$ for $D = 0$ and $k_BT/W \approx 1.54 \cdot 10^{-15} \approx 0$. For the light gray lines, the approximate value of k_BT/W increases from left to right from a) $4.35{\cdot}10^{-4}$ to $6.10{\cdot}10^{-2}$, b) $1.99{\cdot}10^{-7}$ to $6.79{\cdot}10^{-3}$, and c) $4.73{\cdot}10^{-10}$ to $6.79{\cdot}10^{-3}$. Adjacent finite-temperature curves in plots b and c are calculated using truncated Wilson chains whose lengths differ by either four or five lattice sites. Thin vertical lines indicate the respective Zeeman energy $g_S\mu_BB = D$. For the chosen coupling strength $\rho J = 0.07$ and $D = 0$, we have $k_BT_H/W \approx 3.39 \cdot 10^{-7}$ according to Table I.

it determines whether the number and approximate position of the steps in the zero-temperature impurity magnetization curve correspond to the magnetic response of a free spin S with $D > 0$ (for $D/k_BT_H \gg 1$ and little Kondo screening, cf. Fig. 4) or a free spin $S - 1/2$ with $D > 0$ (for $D/k_BT_H \ll 1$ and considerable Kondo screening).

$\mathcal{M}(B, T \approx 0)$ displays a linear dependence on B for

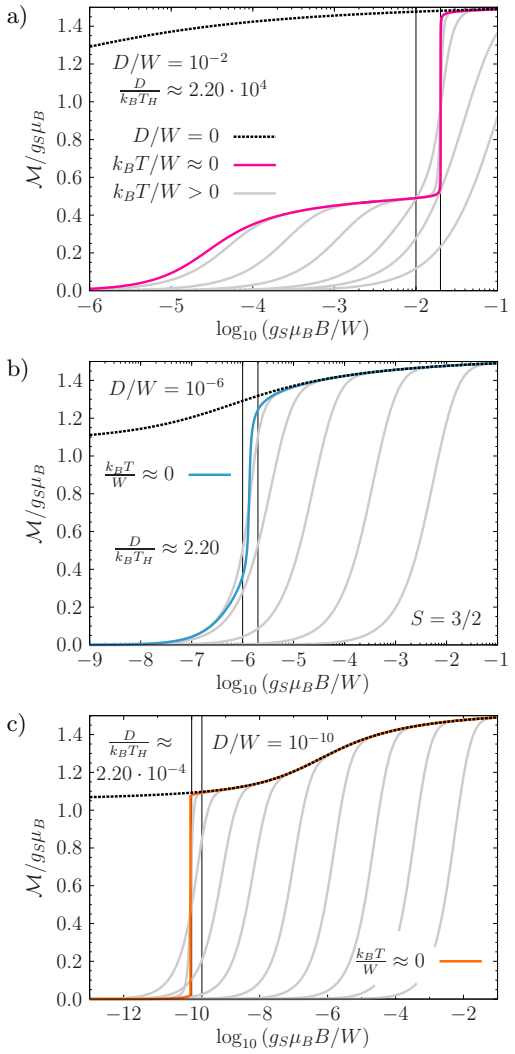

FIG. 7. (Color online) Impurity magnetization $\mathcal{M}$ as function of magnetic field for impurity spin $S = 3/2$ and anisotropy parameter a) $D/W = 10^{-2}$, b) $D/W = 10^{-6}$, and c) $D/W = 10^{-10}$ (solid lines, cf. Fig. 5). As before, dashed lines show $\mathcal{M}(B)$ for $D = 0$ and $k_BT/W \approx 0$. For the light gray lines, the approximate value of k_BT/W increases from left to right from a) $1.61 \cdot 10^{-5}$ to $1.05 \cdot 10^{-1}$, b) $3.45 \cdot 10^{-7}$ to $6.79 \cdot 10^{-3}$, and c) $1.01 \cdot 10^{-11}$ to $6.79 \cdot 10^{-3}$. Adjacent finite-temperature curves in plots b and c are again calculated using truncated Wilson chains whose lengths differ by either four or five lattice sites. Magnetic fields satisfying $g_S\mu_B B = nD$ with $n = 1, 2$ are highlighted by thin vertical lines. According to Table I, $k_BT_H/W \approx 4.55 \cdot 10^{-7}$ for $\rho J = 0.07$ and $D = 0$.

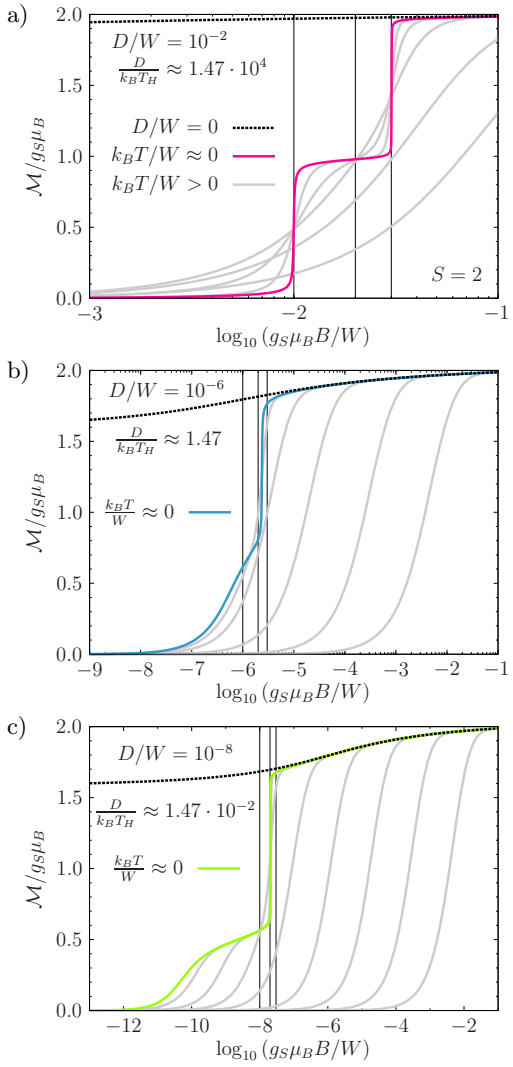

FIG. 8. (Color online) Impurity magnetization $\mathcal{M}$ as function of magnetic field for impurity spin $S = 2$ and anisotropy parameter a) $D/W = 10^{-2}$, b) $D/W = 10^{-6}$, and c) $D/W = 10^{-8}$ (solid lines, cf. Fig. 5). Dashed lines again show $\mathcal{M}(B)$ for $D = 0$ and $k_BT/W \approx 0$. For the light gray lines, the approximate value of k_BT/W increases from left to right from a) $7.54 \cdot 10^{-4}$ to $1.05 \cdot 10^{-1}$, b) $3.45 \cdot 10^{-7}$ to $6.79 \cdot 10^{-3}$, and c) $5.26 \cdot 10^{-11}$ to $6.79 \cdot 10^{-3}$. Adjacent finite-temperature curves in plots b and c are calculated using truncated Wilson chains whose lengths differ by four to six lattice sites. Thin vertical lines indicate magnetic fields satisfying $g_S\mu_B B = nD$, with $n = 1, 2, 3$. For $\rho J = 0.07$ and $D = 0$, we obtain $k_BT_H/W \approx 6.8 \cdot 10^{-7}$.

Zeeman energies that are small compared to all relevant energy scales. If temperature is high so that $k_BT \gg D$, then $\mathcal{M}(T, B)$ is suppressed for magnetic fields of the order of and smaller than $k_BT/g_S\mu_B$. On the other hand, judging by the relative deviation from the zero-temperature curve, finite temperature has negligible effect on the impurity magnetization if the thermal energy falls into the energy regime in which $\mathcal{M}(B, T \approx 0) \propto B$ (such a temperature independence is known for an impurity with $S = 1/2$, as discussed in Sec. IV A). In this regard, $\mathcal{M}$ differs from the magnetization of a free spin with hard axis anisotropy for which non-zero temperature is always relevant. If the impurity magnetization curve features steps, they are smeared out for sufficiently high temperature. In case there is more than one step in $\mathcal{M}(B, T \approx 0)$ (cf. Fig. 8 a), then, as a further difference compared to a free spin with hard axis anisotropy,

non-zero temperature has unequal effect on the different steps. We come back to the last two observations in Sec. VI B.

Ref. 63 arrives at the conclusion that an impurity with additional hard axis anisotropy undergoes exchange-anisotropic pseudo-spin-1/2 Kondo screening if higher-lying impurity states are frozen out so that the impurity is effectively reduced to a spin-1/2 doublet. For $g_S\mu_B B \ll D$ and low temperature, the impurity magnetization is therefore either suppressed if the impurity spin is effectively reduced to a singlet (see Figs. 6 a, 7 c, and 8 a), or it reflects the magnetic response of a Kondo screened pseudo-spin-1/2 doublet (cf. Figs. 6 c, 7 a, and 8 c). For small D and integer impurity spin, the corresponding Kondo temperature decreases faster than linear in D upon reducing the anisotropy (it even drops exponentially fast in the special case $S = 1$).[63] As a result, the pseudo-plateau that appears for $S = 2$ at magnetic fields $g_S\mu_B B \lesssim 2D$ (see Figs. 8 c and 5 c) becomes flatter and broader when decreasing D, whereas a reduction of D eventually leads to quasi-isotropic behavior over the whole considered magnetic field range for $S = 1$ (see Figs. 6 c and 5 a). On the other hand, for large and increasing anisotropy D and half-integer impurity spin, the observed screening effect is increasingly well described by an exchange-anisotropic $S = 1/2$-Kondo model, whose Kondo temperature has a value much smaller than W/k_B.[63] This means that the pseudo-plateau occuring for impurity spin $S = 3/2$ and fields $g_S\mu_B B \lesssim 2D$ (see Figs. 7 a and 5 b) becomes more pronounced for larger anisotropy D. As a final remark, Fig. 8 a once again shows the different width of the two impurity magnetization steps for $S = 2$ and large D.

In App. C we investigate how the magnetization curves $\mathcal{M}(B, T \approx 0)$ are affected by the ratio g_e/g_S of electron and impurity g-factor. It turns out that the difference between the impurity magnetization for a local and a bulk magnetic field can be related to the connection between $\mathcal{M}$ and $M_{\rm imp}$ for equal g-factors.

B. Field-induced Kondo effects

In order to better understand the steps in the low-temperature magnetization curves for large anisotropy $D > 0$ (cf. Figs. 5 and 9 a), we now derive effective models near groundstate level crossings (LCs) of the corresponding free spin with hard axis anisotropy (see Fig. 4). These models are approximations to the full Hamiltonian in the limit of large D.

1. *Effective models near groundstate level crossings in the limit of arbitrarily large anisotropy*

For given impurity spin $S \geq 1$ let us consider one of the groundstate level crossings of the corresponding free spin with hard axis anisotropy (cf. Fig. 4). If D is large, then the two levels which cross in the groundstate are energetically well separated from the rest of the spectrum in the vicinity of the LC field. As an approximation for the full impurity model *near this free LC field*, we therefore project the impurity degrees of freedom in Hamiltonian (1) onto the two impurity states involved in the free LC. This way, the impurity Hilbert space is reduced to two states and the impurity spin S can thus be mapped to an effective spin-1/2. While the projection becomes exact only in the limit $D \to \infty$, we expect it to be a quantitative approximation for $D \gg W$ and $D \gg k_B T$.

The mapping of the impurity spin to a pseudo-spin-1/2 is an extension of the ideas from Refs. 68 and 63. In contrast to the case of zero magnetic field that has been studied there, we do not project onto impurity doublets with $M = \pm 1/2$ (see below). Furthermore, at each LC, i.e., for each step in the magnetization curve, the impurity is reduced to a different pair of states. As a consequence, different parameters of the effective model are obtained at each LC.

We intend to use the effective models to determine the magnetic fields at which steps appear in the impurity magnetization curves for large anisotropy D (cf. Fig. 5), and to investigate how the properties of the full impurity model differ near the various free LCs (as indicated, e.g., by Fig. 9 a). Compared to the full model, the effective models are numerically less demanding as they feature a spin-1/2 impurity independent of the value of S, and they allow to study the effect of the different terms appearing in the effective Hamiltonian.

To be specific, we consider the two impurity states with magnetic quantum numbers $-M$ and $-(M+1)$ (assuming $M \geq 0$), which cross at the free LC field $B_M = (2M+1)D/g_S\mu_B$, and project the impurity and interaction part of Hamiltonian (1) onto them. The effective model is determined by requiring that its matrix representation be equal to that of the full model in the chosen subspace. Note that we have to introduce new impurity states by shifting the magnetic quantum number in order to map the impurity spin to a pseudo-spin-1/2. This mapping then corresponds to the following replacements for the impurity spin operators:

$$\underset{\sim}{S}^x \;\to\; \sqrt{(S-M)(S+M+1)}\;\underset{\sim}{s}^x\,, \tag{17}$$

$$\underset{\sim}{S}^y \;\to\; \sqrt{(S-M)(S+M+1)}\;\underset{\sim}{s}^y\,, \tag{18}$$

$$\underset{\sim}{S}^z \;\to\; \underset{\sim}{s}^z - (M+1/2)\;\underset{\sim}{\mathbb{1}}_s\,. \tag{19}$$

The impurity formally has spin $s = 1/2$ now and the replacement for $(\underset{\sim}{S}^z)^2$ directly follows from that for $\underset{\sim}{S}^z$. In the parameter regime in which the projection is valid, the mapping for $\underset{\sim}{S}^z$ leads to the following connection between the impurity magnetization of the full and effective model:

$$\mathcal{M}/g_S\mu_B = -\langle \underset{\sim}{S}^z \rangle \approx -\langle \underset{\sim}{s}^z \rangle + (M+1/2)\,. \tag{20}$$

There is an analogous relationship for the impurity contribution to the magnetization $M_{\rm imp}$, as seen from Eq. (10). According to its definition, the impurity contribution to the magnetic susceptibility $\chi_{\rm imp}$ is not affected by the shift of the magnetic quantum numbers.

Applying mappings (17) to (19) to the full impurity model (1) and dropping all constant terms, the following Hamiltonian is obtained:

$$\begin{aligned} \underset{\sim}{H}_s(S,M) = &\sum_{\boldsymbol{k},\sigma} \varepsilon_{\boldsymbol{k}\sigma}\, \underset{\sim}{c}^\dagger_{\boldsymbol{k}\sigma} \underset{\sim}{c}_{\boldsymbol{k}\sigma} - \kappa \underset{\sim}{s}^z_0 \\ &+ J_\perp (\underset{\sim}{s}^x_0 \underset{\sim}{s}^x + \underset{\sim}{s}^y_0 \underset{\sim}{s}^y) + J_\parallel \underset{\sim}{s}^z_0 \underset{\sim}{s}^z \\ &+ g_S \mu_B (B - B_M) \underset{\sim}{s}^z \ , \end{aligned} \tag{21}$$

with the set of parameters

$$\varepsilon_{\boldsymbol{k}\sigma} = \varepsilon_{\boldsymbol{k}} + \sigma g_e \mu_B B \quad (\sigma = \pm 1/2) \ , \tag{22}$$

$$\kappa = (M + 1/2)\, J \ , \tag{23}$$

$$J_\perp = \sqrt{(S-M)(S+M+1)}\, J \ , \tag{24}$$

$$J_\parallel = J \ , \tag{25}$$

$$B_M = (2M+1) D / g_S \mu_B \ . \tag{26}$$

In contrast to the full Hamiltonian, $\underset{\sim}{H}_s(S,M)$ is exchange-anisotropic with $J_\perp > J_\parallel$: $J_\perp/J_\parallel$ grows with S and decreases with increasing M (while always present, the exchange anisotropy thus becomes weaker with every further LC). The Zeeman term for the impurity is now expressed relative to the free LC field B_M. $\underset{\sim}{H}_s(S,M)$ furthermore contains the new term $-\kappa \underset{\sim}{s}^z_0$ representing an effective magnetic field, which couples to the electron spin at the origin and points in the opposite direction of the external field B. With respect to NRG, this term can be regarded as spin-dependent scattering at the zeroth site of the Wilson chain. It breaks the invariance under a spinflip transformation ($\underset{\sim}{c}_{\boldsymbol{k}\sigma} \to \underset{\sim}{c}_{\boldsymbol{k}-\sigma}$ and $\underset{\sim}{\boldsymbol{s}} \to (\underset{\sim}{s}^x, -\underset{\sim}{s}^y, -\underset{\sim}{s}^z)$), which $\underset{\sim}{H}_s(S,M)$ would otherwise possess for $B = B_M$. While the scattering parameter κ grows with M, the ratio κ/B_M is independent of M. Starting with the second LC, κ is larger than $J_\parallel$. The ratio $\kappa/J_\perp$, which at first is smaller than 1, also grows with M and eventually becomes greater than 1 if S is large enough.

As an analogue to the free LC field B_M, we call the magnetic field $B_{\rm ELC}$ for which the impurity magnetization vanishes at zero temperature (i.e., the two impurity levels are effectively degenerate) "effective level crossing (ELC) field":

$$\langle \underset{\sim}{s}^z \rangle (B_{\rm ELC}, T=0) = 0 \ . \tag{27}$$

In the parameter regime in which the mapping to a pseudo-spin-1/2 is valid, there is a step in the impurity magnetization curve of the full model at the ELC and, according to Eq. (20), the value of $\mathcal{M}$ at the ELC field is $\mathcal{M}(B_{\rm ELC}, T=0) \approx g_S \mu_B (M+1/2)$. In the following, we discuss the properties of Hamiltonian (21) in more detail for the two different cases $g_e > 0$ and $g_e = 0$.

Let us begin with the case $g_e > 0$. As the free LC field B_M is proportional to D, the limit $D \to \infty$ also corresponds to the limit $B \to \infty$. A non-zero Zeeman coupling of the electrons therefore leads to their complete polarization so that formally they may be replaced with spinless fermions (corresponding to spin-down electrons). Since the remaining fermion band is then completely filled, all interaction terms vanish and the electrons can be completely eliminated from the problem. For $g_e > 0$ and arbitrarily large D, Hamiltonian (21) thus reduces to a pure spin model:

$$\underset{\sim}{H}^{(g_e>0)}_{\rm eff}(\widetilde{B}) = g_S \mu_B \left(\widetilde{B} - \frac{J/2}{g_S \mu_B} \right) \underset{\sim}{s}^z \ . \tag{28}$$

Here, we have introduced a relative magnetic field $\widetilde{B} = B - B_M$. As the only remnant of the interaction between impurity and electrons, a shift of the free LC field remains. This shift is positive for antiferromagnetic coupling $J > 0$ and only depends on the coupling strength, but not on S or M. It is thus the same for all LCs. From the effective model (28) we learn that the ELC fields eventually exceed the free LC fields for $g_e > 0$ and large anisotropy D (cf. Fig. 5).

We now turn to the case of a local magnetic field. Setting $g_e = 0$ and using the relative field $\widetilde{B}$, Hamiltonian (21) becomes the effective model for arbitrarily large D:

$$\underset{\sim}{H}^{(g_e=0)}_{\rm eff}(\widetilde{B}; S, M) = \underset{\sim}{H}_s(S,M)\Big|_{g_e=0} \ . \tag{29}$$

We are particularly interested in the properties of $H^{(g_e=0)}_{\rm eff}(\widetilde{B}; S, M)$ at the ELC field $\widetilde{B}_{\rm ELC} = B_{\rm ELC} - B_M$. Due to the scattering term, the effective model does not exhibit a spinflip-invariance at the ELC. It therefore seems that the ELC is not characterized by special symmetry properties. A spin-*independent* (potential) scattering term can be treated by transforming to scattering states which diagonalize the electronic part of the Hamiltonian (cf. App. C of Ref. 79). Although such a transformation can be easily adapted to the case of spin-*dependent* scattering, it does not seem to yield the intended results. The approximation which is used in the spin-independent case (a modification of the density of states at the Fermi level expressed by an effective coupling parameter)[79] would restore spinflip-invariance for $\widetilde{B} = 0$ in the spin-dependent case and would thus erroneously imply $\langle \underset{\sim}{s}^z \rangle (\widetilde{B} = 0, T) = 0$. Instead, we are going to use NRG to determine the ELC field $\widetilde{B}_{\rm ELC}$ and to study the properties of $H^{(g_e=0)}_{\rm eff}(\widetilde{B}_{\rm ELC}; S, M)$.

For the interpretation of the properties of the full Hamiltonian (1) near the ELCs, we are going to use the

main results for the effective model $\underset{\sim}{H}^{(g_e=0)}_{\rm eff}(\widetilde{B}_{\rm ELC}; S, M)$. These are explicitly demonstrated in Sec. VI B 4 and are summarized in the following. At an ELC the spin-1/2 impurity of the effective model is Kondo screened for $T \to 0$. The temperature dependence of the impurity contribution to the entropy at an ELC is described by the corresponding universal function for the exchange-isotropic $S = 1/2$-Kondo model without scattering term and Zeeman term. Since the parameters of the effective model are different near each free LC (see Eqs. (23) and (24)), there is also a different Kondo temperature $T_K^{\rm ELC}$ at each ELC. It turns out that $T_K^{\rm ELC}$ decreases with increasing M, i.e., $T_K^{\rm ELC}$ becomes smaller with every further ELC.

2. *Magnetic field dependence of impurity contributions near effective level crossing fields*

Armed with the effective model $\underset{\sim}{H}^{(g_e=0)}_{\rm eff}(\widetilde{B}; S, M)$ for a local magnetic field, we now study in detail the field-dependence of typical impurity contributions of the full impurity model for moderately large anisotropy $D > 0$. In Fig. 9 results for $M_{\rm imp}(B)$, $S_{\rm imp}(B)$, and $T\chi_{\rm imp}(B)$ are shown for impurity spin $S = 3$ and anisotropy $D/W = 10^{-3}$. As before, equal g-factors have been assumed.[80]

Let us start with a discussion of the magnetization curves depicted in Fig. 9 a. According to the previously considered behavior of the impurity magnetization $\mathcal{M}$ and its connection with $M_{\rm imp}$, there are also steps in $M_{\rm imp}(B)$ at low temperature. These steps have finite widths for $T \to 0$ and are smeared out for sufficiently high temperature. It is noticeable that the steps have different widths: A step occurring at larger magnetic field is steeper. Fig. 9 a furthermore indicates that the effect of non-zero temperature is different for the different steps. In contrast, for a free spin with hard axis anisotropy the steps in the magnetization become discontinuous for $T \to 0$ and the effect of non-zero (small) temperature is the same for all of them (see Fig. 4). In the chosen representation of Fig. 9 a, the pseudo-plateaus between the steps become flatter in the direction of increasing magnetic field and approach the true zero-temperature plateaus of the free spin with hard axis anisotropy from below for growing D (cf. Fig. 5).

The behavior of $M_{\rm imp}(B)$ as shown in Fig. 9 a can be understood by considering the magnetic field dependence of $M_{\rm imp}$ for the $S = 1/2$-Kondo model with $g_e = g_S$. As discussed in Sec. IV A, $M_{\rm imp}(x, T = 0)$ is described by a universal function $f_{1/2}(x)$ with the variable $x = g_S\mu_B B/k_B T_H$ and $T_H \propto T_K$ according to Eq. (12).[46] $f_{1/2}(x)$ is linear in x for $x \ll 1$ and thus the slope of $M_{\rm imp}(B)$ for small fields is higher if the Kondo temperature is smaller.[46,47] This relation is also expressed by the definition of the Kondo temperature from Eq. (11). Combined with the prediction of the effective model with $g_e = 0$ for the Kondo temperatures at the different ELCs,

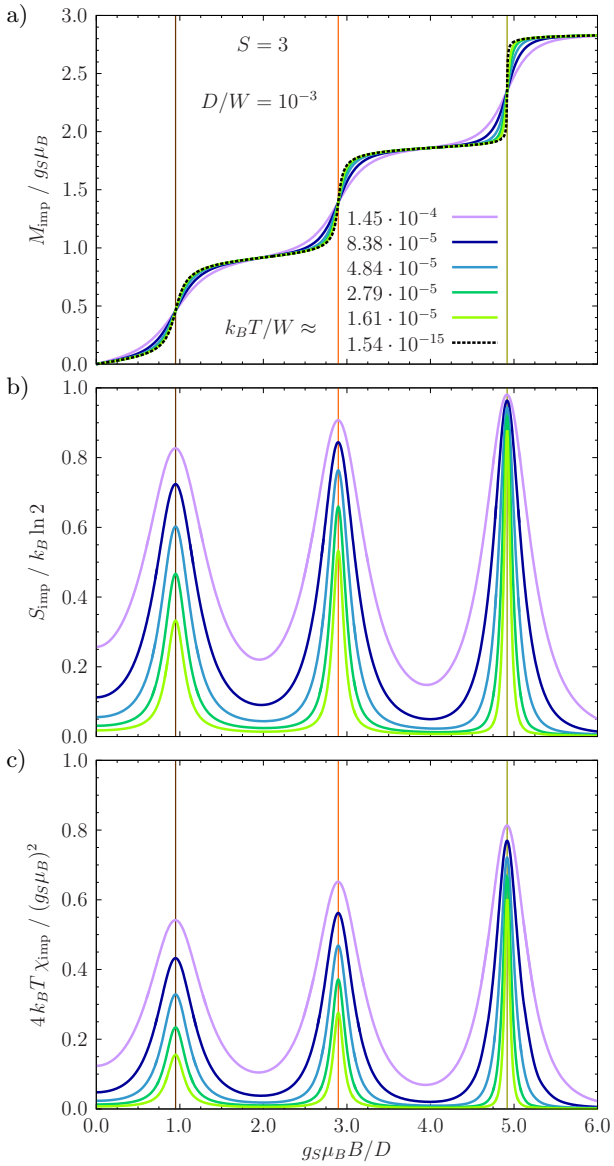

FIG. 9. (Color online) Impurity contribution to a) the magnetization $M_{\rm imp}$, b) the entropy $S_{\rm imp}$, and c) the effective moment $T\chi_{\rm imp}$ as function of magnetic field for impurity spin $S = 3$, hard axis anisotropy $D/W = 10^{-3}$, and several temperature values. In plot a, the dashed curve shows $M_{\rm imp}(B)$ for $k_BT/W \approx 0$, and for the curves in plots b and c temperature increases from bottom to top. Thin vertical lines indicate the (equal) peak positions for $S_{\rm imp}(B)$ and $T\chi_{\rm imp}(B)$. As before, the coupling strength is chosen as $\rho J = 0.07$ and equal g-factors are used.

this observation explains why different steps in a single magnetization curve of the full model have different widths at zero temperature. In case of the $S = 1/2$-Kondo model, temperature has to reach the scale of T_K to become relevant for the zero-field susceptibility.[16] For this reason, thermal broadening of a step in $M_{\rm imp}(B)$ begins at lower temperature if the step occurs at a later ELC with smaller $T_K^{\rm ELC}$. Furthermore, away from an

ELC the magnetization reaches values of the order of the respective saturation value for smaller magnetic fields (relative to the ELC field) if the Kondo temperature at the ELC is lower. It subsequently enters the regime of very slow growth towards saturation, which shows up in Fig. 9 a in the form of a pseudo-plateau. This also explains why pseudo-plateaus between later ELCs with smaller T_K^{ELC} are flatter.

Results for the impurity contribution to the entropy $S_{\mathrm{imp}}(B)$ and the effective moment $T\chi_{\mathrm{imp}}(B)$ at low temperature $k_BT < D$ are shown in Fig. 9 b and c, respectively. In both cases we observe peaks of varying height and width whose positions coincide with those of the steps in $M_{\mathrm{imp}}(B)$. We find that the peaks become both higher and narrower with every further ELC. If the temperature is reduced, the peak heights decline and at the same time, if T is not too low, the peaks become sharper. It is noticeable that there is a temperature below which the width of the first peak in both S_{imp} and $T\chi_{\mathrm{imp}}$ varies only little as a function of T.

At zero temperature both S_{imp} and $T\chi_{\mathrm{imp}}$ vanish for all magnetic fields. In case of the entropy, the reason is that the magnetic field either leads to a non-degenerate groundstate or it creates an effective impurity doublet which is then Kondo screened. The effective moment, on the other hand, has to go to zero since the slope of $M_{\mathrm{imp}}(B)$ at zero temperature, i.e., $\chi_{\mathrm{imp}}(B, T = 0)$, is finite for all fields. For large anisotropy D, the temperature dependence of the peak heights is determined by the pseudo-spin-1/2 Kondo effects that take place at the ELCs (see the next section and Fig. 10 for details). By recollecting results for the $S = 1/2$-Kondo model,[51] we can furthermore understand the different peak widths and their temperature dependence. In case of the $S = 1/2$-Kondo effect, the Zeeman energy $g_S\mu_B B$ has to reach the energy scale of $\max(k_BT, k_BT_H)$ in order to considerably suppress S_{imp} and $T\chi_{\mathrm{imp}}$.[51] In particular, since the lowest temperatures considered in Fig. 9 are smaller than T_K^{ELC} at the first ELC (cf. the indicated temperature range in Fig. 10 a), temperatures are reached for which the thermal broadening of the first peak is small.

3. *Temperature dependence of impurity contributions at effective level crossing fields*

Fig. 10 shows the temperature dependence of S_{imp}, $T\chi_{\mathrm{imp}}$, and χ_{imp} at the three ELCs that occur for the example considered in Fig. 9. In case of entropy and effective moment it is thus demonstrated how the peak heights in Figs. 9 b and c decrease when the temperature is lowered. Note that in this section "anisotropic impurity" always means "exchange-isotropic impurity in the presence of hard axis anisotropy".

$S_{\mathrm{imp}}(T, B = 0)$ for an impurity with $S = 3$ and $D = 0$ interpolates between the limiting values of $k_B \ln 7$ (for $T \to \infty$) and $k_B \ln 6$ (for $T = 0$), according to the

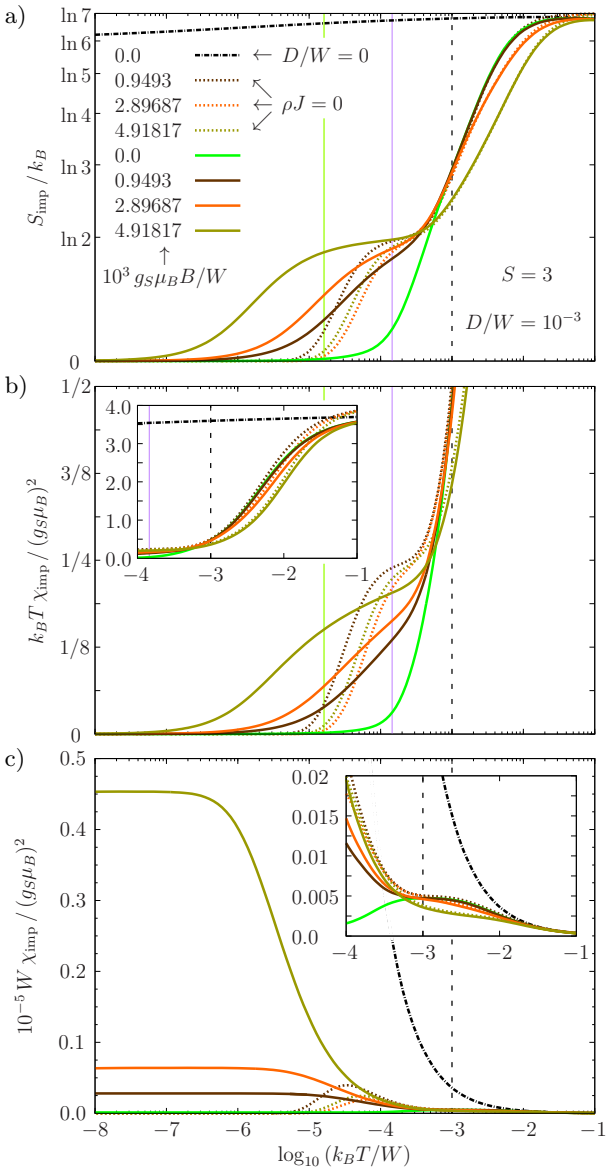

FIG. 10. (Color online) **Main plots:** Impurity contribution to a) the entropy S_{imp}, b) the effective moment $T\chi_{\mathrm{imp}}$, and c) the magnetic susceptibility χ_{imp} as function of temperature for impurity spin $S = 3$ and hard axis anisotropy $D/W = 10^{-3}$. The chosen non-zero magnetic fields correspond to the peak positions for $S_{\mathrm{imp}}(B)$ and $T\chi_{\mathrm{imp}}(B)$ according to Fig. 9. Also shown are NRG results for vanishing coupling strength (dashed lines) and for $D = 0$ (dash-dotted lines). Solid vertical lines delimit the temperature range considered in Fig. 9, whereas dashed vertical lines indicate the thermal energy for which $k_BT = D$. In the **insets**, data from the main plots is presented for a reduced temperature range.

screening of half a magnetic moment (cf. Fig. 10 a). In contrast, for the anisotropic impurity in zero field all higher-lying impurity levels are frozen out on the energy scale $k_BT \approx D$ so that $S_{\mathrm{imp}}(T, B = 0)$ quickly drops to zero.[63] At high temperatures $k_BT \gg D$, on the other hand, the anisotropic impurity behaves more and more

like an impurity with $D = 0$. For the three ELC fields, we observe qualitatively different behavior at low temperature $k_BT < D$ compared to the case of zero field: Starting with $S_{\rm imp} \approx k_B \ln 2$ for $k_BT \lesssim D$, the effective impurity doublet, which is formed due to the magnetic field, undergoes Kondo screening with a value of $T_K^{\rm ELC}$ that decreases with every further ELC. While there is fair agreement with the results for a decoupled impurity at $k_BT > D$, low temperature $k_BT \ll D$ reveals that the ELC fields are not equal to the free LC fields. For this reason, all states except the respective non-degenerate groundstate are ultimately frozen out for $T \to 0$.

For an impurity with $S = 3$ and $D = 0$, $k_BT\chi_{\rm imp}(T, B = 0)/(g_S\mu_B)^2$ obeys a Curie law at both high and low temperature (see Fig. 10 b) and goes from $S(S+1)/3 = 4$ (for $T \to \infty$) to $(S-1/2)(S+1/2)/3 = 35/12$ (for $T = 0$). For the anisotropic impurity in zero magnetic field, on the other hand, the increasing thermal reduction to a non-magnetic groundstate for $k_BT < D$ leads to a vanishing effective moment at zero temperature.[63] At very high temperature $k_BT \lesssim W$ (not shown), we find the expected agreement between $T\chi_{\rm imp}(B = 0)$ for $D = 0$ and for $D > 0$. The effective moment of the decoupled anisotropic impurity first goes to about 1/4 at $k_BT \lesssim D$ (according to the susceptibility of a doublet with $|\Delta M| = 1$), but then quickly drops to zero because of the non-degenerate groundstate with good magnetic quantum number. For the anisotropic impurity at the ELC fields, we again observe Kondo screening for $T \to 0$ with different $T_K^{\rm ELC}$, starting with an effective moment of $k_BT\chi_{\rm imp}/(g_S\mu_B)^2 \approx 1/4$ at $k_BT \lesssim D$.

According to its definition, the impurity contribution to the susceptibility $\chi_{\rm imp}$, for which results are presented in Fig. 10 c, is the slope of $M_{\rm imp}(B)$ and thus directly yields information about the width of the steps in the magnetization curve shown in Fig. 9 a. For an impurity with $D = 0$ and $S \geq 1$, the zero-field susceptibility at low temperature is described by a Curie law and thus diverges for $T \to 0$. In contrast, $\chi_{\rm imp}(T, B = 0)$ for the anisotropic impurity has a maximum at $k_BT \approx D$ and vanishes for zero temperature. Since the ELCs lie close to the free LCs in this example, the susceptibility for the decoupled anisotropic impurity displays a maximum at a thermal energy of the order of the level splitting, but then falls off at low temperature. At the ELCs, $\chi_{\rm imp}(T)$ for the anisotropic impurity saturates at a finite value for $T \to 0$ that increases with decreasing Kondo temperature.

Recently, it has been demonstrated that a field-induced Kondo effect also occurs for Hamiltonian (1) with easy axis anisotropy $D < 0$, additional transverse anisotropy E, and a local magnetic field aligned along the x-axis.[65]

4. *Properties of the effective model for vanishing electron g-factor*

We now return to the effective model for $g_e = 0$ given by Hamiltonian (29) in order to study its properties in greater detail. The ELC field $\widetilde{B}_{\rm ELC}$ and the Kondo temperature $T_K^{\rm ELC}$ *at the ELC field* are determined as function of the parameters $J_\parallel$, $J_\perp$, and κ of the effective model or, respectively, as function of the parameters J, S, and M of the full Hamiltonian (according to Eqs. (23) to (25)). In App. D it is described how to reliably extract these quantities from the NRG results.

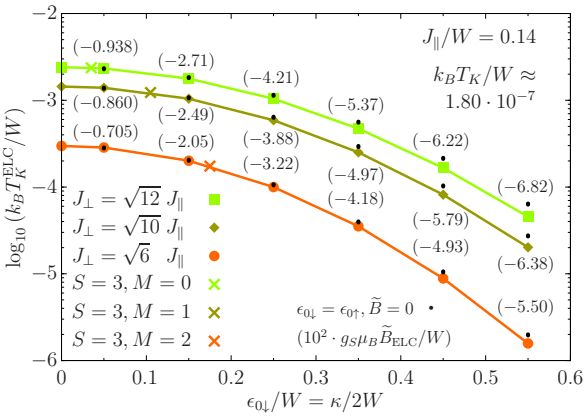

FIG. 11. (Color online) Kondo temperature at the ELC field (cf. App. D) for the effective Hamiltonian with $g_e = 0$ as function of the scattering parameter κ (corresponding to a pair of on-site energies $\epsilon_{0\downarrow} = -\epsilon_{0\uparrow} > 0$ for the zeroth site of the Wilson chain) for fixed $J_\parallel$ and three values of the coupling parameter $J_\perp > J_\parallel$. Numbers in parentheses denote the respective ELC field and lines are intended as a guide to the eye. Pessimistic error bars would be smaller than the symbol size. Additional crosses indicate the Kondo temperature for parameters which, according to Eqs. (23) and (24), correspond to the given values of the quantum numbers S and M. Small dots mark T_K for the case of potential scattering, i.e., for spin-independent on-site energies *and zero magnetic field*. The Kondo temperature given in the upper right corner refers to the exchange-isotropic case without scattering term.

We first investigate how the parameter κ, which corresponds to spin-dependent scattering at the zeroth site of the Wilson chain with on-site energies $\epsilon_{0\downarrow} = -\epsilon_{0\uparrow} > 0$ as seen from Eqs. (21) and (23), affects the values of $\widetilde{B}_{\rm ELC}$ and $T_K^{\rm ELC}$. To this end, we interpret κ as a free parameter of the effective model. For the exchange-isotropic $S = 1/2$-Kondo model in zero magnetic field it is known that ordinary (spin-independent) potential scattering can be approximately mapped to a modified electron DOS at the Fermi level or, equivalently, to an effective coupling parameter $J_{\rm eff}$.[79] This approximation predicts that an increase of the scattering parameter reduces $J_{\rm eff}$ and thus also the Kondo temperature.

In the example shown in Fig. 11, spin quantum number $S = 3$ (as in Fig. 9) is considered and those coupling parameters $J_\perp$ are chosen which, as per Eq. (24), are assigned to the three magnetic quantum numbers allowed for this value of S (i.e., $M = 0, 1, 2$). Without scattering term, the Kondo temperature decreases when $J_\perp$ is reduced.[10,63] Additional spin-dependent scattering further lowers $T_K^{\rm ELC}$ just as standard potential scatter-

ing with $\epsilon_{0\downarrow} = \epsilon_{0\uparrow}$ at zero magnetic field does, but in comparison leads to smaller values of the Kondo temperature. In accordance with the expression for J_{eff} from Ref. 79, the sign of the spin-*independent* on-site energies does not affect T_K. Fig. 11 reveals that the decrease of T_K^{ELC} accelerates with growing scattering strength. Furthermore, we observe that the spin-dependent scattering has a larger influence on the Kondo temperature at the ELC field when the coupling parameter $J_\perp$ is smaller.

Let us now turn to the effect of κ on the position of the ELC field. An additional spin-dependent scattering term breaks the spinflip-invariance and is therefore the very reason for a non-zero value of $\widetilde{B}_{\text{ELC}}$. It thus seems plausible that a larger value of κ also leads to a larger absolute value of the ELC field (cf. the numbers in parentheses in Fig. 11). This increase of $|\widetilde{B}_{\text{ELC}}|$ decelerates with growing scattering strength. A closer look at the data reveals that κ again has a stronger effect when the coupling parameter $J_\perp$ is smaller.

Additional crosses in Fig. 11 mark the Kondo temperature for those values of the scattering parameter κ that follow from Eq. (23) for the three considered M quantum numbers. We observe that the effective model predicts a decrease of T_K^{ELC} with growing M, i.e., with every further ELC. As the example demonstrates, this decline of the Kondo temperature is due to three cooperating effects: 1) According to Eq. (24), $J_\perp$ becomes smaller when M is increased. 2) Simultaneously, κ becomes larger. 3) Because of the decreasing value of $J_\perp$, the scattering parameter additionally gains in importance. For the ELC fields $g_S\mu_B\widetilde{B}_{\text{ELC}}/W$ that belong to the three special values of T_K^{ELC}, we obtain the following results (the error estimates indicate the variance with respect to z, see App. D): $-6.59^{+0.19}_{-0.25}\cdot 10^{-3}$ ($S=3, M=0$), $-1.78^{+0.06}_{-0.07}\cdot 10^{-2}$ ($M=1$), and $-2.36^{+0.06}_{-0.09}\cdot 10^{-2}$ ($M=2$).

Finally, we investigate how the ELC field and the Kondo temperature at the ELC field depend on the parameters of the full Hamiltonian (1), i.e., on J, S, and M, with the parameters of the effective model given by Eqs. (23) to (25). First of all, we note that all obtained (relative) ELC fields are negative. This supports the conclusion that, in the impurity magnetization curves for equal g-factors and large hard axis anisotropy presented in Fig. 5, the free LC fields are only exceeded because of the electrons' non-zero magnetic coupling. For $S = 1$, 3/2, 2 and $J/W = 0.14$ (as in Fig. 5), the following values for $g_S\mu_B\widetilde{B}_{\text{ELC}}/W$ are obtained: $-3.90^{+0.10}_{-0.14}\cdot 10^{-3}$ ($S=1, M=0$), $-8.27^{+0.22}_{-0.30}\cdot 10^{-3}$ ($S=3/2, M=1/2$), $-4.95^{+0.14}_{-0.18}\cdot 10^{-3}$ ($S=2, M=0$), and $-1.31^{+0.04}_{-0.05}\cdot 10^{-2}$ ($S=2, M=1$).

In contrast to the prediction of the effective model with $g_e > 0$ from Eq. (28), the ELC fields depend on the quantum numbers S and M for vanishing electron g-factor (see Fig. 12). With increasing value of S, i.e., with increasing coupling parameter $J_\perp$, the absolute value of the ELC field grows as already seen in Fig. 11. A larger coupling J increases all parameters of the effective model

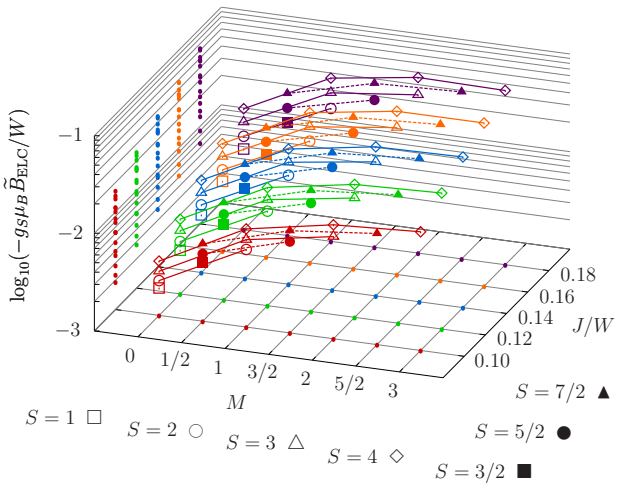

FIG. 12. (Color online) Negative value of the ELC field for a set of parameter combinations of the effective Hamiltonian with $g_e = 0$ which, according to Eqs. (23) to (25), correspond to the indicated spin quantum numbers S, magnetic quantum numbers $0 \leq M < S$, and coupling parameters J. Projections of the data points onto two planes are shown as small dots and lines connect points belonging to the same value of S and J. Pessimistic error bars would be smaller than the symbol size.

($J_\parallel$, $J_\perp$, and κ) and, as demonstrated by Fig. 12, thereby leads to a larger value of $|\widetilde{B}_{\text{ELC}}|$. It is furthermore evident that, with growing J, the quantum number S gains in importance: Fig. 12 shows that the "curves" for fixed coupling strength "fan out" for larger values of J. The dependence of the ELC field on the magnetic quantum number is the result of two counteracting effects: 1) A larger value of M leads to smaller coupling strength $J_\perp$ which, on its own, would lower $|\widetilde{B}_{\text{ELC}}|$. 2) On the other hand, the scattering term becomes stronger with increasing M and would, on its own, enlarge $|\widetilde{B}_{\text{ELC}}|$. For the parameters considered in Fig. 12, there is a growth of $|\widetilde{B}_{\text{ELC}}|$ with M for $S \leq 7/2$ that decelerates with increasing M. In the case of $S = 4$ and both $J/W = 0.16$ and $J/W = 0.18$, we observe a decrease of the absolute value of the ELC field in the last step.

To conclude this section, the Kondo temperatures belonging to the ELC fields shown in Fig. 12 are presented in Fig. 13. As the main result we find that, according to the above explanation, the value of T_K^{ELC} increasingly drops with growing M. On the other hand, a larger value of S increases the coupling strength $J_\perp$ and thus also T_K^{ELC}. It turns out that the influence of S on T_K^{ELC} is reduced for larger coupling J. As a consequence, the "curves" for fixed J are "focussed" in the direction of increasing coupling strength. We find that the dependence of the Kondo temperature on J is the result of two counteracting effects: 1) Both coupling parameters $J_\parallel$ and $J_\perp$ grow with J and would, on their own, lead to a larger value of T_K^{ELC}. 2) However, the scattering parameter κ is also increased and would, on its own, lower the Kondo

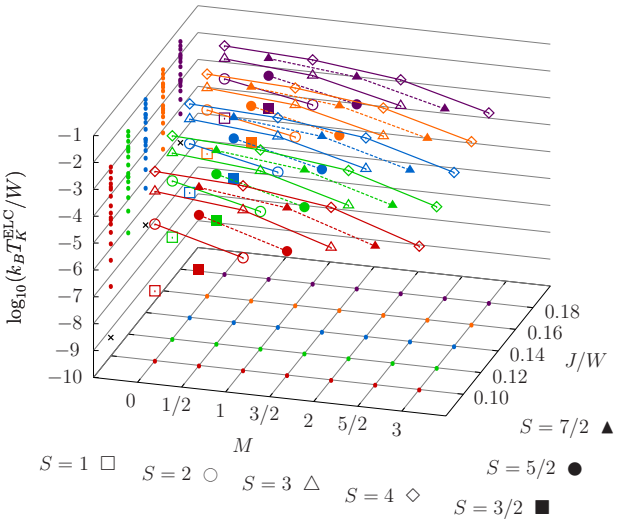

FIG. 13. (Color online) Kondo temperature at the respective ELC field for the same set of parameter combinations of the effective Hamiltonian with $g_e = 0$ as in Fig. 12. Again, pessimistic error bars would be smaller than the symbol size. Three small crosses in the plane spanned by $k_B T_K^{\rm ELC}/W$ and J/W indicate the value of the Kondo temperature for the exchange-isotropic case without scattering term (as inferred from Table I using Eq. (12)).

temperature. For all parameter combinations considered in Fig. 13, $T_K^{\rm ELC}$ is a monotonously increasing function of the coupling strength J. As a final observation, the relative decrease of the Kondo temperature between two consecutive values of M (for fixed J) becomes smaller for larger quantum number S.

5. Comparison of anisotropy- and field-induced pseudo-spin-1/2 Kondo effect for half-integer impurity spin

In the case of half-integer impurity spin $S \geq 3/2$, two different pseudo-spin-1/2 Kondo effects occur for large hard axis anisotropy D. At zero magnetic field, the anisotropy splits up the impurity multiplet and a doublet with magnetic quantum numbers $M = \pm 1/2$ becomes the lowest-lying impurity level (cf. Fig. 4 b). If the energy gap to the impurity states with $M = \pm 3/2$, which is equal to $2D$, is sufficiently large, this doublet undergoes pseudo-spin-1/2 Kondo screening (let us call this Kondo effect "anisotropy-induced").[63] At non-zero magnetic field, on the other hand, ELCs with associated field-induced Kondo effects occur, as discussed in the previous section. Both types of Kondo effect show up in the corresponding impurity magnetization curves. In Fig. 7 a, for example, we observe the magnetic response of the effective impurity doublet at low magnetic fields $g_S \mu_B B/D \ll 1$, which is then followed by a step at $g_S \mu_B B/D \approx 2$ due to the ELC.

One might wonder how the Kondo temperatures of the anisotropy- and field-induced Kondo effects compare. It has been shown in Ref. 63 that the anisotropy-induced Kondo screening in the limit $D/W \to \infty$ is explained by Hamiltonian (29) with $\widetilde{B} = 0$ and parameters $J_\parallel = J$, $J_\perp^D = (S + 1/2)J$, and $\kappa = 0$. On the other hand, for $g_e = 0$ the pseudo-spin-1/2 Kondo effect at the first ELC (i.e., for $M = 1/2$) is described by the same Hamiltonian with $\widetilde{B} = \widetilde{B}_{\rm ELC}$ and parameters $J_\parallel = J$, $J_\perp^{\rm ELC} = \sqrt{(S-1/2)(S+3/2)}\, J$, and $\kappa = J$. In particular, we thus have $J_\perp^{\rm ELC} < J_\perp^D$ for $S \geq 3/2$. Since Fig. 11 shows that additional scattering κ reduces the Kondo temperature, we can conclude that T_K^D for the anisotropy-induced Kondo effect is always larger than $T_K^{\rm ELC}$ at the first ELC and, according to Fig. 13, at all following ELCs, too.

VII. SUMMARY

In this article, we have reported on Numerical Renormalization Group (NRG) calculations for a Kondo model with additional uniaxial anisotropy D. Results have been presented for non-zero magnetic field B and different ratios g_e/g_S of electron and impurity g-factor.

For a bulk field (i.e., for equal g-factors), a comparison of NRG results for the impurity magnetization $\mathcal{M}$ and the impurity contribution to the magnetization $M_{\rm imp}$ reveals that $\mathcal{M}(T, B) = \alpha M_{\rm imp}(T, B)$ as long as all relevant energy scales (i.e., thermal energy, Zeeman energy, and uniaxial anisotropy) are small compared to the half-bandwidth W. The proportionality factor $\alpha > 1$ depends on the coupling strength and decreases for smaller couplings $\rho J_\parallel$ and $\rho J_\perp$. Calculations for isotropic exchange interaction (i.e., $J_\parallel = J_\perp = J$) show that, compared to the case of a local field (i.e., $g_e = 0$), a non-zero electron g-factor effectively rescales the magnetic field argument of the impurity magnetization $\mathcal{M}(B)$ at low temperature. They furthermore suggest that the corresponding values of the rescaling factor $\eta(g_e/g_S = 1)$ and the proportionality factor α coincide.

For an isotropic impurity ($D = 0$), we find that $\mathcal{M}(B, T \approx 0)$, unlike $M_{\rm imp}$, does not display universal behavior in the usual sense as already noticed by Lowenstein.[49]

With additional easy axis anisotropy ($D < 0$), the zero-temperature curve $M_{\rm imp}(B)$ approaches a D-dependent value for small, but non-zero magnetic field, which corresponds to the effective moment of the respective "fractional spin"[63] as given by $k_B T \chi_{\rm imp}(B = 0)$ for $k_B T \ll |D|$. The magnetic response at small fields and low temperature (compared to $|D|$) is thus reminiscent of an ordinary magnetic doublet. Appropriately, the impurity magnetization $\mathcal{M}(B, T > 0)$ is well described by a rescaled and shifted Brillouin function in this regime.

In the case of hard axis anisotropy ($D > 0$), a non-zero magnetic field can lead to "effective level crossings" (ELCs), at which pseudo-spin-1/2 Kondo screening occurs. For $g_e = 0$ and $D/W \to \infty$, these field-induced

Kondo effects are described by an exchange-anisotropic spin-1/2 Kondo model with additional spin-dependent scattering at the zeroth site of the Wilson chain. At the respective ELC field, this scattering leads to a reduction of the Kondo temperature T_K^{ELC} in a similar way as ordinary potential scattering does for zero magnetic field. In particular, the effective model predicts that T_K^{ELC} decreases with every further ELC. This agrees with the observation that the steps in the magnetization curves for large D, which are due to the field-induced Kondo effects, become steeper in the direction of increasing magnetic field.

ACKNOWLEDGMENTS

We thank T. Pruschke and S. Schmitt for helpful discussions. In particular, we would like to thank T. Costi for lots of valuable advice and for carefully reading and critically commenting on the manuscript.

Part of the calculations presented in this article have been done at the Leibniz-Rechenzentrum (LRZ) in Garching near Munich.

Financial support by the Deutsche Forschungsgemeinschaft (DFG) through research group FOR 945 is gratefully acknowledged.

Appendix A: Numerical Renormalization Group calculations with conduction electron Zeeman term

In this first appendix, we briefly describe the changes to the standard NRG procedure[18] which are necessary in order to carry out calculations with an additional Zeeman term for the conduction electrons.

1. Logarithmic discretization

The starting point is the continuous energy representation of the Hamiltonian from Eq. (7) with a restriction to the physically reasonable case $h < W$. In the following it is assumed that the magnetic field, which appears in $h = g_e \mu_B B$, is non-zero and fixed and, to simplify the notation, that the chemical potential is zero. We introduce abbreviations for the absolute value of the integration boundaries in Eq. (7),

$$\mathcal{B}_\mu^\pm = |\pm W + \mu h| \,, \tag{A1}$$

rescale the integration variable ε, and change to rescaled electron operators (cf. Ref. 17):

$$\xi_\mu^+ = \frac{\varepsilon}{\mathcal{B}_\mu^+} \quad \text{for} \quad \varepsilon > 0 \,, \tag{A2}$$

$$\xi_\mu^- = \frac{\varepsilon}{\mathcal{B}_\mu^-} \quad \text{for} \quad \varepsilon < 0 \,, \tag{A3}$$

$$\underset{\sim}{a}_{\xi\mu}^+ = \sqrt{\mathcal{B}_\mu^+}\, \underset{\sim}{a}_{\varepsilon\mu} \quad \text{for} \quad \varepsilon > 0 \,, \tag{A4}$$

$$\underset{\sim}{a}_{\xi\mu}^- = \sqrt{\mathcal{B}_\mu^-}\, \underset{\sim}{a}_{\varepsilon\mu} \quad \text{for} \quad \varepsilon < 0 \,. \tag{A5}$$

Using $\int_{-W}^{W} \mathrm{d}\varepsilon\, \rho(\varepsilon) = 1$ and defining the normalized zeroth state of the Wilson chain as

$$\begin{aligned} \underset{\sim}{f}_{0\mu} = &\int_0^1 \mathrm{d}\xi_\mu^+ \sqrt{\rho\left(\xi_\mu^+ \mathcal{B}_\mu^+ - \mu h\right) \mathcal{B}_\mu^+}\, \underset{\sim}{a}_{\xi\mu}^+ \\ &+ \int_{-1}^0 \mathrm{d}\xi_\mu^- \sqrt{\rho\left(\xi_\mu^- \mathcal{B}_\mu^- - \mu h\right) \mathcal{B}_\mu^-}\, \underset{\sim}{a}_{\xi\mu}^- \quad , \end{aligned} \tag{A6}$$

we obtain an equivalent expression for the electronic and interaction term in Eq. (7):

$$\begin{aligned} \underset{\sim}{H}_{\mathrm{cb+int}} = W \sum_\mu \Bigg(&\frac{\mathcal{B}_\mu^+}{W} \int_0^1 \mathrm{d}\xi_\mu^+\, \xi_\mu^+\, \underset{\sim}{a}_{\xi\mu}^{+\dagger} \underset{\sim}{a}_{\xi\mu}^+ \\ &+ \frac{\mathcal{B}_\mu^-}{W} \int_{-1}^0 \mathrm{d}\xi_\mu^-\, \xi_\mu^-\, \underset{\sim}{a}_{\xi\mu}^{-\dagger} \underset{\sim}{a}_{\xi\mu}^- \Bigg) \\ &+ J\, \underset{\sim}{\boldsymbol{S}} \cdot \sum_{\mu,\nu} \underset{\sim}{f}_{0\mu}^\dagger \frac{\boldsymbol{\sigma}_{\mu\nu}}{2} \underset{\sim}{f}_{0\nu} \quad . \end{aligned} \tag{A7}$$

Next, the logarithmic discretization of the conduction band is carried out according to one of the available discretization schemes[70,71,81–84] by dividing the integration range $[-1, 1]$ into standard intervals $I_m^\pm$ and using the following weight function on the m^{th} positive and negative interval, respectively:

$$\varphi_{m\mu}^\pm(\xi_\mu^\pm) = \sqrt{\frac{\rho\left(\xi_\mu^\pm \mathcal{B}_\mu^\pm - \mu h\right)}{\int_{I_m^\pm} \mathrm{d}\xi_\mu^{\prime\pm}\, \rho\left(\xi_\mu^{\prime\pm} \mathcal{B}_\mu^\pm - \mu h\right)}} \quad . \tag{A8}$$

With $s = \pm$,

$$\gamma_{m\mu}^s = \sqrt{\frac{\mathcal{B}_\mu^s}{W} \int_{I_m^s} \mathrm{d}\xi_\mu^s\, \rho\left(\xi_\mu^s \mathcal{B}_\mu^s - \mu h\right) W} \quad , \tag{A9}$$

and new operators $\underset{\sim}{a}_{m\mu}^s$ corresponding to the weight functions $\varphi_{m\mu}^s(\xi_\mu^s)$ on the intervals I_m^s, we have the following exact representation for the zeroth state of the Wilson chain:

$$\underset{\sim}{f}_{0\mu} = \sum_{s,m} \gamma_{m\mu}^s\, \underset{\sim}{a}_{m\mu}^s \quad . \tag{A10}$$

In addition, a "dimensionless energy" $\mathcal{E}^s_{m\mu}$ has to be assigned to each interval I^s_m for each spin projection μ. This is done according to the chosen discretization scheme by using the weight function (A8) with the shifted DOS, leading to a discrete approximation to Hamiltonian (A7):

$$\underset{\sim}{H}_{\text{cb+int}} \to W \sum_{s,m,\mu} \frac{\mathcal{B}^s_\mu}{W} \mathcal{E}^s_{m\mu}\, \underset{\sim}{a}^{s\dagger}_{m\mu}\, \underset{\sim}{a}^{s}_{m\mu} \qquad \text{(A11)}$$
$$+\; J\, \underset{\sim}{\boldsymbol{S}} \cdot \sum_{\mu,\nu} \underset{\sim}{f}^\dagger_{0\mu} \frac{\boldsymbol{\sigma}_{\mu\nu}}{2} \underset{\sim}{f}_{0\nu} \quad .$$

At this point, the substitution (A11) is still valid for arbitrary $\rho(\varepsilon)$. The above expressions simplify in the case of a constant density of states, $\rho(\varepsilon) = 1/2W$, as a shifted constant DOS is, of course, still a constant DOS:

$$\underset{\sim}{H}_{\text{cb+int}} \to W \sum_{s,m,\mu} \frac{\mathcal{B}^s_\mu}{W} \underbrace{\mathcal{E}^s_{m\mu}(h=0)}_{=\mathcal{E}^s_m}\, \underset{\sim}{a}^{s\dagger}_{m\mu}\, \underset{\sim}{a}^{s}_{m\mu}$$
$$+\; J\, \underset{\sim}{\boldsymbol{S}} \cdot \sum_{\mu,\nu} \underset{\sim}{f}^\dagger_{0\mu} \frac{\boldsymbol{\sigma}_{\mu\nu}}{2} \underset{\sim}{f}_{0\nu} \quad , \qquad \text{(A12)}$$

$$\underset{\sim}{f}_{0\mu} = \sum_{s,m} \sqrt{\frac{\mathcal{B}^s_\mu}{W}} \underbrace{\gamma^s_{m\mu}(h=0)}_{=\gamma_m}\, \underset{\sim}{a}^{s}_{m\mu} \quad . \qquad \text{(A13)}$$

Here, $\mathcal{E}^s_m$ and γ_m are the "energies" and expansion coefficients, respectively, for the system with a *local* magnetic field (i.e., with $g_e = 0$).

2. Tridiagonalization

Since the rescaling factors

$$\frac{\mathcal{B}^s_\mu}{W} = \left| s + \mu \frac{g_e}{g_S} \frac{g_S \mu_B B}{W} \right| \qquad \text{(A14)}$$

depend on spin projection μ and magnetic field B, the tridiagonalization of Hamiltonian (A12), which leads to the Wilson chain with hopping parameters $t_{i\mu}(B)$ and on-site energies $\epsilon_{i\mu}(B)$, has to be done separately for spin-up and spin-down and for each value of B. In case of a constant DOS, Eqs. (A12) and (A13) show that the only necessary modification of an existing code solving the recursion relations given in Ref. 18 is to multiply all "energies" $\mathcal{E}^s_m$ and coefficients γ^2_m with the appropriate factor (A14).

For a particle-hole symmetric DOS we have $\mathcal{E}^s_{m\mu} = -\mathcal{E}^{-s}_{m-\mu}$ and $\gamma^s_{m\mu} = \gamma^{-s}_{m-\mu}$. Using the Ansatz $u_{nm\mu} = (-1)^n v_{nm-\mu}$ and $v_{nm\mu} = (-1)^n u_{nm-\mu}$ for the coefficients of the orthogonal transformation (following the notation of Ref. 18), it can then be shown that $t_{i\uparrow}(B) = t_{i\downarrow}(B)$ and $\epsilon_{i\uparrow}(B) = -\epsilon_{i\downarrow}(B)$ for all sites i of the Wilson chain.

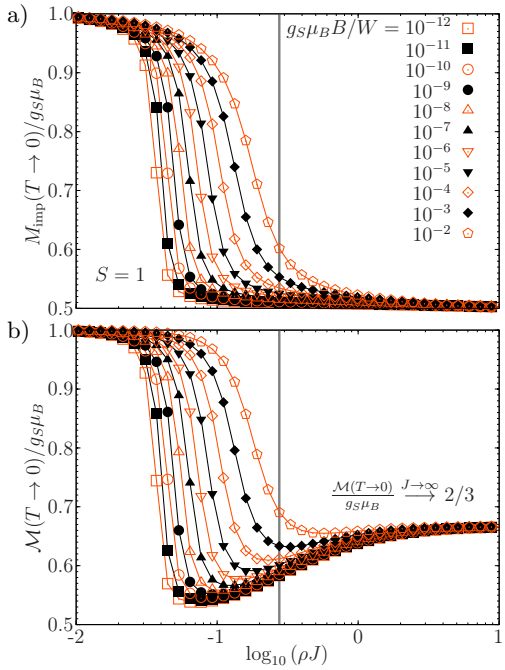

FIG. 14. (Color online) Limiting value for $T \to 0$ of a) the impurity contribution to the magnetization M_{imp} and b) the impurity magnetization $\mathcal{M}$ as function of the coupling strength ρJ for impurity spin $S = 1$, $g_e = g_S$, and several magnetic field values. The vertical lines mark a coupling strength of $\rho J' \approx 0.276$ for which we have checked by comparing with the respective Bethe Ansatz solution shown in Fig. 1 that $M_{\text{imp}}(B, T \approx 0)$ still exhibits universal behavior (a fit of the BA curve gives $k_B T_H/W \approx 8.85 \cdot 10^{-2}$). Remaining lines are intended as a guide to the eye.

Appendix B: Dependence of the zero-temperature magnetization on the coupling strength for $D = 0$

To further illustrate the difference between the impurity contribution to the magnetization M_{imp} and the impurity magnetization $\mathcal{M}$ for vanishing anisotropy $D = 0$, we examine how both quantities depend on the coupling strength ρJ for non-zero magnetic field at zero temperature. As in Sec. IV, the case of equal g-factors for impurity and electrons is considered. NRG results for impurity spin $S = 1$ and $S = 3/2$ are shown in Fig. 14 and Fig. 15, respectively.

Let us begin the interpretation of the plots by considering the limiting cases $J \to 0$ and $J \to \infty$. For vanishing coupling strength, impurity and electrons are decoupled and thus both M_{imp} and $\mathcal{M}$ correspond to the magnetization of the respective free spin (cf. Eqs. (8) and (10)) which takes the value $g_S \mu_B S$ for any positive magnetic field at $T = 0$. However, the behavior in the limit $J \to \infty$ differs for the two quantities, again demonstrating that in general $M_{\text{imp}} \neq \mathcal{M}$. The values of M_{imp} and $\mathcal{M}$ in this limit can be understood by considering a simplified model: In the interaction term (4), the spin operator $\underset{\sim}{\boldsymbol{s}}_0$ depends on the occupation of the lattice site that it is

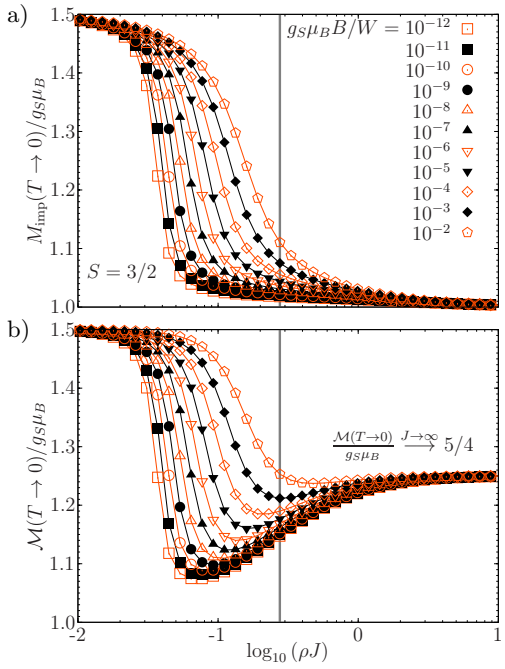

FIG. 15. (Color online) Limiting value for $T \to 0$ of a) the impurity contribution to the magnetization and b) the impurity magnetization as function of the coupling strength ρJ as in Fig. 14, but here for impurity spin $S = 3/2$. $M_{\rm imp}(B, T \approx 0)$ again shows universal behavior for $\rho J' \approx 0.276$ and a fit of the corresponding universal BA curve gives $k_B T_H/W \approx 3.05 \cdot 10^{-1}$.

associated with. For very large values of J it is energetically favorable that this lattice site is singly occupied with a probability near one. We can then replace $\underset{\sim}{\boldsymbol{s}}_0$ by a spin-1/2 operator $\underset{\sim}{\boldsymbol{s}}$ in Eq. (4). Furthermore, all other terms in Hamiltonian (1) that involve degrees of freedom different from the impurity and the lattice site to which it couples can be neglected. We are thus left with a strongly coupled antiferromagnetic dimer in a magnetic field with Hamiltonian

$$\underset{\sim}{H}_{J\to\infty} = J\underset{\sim}{\boldsymbol{S}} \cdot \underset{\sim}{\boldsymbol{s}} + g_S\mu_B B(\underset{\sim}{S}^z + \underset{\sim}{s}^z) \,. \qquad \text{(B1)}$$

To determine the limiting value of $\mathcal{M}(T = 0)/g_S\mu_B$ for $J \to \infty$ and any positive magnetic field, we have to calculate the expectation value of $-\underset{\sim}{S}^z$ with respect to that eigenstate of total spin which has the lowest value of $S_{\rm total}$ and corresponding z-projection $M_{\rm total} = -S_{\rm total}$. Denoting eigenstates of Hamiltonian (B1) as $|S_{\rm total}, M_{\rm total}\rangle$, we find:

$$-\langle 0,0|\underset{\sim}{S}^z|0,0\rangle = 0 \quad \text{for} \quad S = 1/2 \,, \quad \text{(B2)}$$

$$-\left\langle \frac{1}{2},-\frac{1}{2}\left|\underset{\sim}{S}^z\right|\frac{1}{2},-\frac{1}{2}\right\rangle = \frac{2}{3} \quad \text{for} \quad S = 1 \,, \quad \text{(B3)}$$

$$-\langle 1,-1|\underset{\sim}{S}^z|1,-1\rangle = \frac{5}{4} \quad \text{for} \quad S = 3/2 \,. \quad \text{(B4)}$$

In contrast, in the limit $J \to \infty$ the impurity contribution to the magnetization $M_{\rm imp}(T = 0)/g_S\mu_B$ for positive field reduces to $-\langle \underset{\sim}{S}^z + \underset{\sim}{s}^z\rangle$ with respect to the above eigenstates of Hamiltonian (B1). This expectation value gives $S - 1/2$. The case $S = 1/2$ is therefore special since both $M_{\rm imp}$ and $\mathcal{M}$ go to zero for $J \to \infty$. Figs. 14 and 15 show that NRG, as a method that is non-perturbative in J, can in fact reproduce the limiting values for large coupling strength.[85]

Let us now consider the magnetization for intermediate values of ρJ. In the special case $S = 1/2$, both $M_{\rm imp}$ and $\mathcal{M}$ are monotonically decreasing functions of the coupling strength for constant magnetic field B that show similar behavior. We furthermore find that a larger value of B also leads to a larger value of the magnetization. In fact, *all* magnetization curves that we have calculated increase monotonically with B. On the other hand, $M_{\rm imp}(\rho J)$ and $\mathcal{M}(\rho J)$ display qualitatively different behavior for impurity spin $S \geq 1$. While $M_{\rm imp}$ is again a monotonically decreasing function of the coupling strength for given magnetic field (see Figs. 14 a and 15 a), $\mathcal{M}(\rho J)$ displays a minimum for all considered values of B (cf. Figs. 14 b and 15 b).

It is instructive to compare the NRG results with the Bethe Ansatz solution[46,47] for the field-dependence of $M_{\rm imp}(T = 0)$, which takes the form of a universal function $f_S(x)$ of the rescaled magnetic field $x = g_S\mu_B B/k_B T_H$ (cf. Sec. IV A). This function is monotonically increasing for all S (see Fig. 1). The results reported in Table I are furthermore consistent with a monotonic growth of the energy scale $k_B T_H$ as function of the coupling strength ρJ. In the case of impurity spin $S = 1/2$, the standard estimate for the Kondo temperature from Eq. (13) also corresponds to an energy scale $k_B T_H$ that monotonically increases with ρJ. For this reason, an increase of the coupling strength for constant magnetic field ought to lead to a larger scale $k_B T_H$ and hence to a lower rescaled field x and a smaller value of $M_{\rm imp}$. The impurity contribution to the magnetization for fixed positive field should therefore be a monotonically decreasing function of the coupling strength in the scaling regime. This conclusion is in line with the NRG results for $M_{\rm imp}(\rho J)$ shown in Figs. 14 a and 15 a. The vertical lines in the plots mark a coupling strength $\rho J' \approx 0.276$, for which we have checked via a fit to the BA solution that $M_{\rm imp}(B, T \approx 0)$ still displays universal behavior. The scaling regime therefore extends at least up to coupling strengths as large as $\rho J'$ (apart from establishing this bound, the value of $\rho J'$ is arbitrary). In contrast, for low field the impurity magnetization $\mathcal{M}(\rho J)$ has a minimum for coupling strengths smaller than $\rho J'$ (cf. Figs. 14 b and 15 b). We conclude that this behavior of $\mathcal{M}(\rho J)$ is not compatible with the standard scaling picture as described above for $M_{\rm imp}(\rho J)$.

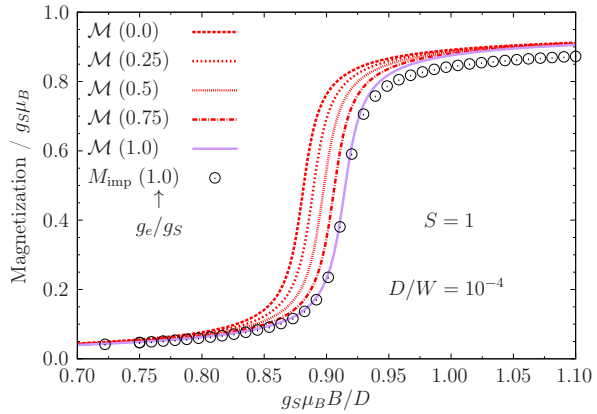

FIG. 16. (Color online) Impurity magnetization $\mathcal{M}$ as function of magnetic field for impurity spin $S = 1$, hard axis anisotropy $D/W = 10^{-4}$, coupling strength $\rho J = 0.07$, and several values of the g-factor ratio g_e/g_S (cf. Fig. 5 a for $g_e = g_S$). For equal g-factors, the impurity contribution to the magnetization $M_{\rm imp}(B)$ is shown, too. The temperature is $k_BT/W \approx 1.54 \cdot 10^{-15} \approx 0$ in all cases.

Appendix C: Effect of the electron g-factor on $\mathcal{M}$ and the connection between $\mathcal{M}$ and $M_{\rm imp}$

We now investigate how the impurity magnetization $\mathcal{M}(B, T \approx 0)$ is affected by a non-zero electron g-factor corresponding to a positive ratio $g_e/g_S > 0$. Because of the sharp features that are found in the magnetization curves for $D > 0$ (see Fig. 5), the case of hard axis anisotropy seems well suited to study the influence of non-zero g_e (alternatively one could examine the effect of the electron g-factor on the basis of the linear magnetic field dependence of $\mathcal{M}(B)$ for small B). As an example, Fig. 16 shows magnetization curves $\mathcal{M}(B, T \approx 0)$ for impurity spin $S = 1$, moderately large D, and several g-factor ratios interpolating between a local field ($g_e = 0$) and a bulk field ($g_e = g_S$).

The results presented in Fig. 16 demonstrate that a positive electron g-factor effectively causes a rescaling of the magnetic field argument of the impurity magnetization: A ratio $g_e/g_S > 0$ shifts the impurity magnetization curve for $g_e = 0$ towards larger fields and thus reduces $\mathcal{M}(B, T \approx 0)$, which is a monotonically increasing function of B, for a fixed magnetic field value. Using the notation $\mathcal{M}(B, T, g_S, g_e)$, this statement can be expressed in the following way:

$$\mathcal{M}(B, T \approx 0, g_S, 0) = \mathcal{M}(B', T \approx 0, g_S, g_e) \ , \quad \text{(C1)}$$

$$B' = \eta(\rho J, g_e/g_S) B \ , \quad \text{(C2)}$$

with a rescaling factor $\eta(\rho J, g_e/g_S) \geq 1$ for $g_e/g_S \geq 0$ that depends on the coupling strength ρJ. Taking the magnetization curve for a local field as reference, we may therefore state that the impurity effectively "feels" a smaller magnetic field if there is also a Zeeman term for the electrons in Hamiltonian (1).

For a bulk field, Fig. 16 additionally shows the impurity contribution to the magnetization $M_{\rm imp}(B, T \approx 0)$ (according to Eq. (10), $\mathcal{M}$ and $M_{\rm imp}$ are equal for a local field). We find that Eq. (14), which was obtained for $D = 0$, is also suitable to describe the relation between $\mathcal{M}(B, T \approx 0)$ and $M_{\rm imp}(B, T \approx 0)$ in the case of easy axis and hard axis anisotropy for magnetic fields $g_S\mu_B B \ll W$. A study of the connection between $\mathcal{M}$ and $M_{\rm imp}$ for $D < 0$ and $D > 0$ with $|D| \ll W$ reveals for impurity spin $S = 1$ and $S = 3/2$ that the magnetic field averaged values for $\alpha(\rho J = 0.07)$ are nearly identical to the results for $D = 0$ reported in Table I, and that the standard deviations have the same order of magnitude. For $S = 2$, the obtained value of the proportionality factor is $\alpha(0.07) = 1.0370(1)$. We conclude that the effect of the uniaxial anisotropy on the value of α must be very small as long as $|D| \ll W$.

An analysis of the impurity magnetization curves for hard axis anisotropy furthermore shows that the values of the rescaling factor $\eta(0.07, 1)$ (approximately 1.038 for $S = 1$, 1.0375 for $S = 3/2$, and 1.037 for $S = 2$) and the corresponding proportionality factor $\alpha(0.07)$ are remarkably similar. In case of $S = 1$ and $D > 0$, we have also studied the difference between $\mathcal{M}(B, T \approx 0)$ for a local and bulk magnetic field for the two other coupling strengths previously considered (i.e., for $\rho J = 0.05$ and $\rho J = 0.09$). The rescaling factors obtained for $D \ll W$ ($\eta(0.05, 1) \approx 1.0265$ and $\eta(0.09, 1) \approx 1.0497$) are again in remarkable agreement with the corresponding values of $\alpha(\rho J)$. Moreover, we find that Eqs. (C1) and (C2), with the values of $\eta(\rho J, 1)$ as determined for $D > 0$, are also suitable to describe the relation between the impurity magnetization curves for a local and bulk magnetic field for anisotropy $D \leq 0$. As $\mathcal{M}(B, T \approx 0)$ lacks sharp features in the $D = 0$ and easy axis case, the effect of a non-zero electron g-factor is more subtle, though.

The numerical results thus strongly suggest that the rescaling factor $\eta(\rho J, 1)$ and the proportionality factor $\alpha(\rho J)$ take the same value. Furthermore, we find our results for the rescaling factor to be compatible with the conclusion of Ref. 49 that, in case of the Kondo model with $S = 1/2$, the g-factor of the electrons (or equivalently their magnetic moment) is irrelevant for impurity properties in the limit of infinite bandwidth, corresponding to $\rho J \to 0$.

In the case of impurity spin $S = 1/2$, it is possible to compare the obtained values for $\eta(\rho J, 1)$ and $\alpha(\rho J)$ with previously published results. For the exchange-anisotropic multichannel $S = 1/2$-Kondo model with transverse coupling strength $\rho J_\perp \ll 1$ (see Eq. (21) for the meaning of the symbols $J_\perp$ and $J_\parallel$), it is known that the impurity contributions to the free energy $F_{\rm imp}(B, T, g_S, g_e)$ for local and bulk magnetic field have the following relation:[86]

$$F_{\rm imp}(B, T, g_S, g_S) = F_{\rm imp}(\bar{B}, T, g_S, 0) \ , \quad \text{(C3)}$$

$$\bar{B} = (1 - 2f\delta/\pi) B \ . \quad \text{(C4)}$$

Here, f is the number of electron channels and δ is the phase shift generated by the longitudinal coupling $J_\parallel$. This result for $F_{\rm imp}$ is a generalization of the conclusion that the impurity contribution to the susceptibility $\chi_{\rm imp}(g_S, g_e)$ *at zero magnetic field* satisfies $\chi_{\rm imp}(g_S, g_e) = \lambda(g_e/g_S, \delta)\,\chi_{\rm imp}(g_S, g_S)$, with a certain factor λ, for the single-channel exchange-anisotropic $S = 1/2$-Kondo model with $\rho J_\perp \ll 1$.[87] Using the definition for the impurity contribution to the magnetization, $M_{\rm imp} = -\partial F_{\rm imp}/\partial B$, and the equivalence of $M_{\rm imp}$ and the impurity magnetization $\mathcal{M}$ for $g_e = 0$ according to Eq. (10), the following relation is obtained from Eqs. (C3) and (C4):

$$M_{\rm imp}(B, T, g_S, g_S) = \\ (1 - 2f\delta/\pi)\,\mathcal{M}((1 - 2f\delta/\pi)B, T, g_S, 0)\,. \quad \text{(C5)}$$

On the other hand, the proportionality $\mathcal{M}(B, T \approx 0, g_S, g_S) = \alpha(\rho J) M_{\rm imp}(B, T \approx 0, g_S, g_S)$ from Eq. (14) that is implied by the NRG results can be combined with Eqs. (C1) and (C2) to give:

$$M_{\rm imp}(B, T \approx 0, g_S, g_S) = \\ \frac{1}{\alpha(\rho J)}\,\mathcal{M}\left(\frac{B}{\eta(\rho J, 1)}, T \approx 0, g_S, 0\right). \quad \text{(C6)}$$

With $f = 1$ and the phase shift for the case of an electron band of width $2W$ with constant DOS $\rho = 1/2W$,[88] $\delta(\rho J_\parallel) = \arctan(\pi\rho J_\parallel/4)$ (note the sign change with respect to Ref. 88), we compare Eqs. (C5) and (C6) and deduce for $\rho J_\perp \ll 1$:

$$\alpha(\rho J_\parallel) = \eta(\rho J_\parallel, 1) = \frac{1}{1 - \frac{2}{\pi}\arctan(\pi\rho J_\parallel/4)}\,. \quad \text{(C7)}$$

This equation predicts, in particular, that both the proportionality factor and the rescaling factor tend to 1 in the limit $\rho J_\parallel \to 0$. From Eq. (C7) the following values for $\alpha(\rho J_\parallel)$ are obtained: $\alpha = 1.02563$ ($\rho J_\parallel = 0.05$), 1.03623 (0.07), and 1.04704 (0.09). In Fig. 17, we present NRG results for $\alpha(\rho J_\parallel, \rho J_\perp)$ for an impurity spin $S = 1/2$ with exchange anisotropy. It is seen that the calculated proportionality factors indeed approach the predictions of Eq. (C7) for decreasing transverse coupling strength $\rho J_\perp$. For $\rho J_\perp = 0.01$ and all three considered values of $\rho J_\parallel$, the relative deviation is about $4 \cdot 10^{-5}$. In the exchange-isotropic case (i.e., $J_\parallel = J_\perp = J$), the relative deviation is less than half a percent, with better agreement for smaller coupling J.

Since Eqs. (C3) and (C4) also hold for non-zero temperature, the connection between $\mathcal{M}(B, T > 0)$ and $M_{\rm imp}(B, T > 0)$ has been studied for impurity spin $S = 1/2, 1$, and $3/2$ in the case of $D = 0$ and isotropic coupling $\rho J = 0.05, 0.07$, and 0.09. Keeping the coupling strength fixed, $\mathcal{M}(B, T)$ and $M_{\rm imp}(B, T)$ are still proportional for non-zero temperature and it is found that, for $g_S\mu_B B/W \in [10^{-13}, 10^{-1}]$, the relative deviation between the proportionality factor and the corresponding value $\alpha(\rho J, T \approx 0)$ is less than 1 ‰ for thermal energies $k_B T/W \leq 10^{-2}$.

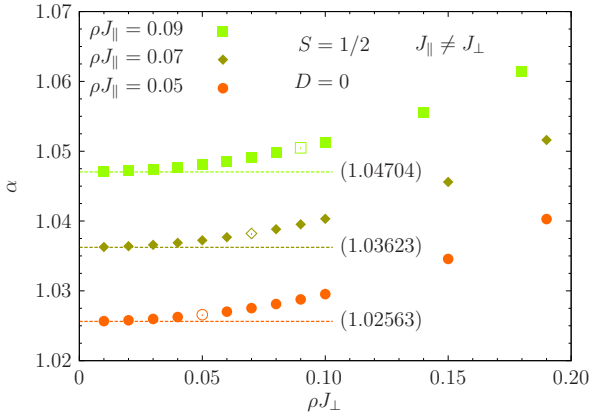

FIG. 17. (Color online) Proportionality factor α appearing in Eq. (14) as function of the transverse coupling strength $\rho J_\perp$ for impurity spin $S = 1/2$ and three values of the longitudinal coupling $\rho J_\parallel$. Dashed horizontal lines mark the values of α, given by the numbers in parentheses, that are predicted by Eq. (C7) for $\rho J_\perp \ll 1$. Open symbols indicate the proportionality factors for the exchange-isotropic case (i.e., $J_\parallel = J_\perp$), which are also found in Table I. As before, α has been averaged over magnetic fields $g_S\mu_B B/W \in [10^{-13}, 10^{-1}]$ for $k_B T/W \approx 1.54 \cdot 10^{-15} \approx 0$. The corresponding standard deviations would amount to error bars smaller than the symbol size.

Appendix D: Technical details regarding the study of the effective model for vanishing electron g-factor

In this last appendix, we describe how to reliably extract the ELC field $\widetilde{B}_{\rm ELC}$ and the Kondo temperature $T_K^{\rm ELC}$ *at the ELC field* from the NRG results for the effective model (29) with $g_e = 0$.

To determine $\widetilde{B}_{\rm ELC}$ as defined in Eq. (27), the impurity magnetization in units of $g_S\mu_B$ for the effective model, $-\langle \underset{\sim}{s}^z \rangle(\widetilde{B})$, is calculated for low temperature $k_B T \ll W$. In the vicinity of an ELC, i.e., near its root, the impurity magnetization depends linearly on the (relative) magnetic field $\widetilde{B}$. The root, which corresponds to $\widetilde{B}_{\rm ELC}$ at $T = 0$, can therefore be determined by performing a linear fit to the numerical data. However, the following complication arises: The position of the root of $\langle \underset{\sim}{s}^z \rangle(\widetilde{B})$ depends on the value of the twist parameter z and thereby on the discretization of the electron band. On the contrary, a physically meaningful result for the ELC field should display only a weak dependence on the numerical parameters of an NRG calculation in order to accurately reflect the continuum limit $\Lambda \to 1$. It turns out that a standard z-averaging, i.e., an averaging of the impurity magnetization curves for different values of z at

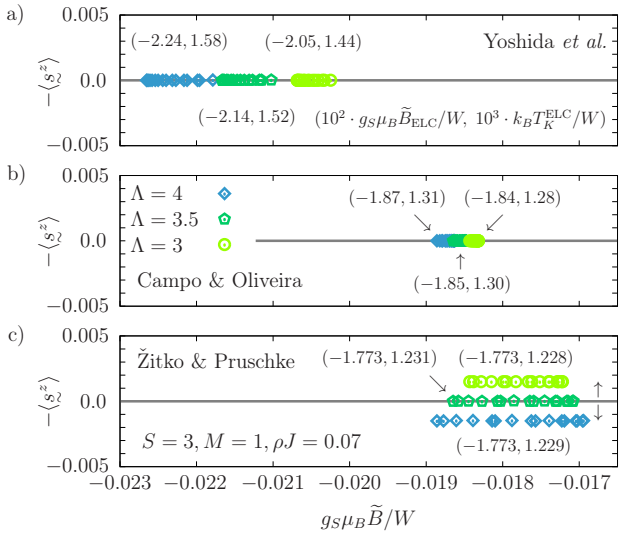

FIG. 18. (Color online) Impurity magnetization (in units of $g_S\mu_B$) for the effective Hamiltonian with $g_e = 0$ and parameters according to Eqs. (23) to (25) versus the relative magnetic field for $k_BT/W \approx 10^{-15} \approx 0$. The results have been calculated using the discretization schemes by a) Yoshida *et al.* (with correction factor[17,18,84] A_Λ),[81–83] b) Campo and Oliveira,[84] and c) Žitko and Pruschke.[70,71] For each discretization scheme, results are presented for three values of the discretization parameter Λ and 16 values of the twist parameter z (i.e., $z_i = i/16$ with $i \in \{1, 2, ..., 16\}$). In plot c, data points are vertically offset to enhance legibility. Numbers in parentheses denote the ELC field $\widetilde{B}_{\rm ELC}$ and the Kondo temperature $T_K^{\rm ELC}$ at the ELC field, respectively (cf. main text).

fixed temperature, is not reasonable at this point. Near an ELC, such an averaging in general introduces artifacts into the averaged curve because of non-linear components which some of the z-dependent curves might already comprise. Similar numerical artifacts are found in the z-averaged magnetization curves of the full impurity model for large hard axis anisotropy. Upon closer inspection, one discovers that z-averaging divides the total height of a magnetization step into smaller "sub-steps" of equal height whose number corresponds to the number of z-values used.

For the effective model with one set of parameters, the dependence of the impurity magnetization root on the discretization of the electron band is demonstrated in Fig. 18. There, the three common discretization schemes are compared for three different values of the discretization parameter Λ and, *only in this example*, for 16 values of the twist parameter z. In all cases, we observe a spread of the position of the impurity magnetization root with respect to z. This variation decreases for smaller values of Λ and is always largest when using the discretization scheme by Žitko and Pruschke (ŽP). The spread due to z defines a magnetic field interval which, in case of the discretization by Yoshida *et al.* (Y) and Campo and Oliveira (CO), moves towards larger fields when Λ is reduced. In contrast, the ŽP discretization leads to nested intervals so that an interval for smaller Λ is wholly contained in an interval for larger Λ. In the special case $z = 1$ (which corresponds to the smallest root), the CO and ŽP discretization give the same result.[70] Note that the Λ-dependence of the data shown in Fig. 18 is consistent with an agreement of the results of all three discretization schemes in the continuum limit $\Lambda \to 1$. However, in order to obtain reliable information about the continuum limit, it would be necessary to perform an impractical extrapolation in Λ when using the Y or CO discretization. On the contrary, the ŽP discretization apparently allows to make a dependable statement about the limit $\Lambda \to 1$ on the basis of results for only a single value of the discretization parameter: Fig. 18 suggests that the continuum value of $\widetilde{B}_{\rm ELC}$ lies in the magnetic field interval that is spanned by the z-dependent roots for $\Lambda > 1$. It turns out that, using the ŽP discretization, one can obtain a better approximation for the ELC field by averaging over the z-dependent impurity magnetization roots since the resulting mean value displays only a weak dependence on Λ (cf. the numbers in parentheses in Fig. 18). The spread of the roots with respect to z then provides a safe error estimate for the mean value (amounting to a relative deviation of about 3 to 4 % for $\Lambda = 3$). However, the dependence of the mean value on Λ indicates that such an error estimate is far too pessimistic. For the ŽP discretization with $\Lambda = 3$ and *four z-values*, we expect that the relative error of the obtained ELC field $\widetilde{B}_{\rm ELC}$ is about one order of magnitude smaller than suggested by the roots' dependency on z.

Having determined $\widetilde{B}^z_{\rm ELC}$ for all values of z, we can study the thermodynamic properties of the effective model at the ELC field by calculating the impurity contribution to the entropy $S^z_{\rm imp}(T, \widetilde{B}^z_{\rm ELC})$ *for each z at the respective ELC field*. For thermal energies that are small compared to the bandwidth, the NRG results for $S^z_{\rm imp}(T, \widetilde{B}^z_{\rm ELC})$ can be aligned with the known universal temperature dependence of the entropy for the Kondo model with $S = 1/2$. We find, however, that there is a dip in the entropy for thermal energies close to the band edge that becomes more pronounced for stronger scattering κ. The Kondo temperature $T_K^{{\rm ELC},z}$ characterizing the temperature dependence of $S^z_{\rm imp}(T, \widetilde{B}^z_{\rm ELC})$ is obtained in the following way for each value of z: By comparing with the Bethe Ansatz solution for the impurity contribution to the magnetization in Sec. IV A, the value of T_K according to the definition (11) is known for the NRG results with $D = 0$ (cf. Table I and Eq. (12)). As a first step, the result for $S^z_{\rm imp}(T, \widetilde{B}^z_{\rm ELC})$ is restricted to the linear low-temperature regime in which a continuous curve is produced using a linear fit. This fit then allows to determine the value of $T_K^{{\rm ELC},z}$ by comparing with an NRG result for $S = 1/2$ with known Kondo temperature. A better approximation for the Kondo temperature at the ELC field $T_K^{\rm ELC}$ is again obtained by averaging over the z-dependent values. Regarding the variation with respect

to z and the error estimate for the mean value, comparable statements hold true as in the case of the ELC field.

We observe that the root of the impurity magnetization depends on temperature. This is possible since its value is apparently not determined by symmetry properties of the effective model. When the temperature exceeds the Kondo temperature at the ELC field, two effects eventually occur: The slope of the magnetization curve decreases and the root moves towards larger relative magnetic fields.

[1] R. Sessoli, D. Gatteschi, A. Caneschi, and M. A. Novak, Nature **365**, 141 (1993).

[2] D. Gatteschi, Adv. Mater. **6**, 635 (1994).

[3] C. J. Milios, A. Vinslava, W. Wernsdorfer, S. Moggach, S. Parsons, S. P. Perlepes, G. Christou, and E. K. Brechin, J. Am. Chem. Soc. **129**, 2754 (2007).

[4] L. Bogani and W. Wernsdorfer, Nat. Mater. **7**, 179 (2008).

[5] G. Rogez, B. Donnio, E. Terazzi, J.-L. Gallani, J.-P. Kappler, J.-P. Bucher, and M. Drillon, Adv. Mater. **21**, 4323 (2009).

[6] D. Gatteschi, A. Cornia, M. Mannini, and R. Sessoli, Inorg. Chem. **48**, 3408 (2009).

[7] A. Cornia, M. Mannini, P. Sainctavit, and R. Sessoli, Chem. Soc. Rev. **40**, 3076 (2011).

[8] N. Domingo, E. Bellido, and D. Ruiz-Molina, Chem. Soc. Rev. **41**, 258 (2012).

[9] D. Gatteschi, R. Sessoli, and J. Villain, *Molecular Nanomagnets* (Oxford University Press, 2006).

[10] C. Romeike, M. R. Wegewijs, W. Hofstetter, and H. Schoeller, Phys. Rev. Lett. **96**, 196601 (2006).

[11] C. Romeike, M. R. Wegewijs, W. Hofstetter, and H. Schoeller, Phys. Rev. Lett. **97**, 206601 (2006); Phys. Rev. Lett. **106**, 019902 (2011).

[12] D. Roosen, M. R. Wegewijs, and W. Hofstetter, Phys. Rev. Lett. **100**, 087201 (2008); Phys. Rev. Lett. **105**, 259901 (2010).

[13] C. F. Hirjibehedin, C.-Y. Lin, A. F. Otte, M. Ternes, C. P. Lutz, B. A. Jones, and A. J. Heinrich, Science **317**, 1199 (2007).

[14] A. F. Otte, M. Ternes, K. von Bergmann, S. Loth, H. Brune, C. P. Lutz, C. F. Hirjibehedin, and A. J. Heinrich, Nat. Phys. **4**, 847 (2008).

[15] H. Brune and P. Gambardella, Surf. Sci. **603**, 1812 (2009).

[16] K. G. Wilson, Rev. Mod. Phys. **47**, 773 (1975).

[17] H. R. Krishna-murthy, J. W. Wilkins, and K. G. Wilson, Phys. Rev. B **21**, 1003 (1980).

[18] R. Bulla, T. A. Costi, and T. Pruschke, Rev. Mod. Phys. **80**, 395 (2008).

[19] M. Mannini, F. Pineider, P. Sainctavit, L. Joly, A. Fraile-Rodriguez, M.-A. Arrio, C. C. d. Moulin, W. Wernsdorfer, A. Cornia, D. Gatteschi, and R. Sessoli, Adv. Mater. **21**, 167 (2009).

[20] M. Mannini, F. Pineider, P. Sainctavit, C. Danieli, E. Otero, C. Sciancalepore, A. M. Talarico, M.-A. Arrio, A. Cornia, D. Gatteschi, and R. Sessoli, Nat. Mater. **8**, 194 (2009).

[21] V. Corradini, F. Moro, R. Biagi, V. De Renzi, U. del Pennino, V. Bellini, S. Carretta, P. Santini, V. A. Milway, G. Timco, R. E. P. Winpenny, and M. Affronte, Phys. Rev. B **79**, 144419 (2009).

[22] S. Stepanow, J. Honolka, P. Gambardella, L. Vitali, N. Abdurakhmanova, T.-C. Tseng, S. Rauschenbach, S. L. Tait, V. Sessi, S. Klyatskaya, M. Ruben, and K. Kern, J. Am. Chem. Soc. **132**, 11900 (2010).

[23] M. Mannini, F. Pineider, C. Danieli, F. Totti, L. Sorace, P. Sainctavit, M. A. Arrio, E. Otero, L. Joly, J. C. Cezar, A. Cornia, and R. Sessoli, Nature **468**, 417 (2010).

[24] R. Biagi, J. Fernandez-Rodriguez, M. Gonidec, A. Mirone, V. Corradini, F. Moro, V. De Renzi, U. del Pennino, J. C. Cezar, D. B. Amabilino, and J. Veciana, Phys. Rev. B **82**, 224406 (2010).

[25] M. Gonidec, R. Biagi, V. Corradini, F. Moro, V. De Renzi, U. del Pennino, D. Summa, L. Muccioli, C. Zannoni, D. B. Amabilino, and J. Veciana, J. Am. Chem. Soc. **133**, 6603 (2011).

[26] A. Lodi Rizzini, C. Krull, T. Balashov, J. J. Kavich, A. Mugarza, P. S. Miedema, P. K. Thakur, V. Sessi, S. Klyatskaya, M. Ruben, S. Stepanow, and P. Gambardella, Phys. Rev. Lett. **107**, 177205 (2011).

[27] V. Corradini, A. Ghirri, E. Garlatti, R. Biagi, V. De Renzi, U. del Pennino, V. Bellini, S. Carretta, P. Santini, G. Timco, R. E. P. Winpenny, and M. Affronte, Adv. Funct. Mater. **22**, 3706 (2012).

[28] C. T. Chen, Y. U. Idzerda, H.-J. Lin, N. V. Smith, G. Meigs, E. Chaban, G. H. Ho, E. Pellegrin, and F. Sette, Phys. Rev. Lett. **75**, 152 (1995).

[29] T. Funk, A. Deb, S. J. George, H. X. Wang, and S. P. Cramer, Coord. Chem. Rev. **249**, 3 (2005).

[30] M. Prinz, K. Kuepper, C. Taubitz, M. Raekers, S. Khanra, B. Biswas, T. Weyhermüller, M. Uhlarz, J. Wosnitza, J. Schnack, A. V. Postnikov, C. Schröder, S. J. George, M. Neumann, and P. Chaudhuri, Inorg. Chem. **49**, 2093 (2010).

[31] F. Meier, L. Zhou, J. Wiebe, and R. Wiesendanger, Science **320**, 82 (2008).

[32] L. Zhou, J. Wiebe, S. Lounis, E. Vedmedenko, F. Meier, S. Blügel, P. H. Dederichs, and R. Wiesendanger, Nat. Phys. **6**, 187 (2010).

[33] J. Wiebe, L. Zhou, and R. Wiesendanger, J. Phys. D: Appl. Phys. **44**, 464009 (2011).

[34] A. A. Khajetoorians, S. Lounis, B. Chilian, A. T. Costa, L. Zhou, D. L. Mills, J. Wiebe, and R. Wiesendanger, Phys. Rev. Lett. **106**, 037205 (2011).

[35] A. A. Khajetoorians, J. Wiebe, B. Chilian, S. Lounis, S. Blügel, and R. Wiesendanger, Nat. Phys. **8**, 497 (2012).

[36] C. Iacovita, M. V. Rastei, B. W. Heinrich, T. Brumme, J. Kortus, L. Limot, and J. P. Bucher, Phys. Rev. Lett. **101**, 116602 (2008).

[37] B. W. Heinrich, C. Iacovita, M. V. Rastei, L. Limot, P. A. Ignatiev, V. S. Stepanyuk, and J. P. Bucher, Eur. Phys. J. B **75**, 49 (2010).

[38] J. Brede and R. Wiesendanger, Phys. Rev. B **86**, 184423 (2012).

[39] P. E. Bloomfield, R. Hecht, and P. R. Sievert, Phys. Rev. B **2**, 3714 (1970).

[40] G. S. Poo, Phys. Rev. B **11**, 4606 (1975); Phys. Rev. B **11**, 4614 (1975).

[41] V. A. Fateev and P. B. Wiegmann, Phys. Lett. A **81**, 179

(1981).
[42] N. Andrei and J. H. Lowenstein, Phys. Rev. Lett. **46**, 356 (1981).
[43] V. A. Fateev and P. B. Wiegmann, Phys. Rev. Lett. **46**, 1595 (1981).
[44] K. Furuya and J. H. Lowenstein, Phys. Rev. B **25**, 5935 (1982).
[45] V. T. Rajan, J. H. Lowenstein, and N. Andrei, Phys. Rev. Lett. **49**, 497 (1982).
[46] A. M. Tsvelick and P. B. Wiegmann, Adv. Phys. **32**, 453 (1983).
[47] N. Andrei, K. Furuya, and J. H. Lowenstein, Rev. Mod. Phys. **55**, 331 (1983).
[48] P. Schlottmann, Z. Phys. B - Condensed Matter **51**, 223 (1983).
[49] J. H. Lowenstein, Phys. Rev. B **29**, 4120 (1984).
[50] A. M. Tsvelick and P. B. Wiegmann, J. Stat. Phys. **38**, 125 (1985).
[51] P. D. Sacramento and P. Schlottmann, Phys. Rev. B **40**, 431 (1989).
[52] K. Takegahara and T. Kasuya, Physica B **163**, 216 (1990).
[53] A. C. Hewson, J. Bauer, and W. Koller, Phys. Rev. B **73**, 045117 (2006).
[54] C. J. Wright, M. R. Galpin, and D. E. Logan, Phys. Rev. B **84**, 115308 (2011).
[55] R. Žitko, in *Physical Properties of Nanosystems*, edited by J. Bonča and S. Kruchinin (Springer, 2011) pp. 247–257.
[56] A. Hackl, M. Vojta, and S. Kehrein, Phys. Rev. B **80**, 195117 (2009).
[57] P. Fritsch and S. Kehrein, Phys. Rev. B **81**, 035113 (2010).
[58] M. Schiró, Phys. Rev. B **81**, 085126 (2010).
[59] M. Pletyukhov, D. Schuricht, and H. Schoeller, Phys. Rev. Lett. **104**, 106801 (2010).
[60] M. Heyl and S. Kehrein, J. Phys.: Condens. Matter **22**, 345604 (2010).
[61] F. B. Anders and A. Schiller, Phys. Rev. Lett. **95**, 196801 (2005); Phys. Rev. B **74**, 245113 (2006).
[62] A. Hackl, D. Roosen, S. Kehrein, and W. Hofstetter, Phys. Rev. Lett. **102**, 196601 (2009).
[63] R. Žitko, R. Peters, and T. Pruschke, Phys. Rev. B **78**, 224404 (2008).
[64] R. Žitko, R. Peters, and T. Pruschke, New J. Phys. **11**, 053003 (2009).
[65] R. Žitko and T. Pruschke, New J. Phys. **12**, 063040 (2010).
[66] A. Bencini and D. Gatteschi, *Electron Paramagnetic Resonance of Exchange Coupled Systems* (Springer-Verlag, 1990).
[67] I. Affleck, A. W. W. Ludwig, and B. A. Jones, Phys. Rev. B **52**, 9528 (1995).
[68] A. Schiller and L. De Leo, Phys. Rev. B **77**, 075114 (2008).
[69] T. Costi, in *Density-Matrix Renormalization – A New Numerical Method in Physics*, Lecture Notes in Physics, Vol. 528, edited by I. Peschel, M. Kaulke, X. Wang, and K. Hallberg (Springer, 1999) pp. 3–25.
[70] R. Žitko and T. Pruschke, Phys. Rev. B **79**, 085106 (2009).
[71] R. Žitko, Comput. Phys. Commun. **180**, 1271 (2009).
[72] A. C. Hewson, *The Kondo Problem to Heavy Fermions* (Cambridge University Press, 1993).
[73] In order to calculate $M_{\rm imp}(x, T=0)/g_S\mu_B$ for magnetic fields $g_S\mu_B B \geq k_B T_H$, we have employed Eq. (5.1.35) of Ref. 46 for all considered values of S. In the regime $g_S\mu_B B < k_B T_H$, Eq. (5.1.37) of Ref. 46 with an additional factor 1/4 has been used for $S = 1/2$ and Eq. (33) of Ref. 41 for $S \geq 1$, respectively. We suspect that the latter equation ought to read (cf. Eq. (5.1.38) of Ref. 46):
$$\frac{M_{\rm imp}(x)}{g_S\mu_B} = S - 1/2 + \frac{1}{2\pi^{3/2}}\int_0^\infty {\rm d}\omega \left(\frac{\sin\left(2\pi\omega(S-1/2)\right)}{\omega} \times \Gamma(1/2-\omega)\, {\rm e}^{-2\omega|\ln(g_S\mu_B B/k_B T_H)|}\, (\omega/{\rm e})^\omega \right) + \frac{1}{2}\sum_{n=0}^{\infty} \dots \quad .$$
For integer impurity spin S (in which case the maxima and minima of the sine coincide with the poles of the gamma function in the integrand), we have been unable to obtain converged results for the above integral in the field regime $g_S\mu_B B \lesssim k_B T_H$. For this reason, part of the BA curve is missing in Fig. 1 b.
[74] D. C. Mattis, Phys. Rev. Lett. **19**, 1478 (1967).
[75] D. M. Cragg and P. Lloyd, J. Phys. C: Solid State Phys. **12**, L215 (1979).
[76] H.-U. Desgranges and K. D. Schotte, Phys. Lett. A **91**, 240 (1982).
[77] A. Okiji and N. Kawakami, Phys. Rev. Lett. **50**, 1157 (1983).
[78] It might seem more natural to compare with the easily obtainable magnetization of a free spin. However, we observe that for the chosen value of Λ and zero coupling NRG is apparently not able to fully reproduce the finite temperature behavior of a free spin. For this reason, we rather use NRG results with $J = 0$ for the comparison.
[79] H. R. Krishna-murthy, J. W. Wilkins, and K. G. Wilson, Phys. Rev. B **21**, 1044 (1980).
[80] It seems permissible to use the effective model for $g_e = 0$ as a *guide* for the interpretation of the results in Fig. 9 since we are primarily interested in the behavior of the impurity magnetization $\mathcal{M}$ whose dependence on g_e we know. As demonstrated in App. C for not too large D, $\mathcal{M}$ is proportional to $M_{\rm imp}$ for equal g-factors and fixed coupling strength, and a reduction of g_e effectively rescales the magnetic field argument of $\mathcal{M}$. This of course changes the ELC field, but preserves the shape of the impurity magnetization curve (cf. Fig. 16).
[81] M. Yoshida, M. A. Whitaker, and L. N. Oliveira, Phys. Rev. B **41**, 9403 (1990).
[82] W. C. Oliveira and L. N. Oliveira, Phys. Rev. B **49**, 11986 (1994).
[83] S. C. Costa, C. A. Paula, V. L. Líbero, and L. N. Oliveira, Phys. Rev. B **55**, 30 (1997).
[84] V. L. Campo and L. N. Oliveira, Phys. Rev. B **72**, 104432 (2005).
[85] However, while being non-perturbative in J, NRG still relies on a discretization of the electronic degrees of freedom. For $\rho J > 0.4$ we observe artifacts in the NRG results: $M_{\rm imp}$ becomes negative for $S = 1/2$, whereas $M_{\rm imp}(\rho J)$-curves for different magnetic fields eventually cross for $S \geq 1$. In contrast, the impurity magnetization $\mathcal{M}$ does not display any obvious anomalies. Figs. 14 and 15 are basically unaffected by the aforementioned problems.
[86] G. Zaránd, T. Costi, A. Jerez, and N. Andrei, Phys. Rev. B **65**, 134416 (2002).
[87] P. B. Vigman and A. M. Finkel'shteĭn, Sov. Phys. JETP **48**, 102 (1978).
[88] T. A. Costi and G. Zaránd, Phys. Rev. B **59**, 12398 (1999).

Summary

This thesis is concerned with Numerical Renormalization Group (NRG) calculations for isotropic and anisotropic single-channel single-impurity Kondo models with impurity spin $S \geq 1/2$ in zero and non-zero magnetic field. In particular, the case of a non-zero coupling of the conduction electrons to the external field, formally corresponding to an electron g-factor $g_e \neq 0$, has been considered. We have focussed on the calculation and interpretation of magnetization curves. The Kondo model with additional uniaxial anisotropy of the impurity spin is relevant to the description of magnetic atoms and molecules that are deposited on a non-magnetic metallic substrate ("surface Kondo effect"). Magnetic molecules, in particular bistable ones such as single molecule magnets, offer the prospect of encoding and storing information in their spin state. Since a controlled deposition on a suitable substrate could solve the problem of addressability (such an approach already allows to study individual deposited atoms and molecules by means of scanning tunneling microscopy and spectroscopy techniques, cf. chapter 8), investigating the magnetic properties of molecules in contact with a surface is also of potential technological interest. Of course, only time will tell whether it is possible (and actually desirable) to represent one bit of information by a single magnetic molecule on any technologically relevant scale.

Chapter 2 of this thesis begins with a brief overview of the history of the Kondo effect, covering its discovery in dilute magnetic alloys and its explanation via the Kondo model. On a technical level, the real-space and $\boldsymbol{k}$-space representations of the Kondo Hamiltonian and the relation between the spin-1/2 Kondo model and the more fundamental single-impurity Anderson model are discussed. Coming to the problem at hand, the general bilinear spin Hamiltonian for the modeling of an isolated magnetic molecule is introduced and the form of the axial and transverse anisotropy terms is clarified. Such terms are included in the impurity part of the Kondo Hamiltonian in order to give a minimal model for the description of the surface Kondo effect as occurring for deposited magnetic atoms and molecules. Chapter 2 closes with a discussion of symmetry properties of the Kondo model, which can be used to make numerical calculations more efficient.

As a supplement to the brief overview of the different steps that a NRG calculation is comprised of in chapter 3, the Numerical Renormalization Group method for the investigation of the thermodynamics of the single-channel Kondo model is described in detail in chapter 4. In particular, it is explained how to carry out NRG calculations with an arbitrary ratio g_e/g_S of electron and impurity g-factors.

As a first application, the canonical example of the single-channel Kondo model with impurity spin $S = 1/2$ in zero magnetic field is studied in chapter 5. The temperature dependence of the impurity contributions to the entropy and the magnetic susceptibility is used to illustrate the concept of Kondo screening, the meaning of

the Kondo temperature T_K, and the universal properties of the model in the scaling regime. A comparison of NRG calculations for small coupling strength $\rho J \ll 1$ with corresponding Bethe ansatz solutions reveals a convincing agreement of the results obtained using the two different methods. Certain generalizations of the spin-1/2 Kondo Hamiltonian (e.g., additional potential scattering and exchange anisotropy) are known to preserve the universal properties of the model. This point is also demonstrated in chapter 5. Lastly, the underscreened Kondo effect is considered: An isotropic impurity spin $S > 1/2$ is only partially screened by a single conduction electron channel, leaving a residual spin $S-1/2$ at low temperature $T \ll T_K$.

With a restriction to the case of equal g-factors, chapter 6 extends the results presented in chapter 5 to the situation with a non-zero magnetic field. In particular, it is illustrated that a fully screened and a partially screened impurity show a different response to an external field at low temperature $T \ll T_K$.

The Bethe ansatz provides solutions in closed form for the zero-temperature field-dependent impurity contribution to the magnetization M_{imp} of the isotropic single-channel single-impurity Kondo model with arbitrary impurity spin. These solutions, along with the corresponding asymptotic low- and high-field expansions, are discussed in chapter 7.

As the main result of this thesis, chapter 8 contains an investigation of the field-dependent magnetization of the single-channel single-impurity Kondo model with and without uniaxial anisotropy. In the isotropic case, a comparison of NRG results for M_{imp} with the corresponding Bethe ansatz solutions considered in chapter 7 shows excellent agreement. The presented NRG calculations clarify the relation between M_{imp} and the impurity magnetization $\mathcal{M}$ and, furthermore, illustrate the effect of the g-factor ratio g_e/g_S on the magnetic properties of the model. In case of additional easy axis anisotropy, the low-field and zero-temperature limit of M_{imp} can be related to the concept of a "fractional spin" and it is demonstrated that the obtained magnetization curves can at least partially be described by an adapted Brillouin function. For impurities with hard axis anisotropy, the magnetization curves can feature steps with characteristic positions and widths. The occurrence and the properties of these steps can be explained by field-induced Kondo effects. In the limit of arbitrarily large anisotropy and for $g_e = 0$, the field-induced Kondo effects are described by an exchange-anisotropic pseudo-spin-1/2 Kondo model with additional spin-dependent scattering. In particular, this effective model predicts a shift of the step positions compared to the corresponding free spin with hard axis anisotropy and, moreover, a smaller Kondo temperature for every further field-induced Kondo effect that occurs when increasing the magnetic field. For a more detailed summary of the results presented in chapter 8, please refer to the summary of the manuscript.

The appendix deals with the initialization of the iterative diagonalization of the Wilson chain. To this end, the analytical solution for the eigensystem of the truncated Wilson chain comprising a spin-1/2 impurity and the zeroth site is presented. Furthermore, one possibility for encoding and storing product basis states of a Kondo-type model in a numerical implementation is described.

Appendix

A. Initialization of the iterative diagonalization of the Wilson chain

In the iterative diagonalization of the Wilson chain for given twist parameter z, a matrix representation of the truncated Hamiltonian in step N is calculated using information (i.e., energy eigenstates and certain matrix elements) from the previous step $N-1$ (cf. Sec. 4.11). In order to "initialize" the iterative diagonalization procedure, the required information has to be provided once by some other method. To this end, the truncated Wilson chain comprising, e.g., the impurity spin and the zeroth lattice site is diagonalized either analytically (see Sec. A.1 for the special case of impurity spin $S = 1/2$) or numerically exact (in Sec. A.2, we describe one possibility of handling product basis states in a numerically exact diagonalization of a truncated Wilson chain) and the matrix elements that are needed for the next step are calculated.

A.1. Analytical results for the eigensystem and certain matrix elements of a truncated Wilson chain comprising a spin-1/2 impurity and the zeroth lattice site

Let us consider the following Hamiltonian for a truncated Wilson chain comprising an impurity spin $\underset{\sim}{\boldsymbol{S}}$ with $S = 1/2$ and the states $\underset{\sim}{f}_{0\mu}$ assigned to the zeroth lattice site:

$$\boxed{\underset{\sim}{H}(z) \equiv J_\perp \big(\underset{\sim}{S}^x \underset{\sim}{s}_0^x + \underset{\sim}{S}^y \underset{\sim}{s}_0^y\big) + J_\parallel \underset{\sim}{S}^z \underset{\sim}{s}_0^z + h_S \underset{\sim}{S}^z + \epsilon_{0\uparrow}(z)\underset{\sim}{n}_{0\uparrow} + \epsilon_{0\downarrow}(z)\underset{\sim}{n}_{0\downarrow} \,.} \tag{A.1}$$

Here, we have $\underset{\sim}{\boldsymbol{s}}_0 = \sum_{\mu,\nu} \underset{\sim}{f}^\dagger_{0\mu} \frac{\boldsymbol{\sigma}_{\mu\nu}}{2} \underset{\sim}{f}_{0\nu}$, $h_S \equiv g_S \mu_B B$, and $\underset{\sim}{n}_{0\mu} = \underset{\sim}{f}^\dagger_{0\mu} \underset{\sim}{f}_{0\mu}$. In order to set up a matrix representation of $\underset{\sim}{H}(z)$, it is convenient to introduce raising and lowering operators $\underset{\sim}{S}^\pm \equiv \underset{\sim}{S}^x \pm \mathrm{i}\underset{\sim}{S}^y$ by using the identity

$$J_\perp \big(\underset{\sim}{S}^x \underset{\sim}{s}_0^x + \underset{\sim}{S}^y \underset{\sim}{s}_0^y\big) = \frac{J_\perp}{2} \big(\underset{\sim}{S}^+ \underset{\sim}{s}_0^- + \underset{\sim}{S}^- \underset{\sim}{s}_0^+\big) \,. \tag{A.2}$$

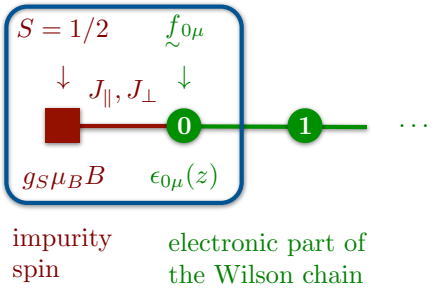

Figure A.1.: The blue frame designates the truncated Wilson chain, consisting of the impurity spin and the zeroth lattice site, that is described by Hamiltonian (A.1) (cf. Figs. 4.4 and 4.5 (a)).

A graphical representation of the truncated Wilson chain that $\underset{\sim}{H}(z)$ describes is shown in Fig. A.1.

A basis of the fermionic Fock space belonging to Hamiltonian (A.1) is given by the product basis $\{|-\rangle, |+\rangle\} \otimes \{|\,\Omega\,\rangle, |\downarrow\rangle, |\uparrow\rangle, |\uparrow\downarrow\rangle\}$. $|-\rangle$ ($|+\rangle$) is the spin-down (spin-up) state of the impurity spin, $|\,\Omega\,\rangle$ denotes the vacuum at the zeroth site of the Wilson chain, and we use the following convention for the doubly occupied state:

$$|\uparrow\downarrow\rangle \equiv \underset{\sim}{f}^\dagger_{0\uparrow} \underset{\sim}{f}^\dagger_{0\downarrow} |\,\Omega\,\rangle\,. \tag{A.3}$$

In the following, we label states with the charge quantum number Q (compare the definition (4.235) of the charge operator $\underset{\sim}{Q}$) and the magnetic quantum number M of the total spin $\underset{\sim}{\boldsymbol{S}}_{\text{total}} \equiv \underset{\sim}{\boldsymbol{S}} + \underset{\sim}{\boldsymbol{s}}_0$ (see Table A.1).

Using the abbreviations

$$E_4(z) \equiv \frac{1}{4}\left(2\big(\epsilon_{0\downarrow}(z) + \epsilon_{0\uparrow}(z)\big) - 2\sqrt{\big(h_S + \epsilon_{0\downarrow}(z) - \epsilon_{0\uparrow}(z)\big)^2 + J_\perp^2} - J_\parallel\right), \tag{A.4}$$

$$E_5(z) \equiv \frac{1}{4}\left(2\big(\epsilon_{0\downarrow}(z) + \epsilon_{0\uparrow}(z)\big) + 2\sqrt{\big(h_S + \epsilon_{0\downarrow}(z) - \epsilon_{0\uparrow}(z)\big)^2 + J_\perp^2} - J_\parallel\right), \tag{A.5}$$

$$\alpha_1(z) \equiv -\frac{1}{J_\perp}\left(h_S + \epsilon_{0\downarrow}(z) - \epsilon_{0\uparrow}(z) + \sqrt{\big(h_S + \epsilon_{0\downarrow}(z) - \epsilon_{0\uparrow}(z)\big)^2 + J_\perp^2}\right), \tag{A.6}$$

$$\alpha_2(z) \equiv -\frac{1}{J_\perp}\left(h_S + \epsilon_{0\downarrow}(z) - \epsilon_{0\uparrow}(z) - \sqrt{\big(h_S + \epsilon_{0\downarrow}(z) - \epsilon_{0\uparrow}(z)\big)^2 + J_\perp^2}\right), \tag{A.7}$$

the eigensystem of Hamiltonian (A.1) is summarized in Table A.2.

In order to set up a matrix representation of the Hamilton operator in the *first* step of the iterative diagonalization (i.e., for an enlarged Wilson chain that

#	product basis state	Q	$2M$	$\lvert Q, 2M; r\rangle$
1	$\lvert-\rangle \otimes \lvert\,\Omega\,\rangle$	-1	-1	$\lvert -1, -1; 1\rangle$
2	$\lvert+\rangle \otimes \lvert\,\Omega\,\rangle$	-1	1	$\lvert -1, \ \ 1; 1\rangle$
3	$\lvert-\rangle \otimes \lvert\downarrow\rangle$	0	-2	$\lvert \ \ 0, -2; 1\rangle$
4	$\lvert-\rangle \otimes \lvert\uparrow\rangle$	0	0	$\lvert \ \ 0, \ \ 0; 1\rangle$
5	$\lvert+\rangle \otimes \lvert\downarrow\rangle$	0	0	$\lvert \ \ 0, \ \ 0; 2\rangle$
6	$\lvert+\rangle \otimes \lvert\uparrow\rangle$	0	2	$\lvert \ \ 0, \ \ 2; 1\rangle$
7	$\lvert-\rangle \otimes \lvert\uparrow\downarrow\rangle$	1	-1	$\lvert \ \ 1, -1; 1\rangle$
8	$\lvert+\rangle \otimes \lvert\uparrow\downarrow\rangle$	1	1	$\lvert \ \ 1, \ \ 1; 1\rangle$

Table A.1.: Product basis of the Fock space belonging to Hamiltonian (A.1). The index r uniquely labels the states in each invariant subspace $(Q, 2M)$.

i	energy eigenvalue E_i	energy eigenstate $\lvert E_i\rangle$
1	$-\frac{h_S}{2}$	$\lvert -1, -1; 1\rangle$
2	$\frac{h_S}{2}$	$\lvert -1, \ \ 1; 1\rangle$
3	$\frac{J_\parallel}{4} - \frac{h_S}{2} + \epsilon_{0\downarrow}(z)$	$\lvert \ \ 0, -2; 1\rangle$
4	$E_4(z)$	$\frac{\alpha_1(z)}{\sqrt{1+\alpha_1^2(z)}}\lvert 0, 0; 1\rangle + \frac{1}{\sqrt{1+\alpha_1^2(z)}}\lvert 0, 0; 2\rangle$
5	$E_5(z)$	$\frac{\alpha_2(z)}{\sqrt{1+\alpha_2^2(z)}}\lvert 0, 0; 1\rangle + \frac{1}{\sqrt{1+\alpha_2^2(z)}}\lvert 0, 0; 2\rangle$
6	$\frac{J_\parallel}{4} + \frac{h_S}{2} + \epsilon_{0\uparrow}(z)$	$\lvert \ \ 0, \ \ 2; 1\rangle$
7	$-\frac{h_S}{2} + \epsilon_{0\downarrow}(z) + \epsilon_{0\uparrow}(z)$	$\lvert \ \ 1, -1; 1\rangle$
8	$\frac{h_S}{2} + \epsilon_{0\downarrow}(z) + \epsilon_{0\uparrow}(z)$	$\lvert \ \ 1, \ \ 1; 1\rangle$

Table A.2.: Eigenvalues and normalized eigenstates of Hamiltonian (A.1).

(a)

i	j	$\langle E_i \lvert \underset{\sim}{f}^\dagger_{0\downarrow} \rvert E_j \rangle$
3	1	1
4	2	$\frac{1}{\sqrt{1+\alpha_1^2(z)}}$
5	2	$\frac{1}{\sqrt{1+\alpha_2^2(z)}}$
7	4	$-\frac{\alpha_1(z)}{\sqrt{1+\alpha_1^2(z)}}$
7	5	$-\frac{\alpha_2(z)}{\sqrt{1+\alpha_2^2(z)}}$
8	6	-1

(b)

i	j	$\langle E_i \lvert \underset{\sim}{f}^\dagger_{0\uparrow} \rvert E_j \rangle$
4	1	$\frac{\alpha_1(z)}{\sqrt{1+\alpha_1^2(z)}}$
5	1	$\frac{\alpha_2(z)}{\sqrt{1+\alpha_2^2(z)}}$
6	2	1
7	3	1
8	4	$\frac{1}{\sqrt{1+\alpha_1^2(z)}}$
8	5	$\frac{1}{\sqrt{1+\alpha_2^2(z)}}$

Table A.3.: The six non-vanishing matrix elements of (a) $\underset{\sim}{f}^\dagger_{0\downarrow}$ and (b) $\underset{\sim}{f}^\dagger_{0\uparrow}$ with respect to the energy eigenstates $|E_i\rangle$ from Table A.2.

additionally includes the first lattice site with states $\underset{\sim}{f}_{1\mu}(z)$, cf. Fig. 4.5 (b)), the matrix elements of the two creation operators $\underset{\sim}{f}^\dagger_{0\downarrow}$ and $\underset{\sim}{f}^\dagger_{0\uparrow}$ with respect to the eigenstates of Hamiltonian (A.1) are required (cf. Sec. 4.11.1). They are given in Table A.3. For a study of the magnetization of the impurity spin, we furthermore need the matrix elements of $\underset{\sim}{S}^z$ with respect to the energy eigenstates (see Table A.4). These matrix elements serve two purposes:

1. The diagonal elements are used in the current step for the calculation of thermodynamic expectation values.
2. All non-vanishing matrix elements from the current step are needed in order to determine the diagonal elements in the next step (cf. Sec. 4.13.4).

When comparing non-diagonal matrix elements from Tables A.3 and A.4 with results obtained by some other method, one should keep in mind that the overall sign of the normalized energy eigenstates is arbitrary. For this reason, the sign convention adopted in Table A.2 corresponds to only one of many possible choices.

A.2. Encoding, manipulating, and creating product basis states of the Wilson chain

In this second appendix, we discuss *one* possibility for encoding and storing product basis states of a Kondo-type model in a numerical implementation.

Let us consider a system that comprises N_s localized spins and N_f spin-1/2 fermions defined on a lattice with L sites. The spins $\underset{\sim}{\boldsymbol{s}}_i$ are characterized by spin quantum numbers $s_i \geq 1/2$ with corresponding magnetic quantum numbers $-s_i \leq m_i \leq s_i$, and the fermions are described by creation operators $\underset{\sim}{c}^\dagger_{j\sigma}$ for lattice

i	j	$\langle E_i \vert \underset{\sim}{S}^z \vert E_j \rangle$
1	1	$-\frac{1}{2}$
2	2	$\frac{1}{2}$
3	3	$-\frac{1}{2}$
4	4	$\frac{1}{2}\frac{1-\alpha_1^2(z)}{1+\alpha_1^2(z)}$
4	5	$\frac{1}{2}\frac{1-\alpha_1(z)\alpha_2(z)}{\sqrt{1+\alpha_1^2(z)}\sqrt{1+\alpha_2^2(z)}}$
5	4	$\frac{1}{2}\frac{1-\alpha_1(z)\alpha_2(z)}{\sqrt{1+\alpha_1^2(z)}\sqrt{1+\alpha_2^2(z)}}$
5	5	$\frac{1}{2}\frac{1-\alpha_2^2(z)}{1+\alpha_2^2(z)}$
6	6	$\frac{1}{2}$
7	7	$-\frac{1}{2}$
8	8	$\frac{1}{2}$

Table A.4.: The ten non-vanishing matrix elements of the z-component of the impurity spin with respect to the eigenstates of Hamiltonian (A.1) from Table A.2. The matrix representation has to be symmetric since $\underset{\sim}{S}^z$ is a Hermitian operator.

site j and spin projection $\sigma \equiv \pm 1/2$. The creation and corresponding destruction operators fulfill standard fermionic anticommutation relations. In accordance with the Pauli exclusion principle, each lattice site has four possible configurations (i.e., empty, occupied by a spin-up (spin-down) fermion, or doubly occupied by two fermions with opposing spin projections) and we have $0 \leq N_f \leq 2L$.

From the basis states $|s_i, m_i\rangle$ of the localized spins in the respective Hilbert spaces $\mathscr{H}_{s_i}$, standard product basis states of the product Hilbert space $\mathscr{H}_s \equiv \bigotimes_{i=0}^{N_s-1} \mathscr{H}_{s_i}$ are constructed (note that numbering always starts at zero in this section):

$$\begin{aligned} |s_0, m_0\rangle \otimes |s_1, m_1\rangle \otimes \ldots \otimes |s_{N_s-1}, m_{N_s-1}\rangle &\equiv |s_0, m_0; s_1, m_1; \ldots; s_{N_s-1}, m_{N_s-1}\rangle \\ &\equiv |m_0, m_1, \ldots, m_{N_s-1}\rangle \,. \end{aligned} \tag{A.8}$$

In a numerical implementation, spin $\underset{\sim}{\boldsymbol{s}}_j = \left(\underset{\sim}{s}_j^x, \underset{\sim}{s}_j^y, \underset{\sim}{s}_j^z\right)$ is represented by the z-component $\underset{\sim}{s}_j^z$ and the raising and lowering operators $\underset{\sim}{s}_j^{\pm} \equiv \underset{\sim}{s}_j^x \pm \mathrm{i}\underset{\sim}{s}_j^y$. Furthermore, it is convenient to change to a so-called *magnon representation* by introducing a *magnon number*

$$\boxed{a_i \equiv s_i - m_i \,,} \tag{A.9}$$

which only takes *non-negative integer* values:

$$\boxed{\begin{aligned} a_i &= 0, 1, \ldots, a_i^{\max} \,, \\ a_i^{\max} &\equiv 2s_i \qquad\qquad\quad . \end{aligned}} \tag{A.10}$$

Instead of working with the magnetic quantum number m_i, the number of "magnetic excitations" a_i relative to the fully polarized state with $m_i = s_i$ is used. $a_i^{\max}$ denotes the maximal number of magnons allowed for spin i. The effect of the operators $\underset{\sim}{s}_i^z$, $\underset{\sim}{s}_i^+$, and $\underset{\sim}{s}_i^-$ on a state $|a_i^{\max}, a_i\rangle$ directly follows from the definition (A.9):

$$\boxed{\begin{aligned} 2\underset{\sim}{s}_i^z \,|a_i^{\max}, a_i\rangle &= (a_i^{\max} - 2a_i) &&|a_i^{\max}, a_i\rangle \quad , \\ \underset{\sim}{s}_i^+ \,|a_i^{\max}, a_i\rangle &= \sqrt{a_i(a_i^{\max} - a_i + 1)} &&|a_i^{\max}, a_i - 1\rangle \,, \\ \underset{\sim}{s}_i^- \,|a_i^{\max}, a_i\rangle &= \sqrt{(a_i^{\max} - a_i)(a_i + 1)} &&|a_i^{\max}, a_i + 1\rangle \,. \end{aligned}} \tag{A.11}$$

Note that $\underset{\sim}{s}_i^+$ $\left(\underset{\sim}{s}_i^-\right)$ decreases (increases) the magnon number a_i and that, in a numerical implementation, $\sqrt{-0.0}$ gives NaN. Using the magnon representation, the product basis states (A.8) are replaced by:

$$\begin{aligned} &|a_0^{\max}, a_0\rangle \otimes |a_1^{\max}, a_1\rangle \otimes \ldots \otimes |a_{N_s-1}^{\max}, a_{N_s-1}\rangle \equiv \\ &|a_0^{\max}, a_0; a_1^{\max}, a_1; \ldots; a_{N_s-1}^{\max}, a_{N_s-1}\rangle \qquad\quad \equiv \\ &|a_0, a_1, \ldots, a_{N_s-1}\rangle \,. \end{aligned} \tag{A.12}$$

For the basis states of the fermionic Hilbert space $\mathscr{H}_f(N)$ with N particles, we employ a standard occupation-number representation with the following convention for the order of the creation operators (cf. Ref. [Jaf08]):

$$\boxed{\begin{aligned}&|n_{0\uparrow}, n_{1\uparrow}, \ldots, n_{L-1\uparrow};\, n_{0\downarrow}, n_{1\downarrow}, \ldots, n_{L-1\downarrow}\rangle \equiv \\ &\big(\underset{\sim}{c}^\dagger_{0\uparrow}\big)^{n_{0\uparrow}} \big(\underset{\sim}{c}^\dagger_{1\uparrow}\big)^{n_{1\uparrow}} \cdots \big(\underset{\sim}{c}^\dagger_{L-1\uparrow}\big)^{n_{L-1\uparrow}} \big(\underset{\sim}{c}^\dagger_{0\downarrow}\big)^{n_{0\downarrow}} \big(\underset{\sim}{c}^\dagger_{1\downarrow}\big)^{n_{1\downarrow}} \cdots \big(\underset{\sim}{c}^\dagger_{L-1\downarrow}\big)^{n_{L-1\downarrow}} |\,\Omega\,\rangle\,.\end{aligned}} \tag{A.13}$$

Here, $|\,\Omega\,\rangle$ is the vacuum state (corresponding to the empty lattice) and, according to the Pauli exclusion principle, the occupation numbers $n_{j\sigma}$, which have to fulfill $\sum_{j,\sigma} n_{j\sigma} = N$, can take the values 0 or 1. The chosen order of the creation operators is convenient for the calculation of typical matrix elements because it simplifies determining the overall sign that results from fermionic anticommutations (see the discussion following Eq. (A.21)).

A product basis of the Hilbert space $\mathscr{H}_s \otimes \mathscr{H}_f(N)$ of the total system, comprising the localized spins and N fermions, is obtained by combining the states (A.12) and (A.13):

$$\boxed{\begin{aligned}&|a_0, a_1, \ldots, a_{N_s-1}\rangle \otimes |n_{0\uparrow}, n_{1\uparrow}, \ldots, n_{L-1\uparrow};\, n_{0\downarrow}, n_{1\downarrow}, \ldots, n_{L-1\downarrow}\rangle \equiv \\ &|a_0, a_1, \ldots, a_{N_s-1};\, n_{0\uparrow}, n_{1\uparrow}, \ldots, n_{L-1\uparrow};\, n_{0\downarrow}, n_{1\downarrow}, \ldots, n_{L-1\downarrow}\rangle \quad \equiv \\ &\big|\psi\big(\{a_i\}, \{n_{j\sigma}\}\big)\big\rangle\,.\end{aligned}} \tag{A.14}$$

A.2.1. Encoding and manipulating product basis states

A product basis state $\big|\psi\big(\{a_i\}, \{n_{j\sigma}\}\big)\big\rangle$ can be stored in the form of a *single* integer variable $\mathcal{I}$ by using the individual bits of the integer for encoding the information about the magnon numbers $\{a_i\}$ and the occupation numbers $\{n_{j\sigma}\}$. Such an approach is advantageous for a number of reasons:

1. It leads to a low memory consumption of the product basis (which, however, might be insignificant compared to the total memory requirements of the numerical code anyway).

2. Product basis states can be manipulated using fast bitwise operations. In particular, the sign resulting from the application of a fermionic operator can be efficiently calculated.

3. Using the same integer variables, different blocks of bits storing different kind of information (such as information about the state of the spins or the fermions) can be treated independently.

4. A comparison of two product basis states simply corresponds to the comparison of two integer variables.

5. In particular, mapping states to integers thus automatically defines an order of the states.

In order to prevent any problems with the sign bit, the integers that are used for storing the basis states should be taken as *unsigned*.

The mapping to integer variables is particularly useful for fermionic systems and for spins with $s_i = 1/2$ since a single bit is sufficient to represent an occupation number $n_{j\sigma}$ or a magnon number a_i with two possible values, respectively. Furthermore, changing the state of a particular lattice site or spin then simply corresponds to flipping a single bit of the respective integer $\mathcal{I}$. In contrast, for $s_i > 1/2$, more than one bit is necessary in order to represent the magnon number a_i. This means that the respective part of $\mathcal{I}$ has to be divided into suitable blocks of bits.

An unsigned integer $\mathcal{I}$ can be partitioned in the following way in order to store the information about a product basis state $\left|\psi\big(\{a_i\},\{n_{j\sigma}\}\big)\right\rangle$ (see Ref. [Jaf08] for a discussion of the fermionic components $\mathcal{I}_\uparrow$ and $\mathcal{I}_\downarrow$):

$$\mathcal{I} \equiv \Big[\underbrace{\mathcal{I}_s}_{\substack{\text{state of the}\\ \textbf{localized spins}\\ (B_s \text{ bits})}}\ \underbrace{\mathcal{I}_\downarrow}_{\substack{\text{state of the}\\ \textbf{spin-down fermions}\\ (L \text{ bits})}}\ \underbrace{\mathcal{I}_\uparrow}_{\substack{\text{state of the}\\ \textbf{spin-up fermions}\\ (L \text{ bits})}}\Big] . \tag{A.15}$$

This division of $\mathcal{I}$ leads to the following relations (% denotes the modulo operator):

$$\begin{aligned} \mathcal{I} &= \mathcal{I}_\uparrow + 2^L\,\mathcal{I}_\downarrow + 2^{2L}\,\mathcal{I}_s \ , \\ \mathcal{I}_s &= \mathcal{I} \,/\, 2^{2L} \ , \\ \mathcal{I}_\downarrow &= \big(\mathcal{I} \,/\, 2^L\big) \,\%\, 2^L \ , \\ \mathcal{I}_\uparrow &= \mathcal{I} \,\%\, 2^L \ . \end{aligned} \tag{A.16}$$

The required constants can be obtained using, e.g., the bitwise left-shift operator $\ll$: $2^j = 1 \ll j$. We need to be able to delete the contents of the different blocks:

$$\begin{aligned} &\text{Delete block } \mathcal{I}_s: && \mathcal{I} = \mathcal{I} \,\%\, 2^{2L} && , \\ &\text{Delete block } \mathcal{I}_\downarrow: && \mathcal{I} = \mathcal{I} \,\&\, {\sim}\big[2^L\big(2^L-1\big)\big] && , \\ &\text{Delete block } \mathcal{I}_\uparrow: && \mathcal{I} = \mathcal{I} \,\&\, {\sim}\big(2^L-1\big) && . \end{aligned} \tag{A.17}$$

Here, & is the bitwise AND operator and $\sim$ is the bitwise NOT operator which inverts the bit pattern of the integer that it is applied to. Once a block has been erased, new information can be encoded. For example, if we want to replace $\mathcal{I}_s$ by $\mathcal{I}'_s$, we first delete $\mathcal{I}_s$ and then use: $\mathcal{I} = \mathcal{I} + 2^{2L}\,\mathcal{I}'_s$. Access to the different blocks would be much easier if the blocks were aligned on byte-boundaries. This is an option that should be considered.

Encoding information in the fermionic components $\mathcal{I}_\downarrow$ and $\mathcal{I}_\uparrow$ (cf. Ref. [Jaf08])

Since the occupation numbers $n_{j\sigma}$ for lattice site j and spin projection σ can only take the values 0 or 1, L bits of the integer $\mathcal{I}_\sigma$ are necessary in order to represent the L lattice sites:

$$\mathcal{I}_\sigma \equiv \Big[\; \underbrace{n_{L-1\sigma}}_{\text{L-1}} \;\; \underbrace{n_{L-2\sigma}}_{\text{L-2}} \;\; \underbrace{n_{L-3\sigma}}_{\text{L-3}} \;\; \ldots \;\; \underbrace{n_{2\sigma}}_{2} \;\; \underbrace{n_{1\sigma}}_{1} \;\; \underbrace{n_{0\sigma}}_{0} \;\Big] \;. \qquad \underbrace{}_{j=} \tag{A.18}$$

Individual bits of $\mathcal{I}_\sigma$ (corresponding to single lattice sites) can be manipulated using the bitwise operators OR (|), AND (&), and XOR (^):

$$\boxed{\begin{array}{lll} \text{Set} \quad \text{bit } j \text{ in } \mathcal{I}_\sigma : & \mathcal{I}_\sigma = \mathcal{I}_\sigma \;|\; & 2^j \;, \\ \text{Delete bit } j \text{ in } \mathcal{I}_\sigma : & \mathcal{I}_\sigma = \mathcal{I}_\sigma \;\&\; \sim 2^j \;, \\ \text{Flip} \quad \text{bit } j \text{ in } \mathcal{I}_\sigma : & \mathcal{I}_\sigma = \mathcal{I}_\sigma \;\hat{}\; & 2^j \;. \end{array}} \tag{A.19}$$

Furthermore, the value of bit j (i.e., the occupation number $n_{j\sigma}$) can be extracted from the integer $\mathcal{I}_\sigma$ in the following way:

$$\boxed{n_{j\sigma} = \left(\mathcal{I}_\sigma \,/\, 2^j\right) \& \, 1 \;.} \tag{A.20}$$

In order to calculate, e.g., a matrix representation of the Hamiltonian, we need to know how to apply creation and destruction operators to a product basis state (compare the partition (A.15) of $\mathcal{I}$):

$$\boxed{\begin{array}{lcll} \underset{\sim}{c}^\dagger_{j\downarrow} \,|\, \mathcal{I} \,\rangle & \cong & \mathcal{S}_{j\downarrow} \,(1 - n_{j\downarrow}) & \big|\, \mathcal{I} = \mathcal{I} \,\hat{}\, 2^{j+L} \,\big\rangle \;, \\ \underset{\sim}{c}^\dagger_{j\uparrow} \,|\, \mathcal{I} \,\rangle & \cong & \mathcal{S}_{j\uparrow} \,(1 - n_{j\uparrow}) & \big|\, \mathcal{I} = \mathcal{I} \,\hat{}\, 2^{j} \,\big\rangle \;, \\ \underset{\sim}{c}_{j\downarrow} \,|\, \mathcal{I} \,\rangle & \cong & \mathcal{S}_{j\downarrow} \, n_{j\downarrow} & \big|\, \mathcal{I} = \mathcal{I} \,\hat{}\, 2^{j+L} \,\big\rangle \;, \\ \underset{\sim}{c}_{j\uparrow} \,|\, \mathcal{I} \,\rangle & \cong & \mathcal{S}_{j\uparrow} \, n_{j\uparrow} & \big|\, \mathcal{I} = \mathcal{I} \,\hat{}\, 2^{j} \,\big\rangle \;. \end{array}} \tag{A.21}$$

$\mathcal{S}_{j\sigma}$ is the total sign that results from all fermionic anticommutations which are necessary, according to Eq. (A.13), to establish the correct order of creation operators or to "remove" the applied destruction operator, respectively. Note that the above equations (A.21) are, strictly speaking, *not* exact because, in a numerical implementation, $\mathcal{I} = 0$ corresponds to a valid state (namely, the state without particles and magnons). From a technical point of view, Eqs. (A.21) show that for the same indices j and σ the application of a creation and a destruction operator is very similar since in both cases the same sign $\mathcal{S}_{j\sigma}$ has to be determined

(provided that applying the operator results in a valid state) and the same bit is flipped in the integer $\mathcal{I}$.

Let us now turn to the calculation of the signs $\mathcal{S}_{j\sigma}$. On the one hand, an operator acting on lattice site j with $\sigma = +1/2$ has to be moved past all spin-up creation operators with indices $k \leq j-1$ in order to be put at the correct position according to Eq. (A.13). On the other hand, to establish the correct order, an operator with $\sigma = -1/2$ and index j has to be moved past *all* spin-up creation operators and, in addition, past all spin-down creation operators with lattice site index $k \leq j-1$. Since each exchange of fermionic operators causes $\mathcal{S}_{j\sigma}$ (being initialized to 1) to be multiplied by -1, the sign can be efficiently calculated using the following algorithm (expressed via C/C++ pseudocode), which effectively counts the number of bits that are set in the relevant part of the respective integer $\mathcal{I}$ (see p. 70 of Ref. [Ouc06]):

```
unsigned int I, j, L;
    ⋮
int sign;
unsigned int IMasked = { I % (1 << j);       // for spin-up
                       { I % (1 << (j+L));   // for spin-down
for(sign = 1; IMasked; sign *= -1)
    IMasked &= (IMasked - 1);
```

Depending on the spin projection σ and the lattice site index j, a certain number of the high-order bits of the integer `I` is removed, resulting in the "masked" integer `IMasked`. The `for`-loop then effectively counts the bits that are set in `IMasked` (by deleting one set bit in each step), multiplying `sign` by -1 for each set bit that is encountered. Note that for non-vanishing matrix elements of the type $\langle\, \mathcal{I} \,|\, \underset{\sim}{c}^{\dagger}_{j\downarrow} \underset{\sim}{c}_{k\downarrow} \,|\, \mathcal{I}' \,\rangle$ the contributions to the signs $\mathcal{S}_{j\downarrow}$ and $\mathcal{S}_{k\downarrow}$ due to the *spin-up* creation operators in $|\, \mathcal{I} \,\rangle$ and $|\, \mathcal{I}' \,\rangle$ cancel and can therefore be neglected (cf. Ref. [Jaf08]).

Encoding information in the spin component $\mathcal{I}_s$ (cf. Ref. [RRSR01])

The spin component $\mathcal{I}_s$ of the integer $\mathcal{I}$ has to be further divided into blocks of suitable lengths in which the information about the state of the different spins can be encoded (see Ref. [RRSR01] and also compare Refs. [Lin90, San10, Läu11]). To this end, we need to know how many bits B_i are necessary for spin i in order to allow for the representation of all possible values of the magnon number a_i:

$$\boxed{B_i = \mathrm{ceiling}\left(\frac{\ln(a_i^{\max} + 1)}{\ln 2} \right) .} \tag{A.22}$$

The total number of required bits is thus $B_s = \sum_{i=0}^{N_s-1} B_i$. The *start bits* $\{b_i\} = \{b_0, b_1, b_2, \ldots, b_{N_s-1}\}$ of the different blocks directly result from Eq. (A.22),

$$\boxed{\begin{aligned} &b_0 \equiv 0\,, \\ &b_i = \sum_{j=0}^{i-1} B_j \quad \text{for} \quad i \geq 1\,, \end{aligned}} \tag{A.23}$$

and lead to the following partition of the integer $\mathcal{I}_s$:

$$\boxed{\begin{array}{l} \mathcal{I}_s \equiv \big[\; \boxed{a_{N_s-1}} \boxed{\ldots} \boxed{a_2} \boxed{a_1} \boxed{a_0} \;\big]\,. \\ \quad\;\; \uparrow \quad\;\; \uparrow \quad\;\; \uparrow \quad\;\; \uparrow \quad\;\; \uparrow \quad\;\; \uparrow \\ \quad\;\; B_s \quad\;\; b_{N_s-1} \quad\;\; b_3 \quad\;\; b_2 \quad\;\; b_1 \quad\;\; b_0 \equiv 0 \end{array}} \tag{A.24}$$

Without any protection against performing an illegal operation that would violate the boundaries of the blocks, a magnon number a_i can be easily changed:

$$\boxed{\begin{aligned} &\text{Increase } a_i \text{ by } 1: \quad \mathcal{I}_s = \mathcal{I}_s + 2^{b_i}\,, \\ &\text{Decrease } a_i \text{ by } 1: \quad \mathcal{I}_s = \mathcal{I}_s - 2^{b_i}\,. \end{aligned}} \tag{A.25}$$

Furthermore, the value of a_i can be extracted and deleted (i.e., set to zero) in the following way:

$$\boxed{\begin{aligned} &\text{Extract } a_i: \quad a_i = \left(\mathcal{I}_s \,\%\, 2^{b_{i+1}}\right) / 2^{b_i}\,, \\ &\text{Delete } \quad a_i: \quad \mathcal{I}_s = \mathcal{I}_s \,\&\, \sim\!\left[2^{b_i}\left(2^{B_i} - 1\right)\right]\,. \end{aligned}} \tag{A.26}$$

After a magnon number a_i has been erased, a new value a_i' can be stored in the integer $\mathcal{I}_s$ by using: $\mathcal{I}_s = \mathcal{I}_s + 2^{b_i} a_i'$.

A.2.2. Creating a product basis subject to constraints

In the following, we discuss one possibility of creating a product basis for a Kondo-type model in a subspace with a certain total magnetic quantum number M and a certain particle number N (corresponding to a particular charge quantum number Q).

Creating a product basis for N_s spins in a subspace with total magnon number A

Although it is possible to create the *complete* product basis (e.g., by using a numeral system with suitable bases) and keep only those states with total magnon number $A \equiv \sum_i a_i$, it seems more elegant to apply an algorithm that directly produces the states which fulfill the constraint. If the size of the total Hilbert

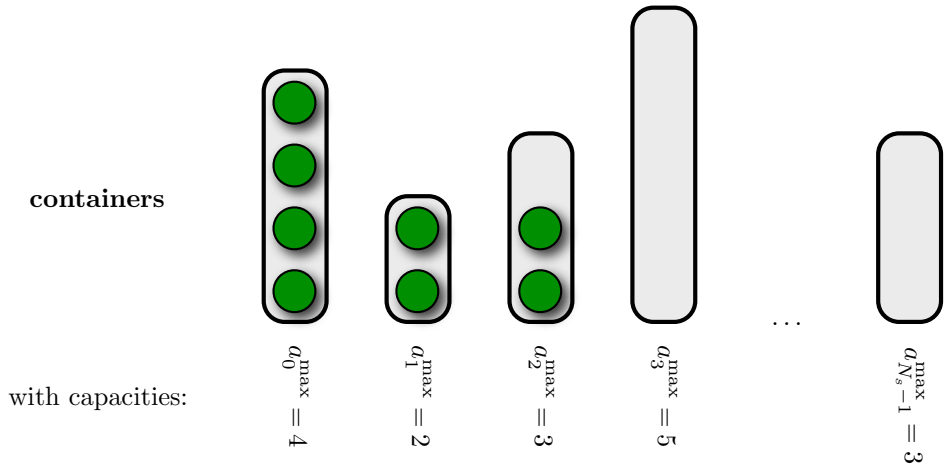

Figure A.2.: Creating the product basis in a subspace with total magnon number A is equivalent to finding all distributions of A balls between N_s containers with capacities $\{a_i^{\max}\}$. For the container sizes in this example and for $A = 8$, the lexicographically lowest state (i.e., the first state) is illustrated.

space becomes huge (e.g., in large-scale Lanczos-based exact diagonalizations of quantum spin models [SHS08]), the ability to create only the states belonging to a certain subspace, without the need for setting up the complete product basis, is clearly advantageous.

Constructing the product basis in a subspace with total magnon number A is equivalent to the problem of finding all possibilities for distributing A balls between N_s containers with capacities $\{a_i^{\max}\}$ (see Fig. A.2). Establishing an order of the distributions (or states) (a lexicographical order seems appropriate), the problem reduces to that of generating the next state for a given state. An algorithm performing this task is presented in Ref. [SHS08]:

1. Create the first (i.e., lexicographically lowest) state by successively filling up the containers, starting with the leftmost container, until there are no remaining balls (cf. Fig. A.2).

2. For a given state, create the next state with respect to lexicographical order:
   a) Find the leftmost box i which is not empty and whose neighboring box to the right is not completely filled. If there is no such box, then the given state is already the last (i.e., lexicographically highest) state.
   b) Move one ball from this container i to its neighboring container to the right $i + 1$.

c) Empty all boxes with indices $j \leq i$ and use the obtained balls to successively fill them up again, starting with the leftmost box, until there are no remaining balls.

Creating a basis for N spin-1/2 fermions on a lattice with L sites in a subspace with total magnetic quantum number M

According to the two constraints,

$$\begin{aligned} N_\uparrow + N_\downarrow &= N \ , \\ \frac{N_\uparrow}{2} - \frac{N_\downarrow}{2} &= M \ , \end{aligned} \tag{A.27}$$

the numbers $N_\uparrow$ and $N_\downarrow$ of spin-up and spin-down fermions, respectively, in a subspace with quantum numbers N and M are given by:

$$\boxed{\begin{aligned} N_\uparrow &= M + \frac{N}{2} \ , \\ N_\downarrow &= -M + \frac{N}{2} \ . \end{aligned}} \tag{A.28}$$

Creating a basis for the fermions again corresponds to the kind of problem illustrated by Fig. A.2: For spin projection σ, N_σ balls have to be distributed between L containers. Since the occupation numbers $n_{j\sigma}$ can only take the values 0 or 1, the containers each have a capacity of one ball. Forming all combinations of the resulting spin-up $\{\mathcal{I}_\uparrow\}$ and spin-down configurations $\{\mathcal{I}_\downarrow\}$, a basis of the subspace with quantum numbers N and M is obtained.

Creating a product basis for N spin-1/2 fermions, on a lattice with L sites, and N_s spins in a subspace with total magnetic quantum number M

According to the definition (A.9) of the magnon numbers, the total magnetic quantum number M_s of the spins can be expressed as:

$$M_s \equiv \sum_i m_i = \underbrace{\sum_i s_i}_{\equiv A_{\max}/2} - \underbrace{\sum_i a_i}_{\equiv A} = \frac{A_{\max}}{2} - A \ . \tag{A.29}$$

The allowed values of A are (cf. Eqs. (A.10)):

$$\boxed{A = 0, 1, \ldots, A_{\max} \ .} \tag{A.30}$$

The situation is more complicated now because there are three types of "balls" with corresponding containers (namely, localized spins, spin-up fermions, and spin-down fermions), but still only two constraints:

$$N_\uparrow + N_\downarrow \;=\; N \;, \tag{A.31}$$

$$\underbrace{\frac{A_{\max}}{2} - A}_{=M_s} \;+\; \underbrace{\frac{N_\uparrow}{2} - \frac{N_\downarrow}{2}}_{\equiv M_f} \;=\; M \;. \tag{A.32}$$

As a pragmatic approach, we can consider all values of M_f that are possible for the total fermion number N,

$$\boxed{\begin{aligned} |M_f|_{\max} &= \begin{cases} \frac{N}{2} & , \quad \text{for} \quad 0 \le N \le L \\ \frac{L}{2} - \frac{N-L}{2} = L - \frac{N}{2} & , \quad \text{for} \quad L < N \le 2L \end{cases} , \\ M_f &= -|M_f|_{\max}, -|M_f|_{\max}+1, \ldots, |M_f|_{\max} \quad , \end{aligned}} \tag{A.33}$$

and search for all combinations of A and M_f that fulfill Eq. (A.32). For each value of M_f thus found, the corresponding particle numbers $N_\uparrow$ and $N_\downarrow$ follow from Eqs. (A.28) setting $M = M_f$. Having determined the set $\big\{(A, N_\uparrow, N_\downarrow)\big\}$ of the allowed combinations of quantum numbers, the algorithm from Ref. [SHS08] can be used to construct the configurations $\{\mathcal{I}_s\}$, $\{\mathcal{I}_\uparrow\}$, and $\{\mathcal{I}_\downarrow\}$ for each element $(A, N_\uparrow, N_\downarrow)$. The product basis states with the quantum numbers $(A, N_\uparrow, N_\downarrow)$ are then obtained by forming all combinations of the corresponding integers $\{\mathcal{I}_s\}$, $\{\mathcal{I}_\uparrow\}$, and $\{\mathcal{I}_\downarrow\}$ according to the partition (A.15) of $\mathcal{I}$.

Bibliography

[AFL83] N. Andrei, K. Furuya, and J. H. Lowenstein, *Solution of the Kondo problem*, Rev. Mod. Phys. **55**, 331 (1983).
URL http://dx.doi.org/10.1103/RevModPhys.55.331

[AL81] N. Andrei and J. H. Lowenstein, *Scales and Scaling in the Kondo Model*, Phys. Rev. Lett. **46**, 356 (1981).
URL http://dx.doi.org/10.1103/PhysRevLett.46.356

[ALJ95] I. Affleck, A. W. W. Ludwig, and B. A. Jones, *Conformal-field-theory approach to the two-impurity Kondo problem: Comparison with numerical renormalization-group results*, Phys. Rev. B **52**, 9528 (1995).
URL http://dx.doi.org/10.1103/PhysRevB.52.9528

[And59] P. W. Anderson, *New Approach to the Theory of Superexchange Interactions*, Phys. Rev. **115**, 2 (1959).
URL http://dx.doi.org/10.1103/PhysRev.115.2

[And61] P. W. Anderson, *Localized Magnetic States in Metals*, Phys. Rev. **124**, 41 (1961).
URL http://dx.doi.org/10.1103/PhysRev.124.41

[And70] P. W. Anderson, *A poor man's derivation of scaling laws for the Kondo problem*, J. Phys. C: Solid State Phys. **3**, 2436 (1970).
URL http://dx.doi.org/10.1088/0022-3719/3/12/008

[And94] N. Andrei, *Integrable models in condensed matter physics*, arXiv:cond-mat/9408101 (1994).
URL http://arxiv.org/abs/cond-mat/9408101

[AS05] F. B. Anders and A. Schiller, *Real-Time Dynamics in Quantum-Impurity Systems: A Time-Dependent Numerical Renormalization-Group Approach*, Phys. Rev. Lett. **95**, 196801 (2005).
URL http://dx.doi.org/10.1103/PhysRevLett.95.196801

[AS06] F. B. Anders and A. Schiller, *Spin precession and real-time dynamics in the Kondo model: Time-dependent numerical renormalization-group study*, Phys. Rev. B **74**, 245113 (2006).
URL http://dx.doi.org/10.1103/PhysRevB.74.245113

[BCP08] R. Bulla, T. A. Costi, and T. Pruschke, *Numerical renormalization group method for quantum impurity systems*, Rev. Mod. Phys. **80**, 395 (2008).
URL http://dx.doi.org/10.1103/RevModPhys.80.395

[Bet31] H. Bethe, *Zur Theorie der Metalle. I. Eigenwerte und Eigenfunktionen der linearen Atomkette.*, Z. Phys. **71**, 205 (1931).
URL http://dx.doi.org/10.1007/BF01341708

[BG90] A. Bencini and D. Gatteschi, *Electron Paramagnetic Resonance of Exchange Coupled Systems*, Springer-Verlag (1990).

[BG09] H. Brune and P. Gambardella, *Magnetism of individual atoms adsorbed on surfaces*, Surf. Sci. **603**, 1812 (2009).
URL http://dx.doi.org/10.1016/j.susc.2008.11.055

[BGK09] L. Borda, M. Garst, and J. Kroha, *Kondo cloud and spin-spin correlations around a partially screened magnetic impurity*, Phys. Rev. B **79**, 100408 (2009).
URL http://dx.doi.org/10.1103/PhysRevB.79.100408

[BHS70] P. E. Bloomfield, R. Hecht, and P. R. Sievert, *Magnetic Field Effects in the s-d Exchange Model of Dilute Magnetic Alloys*, Phys. Rev. B **2**, 3714 (1970).
URL http://dx.doi.org/10.1103/PhysRevB.2.3714

[BK04] M. Bortz and A. Klümper, *The anisotropic multichannel spin-S Kondo model: Calculation of scales from a novel exact solution*, Eur. Phys. J. B **40**, 25 (2004).
URL http://dx.doi.org/10.1140/epjb/e2004-00235-5

[BLTV05] R. Bulla, H.-J. Lee, N.-H. Tong, and M. Vojta, *Numerical renormalization group for quantum impurities in a bosonic bath*, Phys. Rev. B **71**, 045122 (2005).
URL http://dx.doi.org/10.1103/PhysRevB.71.045122

[Blu07] S. J. Blundell, *Molecular magnets*, Contemp. Phys. **48**, 275 (2007).
URL http://dx.doi.org/10.1080/00107510801967415

[Bor07] L. Borda, *Kondo screening cloud in a one-dimensional wire: Numerical renormalization group study*, Phys. Rev. B **75**, 041307 (2007).
URL http://dx.doi.org/10.1103/PhysRevB.75.041307

[BPH97] R. Bulla, T. Pruschke, and A. C. Hewson, *Anderson impurity in pseudo-gap Fermi systems*, J. Phys.: Condens. Matter **9**, 10463 (1997).
URL http://dx.doi.org/10.1088/0953-8984/9/47/014

[BW08] L. Bogani and W. Wernsdorfer, *Molecular spintronics using single-molecule magnets*, Nat. Mater. **7**, 179 (2008).
URL http://dx.doi.org/10.1038/nmat2133

[CGP+04] A. L. Chernyshev, D. Galanakis, P. Phillips, A. V. Rozhkov, and A.-M. S. Tremblay, *Higher order corrections to effective low-energy theories for strongly correlated electron systems*, Phys. Rev. B **70**, 235111 (2004).
URL http://dx.doi.org/10.1103/PhysRevB.70.235111

[CL79a] D. M. Cragg and P. Lloyd, *Kondo Hamiltonians with a non-zero ground-state spin*, J. Phys. C: Solid State Phys. **12**, L215 (1979).
URL http://dx.doi.org/10.1088/0022-3719/12/6/001

[CL79b] D. M. Cragg and P. Lloyd, *Universality and the renormalisability of rotationally invariant Kondo Hamiltonians*, J. Phys. C: Solid State Phys. **12**, 3301 (1979).
URL http://dx.doi.org/10.1088/0022-3719/12/16/018

[CMSS11] A. Cornia, M. Mannini, P. Sainctavit, and R. Sessoli, *Chemical strategies and characterization tools for the organization of single molecule magnets on surfaces*, Chem. Soc. Rev. **40**, 3076 (2011).
URL http://dx.doi.org/10.1039/c0cs00187b

[CO03] V. L. Campo and L. N. Oliveira, *Renormalization-group approach to the problem of conduction through a nanostructure*, Phys. Rev. B **68**, 035337 (2003).
URL http://dx.doi.org/10.1103/PhysRevB.68.035337

[CO04] V. L. Campo and L. N. Oliveira, *Thermodynamics for the two-impurity Kondo model*, Phys. Rev. B **70**, 153401 (2004).
URL http://dx.doi.org/10.1103/PhysRevB.70.153401

[CO05] V. L. Campo and L. N. Oliveira, *Alternative discretization in the numerical renormalization-group method*, Phys. Rev. B **72**, 104432 (2005).
URL http://dx.doi.org/10.1103/PhysRevB.72.104432

[COK98] S. M. Cronenwett, T. H. Oosterkamp, and L. P. Kouwenhoven, *A Tunable Kondo Effect in Quantum Dots*, Science **281**, 540 (1998).
URL http://dx.doi.org/10.1126/science.281.5376.540

[Cos99] T. Costi, *Wilson's Numerical Renormalization Group*, in *Density-Matrix Renormalization – A New Numerical Method in Physics*, vol. 528 of *Lecture Notes in Physics*, edited by I. Peschel, M. Kaulke, X. Wang, and K. Hallberg, pp. 3–25, Springer (1999).
URL http://dx.doi.org/10.1007/BFb0106062

[CP03] P. Coleman and C. Pépin, *Singular Fermi liquid behavior in the underscreened Kondo model*, Phys. Rev. B **68**, 220405 (2003).
URL http://dx.doi.org/10.1103/PhysRevB.68.220405

[CPLO97] S. C. Costa, C. A. Paula, V. L. Líbero, and L. N. Oliveira, *Numerical renormalization-group computation of specific heats*, Phys. Rev. B **55**, 30 (1997).
URL http://dx.doi.org/10.1103/PhysRevB.55.30

[DBRM12] N. Domingo, E. Bellido, and D. Ruiz-Molina, *Advances on structuring, integration and magnetic characterization of molecular nanomagnets on surfaces and devices*, Chem. Soc. Rev. **41**, 258 (2012).
URL http://dx.doi.org/10.1039/c1cs15096k

[DS82] H.-U. Desgranges and K. D. Schotte, *Specific heat of the Kondo model*, Phys. Lett. A **91**, 240 (1982).
URL http://dx.doi.org/10.1016/0375-9601(82)90481-9

[DZ05] K. Ding and B.-H. Zhao, *Wilson number in the Kondo model with arbitrary impurity spin*, Phys. Lett. A **340**, 337 (2005).
URL http://dx.doi.org/10.1016/j.physleta.2005.04.022

[EFG+05] F. H. L. Essler, H. Frahm, F. Göhmann, A. Klümper, and V. E. Korepin, *The One-Dimensional Hubbard Model*, Cambridge University Press (2005).
URL http://dx.doi.org/10.2277/0521802628

[FH89] R. M. Fye and J. E. Hirsch, *Quantum Monte Carlo study of the two-impurity Kondo Hamiltonian*, Phys. Rev. B **40**, 4780 (1989).
URL http://dx.doi.org/10.1103/PhysRevB.40.4780

[FL82] K. Furuya and J. H. Lowenstein, *Bethe-ansatz approach to the Kondo model with arbitrary impurity spin*, Phys. Rev. B **25**, 5935 (1982).
URL http://dx.doi.org/10.1103/PhysRevB.25.5935

[FW81a] V. A. Fateev and P. B. Wiegmann, *The exact solution of the $s-d$ exchange model with arbitrary impurity spin S (Kondo problem)*, Phys. Lett. A **81**, 179 (1981).
URL http://dx.doi.org/10.1016/0375-9601(81)90056-6

[FW81b] V. A. Fateev and P. B. Wiegmann, *Thermodynamics of the $s-d$ Exchange Model with Arbitrary Impurity Spin (Kondo Problem)*, Phys. Rev. Lett. **46**, 1595 (1981).
URL http://dx.doi.org/10.1103/PhysRevLett.46.1595

[FW13] A. Furrer and O. Waldmann, *Magnetic cluster excitations*, Rev. Mod. Phys. **85**, 367 (2013).
URL http://dx.doi.org/10.1103/RevModPhys.85.367

[Fye94] R. M. Fye, *"Anomalous Fixed Point Behavior" of Two Kondo Impurities: A Reexamination*, Phys. Rev. Lett. **72**, 916 (1994).
URL http://dx.doi.org/10.1103/PhysRevLett.72.916

[GCA92] J. Gan, P. Coleman, and N. Andrei, *Coexistence of Fermi Liquid and Magnetism in the Underscreened Kondo Problem*, Phys. Rev. Lett. **68**, 3476 (1992).
URL http://dx.doi.org/10.1103/PhysRevLett.68.3476

[GCMS09] D. Gatteschi, A. Cornia, M. Mannini, and R. Sessoli, *Organizing and Addressing Magnetic Molecules*, Inorg. Chem. **48**, 3408 (2009).
URL http://dx.doi.org/10.1021/ic8013283

[GGGK+98] D. Goldhaber-Gordon, J. Göres, M. A. Kastner, H. Shtrikman, D. Mahalu, and U. Meirav, *From the Kondo Regime to the Mixed-Valence Regime in a Single-Electron Transistor*, Phys. Rev. Lett. **81**, 5225 (1998).
URL http://dx.doi.org/10.1103/PhysRevLett.81.5225

[GGSM+98] D. Goldhaber-Gordon, H. Shtrikman, D. Mahalu, D. Abusch-Magder, U. Meirav, and M. A. Kastner, *Kondo effect in a single-electron transistor*, Nature **391**, 156 (1998).
URL http://dx.doi.org/10.1038/34373

[GJH+07] L. Gao, W. Ji, Y. B. Hu, Z. H. Cheng, Z. T. Deng, Q. Liu, N. Jiang, X. Lin, W. Guo, S. X. Du, W. A. Hofer, X. C. Xie, and H.-J. Gao, *Site-Specific Kondo Effect at Ambient Temperatures in Iron-Based Molecules*, Phys. Rev. Lett. **99**, 106402 (2007).
URL http://dx.doi.org/10.1103/PhysRevLett.99.106402

[GKKR96] A. Georges, G. Kotliar, W. Krauth, and M. J. Rozenberg, *Dynamical mean-field theory of strongly correlated fermion systems and the limit of infinite dimensions*, Rev. Mod. Phys. **68**, 13 (1996).
URL http://dx.doi.org/10.1103/RevModPhys.68.13

[GML+11] E. Gull, A. J. Millis, A. I. Lichtenstein, A. N. Rubtsov, M. Troyer, and P. Werner, *Continuous-time Monte Carlo methods for quantum impurity models*, Rev. Mod. Phys. **83**, 349 (2011).
URL http://dx.doi.org/10.1103/RevModPhys.83.349

[GR88] L. I. Glazman and M. É. Raĭkh, *Resonant Kondo transparency of a barrier with quasilocal impurity states*, JETP Lett. **47**, 452 (1988).

[Grü74] G. Grüner, *Experimental evidence for many-body effects in dilute alloys*, Adv. Phys. **23**, 941 (1974).
URL http://dx.doi.org/10.1080/00018737400101451

[GSV06] D. Gatteschi, R. Sessoli, and J. Villain, *Molecular Nanomagnets*, Oxford University Press (2006).
URL http://dx.doi.org/10.1093/acprof:oso/9780198567530.001.0001

[Gut63] M. C. Gutzwiller, *Effect of correlation on the ferromagnetism of transition metals*, Phys. Rev. Lett. **10**, 159 (1963).
URL http://dx.doi.org/10.1103/PhysRevLett.10.159

[GWPT08] E. Gull, P. Werner, O. Parcollet, and M. Troyer, *Continuous-time auxiliary-field Monte Carlo for quantum impurity models*, EPL **82**, 57003 (2008).
URL http://dx.doi.org/10.1209/0295-5075/82/57003

[GZ74] G. Grüner and A. Zawadowski, *Magnetic impurities in non-magnetic metals*, Rep. Prog. Phys. **37**, 1497 (1974).
URL http://dx.doi.org/10.1088/0034-4885/37/12/001

[HdGF+06] H. B. Heersche, Z. de Groot, J. A. Folk, H. S. J. van der Zant, C. Romeike, M. R. Wegewijs, L. Zobbi, D. Barreca, E. Tondello, and A. Cornia, *Electron Transport through Single* Mn_{12} *Molecular Magnets*, Phys. Rev. Lett. **96**, 206801 (2006).
URL http://dx.doi.org/10.1103/PhysRevLett.96.206801

[HDW91] S. Hershfield, J. H. Davies, and J. W. Wilkins, *Probing the Kondo Resonance by Resonant Tunneling through an Anderson Impurity*, Phys. Rev. Lett. **67**, 3720 (1991).
URL http://dx.doi.org/10.1103/PhysRevLett.67.3720

[Hew93] A. C. Hewson, *The Kondo Problem to Heavy Fermions*, Cambridge University Press (1993).
URL http://dx.doi.org/10.1017/CBO9780511470752

[HF86] J. E. Hirsch and R. M. Fye, *Monte Carlo Method for Magnetic Impurities in Metals*, Phys. Rev. Lett. **56**, 2521 (1986).
URL http://dx.doi.org/10.1103/PhysRevLett.56.2521

[HLO+07] C. F. Hirjibehedin, C.-Y. Lin, A. F. Otte, M. Ternes, C. P. Lutz, B. A. Jones, and A. J. Heinrich, *Large Magnetic Anisotropy of a Single Atomic Spin Embedded in a Surface Molecular Network*, Science **317**, 1199 (2007).
URL http://dx.doi.org/10.1126/science.1146110

[Hof00] W. Hofstetter, *Renormalization Group Methods for Quantum Impurity Systems*, Ph.D. thesis, Universität Augsburg (2000).

[HS13] M. Höck and J. Schnack, *Numerical renormalization group calculations of the magnetization of Kondo impurities with and without uniaxial anisotropy*, Phys. Rev. B **87**, 184408 (2013).
URL http://dx.doi.org/10.1103/PhysRevB.87.184408

[Hub63] J. Hubbard, *Electron correlations in narrow energy bands*, Proc. R. Soc. Lond. A-Math. Phys. Sci. **276**, 238 (1963).
URL http://dx.doi.org/10.1098/rspa.1963.0204

[IDH06] V. Iancu, A. Deshpande, and S.-W. Hla, *Manipulating Kondo Temperature via Single Molecule Switching*, Nano Lett. **6**, 820 (2006).
URL http://dx.doi.org/10.1021/nl0601886

[Jaf08] S. A. Jafari, *Introduction to Hubbard Model and Exact Diagonalization*, arXiv:0807.4878 (2008).
URL http://arxiv.org/abs/0807.4878

[JGB+06] M.-H. Jo, J. E. Grose, K. Baheti, M. M. Deshmukh, J. J. Sokol, E. M. Rumberger, D. N. Hendrickson, J. R. Long, H. Park, and D. C. Ralph, *Signatures of Molecular Magnetism in Single-Molecule Transport Spectroscopy*, Nano Lett. **6**, 2014 (2006).
URL http://dx.doi.org/10.1021/nl061212i

[JVW88] B. A. Jones, C. M. Varma, and J. W. Wilkins, *Low-Temperature Properties of the Two-Impurity Kondo Hamiltonian*, Phys. Rev. Lett. **61**, 125 (1988).
URL http://dx.doi.org/10.1103/PhysRevLett.61.125

[Kas56] T. Kasuya, *A Theory of Metallic Ferro- and Antiferromagnetism on Zener's Model*, Prog. Theor. Phys. **16**, 45 (1956).
URL http://dx.doi.org/10.1143/PTP.16.45

[KIL+11] T. Komeda, H. Isshiki, J. Liu, Y.-F. Zhang, N. Lorente, K. Katoh, B. K. Breedlove, and M. Yamashita, *Observation and electric current control of a local spin in a single-molecule magnet*, Nat. Commun. **2**, 217 (2011).
URL http://dx.doi.org/10.1038/ncomms1210

[KJ04] P. Kakashvili and G. I. Japaridze, *Effective Hamiltonian for a half-filled Hubbard chain with alternating on-site interactions*, J. Phys.: Condens. Matter **16**, 5815 (2004).
URL http://dx.doi.org/10.1088/0953-8984/16/32/017

[KKH11] A. Kiss, Y. Kuramoto, and S. Hoshino, *Numerical study of Kondo impurity models with strong potential scattering: Reverse Kondo effect and antiresonance*, Phys. Rev. B **84**, 174402 (2011).
URL http://dx.doi.org/10.1103/PhysRevB.84.174402

[KmWW75] H. R. Krishna-murthy, K. G. Wilson, and J. W. Wilkins, *Temperature-Dependent Susceptibility of the Symmetric Anderson Model: Connection to the Kondo Model*, Phys. Rev. Lett. **35**, 1101 (1975).
URL http://dx.doi.org/10.1103/PhysRevLett.35.1101

[KmWW80a] H. R. Krishna-murthy, J. W. Wilkins, and K. G. Wilson, *Renormalization-group approach to the Anderson model of dilute magnetic alloys. I. Static properties for the symmetric case*, Phys. Rev. B **21**, 1003 (1980).
URL http://dx.doi.org/10.1103/PhysRevB.21.1003

[KmWW80b] H. R. Krishna-murthy, J. W. Wilkins, and K. G. Wilson, *Renormalization-group approach to the Anderson model of dilute magnetic alloys. II. Static properties for the asymmetric case*, Phys. Rev. B **21**, 1044 (1980).
URL http://dx.doi.org/10.1103/PhysRevB.21.1044

[Kon64] J. Kondo, *Resistance Minimum in Dilute Magnetic Alloys*, Prog. Theor. Phys. **32**, 37 (1964).
URL http://dx.doi.org/10.1143/PTP.32.37

[Kon68] J. Kondo, *Effect of Ordinary Scattering on Exchange Scattering from Magnetic Impurity in Metals*, Phys. Rev. **169**, 437 (1968).
URL http://dx.doi.org/10.1103/PhysRev.169.437

[KSD+02] N. Knorr, M. A. Schneider, L. Diekhöner, P. Wahl, and K. Kern, *Kondo Effect of Single Co Adatoms on Cu Surfaces*, Phys. Rev. Lett. **88**, 096804 (2002).
URL http://dx.doi.org/10.1103/PhysRevLett.88.096804

[Läu11] A. M. Läuchli, *Numerical Simulations of Frustrated Systems*, in *Introduction to Frustrated Magnetism*, vol. 164 of *Springer Series in Solid-State Sciences*, edited by C. Lacroix, P. Mendels, and F. Mila, pp. 481–511, Springer (2011).
URL http://dx.doi.org/10.1007/978-3-642-10589-0

[LCNJ05] C.-Y. Lin, A. H. Castro Neto, and B. A. Jones, *Microscopic theory of the single impurity surface Kondo resonance*, Phys. Rev. B **71**, 035417 (2005).
URL http://dx.doi.org/10.1103/PhysRevB.71.035417

[Lin90] H. Q. Lin, *Exact diagonalization of quantum-spin models*, Phys. Rev. B **42**, 6561 (1990).
URL http://dx.doi.org/10.1103/PhysRevB.42.6561

[Low84] J. H. Lowenstein, *Absence of significant conduction-electron polarization in the Kondo effect*, Phys. Rev. B **29**, 4120 (1984).
URL http://dx.doi.org/10.1103/PhysRevB.29.4120

[LSB+02] W. Liang, M. P. Shores, M. Bockrath, J. R. Long, and H. Park, *Kondo resonance in a single-molecule transistor*, Nature **417**, 725 (2002).
URL http://dx.doi.org/10.1038/nature00790

[LSBD98] J. Li, W.-D. Schneider, R. Berndt, and B. Delley, *Kondo Scattering Observed at a Single Magnetic Impurity*, Phys. Rev. Lett. **80**, 2893 (1998).
URL http://dx.doi.org/10.1103/PhysRevLett.80.2893

[MAC+05] P. Mehta, N. Andrei, P. Coleman, L. Borda, and G. Zarand, *Regular and singular Fermi-liquid fixed points in quantum impurity models*, Phys. Rev. B **72**, 014430 (2005).
URL http://dx.doi.org/10.1103/PhysRevB.72.014430

[Mat67] D. C. Mattis, *Symmetry of ground state in a dilute magnetic metal alloy*, Phys. Rev. Lett. **19**, 1478 (1967).
URL http://dx.doi.org/10.1103/PhysRevLett.19.1478

[MCJ+98] V. Madhavan, W. Chen, T. Jamneala, M. F. Crommie, and N. S. Wingreen, *Tunneling into a Single Magnetic Atom: Spectroscopic Evidence of the Kondo Resonance*, Science **280**, 567 (1998).
URL http://dx.doi.org/10.1126/science.280.5363.567

[MCJ+01] V. Madhavan, W. Chen, T. Jamneala, M. F. Crommie, and N. S. Wingreen, *Local spectroscopy of a Kondo impurity: Co on Au(111)*, Phys. Rev. B **64**, 165412 (2001).
URL http://dx.doi.org/10.1103/PhysRevB.64.165412

[MGY88] A. H. MacDonald, S. M. Girvin, and D. Yoshioka, *t/U expansion for the Hubbard model*, Phys. Rev. B **37**, 9753 (1988).
URL http://dx.doi.org/10.1103/PhysRevB.37.9753

[MGY90] A. H. MacDonald, S. M. Girvin, and D. Yoshioka, *Reply to "Comment on 't/U expansion for the Hubbard model'"*, Phys. Rev. B **41**, 2565 (1990).
URL http://dx.doi.org/10.1103/PhysRevB.41.2565

[MGY91] A. H. MacDonald, S. M. Girvin, and D. Yoshioka, *Erratum: Reply to "Comment on 't/U expansion for the Hubbard model'"*, Phys. Rev. B **43**, 6209 (1991).
URL http://dx.doi.org/10.1103/PhysRevB.43.6209

[MJN+02] V. Madhavan, T. Jamneala, K. Nagaoka, W. Chen, J.-L. Li, S. G. Louie, and M. F. Crommie, *Observation of spectral evolution during the formation of a Ni_2 Kondo molecule*, Phys. Rev. B **66**, 212411 (2002).
URL http://dx.doi.org/10.1103/PhysRevB.66.212411

[MV89] W. Metzner and D. Vollhardt, *Correlated Lattice Fermions in $d = \infty$ Dimensions*, Phys. Rev. Lett. **62**, 324 (1989).
URL http://dx.doi.org/10.1103/PhysRevLett.62.324

[MWC12] L. Merker, A. Weichselbaum, and T. A. Costi, *Full density-matrix numerical renormalization group calculation of impurity susceptibility and specific heat of the Anderson impurity model*, Phys. Rev. B **86**, 075153 (2012).
URL http://dx.doi.org/10.1103/PhysRevB.86.075153

[MWL93] Y. Meir, N. S. Wingreen, and P. A. Lee, *Low-Temperature Transport Through a Quantum Dot: The Anderson Model Out of Equilibrium*, Phys. Rev. Lett. **70**, 2601 (1993).
URL http://dx.doi.org/10.1103/PhysRevLett.70.2601

[NL88] T. K. Ng and P. A. Lee, *On-Site Coulomb Repulsion and Resonant Tunneling*, Phys. Rev. Lett. **61**, 1768 (1988).
URL http://dx.doi.org/10.1103/PhysRevLett.61.1768

[Noz74] P. Nozières, *A "Fermi-Liquid" Description of the Kondo Problem at Low Temperatures*, J. Low Temp. Phys. **17**, 31 (1974).
URL http://dx.doi.org/10.1007/BF00654541

[NR09] W. Nolting and A. Ramakanth, *Quantum Theory of Magnetism*, Springer (2009).
URL http://dx.doi.org/10.1007/978-3-540-85416-6

[OO94] W. C. Oliveira and L. N. Oliveira, *Generalized numerical renormalization-group method to calculate the thermodynamical properties of impurities in metals*, Phys. Rev. B **49**, 11986 (1994).
URL http://dx.doi.org/10.1103/PhysRevB.49.11986

[OTvB+08] A. F. Otte, M. Ternes, K. von Bergmann, S. Loth, H. Brune, C. P. Lutz, C. F. Hirjibehedin, and A. J. Heinrich, *The role of magnetic anisotropy in the Kondo effect*, Nat. Phys. **4**, 847 (2008).
URL http://dx.doi.org/10.1038/nphys1072

[Ouc06] F. Ouchni, *Exact diagonalization studies of a one-dimensional system at electron density $\rho = 0.4$: effect of the Coulomb repulsions and distant transfer*, Ph.D. thesis, Universität Osnabrück (2006).

[PCC+10] J. J. Parks, A. R. Champagne, T. A. Costi, W. W. Shum, A. N. Pasupathy, E. Neuscamman, S. Flores-Torres, P. S. Cornaglia, A. A. Aligia, C. A. Balseiro, G. K.-L. Chan, H. D. Abruña, and D. C. Ralph, *Mechanical Control of Spin States in Spin-1 Molecules and the Underscreened Kondo Effect*, Science **328**, 1370 (2010).
URL http://dx.doi.org/10.1126/science.1186874

[PKWH99] I. Peschel, M. Kaulke, X. Wang, and K. Hallberg (eds.), *Density-Matrix Renormalization – A New Numerical Method in Physics*, vol. 528 of *Lecture Notes in Physics*, Springer (1999).
URL http://dx.doi.org/10.1007/BFb0106062

[PPG+02] J. Park, A. N. Pasupathy, J. I. Goldsmith, C. Chang, Y. Yaish, J. R. Petta, M. Rinkoski, J. P. Sethna, H. D. Abruña, P. L. McEuen, and D. C. Ralph, *Coulomb blockade and the Kondo effect in single-atom transistors*, Nature **417**, 722 (2002).
URL http://dx.doi.org/10.1038/nature00791

[QWW+04] N. Quaas, M. Wenderoth, A. Weismann, R. G. Ulbrich, and K. Schönhammer, *Kondo resonance of single Co atoms embedded in Cu(111)*, Phys. Rev. B **69**, 201103 (2004).
URL http://dx.doi.org/10.1103/PhysRevB.69.201103

[RDT+09] G. Rogez, B. Donnio, E. Terazzi, J.-L. Gallani, J.-P. Kappler, J.-P. Bucher, and M. Drillon, *The Quest for Nanoscale Magnets: The example of [Mn12] Single Molecule Magnets*, Adv. Mater. **21**, 4323 (2009).
URL http://dx.doi.org/10.1002/adma.200803020

[RFC+09] N. Roch, S. Florens, T. A. Costi, W. Wernsdorfer, and F. Balestro, *Observation of the Underscreened Kondo Effect in a Molecular Transistor*, Phys. Rev. Lett. **103**, 197202 (2009).
URL http://dx.doi.org/10.1103/PhysRevLett.103.197202

[RK54] M. A. Ruderman and C. Kittel, *Indirect Exchange Coupling of Nuclear Magnetic Moments by Conduction Electrons*, Phys. Rev. **96**, 99 (1954).
URL http://dx.doi.org/10.1103/PhysRev.96.99

[RLA82] V. T. Rajan, J. H. Lowenstein, and N. Andrei, *Thermodynamics of the Kondo Model*, Phys. Rev. Lett. **49**, 497 (1982).
URL http://dx.doi.org/10.1103/PhysRevLett.49.497

[RRSR01] C. Raghu, I. Rudra, D. Sen, and S. Ramasesha, *Properties of low-lying states in some high-nuclearity Mn, Fe, and V clusters: Exact studies of Heisenberg models*, Phys. Rev. B **64**, 064419 (2001).
URL http://dx.doi.org/10.1103/PhysRevB.64.064419

[RWH08] D. Roosen, M. R. Wegewijs, and W. Hofstetter, *Nonequilibrium Dynamics of Anisotropic Large Spins in the Kondo Regime: Time-Dependent Numerical Renormalization Group Analysis*, Phys. Rev. Lett. **100**, 087201 (2008).
URL http://dx.doi.org/10.1103/PhysRevLett.100.087201

[RWH10] D. Roosen, M. R. Wegewijs, and W. Hofstetter, *Erratum: Nonequilibrium Dynamics of Anisotropic Large Spins in the Kondo Regime: Time-Dependent Numerical Renormalization Group Analysis [Phys. Rev. Lett. 100, 087201 (2008)]*, Phys. Rev. Lett. **105**, 259901 (2010).
URL http://dx.doi.org/10.1103/PhysRevLett.105.259901

[RWHS06a] C. Romeike, M. R. Wegewijs, W. Hofstetter, and H. Schoeller, *Kondo-Transport Spectroscopy of Single Molecule Magnets*, Phys. Rev. Lett. **97**, 206601 (2006).
URL http://dx.doi.org/10.1103/PhysRevLett.97.206601

[RWHS06b] C. Romeike, M. R. Wegewijs, W. Hofstetter, and H. Schoeller, *Quantum-Tunneling-Induced Kondo Effect in Single Molecular Magnets*, Phys. Rev. Lett. **96**, 196601 (2006).
URL http://dx.doi.org/10.1103/PhysRevLett.96.196601

[RWHS11] C. Romeike, M. R. Wegewijs, W. Hofstetter, and H. Schoeller, *Erratum: Kondo-Transport Spectroscopy of Single Molecule Magnets [Phys. Rev. Lett. 97, 206601 (2006)]*, Phys. Rev. Lett. **106**, 019902 (2011).
URL http://dx.doi.org/10.1103/PhysRevLett.106.019902

[RZK66] L. M. Roth, H. J. Zeiger, and T. A. Kaplan, *Generalization of the Ruderman-Kittel-Kasuya-Yosida Interaction for Nonspherical Fermi Surfaces*, Phys. Rev. **149**, 519 (1966).
URL http://dx.doi.org/10.1103/PhysRev.149.519

[San10] A. W. Sandvik, *Computational Studies of Quantum Spin Systems*, in *Lectures on the physics of strongly correlated systems XIV*, vol. 1297 of *AIP Conf. Proc.*, edited by A. Avella and F. Mancini, pp. 135–338 (2010).
URL http://dx.doi.org/10.1063/1.3518900

[Sch05] U. Schollwöck, *The density-matrix renormalization group*, Rev. Mod. Phys. **77**, 259 (2005).
URL http://dx.doi.org/10.1103/RevModPhys.77.259

[SDL08] A. Schiller and L. De Leo, *Phase diagram of the anisotropic multichannel Kondo Hamiltonian revisited*, Phys. Rev. B **77**, 075114 (2008).
URL http://dx.doi.org/10.1103/PhysRevB.77.075114

[SHS08] J. Schnack, P. Hage, and H.-J. Schmidt, *Efficient implementation of the Lanczos method for magnetic systems*, J. Comput. Phys. **227**, 4512 (2008).
URL http://dx.doi.org/10.1016/j.jcp.2008.01.027

[SS89] P. D. Sacramento and P. Schlottmann, *Thermodynamics of the single-channel Kondo impurity of spin $S(\leq \frac{7}{2})$ in a magnetic field*, Phys. Rev. B **40**, 431 (1989).
URL http://dx.doi.org/10.1103/PhysRevB.40.431

[SS91] P. D. Sacramento and P. Schlottmann, *Thermodynamics of the n-channel Kondo model for general n and impurity spin S in a magnetic field*, J. Phys.: Condens. Matter **3**, 9687 (1991).
URL http://dx.doi.org/10.1088/0953-8984/3/48/010

[SW66] J. R. Schrieffer and P. A. Wolff, *Relation between the Anderson and Kondo Hamiltonians*, Phys. Rev. **149**, 491 (1966).
URL http://dx.doi.org/10.1103/PhysRev.149.491

[TC69] G. Toulouse and B. Coqblin, *Remarks on potential scattering and effective J values in the Kondo problem*, Solid State Commun. **7**, 853 (1969).
URL http://dx.doi.org/10.1016/0038-1098(69)90776-5

[TSU97] H. Tsunetsugu, M. Sigrist, and K. Ueda, *The ground-state phase diagram of the one-dimensional Kondo lattice model*, Rev. Mod. Phys. **69**, 809 (1997).
URL http://dx.doi.org/10.1103/RevModPhys.69.809

[TW83] A. M. Tsvelick and P. B. Wiegmann, *Exact results in the theory of magnetic alloys*, Adv. Phys. **32**, 453 (1983).
URL http://dx.doi.org/10.1080/00018738300101581

[ÚZ98] O. Újsághy and A. Zawadowski, *Spin-orbit-induced magnetic anisotropy for impurities in metallic samples. I. Surface anisotropy*, Phys. Rev. B **57**, 11598 (1998).
URL http://dx.doi.org/10.1103/PhysRevB.57.11598

[ÚZG96] O. Újsághy, A. Zawadowski, and B. L. Gyorffy, *Spin-Orbit-Induced Magnetic Anisotropy for Impurities in Metallic Samples of Reduced Dimensions: Finite Size Dependence in the Kondo Effect*, Phys. Rev. Lett. **76**, 2378 (1996).
URL http://dx.doi.org/10.1103/PhysRevLett.76.2378

[vdWDFF$^+$00] W. G. van der Wiel, S. De Franceschi, T. Fujisawa, J. M. Elzerman, S. Tarucha, and L. P. Kouwenhoven, *The Kondo Effect in the Unitary Limit*, Science **289**, 2105 (2000).
URL http://dx.doi.org/10.1126/science.289.5487.2105

[WDW$^+$05] P. Wahl, L. Diekhöner, G. Wittich, L. Vitali, M. A. Schneider, and K. Kern, *Kondo Effect of Molecular Complexes at Surfaces: Ligand Control of the Local Spin Coupling*, Phys. Rev. Lett. **95**, 166601 (2005).
URL http://dx.doi.org/10.1103/PhysRevLett.95.166601

[Wei11] A. Weichselbaum, *Discarded weight and entanglement spectra in the numerical renormalization group*, Phys. Rev. B **84**, 125130 (2011).
URL http://dx.doi.org/10.1103/PhysRevB.84.125130

[Wil75] K. G. Wilson, *The renormalization group: Critical phenomena and the Kondo problem*, Rev. Mod. Phys. **47**, 773 (1975).
URL http://dx.doi.org/10.1103/RevModPhys.47.773

[WM94] N. S. Wingreen and Y. Meir, *Anderson model out of equilibrium: Noncrossing-approximation approach to transport through a quantum dot*, Phys. Rev. B **49**, 11040 (1994).
URL http://dx.doi.org/10.1103/PhysRevB.49.11040

[Yos57] K. Yosida, *Magnetic Properties of Cu-Mn Alloys*, Phys. Rev. **106**, 893 (1957).
URL http://dx.doi.org/10.1103/PhysRev.106.893

[Yos66] K. Yosida, *Bound State Due to the $s-d$ Exchange Interaction*, Phys. Rev. **147**, 223 (1966).
URL http://dx.doi.org/10.1103/PhysRev.147.223

[YWO90] M. Yoshida, M. A. Whitaker, and L. N. Oliveira, *Renormalization-group calculation of excitation properties for impurity models*, Phys. Rev. B **41**, 9403 (1990).
URL http://dx.doi.org/10.1103/PhysRevB.41.9403

[Zen51] C. Zener, *Interaction Between the d Shells in the Transition Metals*, Phys. Rev. **81**, 440 (1951).
URL http://dx.doi.org/10.1103/PhysRev.81.440

[Žit07] R. Žitko, *Many-particle effects in resonant tunneling of electrons through nanostructures*, Ph.D. thesis, University of Ljubljana (2007).

[Žit09] R. Žitko, *Adaptive logarithmic discretization for numerical renormalization group methods*, Comput. Phys. Commun. **180**, 1271 (2009).
URL http://dx.doi.org/10.1016/j.cpc.2009.02.007

[Žit11a] R. Žitko, *Magnetization curves for anisotropic magnetic impurities adsorbed on a normal metal substrate*, in *Physical Properties of Nanosystems*, edited by J. Bonča and S. Kruchinin, pp. 247–257, Springer (2011).
URL http://dx.doi.org/10.1007/978-94-007-0044-4_20

[Žit11b] R. Žitko, *Quantitative determination of the discretization and truncation errors in numerical renormalization-group calculations*

of spectral functions, Phys. Rev. B **84**, 085142 (2011).
URL http://dx.doi.org/10.1103/PhysRevB.84.085142

[ŽP09] R. Žitko and T. Pruschke, *Energy resolution and discretization artifacts in the numerical renormalization group*, Phys. Rev. B **79**, 085106 (2009).
URL http://dx.doi.org/10.1103/PhysRevB.79.085106

[ŽP10] R. Žitko and T. Pruschke, *Many-particle effects in adsorbed magnetic atoms with easy-axis anisotropy: the case of Fe on the CuN/Cu(100) surface*, New J. Phys. **12**, 063040 (2010).
URL http://dx.doi.org/10.1088/1367-2630/12/6/063040

[ŽPP08] R. Žitko, R. Peters, and T. Pruschke, *Properties of anisotropic magnetic impurities on surfaces*, Phys. Rev. B **78**, 224404 (2008).
URL http://dx.doi.org/10.1103/PhysRevB.78.224404

[ŽPP09] R. Žitko, R. Peters, and T. Pruschke, *Splitting of the Kondo resonance in anisotropic magnetic impurities on surfaces*, New J. Phys. **11**, 053003 (2009).
URL http://dx.doi.org/10.1088/1367-2630/11/5/053003

[ZWL+10] L. Zhou, J. Wiebe, S. Lounis, E. Vedmedenko, F. Meier, S. Blügel, P. H. Dederichs, and R. Wiesendanger, *Strength and directionality of surface Ruderman-Kittel-Kasuya-Yosida interaction mapped on the atomic scale*, Nat. Phys. **6**, 187 (2010).
URL http://dx.doi.org/10.1038/NPHYS1514